

NASA Conference Publication 2045

Part 2

(NASA-CP-2045) ADVANCED TECHNOLOGY AIRFOIL
RESEARCH, VOLUME 1, PART 2 (NASA) 303 p HC
A14/MF A01 CSCL 02A

N79-19989
THRU
N79-20007
Unclass
16558

G3/01

Advanced Technology Airfoil Research

Volume I

Proceedings of a conference
Langley Research Center
Hampton, Virginia, March 7-9, 1978



NASA

PREFACE

This NASA Conference Publication contains the proceedings of the NASA Conference on Advanced Technology Airfoil Research held at Langley Research Center on March 7-9, 1978, which have unlimited distribution. Conference cochairmen were Alfred Gessow, NASA Headquarters, and Robert F. Bower, Langley Research Center. Honorary cochairmen were Ira H. Abbott, NASA Headquarters (retired), and Richard T. Whitcomb, Langley Research Center.

The conference was planned to provide a comprehensive review of all NASA airfoil research, conducted both in-house and under grant and contract. In addition, a broad spectrum of airfoil research outside of NASA was reviewed. A total of 64 technical papers were presented at 12 sessions. Six workshops were also held to discuss progress, further immediate and long-range research needs, and important unresolved issues. A roundtable discussion summarized the technical sessions and workshops.

This volume contains papers presented at technical sessions covering the following subjects:

- (1) Airfoil Analysis and Design of Single-Element Airfoils
- (2) Airfoil Analysis and Design of Multielement Airfoils
- (3) Airfoil Analysis and Design Topics
- (4) Research Facilities and Test Techniques
- (5) Facilities and Test Technique Topics
- (6) Unsteady Aerodynamics

The major thrusts of the technical sessions were in three areas: development of computational aerodynamic codes for airfoil analysis and design, development of experimental facilities and test techniques, and all types of airfoil applications. The conference proceedings are presented in two volumes: Volume I is unclassified with unlimited distribution and Volume II is unclassified but with limited distribution.

The included papers are largely as submitted as camera-ready copy. Only minor editorial revisions have been made and a title page and abstract have been added.

Use of trade names or names of manufacturers in this report does not constitute an official endorsement of such products or manufacturers, either expressed or implied, by the National Aeronautics and Space Administration.

P. K. Pierpont, Conference Organizer

PRECEDING PAGE BLANK NOT FILMED

CONTENTS

PREFACE 111

PART 1*

1. NASA RESEARCH OBJECTIVES AND ROLES 1
Alfred Gessow

2. LANGLEY AIRFOIL-RESEARCH PROGRAM 11
Percy J. Bobbitt

3. OVERVIEW OF TWO-DIMENSIONAL AIRFOIL RESEARCH AT
AMES RESEARCH CENTER 39
Gary T. Chapman

AIRFOIL ANALYSIS AND DESIGN FOR SINGLE-ELEMENT AIRFOILS

Chairman: Jerry C. South
NASA Langley Research Center

4. TRANSONIC AIRFOIL CODES 45
P. R. Garabedian

5. APPLICATION OF DIRECT-INVERSE TECHNIQUES TO AIRFOIL
ANALYSIS AND DESIGN 55
Leland A. Carlson and Bruce M. Rocholl

6. LOW SPEED AIRFOIL DESIGN AND ANALYSIS 73
Richard Eppler and Dan M. Somers

7. A CONSISTENT DESIGN PROCEDURE FOR SUPERCRITICAL AIRFOILS
IN FREE AIR AND A WIND TUNNEL 101
Vijaya Shankar, Norman D. Malmuth, and Julian D. Cole

8. PROSPECTS FOR COMPUTING AIRFOIL AERODYNAMICS WITH REYNOLDS
AVERAGED NAVIER-STOKES CODES 119
George S. Deiwert and H. E. Bailey

9. AN EVALUATION OF FOUR SINGLE ELEMENT AIRFOIL ANALYTIC METHODS . . . 133
R. J. Freuler and G. M. Gregorek

AIRFOIL ANALYSIS AND DESIGN FOR MULTIELEMENT AIRFOILS

Chairman: Paul R. Garabedian
New York University

10. UPGRADED VISCOUS FLOW ANALYSIS OF MULTIELEMENT AIRFOILS 163
Guenter W. Brune and Joseph W. Manke

*Papers 1 to 29 are presented under separate cover.

11. NUMERICAL SOLUTION OF THE NAVIER-STOKES EQUATIONS FOR ARBITRARY TWO-DIMENSIONAL MULTI-ELEMENT AIRFOILS	183
Joe F. Thompson, Louie Turner, W. Serrill Long, and John H. Bearden	
12. THE ANALYSIS AND DESIGN OF TRANSONIC TWO-ELEMENT AIRFOIL SYSTEMS	209
G. Volpe and B. Grossman	
13. IMPROVEMENTS IN SURFACE SINGULARITY ANALYSIS AND DESIGN METHODS	221
Dean R. Bristow	
14. OPTIMIZATION OF MULTIELEMENT AIRFOILS FOR MAXIMUM LIFT	237
Lawrence E. Olson	

AIRFOIL ANALYSIS AND DESIGN TOPICS - SESSION I

Chairman: Paul R. Garabedian
New York University

15. WAKE CURVATURE AND TRAILING EDGE INTERACTION EFFECTS IN VISCOUS FLOW OVER AIRFOILS	255
R. E. Melnik	
16. A STUDY OF THE INTERACTION OF A NORMAL SHOCK WAVE WITH A TURBULENT BOUNDARY LAYER AT TRANSONIC SPEEDS	271
A. F. Messiter and T. C. Adamson, Jr.	
17. RECENT DEVELOPMENTS IN FINITE ELEMENT ANALYSIS FOR TRANSONIC AIRFOILS	281
M. M. Hafez and E. M. Murman	
18. SUPERCRITICAL TESTS OF A SELF-OPTIMIZING, VARIABLE-CAMBER WIND TUNNEL MODEL	297
Ely S. Levinsky and Richard L. Palko	
19. APPLICATION OF NUMERICAL OPTIMIZATION TO THE DESIGN OF ADVANCED SUPERCRITICAL AIRFOILS.	315
Raymond R. Johnson and Raymond M. Hicks	

AIRFOIL ANALYSIS AND DESIGN TOPICS - SESSION II

Chairman: Jerry C. South
NASA Langley Research Center

20. IMPROVED PREDICTION OF LAMINAR LEADING EDGE SEPARATION	327
R. N. Herring and W. L. Ely	

21. THE PREDICTION OF TWO-DIMENSIONAL AIRFOIL STALL PROGRESSION	335
Lloyd W. Gross	
22. APPLICATION OF THE AMI $C_{l_{max}}$ PREDICTION METHOD TO A NUMBER OF AIRFOILS	347
F. A. Dvorak and B. Maskew	
23. A NEW FLOW MODEL FOR HIGHLY SEPARATED AIRFOIL FLOWS AT LOW SPEEDS	367
Glen W. Zumwalt and Sharad N. Naik	
24. INVERSE BOUNDARY-LAYER TECHNIQUE FOR AIRFOIL DESIGN	383
M. L. Henderson	

RESEARCH FACILITIES AND TEST TECHNIQUES

Chairman: Richard W. Barnwell
NASA Langley Research Center

25. LANGLEY'S TWO-DIMENSIONAL RESEARCH FACILITIES - CAPABILITIES AND PLANS	399
Edward J. Ray	
26. DEVELOPMENTS IN AIRFOIL TESTING TECHNIQUES AT UNIVERSITY OF SOUTHAMPTON	415
Michael J. Goodyer	
27. A NEW AIRFOIL RESEARCH CAPABILITY	425
Charles L. Ladson	
28. DESIGN AND CALIBRATION OF SLOTTED WALLS FOR TRANSONIC AIRFOIL WIND TUNNELS	433
Richard W. Barnwell, William G. Sewall, and Joel L. Everhart	
29. PROGRESS REPORT: SOME STEADY AND OSCILLATING AIRFOIL TEST RESULTS, INCLUDING THE EFFECTS OF SWEEP, FROM THE TUNNEL SPANNING WING	445
Franklin O. Carta, Arthur O. St. Hilaire, James B. Rorke, and W. Donald Jepson	

PART 2

FACILITIES AND TEST TECHNIQUE TOPICS - SESSION I

Chairman: John D. Lee
The Ohio State University

30. A PARAMETRIC EXPERIMENTAL STUDY OF THE SLOTTED-WALL BOUNDARY CONDITION	459
Joel L. Everhart and Richard W. Barnwell	
31. TRANSONIC ASSESSMENT OF TWO-DIMENSIONAL WIND TUNNEL WALL INTERFERENCE USING MEASURED WALL PRESSURES	473
William B. Kemp, Jr.	
32. RESEARCH ON SELF-CORRECTING WIND TUNNELS	487
R. J. Vidal and J. C. Erickson, Jr.	
33. ANALYTICAL DESIGN OF A CONTOURED WIND-TUNNEL LINER FOR SUPERCRITICAL TESTING	499
Perry A. Newman and E. Clay Anderson	
34. EVALUATION OF INTERFERENCE IN THE OSU 6 IN. BY 22 IN. TRANSONIC AIRFOIL TUNNEL	511
John D. Lee	

FACILITIES AND TEST TECHNIQUE TOPICS - SESSION II

Chairman: Richard W. Barnwell
NASA Langley Research Center

35. VISUALIZATION OF THE SEPARATION AND SUBSEQUENT TRANSITION NEAR THE LEADING EDGE OF AIRFOILS	527
Anthony V. Arena and Thomas J. Mueller	
36. INSTRUMENTATION, TECHNIQUES AND DATA REDUCTION ASSOCIATED WITH AIRFOIL TESTING PROGRAMS AT WISCONSIN STATE UNIVERSITY	539
Edward J. Rodgers, William H. Wentz, Jr., and H. C. Seetharam	
37. APPLICATION OF THE LASER VELOCIMETER TO AIRFOIL RESEARCH	559
Danny R. Hoad	
38. APPLICATIONS OF DYNAMIC MEASUREMENT TECHNIQUES TO WIND-TUNNEL TESTING	571
F. K. Owen	
39. HOLOGRAPHY AND LDV TECHNIQUES, THEIR STATUS AND USE IN AIRFOIL RESEARCH	589
D. A. Johnson and W. D. Bachalo	

40. SECTION DRAG COEFFICIENTS FROM PRESSURE PROBE TRAVERSES OF A WING WAKE AT LOW SPEEDS	601
Lawrence C. Montoya, Paul F. Bikle, and Richard D. Banner	
41. FLIGHT TEST TECHNIQUES FOR LOW SPEED AIRFOIL EVALUATION	623
M. J. Hoffmann, G. M. Gregorek, and G. S. Weislogel	
42. IN-FLIGHT THREE-DIMENSIONAL BOUNDARY LAYER AND WAKE MEASUREMENTS FROM A SWEEPED SUPERCRITICAL WING	643
David P. Lux	

UNSTEADY AERODYNAMICS

Chairman: Samuel R. Bland
NASA Langley Research Center

43. A PROCEDURE FOR ANALYZING TRANSONIC FLOW OVER HARMONICALLY OSCILLATING AIRFOILS	657
Warren H. Weatherill, F. Edward Ehlers, and James D. Sebastian	
44. A NEW TWO-DIMENSIONAL OSCILLATING WING APPARATUS FOR UNSTEADY AERODYNAMICS RESEARCH	671
Sanford S. Davis and Gerald N. Malcolm	
45. SOME CALCULATIONS OF TRANSONIC POTENTIAL FLOW FOR THE NACA 64A006 AIRFOIL WITH AN OSCILLATING FLAP	689
Robert M. Bennett and Samuel R. Bland	
46. OBSERVATIONS ON THE DYNAMIC STALL CHARACTERISTICS OF ADVANCED HELICOPTER ROTOR AIRFOILS	701
L. Dadone	
47. TRANSONIC FLOW OVER THE NACA 64A006 WITH AN OSCILLATING FLAP - CALCULATIONS BASED ON THE EULER EQUATIONS	717
R. J. Magnus	
48. ROUNDTABLE SUMMARY AND CONFERENCE CONCLUSION	729
Cochairmen: Alfred Gessow and Robert E. Bower	

SLOTTED-WALL BOUNDARY CONDITION

Joel L. Everhart* and Richard W. Barnwell
NASA Langley Research Center

SUMMARY

An experimental study of slotted upper and lower walls in a two-dimensional transonic wind tunnel with solid sidewalls is reported. Results are presented for several slot spacings and slot openness ratios. The experimental data are pressure measurements which were made on an airfoil model and on a sidewall near one of the slotted walls. The slotted-wall boundary-condition coefficient, which relates the pressure and streamline curvature near the wall, is determined from the wall pressure measurements. The measured wall-induced interference is correlated with the experimental values for the boundary-condition coefficient. This correlation is compared with theory.

INTRODUCTION

Slotted walls have been used to relieve blockage effects in transonic wind tunnels for three decades. In this paper an experimental study of slotted walls with different slot spacings and openness ratios in a two-dimensional transonic tunnel with solid sidewalls is reported. Pressure measurements were made both on a model in the tunnel and near one of the slotted walls so that the wall-induced interference on the model and the nature of the flow near the slotted wall could be determined and correlated. These results can be used in the design and estimation of interference of other wind tunnels with slotted walls.

There was a practical incentive for the present test. The amount of experimental data on the flow near slotted walls is scarce (only three experimental data points (refs. 1, 2, and 3) are known to have been published prior to this test), and the data that have been published do not agree with either of the basic theoretical models (refs. 4 and 5). It should be noted that the theoretical model presented in reference 3 is, in effect, an empirical modification to the method of reference 4. It should also be noted that the theoretical model of reference 5 is simply a correction to that of reference 1. An analysis of the theoretical and experimental results (ref. 6) has shown that the design of two-dimensional tunnels with little or no blockage and streamline curvature effects is feasible if the experimental results are correct but unfeasible if the generally-accepted theoretical model of Davis and Moore (ref. 4) is correct. It was concluded that a parametric study involving wall-geometry parameters, Mach number and angle of attack should be made. The Reynolds number could not be varied independently since an atmospheric facility was used.

*Former Graduate Research Scholar Assistant with Joint Institute for Advancement of Flight Sciences, George Washington University.

There are three major steps in the estimation of interference effects caused by slotted walls. First, the general form of the boundary condition for flow near the wall must be determined. Second, the unknown coefficients in this boundary condition must be evaluated in terms of the slotted wall geometry. Third, the relationship between the wall-induced interference and the values of the boundary-condition coefficients must be determined. In this paper, results which affect each of these three major steps will be presented. In the case of the first step, the ideal slotted-wall boundary condition is used. For the second and third steps, correlations of parametric experimental data for the tunnel-geometry to boundary-condition-coefficient relationship and the boundary-condition-coefficient to interference-effects relationships are presented.

SYMBOLS

A	empirical boundary-condition coefficient
a	slot spacing
B	porous wall boundary-condition coefficient
C_N	normal-force coefficient
C_{N_α}	slope of the normal force curve
C_m	pitching-moment coefficient
C_p	pressure coefficient
C_p^*	critical pressure coefficient
$C_{p,PLENUM}$	pressure coefficient in the plenum chamber
c	airfoil chord
h	tunnel semi-height
K	slotted-wall boundary-condition coefficient
k	slotted-wall correlation parameter, $k = \frac{a}{h}K$
M_{PLENUM}	Mach number based on plenum pressure
P_{PLENUM}	plenum pressure
R	Reynolds number
x	distance along tunnel center line

x_0	upstream location used in evaluation of equation (7)
y	distance normal to tunnel center line
α	angle of attack
δ	slot width
θ	flow angle
θ_0	value of θ at x_0

SLOTTED-WALL BOUNDARY CONDITION

The terms used in the slotted-wall boundary condition are illustrated in figure 1. The usual form of the boundary condition is derived from the ideal slot condition, which states that the pressure in the slots is equal to the plenum pressure. The resulting boundary condition is

$$C_p - \frac{a^2 \theta^2}{\delta^2} - 2Ka \frac{\partial \theta}{\partial x} = C_{p,PLENUM} \quad (1)$$

where C_p and $C_{p,PLENUM}$ are the pressure coefficients in the tunnel near the wall and in the plenum, respectively. The quantities δ , a , and θ are the slot width, the slot spacing, and the flow angle in the tunnel near the wall. Note that the quantity $\theta a/\delta$ is the nondimensional cross-flow velocity at the slot. The coordinate x is the distance along the tunnel axis, and K is the slotted-wall boundary-condition coefficient.

When the cross flow at the slot is small, equation (1) can be approximated as

$$C_p - 2Ka \frac{\partial \theta}{\partial x} = C_{p,PLENUM} \quad (2)$$

DETERMINATION OF BOUNDARY-CONDITION COEFFICIENT

The experimental procedure which was used to measure the boundary-condition coefficient is described in this section. Since the flow in the tunnel near the slotted walls is irrotational and the disturbances are small, the small-disturbance irrotational condition

$$\frac{\partial \theta}{\partial x} = -\frac{1}{2} \frac{\partial C_p}{\partial y} \quad (3)$$

can be used to rewrite equation (1) as

$$C_p - \frac{a^2 \theta^2}{\delta^2} + K_u \frac{\partial C_p}{\partial y} = C_{p, \text{PLENUM}} \quad (4)$$

The coordinate y is measured perpendicular to the slotted top and bottom walls of the tunnel. Finite-difference approximations for the pressure coefficient C_p and the derivative $\partial C_p / \partial y$ are made and are evaluated with pressures obtained from pairs of orifices drilled in the solid sidewall near the slotted top wall. The location of these orifices is indicated in figure 2. The expressions for these quantities are

$$C_p = \frac{1}{2} \{C_p(x, y_1) + C_p(x, y_2)\} \quad (5)$$

and

$$\frac{\partial C_p}{\partial y} = \left\{ \frac{C_p(x, y_1) - C_p(x, y_2)}{y_1 - y_2} \right\} \quad (6)$$

where y_1 and y_2 are values of the y coordinate for two orifice rows. The flow angle θ is obtained from an integration of the irrotational condition as

$$\theta = -\frac{1}{2} \int_{x_0}^x \frac{\partial C_p}{\partial y} dx + \theta_0 \quad (7)$$

The boundary-condition coefficient K is obtained from a comparison of distributions of C_p and $\partial C_p / \partial y$.

EXPERIMENTAL FACILITY AND TEST CONDITIONS

The experimental facility is the Langley 6- by 19-inch transonic tunnel. This is a two-dimensional blowdown tunnel in which transonic airfoils are tested. The model used for the present study was an NACA 0012 airfoil with a chord of 15.24 cm (6 in.). Pressures on the airfoil surface were measured with strain-gage pressure transducers with a range of $\pm 10.34 \text{ N/cm}^2$ ($\pm 15 \text{ psi}$). The accuracy of these gages is 1 percent of full scale.

Three rows of pressure orifices have been drilled in one of the solid sidewalls at distances of 2.54 cm (1 in.), 3.81 cm (1.5 in.), and 5.08 cm (2 in.) from the slotted upper wall. Two of the orifice rows extend upstream beyond the point where the slots start so that the integration to determine the flow angle θ can start at a point where θ is known. The sidewall pressures were measured with variable capacitance precision transducers which

have reading errors no larger than .5 percent of reading. The transducers were referenced to the plenum pressure in order to keep the reading small and hence minimize measurement error. Near the model, transducers with a range of $+5.17 \text{ N/cm}^2$ ($+7.5 \text{ psi}$) were used. At other orifices where the measurements were less critical, transducers with a range of $+10.34 \text{ N/cm}^2$ ($+15 \text{ psi}$) were used. In all, there are 52 orifices on the sidewall where pressure measurements were made.

It should be noted that the pressure measurements on the tunnel sidewall and on the model were all made at the same time. In references 1, 2, and 3, the flow angle was measured one point at a time. This noncoincident data was then differentiated numerically to determine the derivative $\partial\theta/\partial x$.

The test conditions are shown in figure 3. Tests were conducted for slotted walls with openness ratios of .01, .025, .05, .075, .10, and .15 and slot spacings of 3.81 cm (1.5 in.), 7.62 cm (3 in.), and 15.24 cm (6 in.). These slot spacings correspond to 4, 2, and 1 slots, respectively, in the 6-inch-wide slotted wall. Some data were also obtained in a closed tunnel. It should be noted that some combinations of the openness ratio and slot spacing values listed above were not tested. It should also be noted that some of the combinations were tested in two different configurations. For example, some of the single-slot combinations were tested with a single slot in the middle and with 1/2 slot at each sidewall. The basic wall configurations are shown in figure 3.

The wall configurations were tested at Mach numbers of .5, .6, .7, .8, .825, .85, .875, and .9. Each wall was tested with the airfoil at several different angles of attack. Since the airfoil model is symmetric, results for the upper and lower slotted walls were obtained with the present experimental facility, which is only instrumented near the upper slotted wall, by placing the airfoil at positive and negative angles of attack.

EVALUATION OF BOUNDARY-CONDITION COEFFICIENT

An example of the evaluation of the coefficient K is depicted in figure 4. It is assumed that the boundary condition is the combined slotted-wall, porous-wall condition with an added constant term. This boundary condition is written as

$$C_p - \frac{a^2 \theta^2}{\delta^2} - C_{p, \text{PLENUM}} = -Ka \frac{\partial C_p}{\partial y} + B\theta + A \quad (8)$$

The constant A is added to account for the fact that the plenum pressure is slightly lower than the average pressure in the tunnel even when no model is present.

Results for the distributions of C_p , $\partial C_p/\partial y$, and θ are plotted against tunnel station. It can be seen that the distribution of C_p is

similar to that of $\partial C_p/\partial y$ but unlike that of θ . For example, the local maximum and minimum on the curve for θ do not occur near similar features on the curve for C_p , but the local maximums on the curves for C_p and $\partial C_p/\partial y$ occur at the same place. It is concluded that, for all means and purposes, the coefficient B is zero. A good match of the curves for C_p and $\partial C_p/\partial y$ is obtained when the coefficients K and A have the values 1.7 and .022, respectively.

Results for the value of the slotted-wall coefficient K for several openness ratios and slot spacings are depicted in figure 5. All of the present data shown are for a Mach number based on plenum pressure of .7. Also shown on the figure are the three previous experimental data points (refs. 1, 2, and 3) and the results of two theoretical models (refs. 4 and 5). It can be seen that the four present data points for the two-slot configuration vary consistently with openness ratio. It can also be seen that the coefficient K appears to be dependent on the slot-spacing to tunnel-height ratio.

DETERMINATION OF INTERFERENCE EFFECTS

Blockage Interference

Blockage interference is a result of either the underexpansion or the overexpansion of the fluid about the model as compared to free-air flow. This effect is directly related to the wall characteristics (i.e., openness ratio, number of slots, slot arrangement, etc.). In figure 6 the effect of the openness ratio on the shock location is shown at non-lifting conditions for a wall with 1 slot. The Mach number is about .833. The openness ratio has been varied from .01 to .05. On this airfoil at this Mach number, a 30-percent chord change in shock location is indicated with a change of 4 percent in openness ratio.

The effect of the number of slots and their arrangement in the wind tunnel is a constraint which, in general, has been overlooked. In figure 7 the effect of slot arrangement on shock location for an openness ratio of .05 and Mach number of about .83 is shown. The open circles represent a wall with one slot in the middle of the tunnel. The closed circles represent a wall with one-half slot located at each sidewall. Open squares are data obtained from a two-slot wall with each slot located a distance of one-half the slot spacing from the nearest wall, while the closed squares represent a two-slot wall with one slot in the center and one-half slot on each sidewall. The difference in the shock wave location obtained with the two one-slot walls and the difference obtained with the two two-slot walls is about 2 percent in each case. Differences of this magnitude can be expected from either instrumentation error or the inability to repeat test conditions. These data indicate that shock location is relatively insensitive to slot arrangement. However, there is a larger difference in shock wave location between the one-slot and two-slot results. This difference is between 5 and 10 percent for the case shown.

Lift Interference

Lift interference is a result of the tunnel walls constraining the streamlines to a slope which is different from that in free air. The effects of lift interference on an NACA 0012 airfoil are shown in figure 8 for a Mach number of .7. On the left side of the figure results for the slope of the normal-force curve are plotted against openness ratio, where circles, squares, and diamonds represent data obtained using 1, 2, and 4 slots, respectively. Also presented are data obtained during a previous investigation with a different slotted-wall configuration in the same tunnel (ref. 7).

On the right side of the figure the present results are plotted in terms of the parameter $k = Ka/h$. This is the theoretical correlation parameter obtained in references 4 and 6. The results of reference 7 are not plotted on the right side of the figure because the coefficients K for these cases are not known. It can be seen that the parameter k correlates the present data, although the correlated data do not fall on the curve obtained from slotted-wall theory (ref. 8).

The "zero interference" data were obtained in the 6- by 19-inch tunnel with a closed wall. It is so labelled because the theory indicates that lift interference in a closed tunnel is zero (except for streamline curvature effects). The slotted-wall theory is plotted through this point.

Streamline Curvature Interference

Streamline curvature is the rate of change of the local flow angle. Since streamline curvature results in an effective recambering of the airfoil, its effect will appear as a change in the airfoil pitching moment. These effects are determined by correlating pitching-moment variations with the tunnel-wall parameters.

On the left-hand side of figure 9 are presented pitching-moment versus openness-ratio results for an angle of attack of 4° and a Mach number based on plenum pressure of .7. Also shown is a theoretical free-air prediction (ref. 9), which accounts for the effects of transonic flow and nonsymmetrical boundary-layer growth on the upper and lower surfaces of a lifting airfoil. The correlation of the data with the slotted-wall parameter k is shown on the right-hand side of figure 9. The theoretical results shown on the right-hand side account for transonic and boundary-layer effects (ref. 9) and for wall-interference effects (ref. 8). The parameter k correlates the two-slot and four-slot data although these data do not fall on the theoretical curve. The one-slot datum point does not fall in the correlation band for the two- and four-slot data.

It should be noted that the theoretical pitching-moment coefficient for this airfoil is zero if transonic, boundary-layer, and wall effects are neglected because the airfoil is symmetric.

CONCLUDING REMARKS

It has been shown that the unknown coefficients in the expression for the boundary condition can be evaluated with sidewall pressure measurements. The results have been correlated with airfoil data to demonstrate the effects of wall geometry on the interference and, in general, it has been seen that the slotted-wall coefficient is the correct parameter for data correction and tunnel design. Deficiencies in the existing theories have been demonstrated.

REFERENCES

1. Chen, C. F.; and Mears, J. W.: Experimental and Theoretical Study of Mean Flow Boundary Conditions at Perforated and Longitudinally Slotted Wind Tunnel Walls. Arnold Engineering and Development Center, TR-57-20, 1957.
2. Baronti, P.; Ferri, A.; and Weeks, T.: Analysis of Wall Modifications in a Transonic Wind Tunnel. Advanced Technology Laboratories, TR-181, 1973.
3. Berndt, S. B.; and Sorensen, H.: Flow Properties of Slotted Walls for Transonic Test Sections. AGARD Conference Proceedings No. 174. Paper No. 17, 1975.
4. Davis, Don D., Sr.; and Moore, Dewey: Analytical Studies of Blockage and Lift Interference Corrections for Slotted Tunnels Obtained by the Substitution of an Equivalent Homogeneous Boundary for the Discrete Slots. NACA TM L53E076, 1953.
5. Barnwell, Richard W.: Improvements in the Slotted-Wall Boundary Condition. Proc. AIAA Ninth Aerodynamic Testing Conf., June 1976, pp. 21-30.
6. Barnwell, Richard W.: Design and Performance of Slotted Walls for Two-Dimensional Wind Tunnels. NASA TM X-78648, 1978.
7. Ladson, Charles L.: Description and Calibration of the Langley 6-By-19-Inch Transonic Tunnel. NASA TN D-7182, 1973.
8. Wright, R. H.: The Effectiveness of the Transonic Wind Tunnel as a Device for Minimizing Tunnel-Boundary Interference for Model Tests at Transonic Speeds. AGARD Report 294, 1959.
9. Bauer, Frances; Garabedian, Paul; Korn, David; and Jameson, Antony: Supercritical Wing Sections II. Lecture Notes in Economics and Mathematical Systems, vol. 108, M. Bechmann and H. P. Lunzi, eds., Springer-Verlag, c. 1975.
10. Berndt, Sune B.: Inviscid Theory of Wall Interference in Slotted Test Sections. AIAA Journal, vol. 15, no. 9, September 1977, pp. 1278-1287.

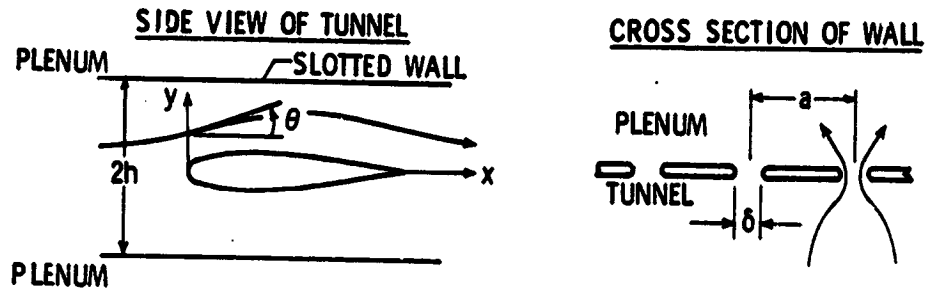


Figure 1.- Slotted-wall boundary condition.

LANGLEY 6- BY 19-INCH TRANSONIC TUNNEL

$P_{\text{PLENUM}} \approx 1$ ATMOSPHERE

$0.5 < M_{\text{PLENUM}} < 1.2$

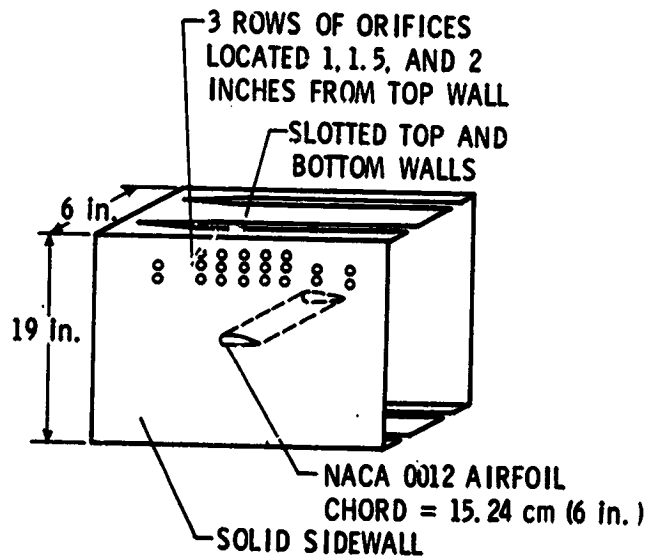


Figure 2.- Experimental facility.

TEST CONDITIONS

$M_{\text{PLENUM}} = 0.5, 0.6, 0.7, 0.8, 0.825, 0.85, 0.875, 0.9$
 $\alpha = -4, -2, -1, 0, 1, 2, 4$
 $1.5 \times 10^6 < R < 4.0 \times 10^6$

SLOTS TESTED

OPENNESS RATIO	NUMBER OF SLOTS
0.01	1
0.025	1, 2
0.05	1, 2
0.075	2
0.10	2, 4
0.15	2

SLOT ARRANGEMENTS

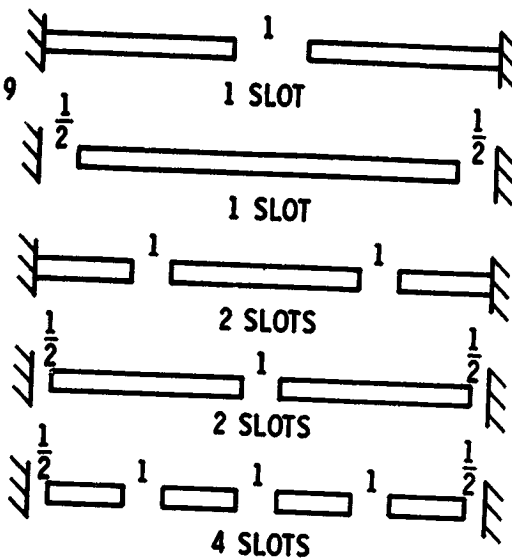


Figure 3.- Test conditions and slotted-wall arrangements.

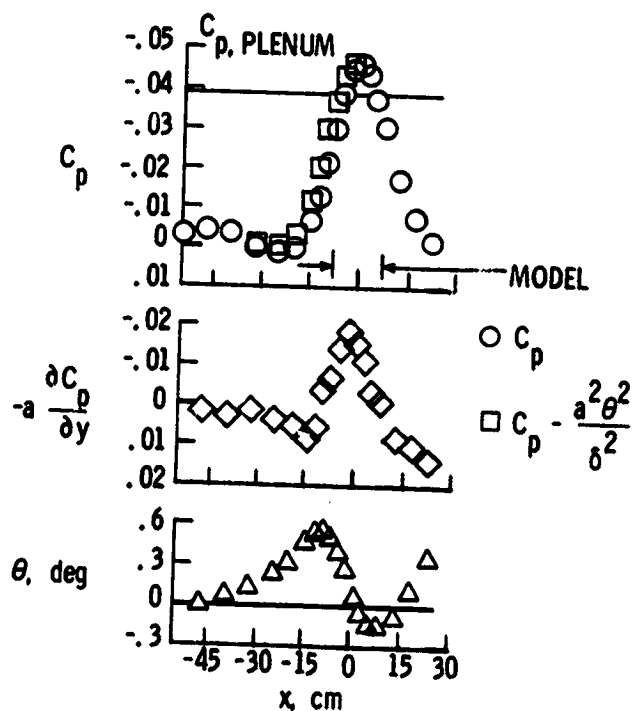


Figure 4.- Evaluation of coefficient K for a 10-percent open wall with 2 slots. $M_{\text{PLENUM}} = 0.7$.

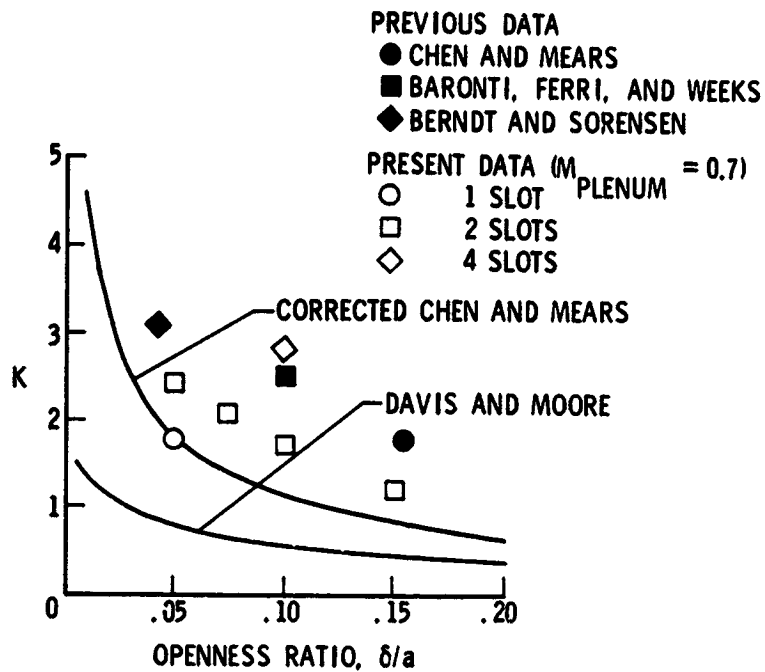


Figure 5.- Slotted-wall coefficient K.

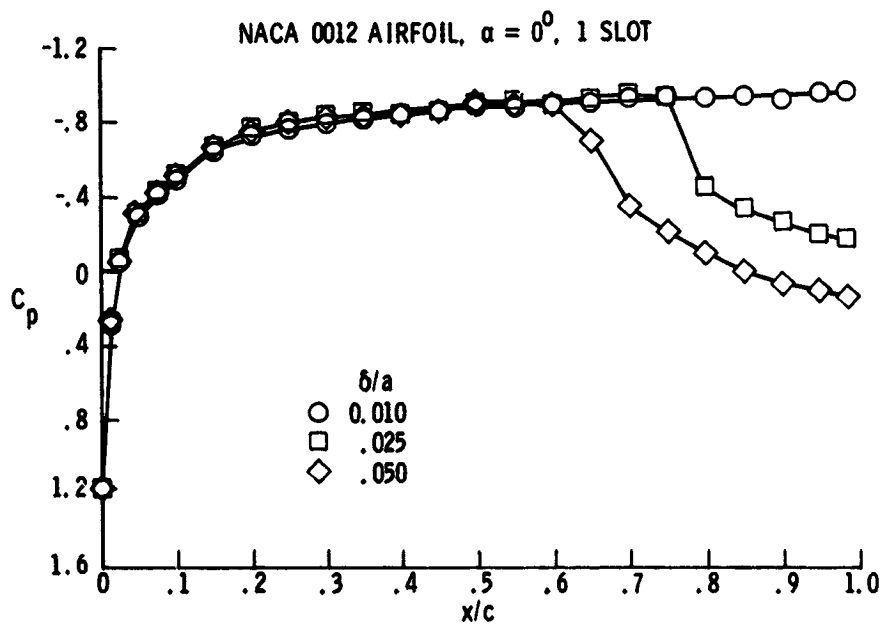


Figure 6.- Effect of openness ratio on airfoil pressure distribution.
 $M_{\text{PLENUM}} = 0.833$.

NACA 0012 AIRFOIL, $\alpha = 0^\circ$, OPENNESS RATIO = 0.05

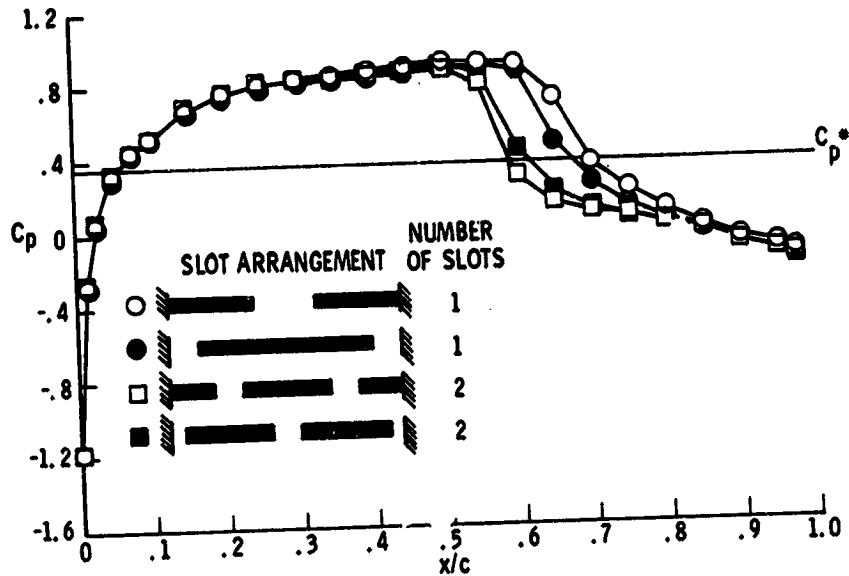


Figure 7.- Effect of slot arrangement on airfoil pressure distribution.
 $M_{\text{PLENUM}} = 0.83$.

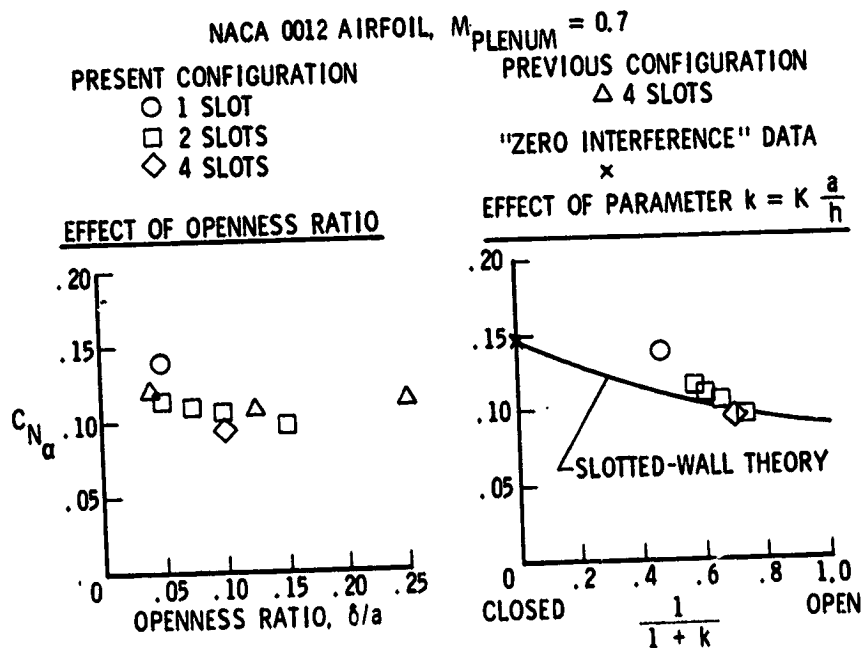


Figure 8.- Lift interference induced by slotted walls.

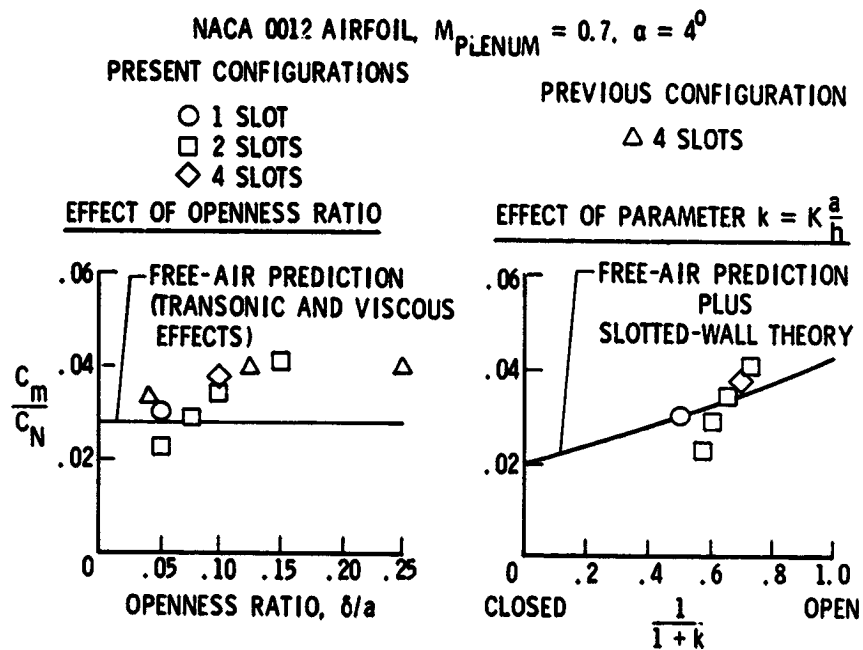


Figure 9.- Streamline curvature effects induced by slotted wall.

TRANSONIC ASSESSMENT OF TWO-DIMENSIONAL WIND
TUNNEL WALL INTERFERENCE USING MEASURED WALL PRESSURES

William P. Kemp, Jr.
NASA Langley Research Center

SUMMARY

A method is described for assessing wall interference in two-dimensional wind tunnels with better realism and accuracy than is achieved with methods based on classical wall interference theory. Measured pressure distributions are imposed as boundary conditions on a nonlinear transonic form of the potential equation to obtain an accurate computational reproduction of the actual tunnel flow. Wall-induced velocity perturbations are then extracted to yield both corrections to the tunnel test conditions and a measure of the adequacy of these corrections to account for tunnel interference. Application of the method to a transonic tunnel with variable porosity walls is illustrated.

INTRODUCTION

The methods used most frequently for predicting wall interference in two-dimensional tunnels draw their basic principles from the classical wall interference theory evolved by such pioneers as Glauert (ref. 1) and Goldstein (ref. 2). Specifically, a theoretical representation of the tunnel flow is built up by linear superposition of two-dimensional potential fields due to model lift, thickness, drag, and the wall reaction to each, and the wall boundary conditions are satisfied uniformly along surfaces extending from upstream to downstream infinity. This approach has been satisfactory in general when applied to solid wall wind tunnels at purely subsonic speeds.

With the advent of transonic test sections having either slotted or perforated walls, boundary condition expressions were developed in linear form to represent these walls in the classically based procedures. Subsequent experience has shown that the resulting wall interference predictions are often inadequate for correlating airfoil test results from different facilities. In the present paper, several areas from which inaccuracies arise will be identified and a new procedure will be described which should lead to significantly improved accuracy for wall interference assessment.

SYMBOLS

C_p	pressure coefficient
c	airfoil chord
C_n	airfoil section normal-force coefficient
h	tunnel height
M	Mach number
u, v	total perturbation velocity components in x and y directions, respectively; normalized by tunnel reference velocity
u_w, v_w	wall-induced perturbation velocity components in x and y directions, respectively; normalized by tunnel reference velocity
V_n	velocity component normal to wall
x, y	coordinates in streamwise and crossflow directions, respectively
α	angle of attack
τ	open area ratio of perforated wall

SOURCES OF INACCURACY

Several problem areas which contribute to inaccuracy in wall interference prediction, especially in transonic test sections, are pointed out in figure 1. Although the primary reason for using a transonic test section in an airfoil test facility is to minimize the exaggeration of wall interference by the supercritical flows occurring at high subsonic speeds, the limitations of the linearized potential flow representation used in the classical wall interference theory are violated in this speed range.

The imposition of wall boundary conditions uniformly on infinitely long surfaces in the classical approach overlooks such real tunnel geometry features as the finite length of a ventilated wall, the possible existence of diffuser entry flaps, a choked diffuser entrance, or the presence of a wake survey rake and its support. An additional source of error is the boundary layer on the tunnel side walls. The pressure field around the test airfoil causes variations in the displacement thickness of this wall boundary layer, thereby violating the two-dimensional flow assumption of the classical theory. The resulting effects include not only localized three-dimensional flow distortions but also the one-dimensional distortion of the effective tunnel stream tube area.

The problem area which is probably most significant, however, arises from the complex and variable nature of the flow constraint characteristics of both perforated and slotted walls. As a result, it is difficult to specify a boundary condition in linear form which accurately represents the constraint imposed by such walls in the presence of the wall boundary layer and model disturbance existing at a particular test condition.

FEATURES OF IMPROVED METHOD

The computation of a wall interference velocity field involves first the computational representation of the flow in the tunnel and second, the isolation of the perturbation in that flow that is attributable to the constraint imposed by the tunnel walls. To minimize inaccuracies from the problem areas previously discussed, the tunnel flow computation should reproduce as accurately as possible the flow actually existing in the tunnel. Two significant departures from the classical approach are incorporated in the method described herein to improve the accuracy of the tunnel flow representation. A nonlinear transonic form of the potential equation is used instead of the linearized form, and boundary conditions both at the model and at or near the upper and lower walls are imposed in the form of static pressure distributions actually measured during the tunnel test. This form of boundary condition eliminates the need for any specification of ventilated wall constraint characteristics and reflects into the computation the effects of the actual tunnel geometry and even the one-dimensional aspects of the side wall boundary layer effects.

To explore the feasibility of using experimental pressures directly as boundary conditions, they were first tried in a linearized potential flow procedure described in detail in reference 3. A sample of the results given in reference 3 is compared in figure 2 with predictions from the classical approach as implemented in reference 4. The experimental data analyzed were obtained at the University of Southampton, Southampton, England, during the course of a self-streamlining wall study (ref. 5) sponsored by Langley Research Center. The test Mach number was low enough to justify use of the linearized potential flow representation, and the straight solid tunnel wall configuration should be represented with good accuracy by the zero normal velocity boundary condition used in the classical theory. The NACA 0012-64 test airfoil with a chord of 90 percent of the tunnel height could be expected to produce unusually large wall interference effects.

The results shown in figure 2 are the distributions along the tunnel center line of the blockage and upwash components of the wall-induced velocity (u_w and v_w , respectively) normalized by the tunnel reference velocity. At an airfoil angle of attack of 40° , the use of measured pressures as boundary conditions gave results in good agreement with wall interference predictions from the classical approach. At an angle of attack of 12° , the two methods again yielded similar wall-induced upwash distributions but significantly different blockage velocities. It should be noted that the airfoil was stalled at this angle and the blockage due to the thickened airfoil wake is accounted for in the classical method. The additional blockage that is indicated

by the method using measured boundary conditions is probably caused by the influence of the model on the tunnel wall boundary layers, including a probable flow separation on the side walls. This result illustrates that the measured boundary conditions can account implicitly for flow phenomena which must be either modeled directly or be ignored in other methods.

To extend this capability to supercritical flows, the measured boundary conditions are imposed on a potential flow representation which is appropriate to transonic speeds. The tunnel flow is calculated as an iterative line overrelaxation solution of a finite difference representation of the transonic small disturbance equation in quasi-conservative form. The computational domain is the rectangular region included between the upper and lower wall pressure measurement locations. The measured pressure distributions on these upper and lower boundaries as well as on the airfoil upper and lower surfaces are imposed as boundary conditions in forms analogous to those described in reference 3. Potential distributions on the upstream and downstream boundaries are developed as polynomials compatible with all prescribed data, including prescribed flow directions at the two upstream corners. Prescribed values of airfoil lift and drag coefficients are used to constrain the total circulation and the trailing edge thickness by means of a special difference scheme at the mesh interval bracketing the airfoil leading edge.

The wind tunnel flow calculated by this method combines the realism introduced by the experimental boundary conditions with the accurate treatment of supercritical flows made possible by the nonlinear transonic potential equation. Because, however, the wall-induced perturbation is not an explicitly identified part of the nonlinear tunnel flow solution, it cannot be isolated as directly as in the linearized formulation. In the present method, the wall-induced perturbation field is determined as the difference between the total perturbation in the tunnel flow solution and a separately calculated perturbation representing that part of the tunnel flow perturbation which is directly attributable to the model. In the classical linearized formulation, the model-induced part of the tunnel flow perturbation is determined completely by the types and strengths of singularities at the model. Neither model shape nor pressure distribution is appropriate for characterizing the model perturbation because both would change if the wall-induced perturbations were removed. In the present method, therefore, the model singularity distributions are extracted from the tunnel flow solution in the form of velocity component jumps between the upper and lower surfaces of the model and are imposed in this form as the model boundary conditions in a free-air flow computation to define the model-induced perturbation.

To facilitate both the boundary condition transfer and the subsequent subtraction of the model perturbation from the total, the two computations are performed on coordinate grids which are identical within the domain of the tunnel flow computation. The free-air computational grid is, in general, extended beyond this domain and far field boundary conditions are imposed in the asymptotic form given in reference 6 with an additional term to account for the net model source strength corresponding to the prescribed drag coefficient.

Because at transonic speeds the perturbation solution becomes strongly coupled to the Mach number of the uniform flow that is used as a perturbation base, the Mach number of this uniform base flow (that is, the far field Mach number) is corrected in the free air computation to account for wall interference. The streamwise component of the wall-induced velocity is calculated at a prescribed chordwise location on the model after each iteration of the free air flow solution and is used to update the far field Mach number for the next iteration. After convergence, the local Mach number at this location in the free air flow matches that in the tunnel flow because the wall-induced contribution simply has been shifted from the perturbation in the tunnel case to the uniform base flow in the free air case. This location, therefore, will be called the match point. Because of the velocity jump boundary condition, this match occurs on both the upper and lower model surfaces. It follows that if the wall-induced blockage velocity were uniform over the model chord, the entire Mach number distribution (or static pressure distribution) over the model in the free air flow would match that in the tunnel flow.

It is not necessary to iteratively correct the far field flow direction to account for the wall-induced upwash because the transonic small disturbance equation used in the present method treats such crossflow perturbations linearly. Instead, one might imagine rotating the entire free-air flow solution to align the local flow direction at the match point with that in the tunnel flow. Then if the wall induced upwash velocity were uniform over the model chord, the entire model shape would match that in the tunnel flow and the far field velocity vector would define the free-air Mach number and angle of attack to which the data measured in the tunnel should be applied. In general, however, the wall-induced blockage and upwash velocities will not be found uniform over the model chord and the amount of nonuniformity is indicative of the residual error in the data after correcting for mean values of the wall-induced increments in Mach number and angle of attack. Although at low speeds data corrections sometimes are applied as linearly superimposed first order effects of gradients in wall-induced velocity, these corrections overlook such nonlinear phenomena as shock movement and are, therefore, of questionable validity at supercritical speeds.

ILLUSTRATION OF TRANSONIC ASSESSMENT

Data obtained during tests of a 10-percent thick supercritical airfoil in the Lockheed Compressible Flow Facility and discussed in reference 7 have been assessed for wall interference using the present method. This facility has perforated top and bottom walls with variable porosity control and was equipped with pressure measurement rails to determine the static pressure distributions near the top and bottom walls. Because the pressure rails did not extend upstream into the solid wall nozzle, the upstream boundary of the tunnel flow computation region was located within the perforated region of the real tunnel test section and consequently the flow directions at the two upstream corners were not accurately known. To analyze the test results from this facility, therefore, the flow angle at these points was input as zero and the calculated tunnel flow was then rotated to achieve a best

alignment of the model surface streamlines in the calculated flow with the known airfoil shape and angle of attack setting. The flow direction was thereby resolved within about 0.02° . Experience has shown that the calculated airfoil surface streamline shape is sufficiently reliable for this approach if the angle of attack is small and the airfoil pressure data are of good quality.

Airfoil pressure distributions measured at a Mach number of 0.8 with two different wall porosities are compared in figure 3. In each case the angle of attack in the experiment was set to obtain a normal force coefficient equal to the airfoil design value. The angle of attack settings required with the two porosities differed by more than 1° , and, even at the same C_n , the large differences observed between the two pressure distributions indicate changes in wall interference which cannot be accounted for simply by adjusting angle of attack.

Wall interference results obtained by applying the present method to the 0.013 wall porosity case are shown in figure 4 for two prescribed locations of the match point used in updating the far field Mach number. Again, the results are given as distributions along the tunnel center line of the blockage and upwash components of the wall-induced velocity normalized by the tunnel reference velocity. Observe that although the blockage velocities used for the far field update differed by only about 0.005 between the two match point locations, the resulting wall-induced velocity distributions are very sensitive to this change, particularly in the vicinity of the shock terminating the upper surface supercritical region. Observe also that the discontinuity in wall-induced velocity across the shock is essentially eliminated by choosing a match point location just ahead of the shock. This is because the shock strength is equalized in the two flows by matching the local Mach number entering the shock.

One might be disturbed at this point by the apparent dependence of the wall interference results on an arbitrarily chosen match point location. Note, however, that this dependence arises from the gradient in wall-induced velocity and would vanish if the wall properties were such as to produce a uniform wall-induced velocity over the model. In such a case, the free-air condition to which the tunnel data properly should be applied would be indicated by the present method regardless of match point location. In the more general case, the nonuniformities in wall-induced velocity yield an uncorrectable residual error and the arbitrary match point location provides a means of minimizing this residual error by seeking a most nearly uniform wall-induced perturbation, thereby identifying that free-air condition to which the tunnel data are most nearly applicable. The experience gained to date in applying the method to supercritical flow cases has indicated that locating the match point just ahead of the shock is a generally effective way to minimize the nonuniformities.

The wall-induced velocity distributions in the vicinity of the model with four different wall porosities are compared in figure 5. For each case, representative single values of wall-induced blockage and downwash would be used to correct the Mach number and angle of attack. Best accuracy

of the resulting data requires minimizing not the magnitude of the wall-induced velocities but rather their nonuniformity over the model. The nonuniformities in the results shown in figure 5 include localized irregularities in the supercritical flow region which are most pronounced for the minimum porosity wall. With increasing porosity, the localized irregularities diminish and essentially vanish at 0.06 porosity, only to reappear with a somewhat altered nature at 0.08 porosity. The localized irregularities are superimposed on a general gradient which, in the case of the blockage component, is also largest for the minimum porosity and nearly vanishes at 0.06 porosity. The general gradient of the wall-induced downwash, however, crosses zero between the 0.013 and 0.04 porosity cases and is clearly negative at 0.06 porosity. The results shown in figure 5 indicate, therefore, that none of the wall porosities produce data which are completely correctable for wall interference. The residual error is probably minimized with a porosity of slightly less than 0.06.

It is tempting to speculate that the previously noted localized irregularities of wall-induced velocity in the supercritical region might arise from the same wall properties that govern the wave reflection characteristics of the wall at higher Mach numbers. To date no cases have been analyzed at sufficiently high Mach number to either support or refute this speculation.

In order to compare the results shown in figure 5 with predictions from the classical approach, values are needed of the wall porosity parameter which appears as a coefficient in the perforated wall boundary condition. Inasmuch as the tunnel flow computation in the present method is an accurate reproduction of the actual tunnel flow, it can be used to provide a wall crossflow calibration from the actual test data. The procedure is illustrated in figure 6 for wall porosities of 0.013 and 0.08 although it was performed for all porosities. The variation of crossflow velocity v (positive inward) with longitudinal perturbation velocity u along both the top and bottom walls is plotted for each porosity. The slope of this variation is taken as the wall porosity parameter. In determining the slope, the portions of the walls nearest the model, which generally included the largest magnitude of velocity perturbations, were considered most significant. The curly variations near the origin in figure 6 occurred far upstream of the model and were ignored.

The porosity parameters thus determined were used with the charts of reference 4 to predict the magnitude and gradient of the wall-induced velocities for each wall porosity. These predictions are shown in figure 7 as dashed lines and are compared in this figure with the results of the present method reproduced from figure 5. Considering first the wall-induced downwash results, the gradients predicted from reference 4 agree well with the general gradients obtained by ignoring the localized irregularities near the shock in the results of the present method. The downwash magnitude agrees reasonably well between the two methods for the 0.04 porosity case but significant discrepancies are apparent for the higher porosities. Additional information on the wall-induced downwash magnitude can be obtained from the angle of attack settings during the experiment. It is reasoned that because the airfoil normal force coefficient was the same for all four

wall porosity cases, the change in angle of attack setting between any two porosities should reflect with fair accuracy the change in wall-induced downwash. Accordingly, the negative of the actual angle of attack settings (in radians) is indicated in figure 7 by the tick marks. Although the agreement in absolute level with the results of the present method is only coincidental, the increments due to changes in wall porosity corroborate the results of the present method rather than those from the classical predictions.

The magnitudes of the wall-induced blockage velocity that were predicted using reference 4 are shown in figure 7 to be smaller in general and much less sensitive to changes in wall porosity than those assessed by the present method. The large sensitivity of the wall-induced blockage to wall porosity changes indicated by the results of the present method at low porosities is corroborated by the discussion in reference 7 of the same experimental data. In reference 7 it was shown that the airfoil pressure distribution measured with 0.02 porosity walls at a reference Mach number of 0.796 but reduced as though the Mach number were 0.817 agreed very well with that measured with 0.04 porosity walls at a reference Mach number of 0.817. This implies that the normalized blockage velocity u_w was 0.023 more positive for a wall porosity of 0.02 than for a porosity of 0.04; this agrees much better with the trend of the present method on figure 7 than with that of the predictions using reference 4.

Although the reasons for discrepancy in the particular cases shown are not known, it should be pointed out that the present method is responsive to several phenomena which are overlooked by the classical approach. These include the effect of discrepancies in the empty tunnel calibration, the interaction between the model and the tunnel reference pressure source, and the change in effective wall boundary layer thickness due to model-induced flow through the wall perforations as well as the sources of inaccuracy discussed in a previous section.

In addition, an anomaly in the method of reference 4 with respect to the wake blockage prediction should be noted. In the classical approach, the test section walls are extended an infinite distance upstream from the model to the reference flow. For perforated walls, the establishment of the reference flow is dominated by a pressure balance condition, even in the limit of zero porosity, rather than by the mass conservation condition which dominates the solid wall case. As a result, the predicted perforated wall wake blockage increases negatively with decreasing porosity and reaches a limit at zero porosity which is equal in magnitude but opposite in sign to that for solid walls. This result is clearly inappropriate for real perforated tunnels in which the reference pressure is measured much closer to the model.

CONCLUDING REMARKS

The method described in this paper for assessing the wall interference in transonic two-dimensional tunnel tests embodies two significant departures from the methods generally used for wall interference prediction. The use of experimentally measured boundary conditions provides the means of accounting realistically for a number of tunnel interference phenomena which are either overlooked or represented less accurately by other methods. The use of a nonlinear transonic potential equation to represent the tunnel flow assures applicability of the method to supercritical test conditions. The method yields corrections to the test Mach number and angle of attack and also yields a measure of the adequacy of these corrections to account for the interference existing during the test. The improved accuracy and realism illustrated in this paper should lead to increased confidence in the use of airfoil test facilities, particularly at supercritical speeds.

REFERENCES

1. Clauert, H.: Wind-Tunnel Interference on Wings, Bodies and Airscrews. R. & M. No. 1566, British A.R.C., 1933.
2. Goldstein, S.: Steady Two-Dimensional Flow Past a Solid Cylinder in a Non-Uniform Stream and Two-Dimensional Wind-Tunnel Interference. R. & M. No. 1902, British A.R.C., 1942.
3. Kemp, William B., Jr.: Toward the Correctable-Interference Transonic Wind Tunnel. AIAA 9th Aerodynamic Testing Conference, 1976, pp. 31-38.
4. Pindzola, M.; and Lo, C. F.: Boundary Interference at Subsonic Speeds in Wind Tunnels with Ventilated Walls. AEDC-TR-69-47, 1969.
5. Goodyer, Michael J.: The Self Streamlining Wind Tunnel. NASA TM X-72699, 1975.
6. Klunker, E. B.: Contribution to Methods for Calculating the Flow About Thin Lifting Wings at Transonic Speeds - Analytic Expressions for the Far Field. NASA TN D-6530, 1971.
7. Blackwell, James A., Jr.; and Pounds, Gerald A.: Wind-Tunnel Wall Interference Effects on a Supercritical Airfoil at Transonic Speeds. J. Aircraft, vol. 14, no. 10, Oct. 1977, pp. 929-935.

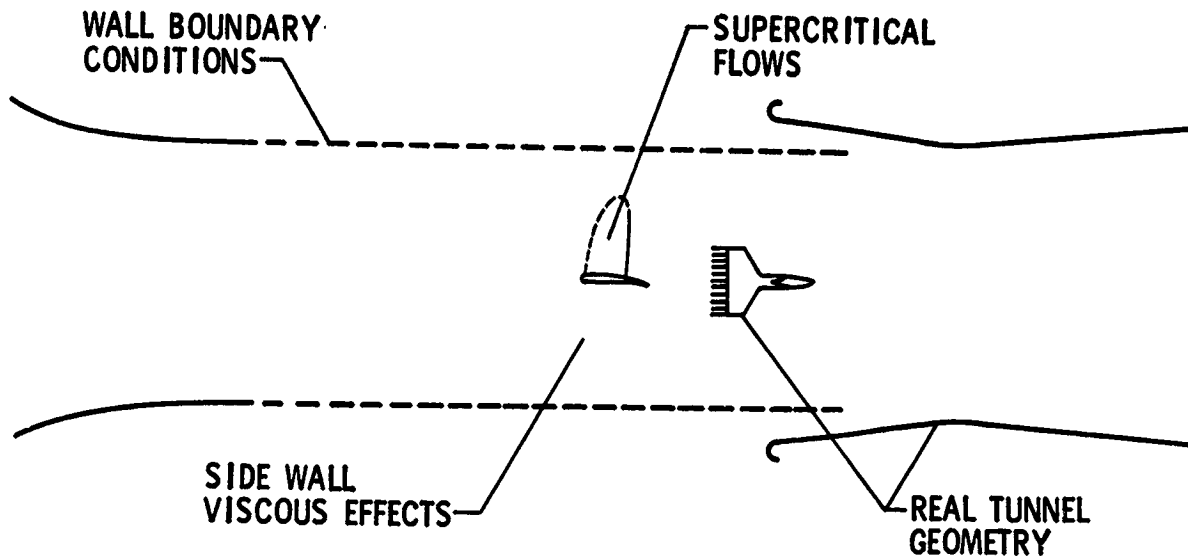


Figure 1.- Wall interference problem areas.

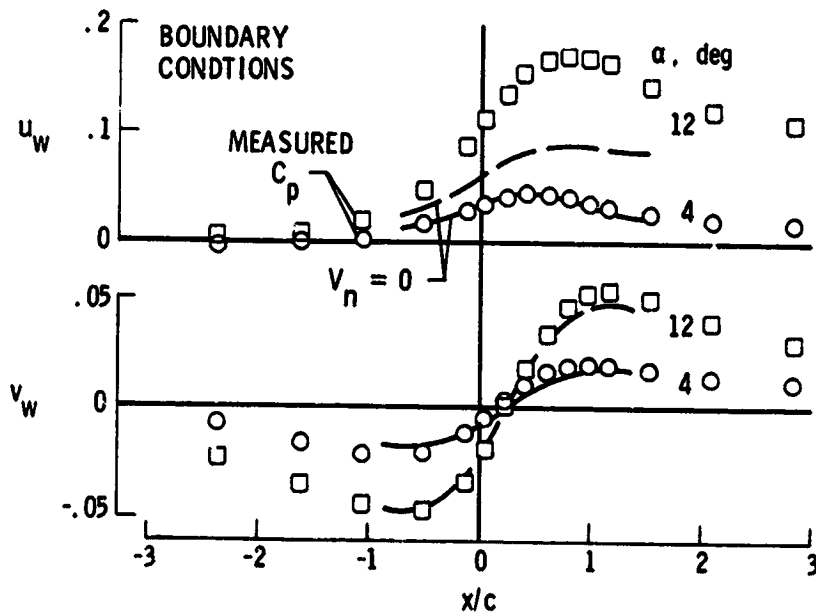


Figure 2.- Comparison of wall-induced velocities calculated at tunnel center line using measured pressures with predictions by classical approach. NACA 0012-64 airfoil in University of Southampton tunnel with straight solid walls; $c/h = 0.9$; $M = 0.1$.

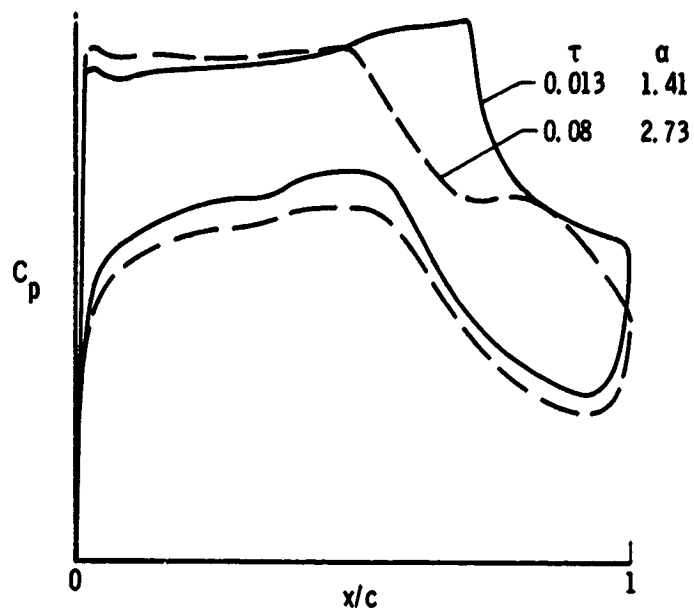


Figure 3.- Effect of wall porosity on airfoil pressure distribution.
 10-percent thick supercritical airfoil in Lockheed CFF; $c/h = 0.25$;
 $M = 0.8$; design c_n .

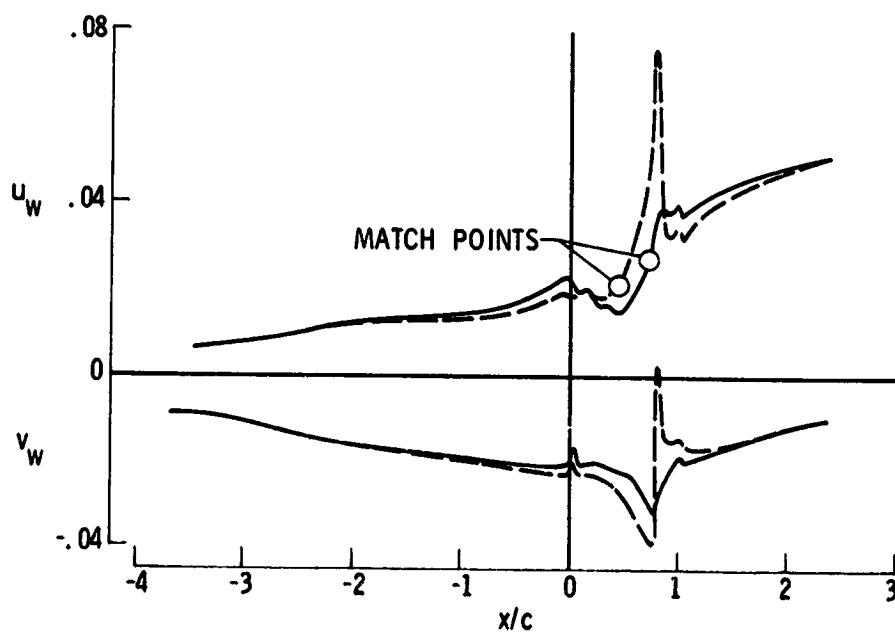


Figure 4.- Effect of far-field Mach number update on calculated wall-induced velocities. $\tau = 0.013$; $M = 0.8$; design c_n .

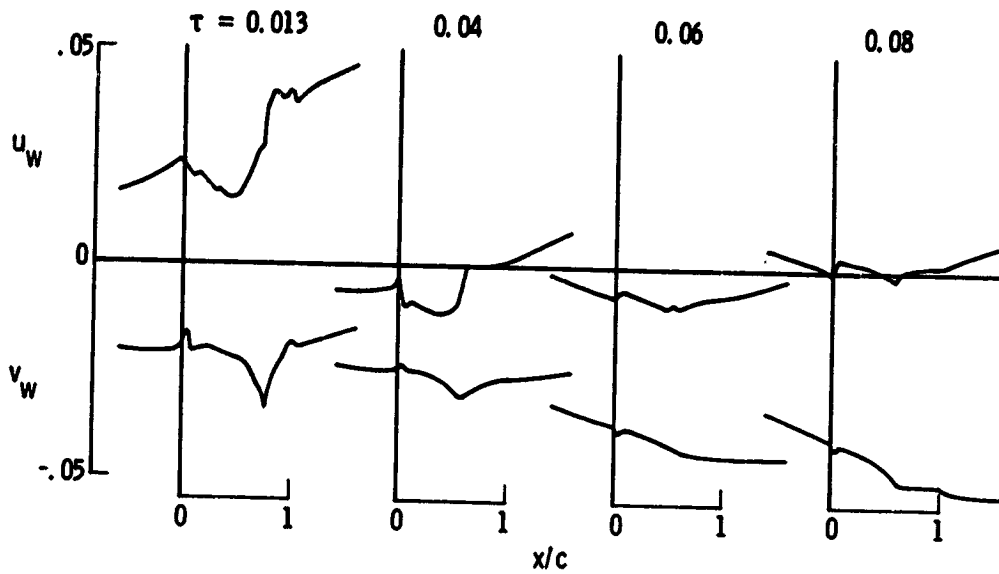


Figure 5.- Effect of wall porosity on wall-induced velocity distribution at tunnel center line; $M = 0.8$; design c_n .

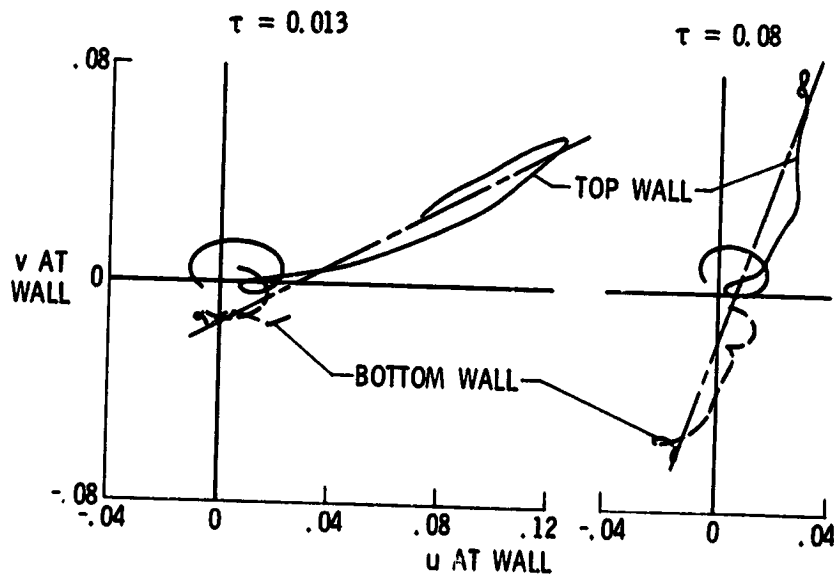


Figure 6.- Illustration of wall calibration during test.

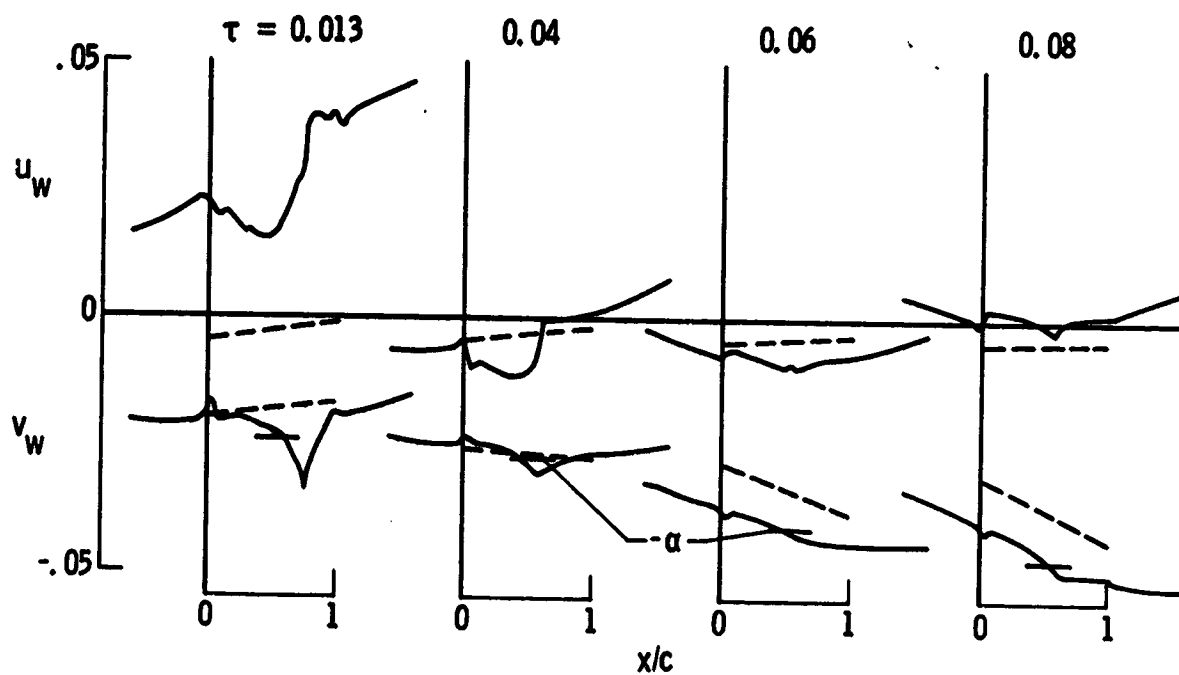


Figure 7.- Comparison of results of present method with predictions by method of reference 4.

RESEARCH ON SELF-CORRECTING WIND TUNNELS*

R. J. Vidal and J. C. Erickson, Jr.
Calspan Corporation

SUMMARY

The Calspan Self-Correcting Wind Tunnel is a two-dimensional facility in which the flow field in the vicinity of the walls is actively controlled, and a theoretical evaluation is used in conjunction with flow-field measurements to confirm that wall interference has been minimized. The facility is described and the results of experiments with a 6% blockage model are presented to show that iterative application of wall control effectively eliminates the interference. Experiments were performed at conditions where the flow at the walls was supercritical, and a new operating procedure is described for these conditions. The results of an analysis of the flow in the auxiliary suction system and test section illustrate the trade-offs available in the design of self-correcting wind tunnel test sections and in model sizing for such tunnels.

INTRODUCTION

A program of research is in progress at the Calspan Corporation to develop a self-correcting wind tunnel and to demonstrate that interference-free flows can be achieved by controlling the flow field in the vicinity of the walls. The concept of a self-correcting, or adaptive-wall, wind tunnel has been described in the literature (refs. 1 and 2). Briefly, it is based on the idea of measuring the components of the disturbance velocity at discrete points along imaginary control surfaces, or interfaces, in the flow field within the tunnel. A theoretical formulation for the flow field external to the control surfaces, including the boundary condition for unconfined flow, i.e., that all disturbances vanish at infinity, is used to determine if those measured velocity components satisfy functional relationships which are consistent with interference-free flow. If they are not, an iteration procedure provides a new approximation for the flow field at the interfaces, and the flow through the tunnel walls is readjusted until the measured quantities are consistent with the boundary condition for unconfined flow. In this way, the best theoretical and experimental features are combined to minimize wall interference. The flow chart for the self-correcting tunnel scheme is shown in

* Research sponsored by the Office of Naval Research and the Air Force Office of Scientific Research under Contract No. N00014-72-C-0102, with supplemental support by the NASA/Langley Research Center; by the ONR and AFOSR under Contract No. N00014-77-C-0052; and by the Arnold Engineering Development Center under Contract No. F40600-76-C-0011.

figure 1.

Experiments have been completed with a two-dimensional airfoil model, which has a solid blockage of 6%, at test conditions where the model flow field was supercritical, but the flow at the walls was subcritical. Those results have been reported (refs. 3 and 4), but are reviewed here to illustrate the wall-interference effects present in conventional tunnels, and to demonstrate that active flow-field control effectively minimizes these effects. Then, the results of our recent experiments, in which the flow at the walls was supercritical, are presented to show that new operating procedures are required which are different from those for subcritical walls. Finally, a brief description is given of an analysis for the flow in the auxiliary suction system and test section. The results of this analysis are discussed with respect to trade-offs which can be made in test section design and model sizing.

SYMBOLS

Values are given in both SI and U.S. Customary Units. The measurements and calculations were made in U.S. Customary Units.

c	airfoil chord length, m (in.)
c_l, c_d, c_m	airfoil section lift, drag, and pitching-moment coefficients
c_p	pressure coefficient
M	Mach number
U	stream velocity, m/sec (ft/sec)
v_n, v_x	normal and streamwise components of disturbance velocity, m/sec (ft/sec)
x	streamwise coordinate with origin at airfoil leading edge, m (in.)
α	airfoil angle of attack
β	$(1-M_\infty^2)^{1/2}$

Subscripts:

c	calculated value
m	measured value
∞	free-stream conditions

THE CALSPAN SELF-CORRECTING WIND TUNNEL

The Calspan 0.30 m (1 ft.) Self-Correcting Wind Tunnel (figs. 2 and 3) is a continuous-flow facility. The test section is two dimensional with porous top and bottom walls of 22.5% open area. The plenum chambers behind the porous walls have been divided into 18 segments, 10 on the top and 8 on the bottom, and each segment is connected to a pressure and a suction source through individual control valves. The pressure source is the tunnel stilling chamber, and the suction source is an auxiliary compressor discharging into the tunnel circuit in the diffuser. Six plenum chambers in the immediate vicinity of the model have provisions for a distributed porosity which can be varied linearly in the streamwise direction.

The model and test section are shown in figure 4. The model is an NACA 0012 airfoil section with a 0.15 m (6 in.) chord (6% solid blockage) and is instrumented with a row of pressure orifices and with a three-component force balance supporting a metric section on the tunnel centerline. The test section instrumentation (fig. 4) consists of two static-pressure pipes, each with 52 pressure orifices, and 18 flow-angle probes, with each probe located above the center of a plenum segment. These sensors are located outside the wall boundary layers and enable us to infer the normal and streamwise components of the disturbance velocity. Further details of the test section, model and instrumentation are given in references 3 and 4.

EXPERIMENTS

The first experiments were performed with the 0.15 m (6 in.) chord model in the Calspan 2.44 m (8 ft.) tunnel (0.75% solid blockage) to acquire a body of data that could be regarded as essentially free from wall interference. These data are presented and analyzed in reference 5.

Initial experiments with the model in the 0.30 m (1 ft.) tunnel were made to simulate tests in a conventional porous-wall facility. This simulation consisted of using wall control to establish a uniform axial pressure distribution in the empty test section. The model was then installed and tested with the same valve settings. The lift, drag and pitching-moment results obtained at $M_{\infty} = 0.725$ are compared with the 2.44 m (8 ft.) tunnel data in figure 5. In general, this comparison shows that there are wall-interference effects on the model forces and moment in this simulation. The effects on lift are moderate and on pitching-moment are large, and each is qualitatively consistent with solid-wall interference for lift coefficients greater than 0.1. The effects on drag are appreciable and indicate open-jet interference for subcritical conditions. If the available porous-wall theoretical and experimental data (refs. 6 and 7) are applied to these cases, they would predict wall

interference equal to about one-fourth the solid-wall interference. The data shown here are contradictory as to open-jet or solid-wall interference, and this probably reflects the fact that it is an oversimplification to attempt to categorize these results within the usual concepts of solid-wall or open-jet interference. The interference includes effects such as changes in the separation point and changes in the shock-wave position at supercritical conditions. This latter effect can be seen in the comparison of airfoil-surface pressure distributions at this Mach number for $\alpha = 2^\circ$ in figure 6.

Iterations for Subcritical Walls

Experiments were performed in the self-correcting mode by iterating with the model at $\alpha = 2^\circ$ and $M_\infty = 0.725$. The method we used to begin the iterations was to estimate the streamwise disturbance velocities at the control surfaces by Prandtl-Glauert theory. The free-stream Mach number is established in the test section, and wall control is then applied to obtain the desired distributions of the streamwise disturbance velocities, i.e., local static pressures. All data then are recorded and used in evaluating the functional relationships to obtain a second approximation. The pressure distribution after this first iterative step is presented in figure 7. It can be seen that the shock wave already is located at its interference-free position, as indicated by comparison with the 2.44 m (8 ft.) tunnel data.

The results of the iteration are shown in figure 5 by the numbered data points, where each number indicates the iterative step. The solid triangle indicates the equivalent data point in the simulated conventional facility. It can be seen that after three iterations we have largely eliminated the wall-interference effects in that the lift and drag agree with the 2.44 m (8 ft.) tunnel data, within the scatter in that data, and the pitching moment agrees to within 5% to 7%. Normally, we would have continued the iterations because the evaluation of the functional relationships did not indicate complete convergence, but we were at the limits of control at one plenum section above the model and could not achieve the next iterative step. Nevertheless, we regard these results, and those obtained at lower Mach numbers and higher angles of attack (refs. 3 and 4), as a convincing demonstration of the concept.

Operating Procedure for Supercritical Walls

Experiments were performed with the 0.15 m (6 in.) chord model in the 0.30 m (1 ft.) tunnel at $M_\infty = 0.85$, $\alpha = 1^\circ$. We followed the same procedure outlined in the previous paragraphs; namely we obtained a theoretical estimate of the flow field at the control surfaces and used that as the first approximation. We established the free-stream Mach number and then applied wall control, beginning at the upstream end of the test section, to obtain the de-

sired distributions of the streamwise disturbance velocities. We were able to establish the desired distributions upstream of the model quarter chord, but could not control the flow downstream of the quarter chord. The resulting flow field is illustrated by the schlieren photograph in figure 8. The pressure data from the model and the static pipes showed that the Mach number downstream of the quarter chord was about 1.3, and that the flow contained multiple shock waves in the remainder of the test section.

We were able to exert the desired flow-field control by modifying our operational procedures. We found that the best technique is to establish control at a Mach number where the walls are subcritical, and then sequentially to increase the Mach number and readjust the wall control until we reach the desired Mach number and distributions of the streamwise disturbance velocities. In this particular case, we established flow-field control by setting the first approximation at $M_{\infty} = 0.80$, increased the Mach number to 0.85, readjusted the wall control to the desired first approximation, and obtained the flow field shown in figure 9. The shock waves are close to the correct position, as evidenced by the 2.44 m (8 ft.) tunnel data, and the walls are supercritical, as evidenced by the shock wave emanating from the flow-angle probe. The data from the static-pressure pipes showed that the Mach number near the wall was about 1.05. We could not iterate at this condition, again, because one of the plenum sections was at its limit of control.

CHARACTERISTICS OF THE AUXILIARY SUCTION SYSTEM

The recurring inability to achieve full control of the flow field at all plenum sections led to an analysis of the flow in the auxiliary suction system and the test section. Details are given in reference 8 and only some highlights and conclusions of the analysis are given here.

Basically, the analysis consists of writing a pressure balance for the auxiliary suction system, which is shown in figure 3. The analysis includes the operating characteristics of the auxiliary compressor, the losses in the pipes, the recompression pressure loss arising from the compressor discharge into the diffuser, the pressure drop across the porous walls, and the required unconfined-flow pressure at the wall locations due to the model. When suitable engineering approximations for these pressure terms are made, using, in part, data measured in the 0.30 m (1 ft.) tunnel, the predicted limits on available control agree reasonably well with experimental observations.

One conclusion from this analysis was that the recompression penalty could be reduced considerably. This could be accomplished by introducing an area change in the tunnel diffuser at the location where the flow from the auxiliary blower is vented into the tunnel circuit. The best arrangement is to generate sonic flow at that location, so that there would be suction on the blower discharge. This area change modification promises a considerable improvement in the circuit performance and has been carried out.

The analysis also illustrates the three major trade-offs available in the design and application of self-correcting wind tunnels with porous walls; namely, compression ratio, porosity, and model size. The results in reference 8 show that the tunnel performance could be improved by increasing the compression ratio from 1.43 to 2.0, but the improvement would be available only at Mach numbers above about 0.75 because the wall perforations would be choked at Mach numbers below that value. That restriction could be relaxed considerably by using a higher porosity, although the shock-wave reflection characteristics may not be as favorable. Decreasing the model size from 6% blockage to a smaller value would decrease the magnitude of the disturbance velocities at the walls and would improve the tunnel performance. The latter alternative, decreasing the model size, has been selected for the Calspan facility and iteration experiments have begun at higher Mach numbers with a model having 4% solid blockage.

CONCLUDING REMARKS

A two-dimensional self-correcting wind tunnel has been built and tested at the Calspan Corporation to demonstrate that wall-interference effects can be minimized by actively controlling the flow in the vicinity of the tunnel walls. Experiments were made with a 6%-blockage airfoil model, using the facility to simulate a conventional wind tunnel, to show that the wall-interference effects can be large in such tunnels. Several cases have been iterated successfully in the self-correcting mode. In one supercritical flow over the airfoil, we iterated three times and were able to reproduce the correct shock position, eliminate wall-interference effects on lift and drag, and decrease them to 5% to 7% on pitching moment. Experiments with supercritical walls showed that it is necessary to establish wall control initially when the flow at the walls is subcritical, and then sequentially to increase the Mach number and readjust the wall control until the desired test condition is achieved. We have devised a method for analyzing the performance of a self-correcting test section with porous walls. This method makes it possible to examine the trade-offs between compression ratio, wall porosity, and model size. It should be a useful tool in future design studies of self-correcting wind tunnels.

REFERENCES

1. Sears, W. R.: Self-Correcting Wind Tunnels (The Sixteenth Lanchester Memorial Lecture). The Aeronautical Journal, vol. 78, no. 758/759, February/March 1974, pp. 80-89.
2. Ferri, A. and Baronti, P.: A Method for Transonic Wind Tunnel Corrections. AIAA Journal, vol. 11, no. 1, January 1973, pp. 63-66.
3. Vidal, R.J., Erickson, J.C., Jr. and Catlin, P.A.: Experiments with a Self-Correcting Wind Tunnel. Paper No. 11, AGARD Conference Proceedings No. 174 on Wind Tunnel Design and Testing Techniques (London, England), 6-8 October 1975.
4. Sears, W. R., Vidal, R.J., Erickson, J.C., Jr. and Ritter, A.: Interference-Free Wind-Tunnel Flows by Adaptive-Wall Technology. Journal of Aircraft, vol. 14, no. 11, November 1977, pp. 1042-1050.
5. Vidal, R.J., Catlin, P.A. and Chudyk, D.W.: Two-Dimensional Subsonic Experiments with an NACA 0012 Airfoil. Calspan Report No. RK-5070-A-3, December 1973.
6. Pindzola, M. and Lo, C.F.: Boundary Interference at Subsonic Speeds in Wind Tunnels with Ventilated Walls. AEDC-TR-68-47, May 1969.
7. Chew, W.L.: Cross-Flow Calibration at Transonic Speeds of Fourteen Perforated Plates with Round Holes and Airflow Parallel to the Plates. AEDC-TR-54-65, July 1955.
8. Vidal, R.J. and Erickson, J.C., Jr.: Experiments on Supercritical Flows in a Self-Correcting Wind Tunnel. AIAA Paper No. 78-788, AIAA 10th Aerodynamic Testing Conference, San Diego, April 19-21, 1978.

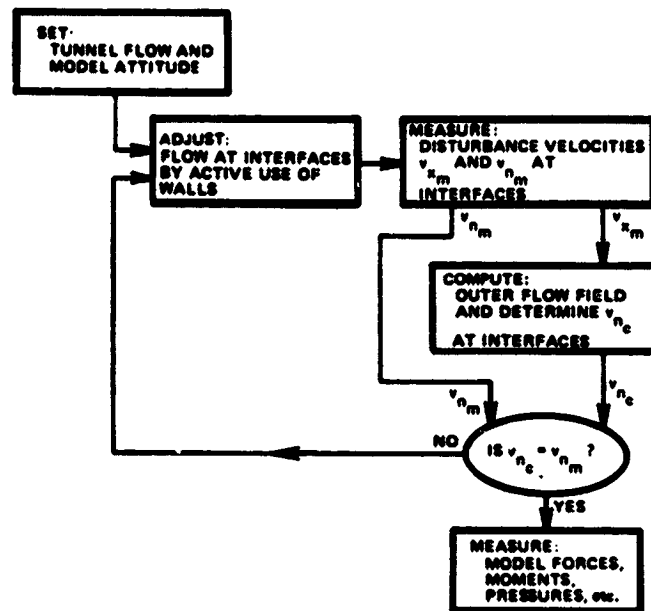


Figure 1.- Self-correcting wind-tunnel scheme.

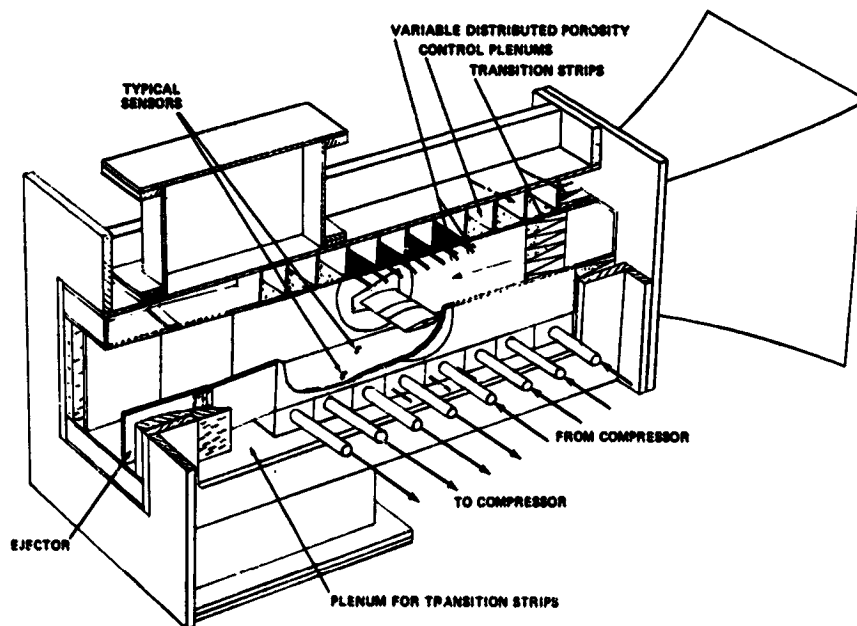


Figure 2.- Cutaway sketch of Calspan two-dimensional self-correcting wind tunnel.

ORIGINAL PAGE IS
OF POOR QUALITY

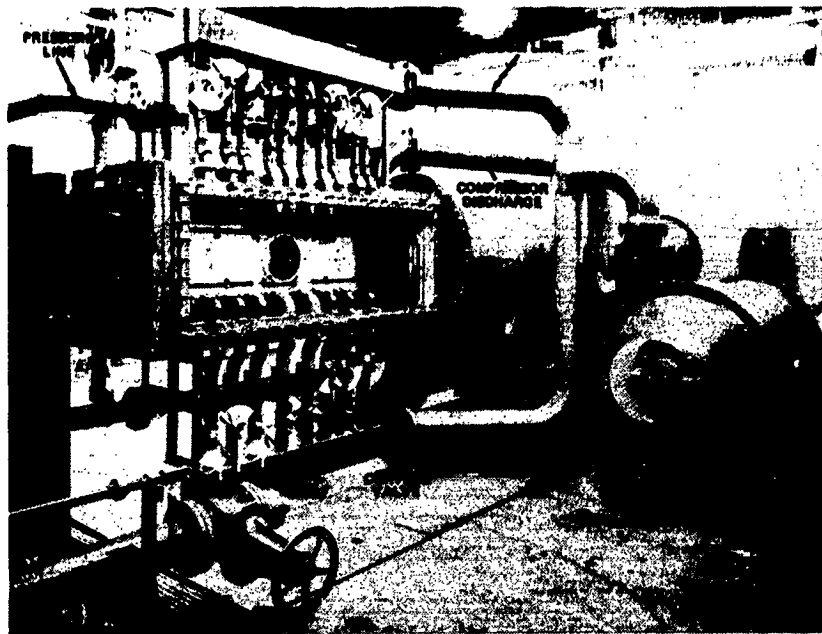


Figure 3.- The Calspan self-correcting wind tunnel.

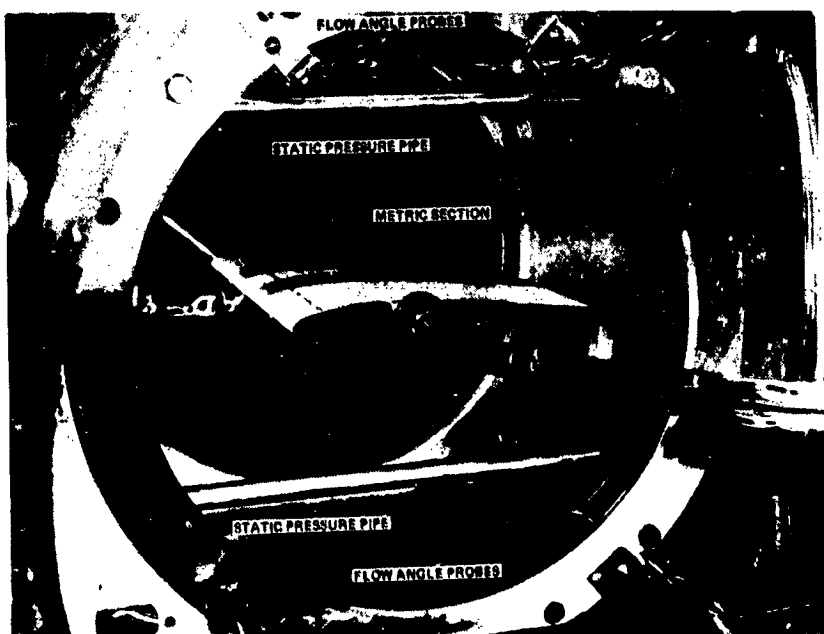


Figure 4.- Test section of the self-correcting wind tunnel.

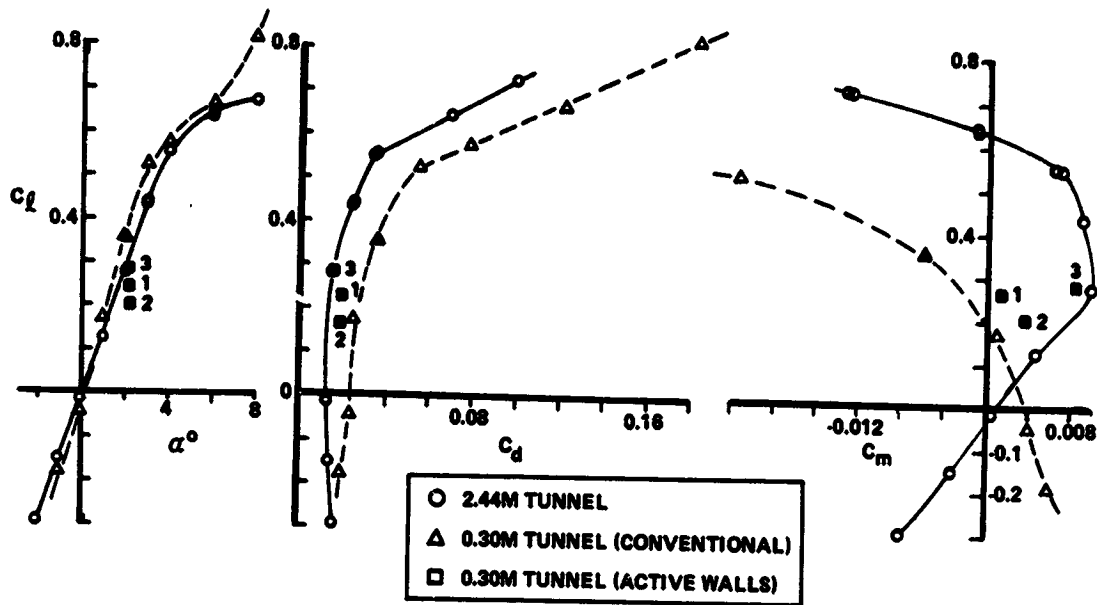


Figure 5.- Wall effects on force data. $M_\infty = 0.725$.

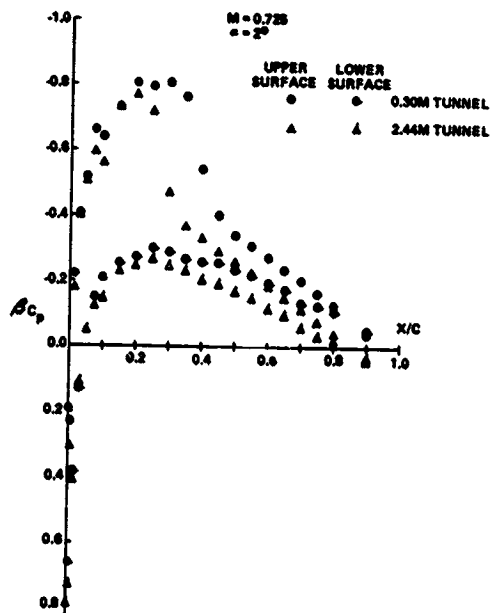
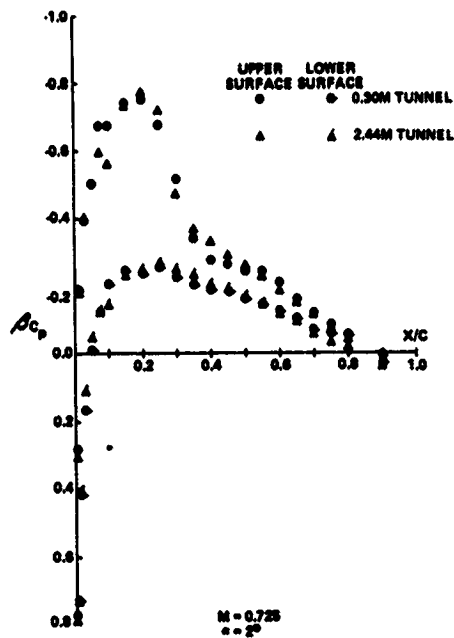


Figure 6.- Simulated conventional wind tunnel.



ORIGINAL PAGE IS
OF POOR QUALITY

Figure 7.- First wall adjustment.

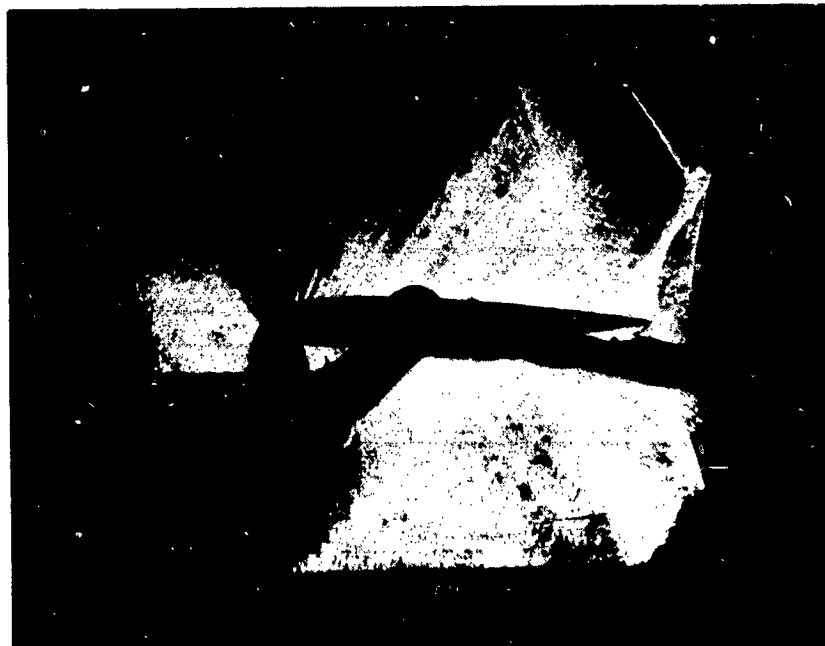


Figure 8.- Schlieren view of the flow field with incorrect wall control.
 $M_\infty = 0.85$; $\alpha = 1^\circ$.



Figure 9.- Schlieren view of the flow field with correct wall control.
 $M_{\infty} = 0.85$; $\alpha = 1^{\circ}$.

ANALYTICAL DESIGN OF A CONTOURED WIND-TUNNEL
LINER FOR SUPERCRITICAL TESTING

Perry A. Newman and E. Clay Anderson*

NASA Langley Research Center

SUMMARY

The present analytical design procedure is being developed in order to determine the shape of a contoured nonporous wind-tunnel liner for use in the Ames 12-foot-pressure-wind-tunnel test of a large-chord, laminar flow control (LFC), swept-wing panel which has a supercritical airfoil section. This procedure is applicable to the two-dimensional streamlined tunnel problem and a first check on its validity would be a comparison of the calculated tunnel-wall shape with that found experimentally. Results for such a comparison are given and the favorable agreement is encouraging.

INTRODUCTION

The analytical design procedure discussed herein is being developed in order to meet the special requirements of a laminar flow control (LFC) test. A transonic test condition is needed in order to establish the compatibility of an active LFC wing suction system with the current high-performance supercritical airfoil technology. This test must be done in a wind tunnel which has low levels of stream turbulence and acoustic noise so that the laminar flow is not unduly disturbed. Conventional slotted- or porous-walled transonic tunnels are, therefore, inappropriate in this regard. Transport aircraft presently envisioned for LFC applications have moderately swept wings; thus, the laminar boundary-layer crossflow stability must be investigated at the appropriate flight crossflow Reynolds number. This requirement, together with the physical-size limitations set by slot/duct construction and the required roughness-height Reynolds number for laminar flow, results in a large-chord, swept-wing panel. In order to produce a transonic wind-tunnel flow which simulates free-air flow about an infinite yawed wing, one must contour all the nonporous bounding walls. The ratio of total tunnel height to chord for this test is about 1 for the Ames 12-foot pressure wind-tunnel.

The design procedure is based on a simple idea and several existing computational tools which make it feasible. Basically, one determines bounding streamlines in the desired flow, makes all required blockage corrections, and

*E. Clay Anderson, a consultant, has performed the boundary-layer analyses for this study under NASA contract NAS1-14517.

then builds the resulting contoured nonporous tunnel liner. At supercritical flow conditions, one must use an appropriate transonic analysis in order to determine the desired flow-field and bounding streamlines. In order to account for the blockage due to viscous effects on the liner, a boundary-layer analysis must be made along the bounding streamlines with (local) edge conditions determined by the local flow properties. The bounding streamlines are then displaced to relieve the viscous blockage. This displaced shape is the geometric nonporous contour to be built. The liner is restricted to a given airfoil configuration at a single design-point condition. Currently available two-dimensional transonic analysis codes (refs. 1 and 2) and a laminar-turbulent boundary-layer code (ref. 3) have been used. The procedure, however, has a general utility which is restricted by our current ability to calculate the viscous transonic flow field about arbitrary configurations.

This design procedure is, of course, directly applicable to the two-dimensional streamlined tunnel problem. One should be able to predict the tunnel-wall shape required to simulate free-air flow about an airfoil. A first check of its validity is provided by a direct comparison of the analytically determined tunnel wall shape with one determined experimentally in a streamlined tunnel experiment. Barnwell and Everhart¹ have recently completed such an experiment for a symmetric airfoil at zero lift in the Langley 6- by 19-inch transonic tunnel. In that test, the slotted walls of the tunnel were replaced by nonporous flexible plates which were adjusted using an experimental/analytical procedure until a simulated free-air flow over the airfoil section was obtained. Thus, the tunnel-wall displacement required to produce equivalent free-air flow is determined as a result of the experiment. Their iterative experimental/analytical technique is similar to that presented by Goodyer (ref. 4).

This paper should be viewed as a progress report in the continuing development of the design procedure for the LFC swept-wing test application. Some (preliminary) test-section contours which were generated to check the numerical procedure are given in the next section. The following section summarizes an application for a two-dimensional streamlined tunnel experiment and compares present analytical predictions and experimental results for tunnel-wall shapes.

SYMBOLS

c	airfoil chord length, cm (inch)
M_{∞}	free-stream Mach number

¹A streamlining procedure (unpublished) has been developed by Richard W. Barnwell and Joel L. Everhart of Langley Research Center. The present analytical results are compared with the wall shape experimentally determined by this procedure.

- $N_{Re,\infty}$ free-stream Reynolds number based on airfoil chord
- x streamwise tunnel coordinate measured from test section origin indicated (\oplus) in figure 4, cm (inch)
- y lateral tunnel coordinate normal to tunnel span, measured from test section origin indicated (\oplus) in figure 4, cm (inch)
- α angle of attack, deg
- $\delta^*(x,y)$ local boundary-layer displacement-thickness correction, measured normal to tunnel wall, cm (inch)

LFC SWEEP-WING PANEL TEST LINER

Current plans for the LFC swept-wing panel test are to utilize the Ames 12-foot pressure wind-tunnel to test a large-chord model, which has a cambered supercritical airfoil section, at lift. Recall (as shown in fig. 1) that for flow over a lifting yawed wing the streamline which divides around the leading edge of the airfoil develops a different spanwise displacement on the two wing surfaces. The resulting displacement at the trailing edge persists downstream and one must contour the end walls to properly simulate the inviscid crossflow.

The LFC airfoil section design and its aerodynamic characteristics are for a given set of wing-normal conditions. (See ref. 5, for example.) However, as indicated in the last section, considerations of crossflow Reynolds number, unit Reynolds number, and slot/duct construction bear on the selection of a model chord length and test conditions. These are certainly not independent of the tunnel operating characteristics and it appears that the required conditions may well be near the tunnel power limitations. All of these aspects result in a ratio of tunnel height to chord of approximately 1. The contraction ratio of the tunnel is 25 to 1 and an appreciable increase could easily result in unsatisfactory diffuser performance. A liner of "octagonal" cross-section results in less additional contraction from the existing circular cross-section than would result from a "rectangular" liner. Figure 2 is a view of the tunnel showing an "octagonal" cross-section liner and the large-chord swept-wing panel.

All walls are contoured in order to simulate free-air flow about an infinite-aspect-ratio yawed wing at the design condition. A preliminary design of an "octagonal" liner shape has been made, considering only the inviscid streamline shapes, in order to check the numerical procedure. This was done using an early LFC supercritical airfoil design of chord length 2.44 m (8 feet), swept 35° , at a tunnel Mach number of 0.89. Schematic views of this contoured liner shape near the LFC model are shown in figure 3. The section views clearly show the development of the end-wall steps which persist downstream of the trailing edge. It is also seen that some of the streamlines fall outside the existing tunnel in places for this first try. A turbulent boundary layer will exist on all tunnel walls and the local viscous blockage correction for it has not been included in this shape. This correction will move the liner even

further outside the existing tunnel in places. The sizing will be done iteratively in order to minimize the additional contraction. Section D-D in figure 3 shows the distorted flow which will have to be reshaped by a transition section in the liner in order to fair into the existing diffuser. This fairing will be shaped to minimize the degradation of the existing tunnel performance.

2-D STREAMLINED TUNNEL WALL SHAPE

The liner design procedure being developed for the LFC swept-wing test is applicable to the prediction of wall shapes for two-dimensional streamlined tunnels. Details concerning application of the present approach to a two-dimensional tunnel are given in reference 6. The results from that study are summarized in this section.

In the Barnwell-Everhart experiment the slotted lateral walls in the Langley 6- by 19-inch transonic tunnel were replaced by nonporous flexible walls (as indicated in fig. 4) in order to investigate the streamlined tunnel concept for minimizing wall interference in transonic tests. Basically, their experimental/analytical procedure iterates on the contoured-wall shape until consistency is obtained between near-field and far-field solutions. The wind tunnel determines the near-field solution for a given wall shape (i.e., experimentally "solves" a direct, viscous, boundary-value problem). The inverse far-field solution corresponding to uniform parallel flow at infinity is determined numerically using the experimental wall pressures as input data to predict a new wall shape. Thus, the tunnel-wall shape is determined as a result of the experiment. Their procedure has been used to find the wall shape for only one model and test condition. However, the first step in their procedure is to determine a wall shape which produces uniform pressures in the test section for the empty tunnel (i.e., no model).

For the empty tunnel the lateral wall shape required to produce uniform test-section pressures is a weighted relative (differential) δ^* correction due to all of the tunnel wall boundary layers. That is, the local δ^* (x,y), minus that at the upstream flexible-wall/rigid-wall junction, is integrated around the perimeter of the tunnel cross section to obtain a local area correction which is then applied at the two adjustable walls. Comparison of the analytically determined wall shape and that found experimentally by Barnwell and Everhart is shown in figure 5. The tunnel was operating at a Mach number of 0.902 and a unit Reynolds number of $2.24 \times 10^5/\text{cm}$ (3.41×10^6 based on model chord). The maximum difference in the wall shapes is not inconsistent with the pressure measurement accuracies. (See ref. 6.)

The model test was conducted at a Mach number of 0.765 using a 15.24-cm (6-inch) chord symmetric NACA 0012 airfoil section at zero lift. This size model results in a ratio of tunnel height to chord of approximately 3. There is a turbulent boundary layer on all of the walls and the model. As indicated in figure 4, only the narrow lateral tunnel walls were flexible and these were deformed to simulate free-air flow about the model at one condition. The model is centered at the location (\oplus) indicated in figure 4; this is taken to be the origin for streamwise and lateral coordinates in what follows. Each flexible

wall is supported by 11 adjustable screw jacks which are located 10.16 cm (4 inches) apart. The streamwise extent of the flexible-walled section is from 4.333 chords upstream of the leading edge to 2.833 chords downstream of the trailing edge.

Calculations were made along 48 free-air streamlines about the NACA 0012 airfoil in order to estimate the tunnel-wall boundary layer in the presence of the model. Boundary-layer displacement-thickness distributions across the tunnel rigid walls (at several streamwise locations) are shown in figure 6. These clearly show a significant local influence due to the pressure field of the airfoil. Note that the y/c axis is located at a value of $\delta^*/c = 0.014$ on all plots; the maximum value of δ^*/c (shown on the last curve in fig. 6(a)) is 0.03. At the lateral wall (largest y/c shown) the displacement thickness exhibits a monotonic increasing behavior. However, along streamlines near the airfoil surface, δ^*/c undergoes very rapid streamwise changes. There is a pronounced local boundary-layer thickening near the leading and trailing edges of the model with a thinning near the expansion peak just downstream of the leading edge. The distribution in the wake region may not be very realistic since the wake is not properly modeled in the transonic airfoil program.

The flexible wall shape is determined as the sum of the deflection of the outermost lateral streamline (i.e., the inviscid compressible blockage correction) and the viscous correction due to the local boundary-layer displacement thickness on all walls (i.e., flexible and rigid). The method for determining this latter δ^* correction was indicated when discussing the empty tunnel results. Comparisons of analytical and experimental flexible wall shapes are shown in figure 7. The agreement is seen to be very good. The outermost lateral inviscid streamline is shown as a dashed line so that the relative contributions to the wall displacement can be seen. The viscous wall effect is not small; the boundary layer on the rigid wall near the model produces a rapid streamwise variation in blockage which must be accounted for in the flexible wall. One must have sufficient resolution in the wall control at lateral regions around the model in order to accommodate this behavior.

CONCLUDING REMARKS

The present design procedure has a general utility which is restricted by our current ability to calculate transonic flow about arbitrary configurations including a proper account of the viscous phenomena. However, continuing rapid advances in computational machinery and methods will allow for better numerical modeling of these aspects. Comparisons with the Barnwell-Everhart streamlined tunnel experiment provide some degree of verification of the numerical design procedure which is being developed for the LFC application. These comparisons demonstrate that the blockage due to the viscous-boundary layer on the rigid (side) wall cannot be neglected in tunnel streamlining. In fact, it is primarily this wall boundary layer near the model which responds to the pressure field of the model and produces the rapidly varying streamwise character in the lateral wall shape. For more severe conditions of transonic flow with strong shockwaves and high lift, it is felt that the local rigid-(side-) wall boundary-layer effects will distort the test so that the desired

simulation is not achieved (i.e., 2-D flow will not be achieved in the tunnel). The present design procedure contains an option for direct calculation of suction rate distributions required to maintain attached boundary-layer flow. This option provides a means for determining suction requirements needed for boundary-layer control near the model/liner junction.

REFERENCES

1. Bauer, F.; Garabedian, P.; Korn, D.; and Jameson, A.: Supercritical Wing Sections II. Springer-Verlag, New York, 1975.
2. Carlson, Leland A.: TRANDES: A Fortran Program for Transonic Airfoil Analysis or Design. NASA CR-2821, 1977.
3. Anderson, E. C.; and Lewis, C. H.: Laminar or Turbulent Boundary-Layer Flows of Perfect Gases or Reacting Gas Mixtures in Chemical Equilibrium. NASA CR-1893, 1971.
4. Goodyer, M. J.: The Self-Streamlining Wind Tunnel. NASA TM X-72699, 1975.
5. Allison, Dennis O.; and Dagenhart, John R.: Design of a Laminar-Flow-Control Supercritical Airfoil for a Swept Wing. CTOL Transport Technology - 1978, NASA CP-2036, Pt. I, 1978, pp. 395-408.
6. Newman, Perry A.; and Anderson, E. Clay; Numerical Design of Streamlined Tunnel Walls for a Two-Dimensional Transonic Test. NASA TM-78641, 1978.

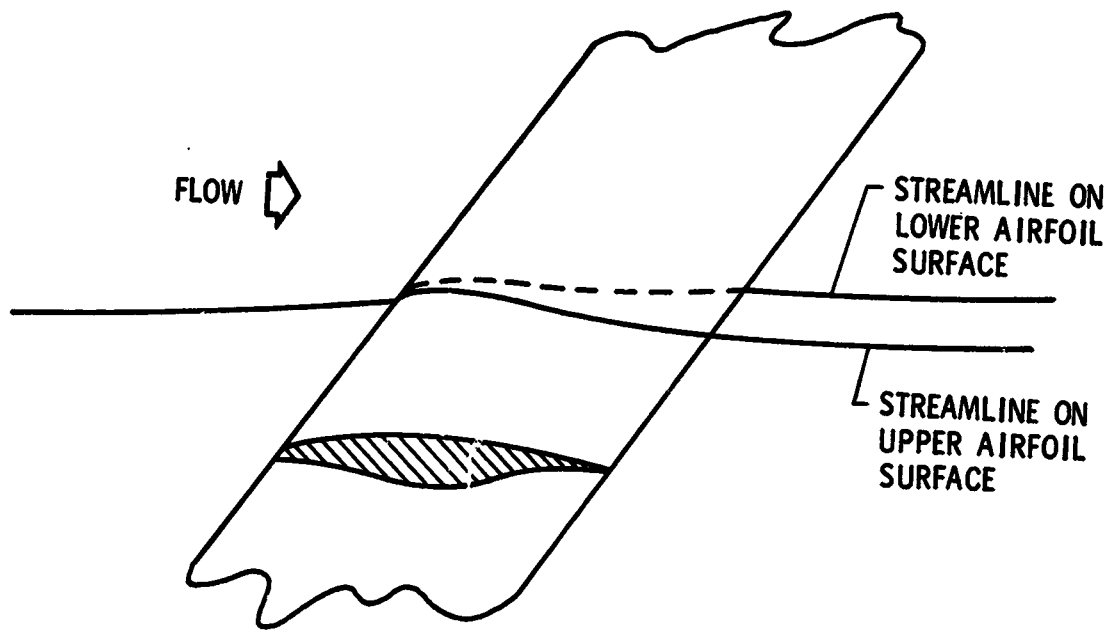


Figure 1.- Spanwise streamline displacement in lifting flow over a yawed wing.

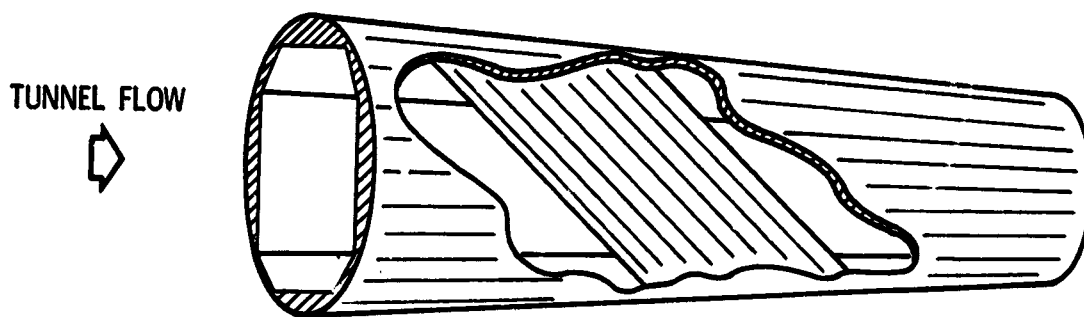


Figure 2.- View of the Ames 12-foot pressure wind tunnel showing "octagonal" test-section liner and large-chord swept-wing panel for LFC test.

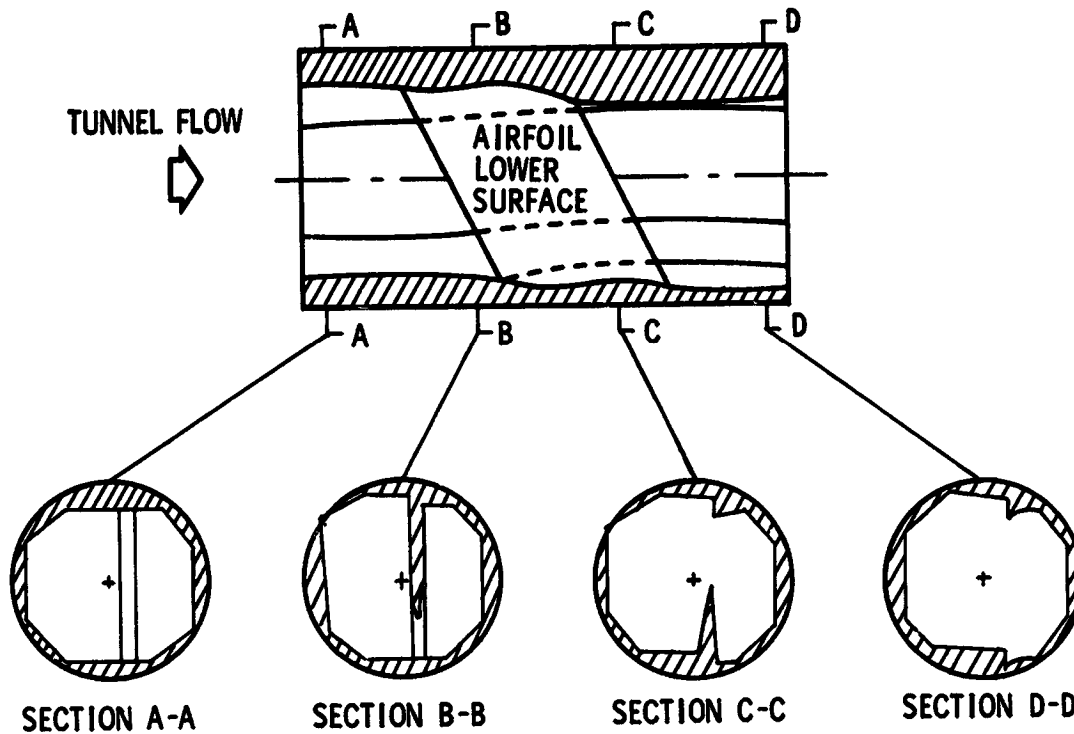
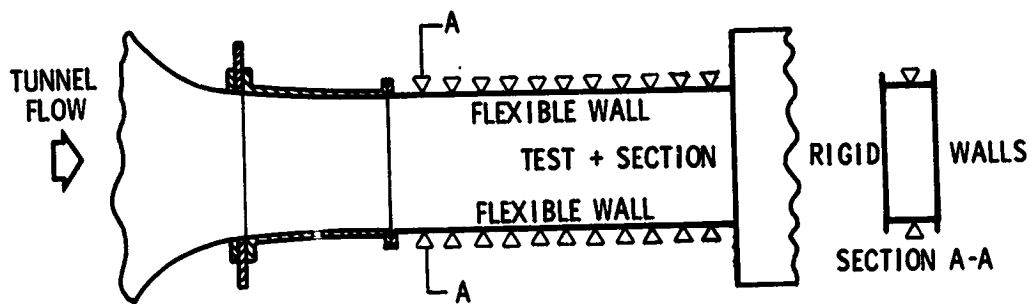


Figure 3.- Schematic view of test-section liner for an LFC model in the Ames 12-foot pressure wind tunnel. Liner was contoured for a preliminary LFC section neglecting viscous wall effects.



▽ DENOTES WALL JACK LOCATION

Figure 4.- Schematic of two-dimensional streamlined tunnel (Langley 6- by 19-inch transonic tunnel) used by Barnwell and Everhart.

$$M_\infty = 0.90, N_{Re, \infty} = 3.41 \times 10^6$$

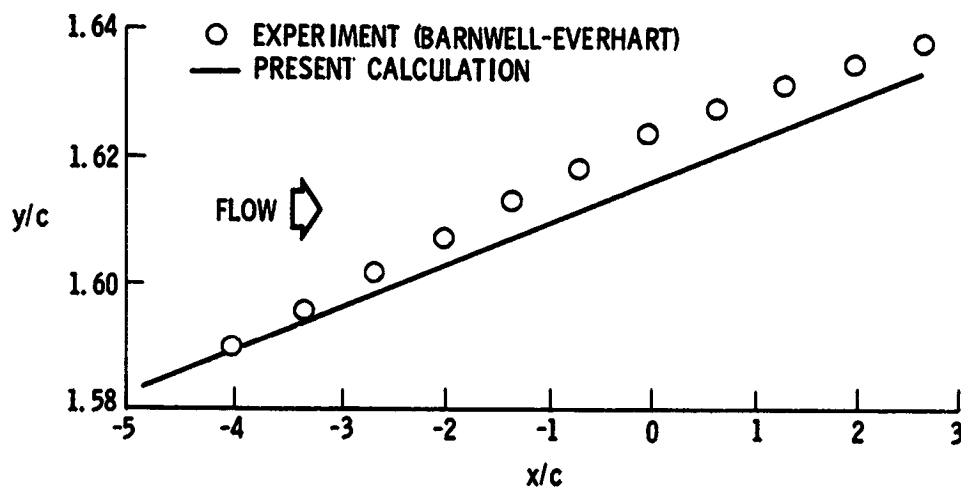
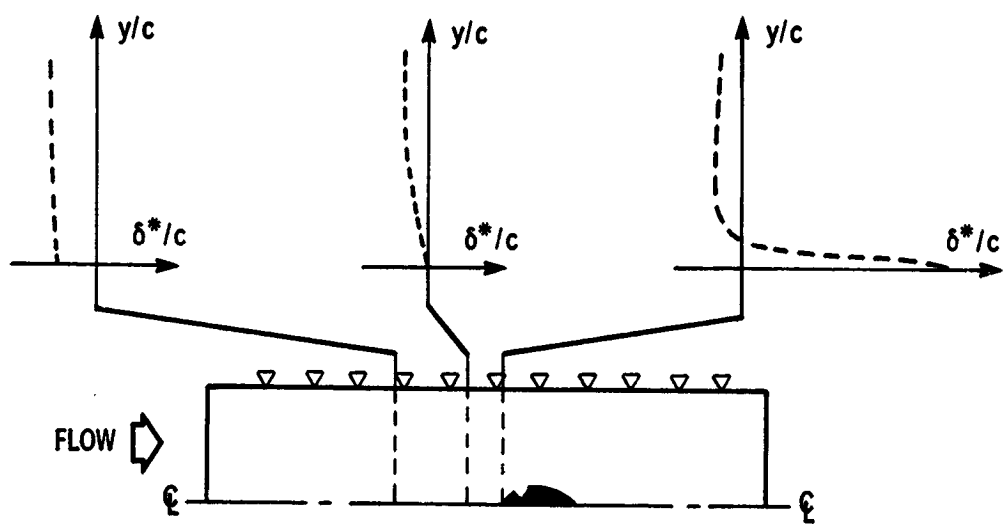
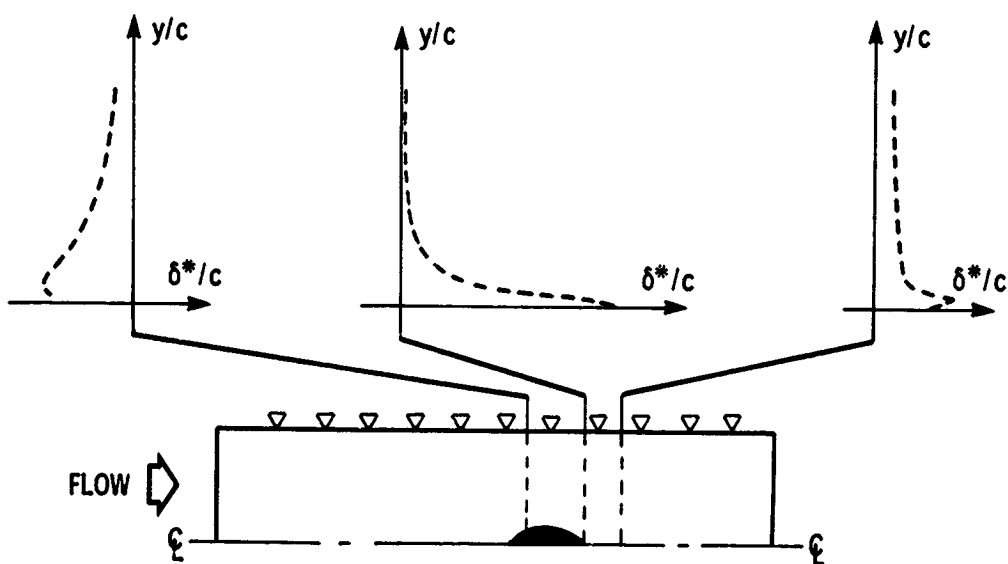


Figure 5.- Comparison of flexible nonporous wall shapes required to produce uniform parallel flow in the Langley 6- by 19-inch transonic tunnel.



(a) Upstream of model.



(b) At and downstream of model.

Figure 6.- Calculated distribution of boundary-layer displacement thickness δ^*/c across the tunnel rigid wall.

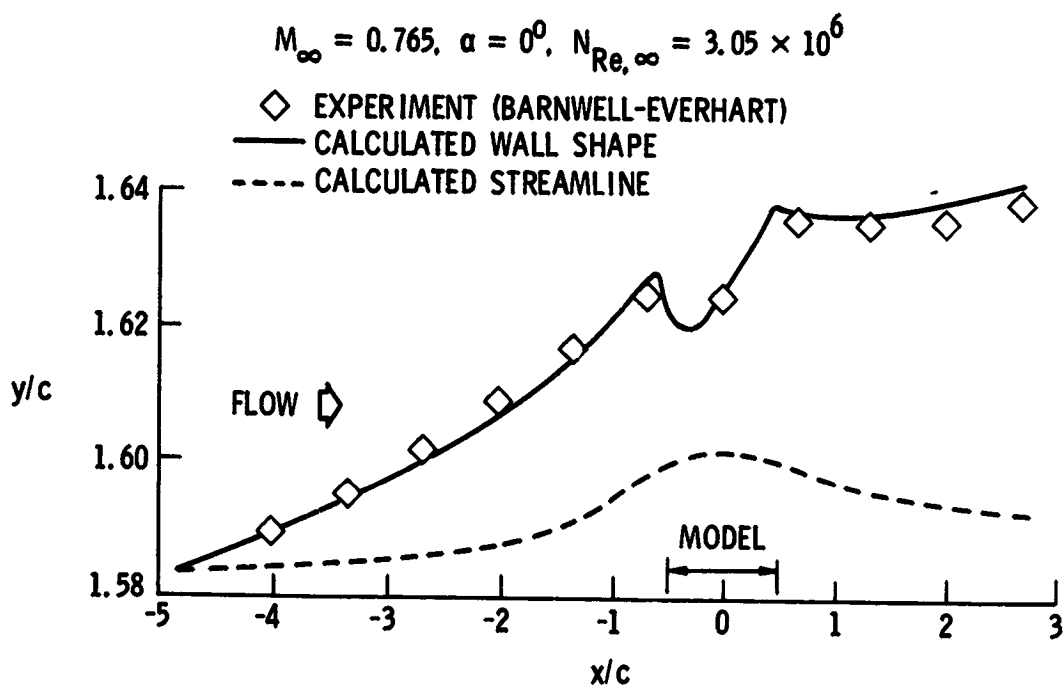


Figure 7.- Comparison of flexible nonporous wall shapes for an NACA 0012 airfoil test at zero lift in the Langley 6- by 19-inch transonic tunnel.

PRECEDING PAGE BLANK NOT FILMED

34

EVALUATION OF INTERFERENCE IN THE OSU
6 IN. BY 22 IN. TRANSONIC AIRFOIL TUNNELJohn D. Lee
The Aeronautical and Astronautical Research Laboratory
The Ohio State University

PRECEDING PAGE BLANK NOT FILMED

SUMMARY

Interference in a 6 in. by 22 in. "two-dimensional" wind tunnel has been evaluated at Mach numbers up to 1.06 by comparing pressure distributions from airfoil models of differing size. Models of the NACA 0012 profile having chords of 76, 152, and 305 mm were used in one phase of the evaluation program and models of a supercritical profile having chords of 76 and 152 mm were used in another. This report documents the confinement interference, i.e., blockage, downwash and streamline curvature, all of which are quite small on a model having a chord of 152 mm and which can, for most applications, be ignored. Specifically the corrections are lumped into an attack angle adjustment of -0.16 degrees per unit lift coefficient on a 152 mm model.

INTRODUCTION

The interpretation of wind tunnel data in terms of equivalent "free-air" information has always been hindered by considerations of the constraints of the boundaries. For some situations, theoretical analyses, moderated by experience have yielded suitable correction procedures. In the transonic range two features have led to serious difficulties: (a) the use of ventilated walls introduced peculiar constraints which are not yet properly understood and (b) local shock waves interacting with the boundary layers on the tunnel walls will often disrupt those layers and produce extensive lateral disturbances. For the past 25 years in which tests have been conducted in the transonic range, there has been a multitude of innovations but there is yet no simple, direct procedure by which valid "free-air" data may be acquired from a ground test facility other than by using models which are relatively small in a given facility.

Due to peculiarities in design and operation, each facility has interference effects which are unlike those in another, with the result that procedures for testing and for modifying the data in one facility will not, in general, apply to another facility. It is necessary to examine three areas: the facility design, the data acquisition technique and the procedure for determining the nature and degree of wall interference, in order to adjust the data to equivalent "free-air" information.

The OSU airfoil tunnel was designed for the specific task of airfoil testing and its configuration was based upon previous research with three other transonic tunnels. A wide variety of airfoils has been tested to date and a series of careful programs has been conducted to define and evaluate interference of all types. This paper describes results from tests utilizing models of the NACA 0012 profile to define the interference from the confining boundaries, i.e. the ventilated walls. A similar evaluation program was conducted using an "aft-loaded" or "supercritical" profile to support the results with the 0012 model. The program was based on the premise that final reduced and/or "corrected" data from similar models differing in chord by factors of two and four must agree with each other. As a further test, such data must also agree with theory, to an acceptable degree, and with data from other facilities which were relatively much larger in comparison to the model size.

The symbols are defined in an appendix.

THE 6" X 22" WIND TUNNEL SYSTEM

A schematic of the 6" x 22" airfoil wind tunnel is shown in figure 1. The dimensions of the test section are 6" x 22" x 44" long in a two-dimensional configuration; i.e., the two 22" side walls are solid while the 6" walls are perforated with a porosity of about 7% and overlie individual plenum chambers. The plenums are open to the mixing zone downstream of the test section and thus can respond individually to pressure changes caused by models in the test section. This isolated plenum configuration leads to the extremely low interference as indicated by experimental data for two-dimensional airfoils over a wide range of operating conditions and model attitudes.

Models are mounted in the test section between two ports in the 22" side walls midway in the test section, and the angle of attack of the airfoil can be varied by rotating the ports. The nozzle consists of two solid aluminum blocks machined to coordinates specifying continuous first and second derivatives vanishing at the nozzle exit. A pressure drop device and a two-staged bellmouth from the screened settling chamber with a contraction ratio of 15:1 are used to maximize flow uniformity.

Test section Mach number is fixed by a choke consisting of an array of bars across the flow downstream from the induction/mixing zone. The Mach number can be varied by changing the number and/or the diameter of the bars. With a typical model installed, the Mach number can be varied from 0.3 to 1.1 with a tolerance of ± 0.001 . The Reynolds number can be varied by changing the total pressure in the stagnation chamber providing a range in Re/m from 1 to 100 million at a fixed Mach number if desired. This particular feature is extremely important in studying the Mach/Reynolds number effects on two-dimensional airfoils. The facility operating envelope is given in figure 2.

The tunnel is operated by pre-setting the control valve (fig. 1) to achieve the desired reservoir pressure. The plug valve is opened and the circuit pressurizes in a few seconds. Thereafter, the pressure drops in proportion to the

mass flow from the storage tanks. The storage system provides 140 cubic meters of air at pressures up to $18 \times 10^6 \text{ N/m}^2$. Conventional air driers and oil separators are used to maintain a very high purity of the airflow.

Figure 3 shows the pressure history for the facility during a typical test run. Data are normally taken immediately after the pressure peak when a period of nearly constant pressure is available. For the conditions of figure 3, tunnel shutdown was delayed for purposes of evaluating the response of the overall system, where the good uniformity of pressure ratio is evident.

Calibration

The basic characteristics of the tunnel were determined by means of static pressure distributions through the test section. The calibration of the tunnel was based upon the average of seven static pressures at the model-mounting site (with no model present) referred to the plenum pressure. Calibration tests were also performed with one plenum vented in order to evaluate the effects of the small unbalance which occurs when testing with a lifting model.

The validity of applying such an "empty-tunnel" calibration when a model is installed is based on the assumption that the plenums, through the perforated boundaries, supply the necessary environment to simulate the far-field. The assumption has been verified by the correlations of the data.

Data Acquisition and Processing

Steady-state pressure measurements are made with a Scanivalve and a trapped-volume system. Tubes from model and tunnel taps are ducted to a Scanivalve system, consisting of a set of valves (basically rotary guillotines) preceding a regular Scanivalve. At the data point, the valves are closed, thus trapping samples of all the pressures at the same tunnel operating pressure. The pressures are subsequently read through the Scanivalve as the tunnel is shutting down. Due to the small but finite volume in the transducer cavity, adjustments to the raw data are necessary to account for pressure differences as the Scanivalve is cycled between ports. This is accomplished with simple calibration procedures, during which the Scanivalve is cycled two or more times. The multi-cycle calibration is frequently repeated during a test program as a cross check on the system and for detection of leaks.

Data taken during the run as well as those from the Scanivalve are digitized and stored on magnetic tape in the Digital Computational Facility of the Aeronautical and Astronautical Research Laboratory. The data is reduced to coefficient form, reviewed on a CRT display, then integrated to lift and pitching moment coefficients, printed and plotted in hard copy form in five minutes from the run.

The wake is traversed by a motor-driven pitot probe, 25 cm downstream from the trailing edge, and the pressure recorded as a continuous trace of deficit from the stagnation pressure. Again, this datum is stored during the run cycle,

to be evaluated by "quick-look" on the CRT before proceeding to the next test point. Such profiles are then reduced and integrated to drag coefficients.

Models

Pressure models as used in this study were fabricated from solid brass on a computer-controlled milling machine using a minimum of 600 coordinate sets. Pressure taps are incorporated by blind drilling so that the surface is not marred by inlaying tubes, and then the terminal tubes are soldered or epoxyed into the ends of the model. Typical models are shown in figure 4 while figure 5 shows a model in the test section with taps connected to Scanivalve system.

INTERFERENCE EVALUATION

I. Flow Quality

The basic characteristics of the flow field were determined by means of static pressure measurements through the test section; two such sets of data are given in figure 6.

The flow quality at different Mach numbers and a verification of the calibration procedure may be deduced from data such as those presented in figures 7 and 8. For such purposes the 0012 model may be regarded as a probe. It should be noted that a relatively small error in Mach number will shift the data out of agreement.

II. Blockage

Figures 9(a) and 9(b) show measurements from the 0012 profile at zero attack-angle. The scale of C_p has been expanded to clarify the small differences between the three models. Note that the data (from the 12-inch model) is in the direction to be expected from boundary "openness".

III. Lift Interference

The low level of interference in the 6 in. by 22 in. airfoil tunnel has been documented by means of data from the three models of the 0012 profile and from two models of a supercritical (aft-loaded) section both tested over wide ranges in Mach number and attack angle. Interference may be deduced by comparisons of the data between models with data from other facilities and with theoretical predictions (including viscous effects). (See ref. 1.) Only a few examples are presented here in figures 10 through 13. Such comparisons lead to the conclusion that the interference on a 152 mm model is negligibly small over the full range of Mach number and, in fact, is quite small even on a model of 305 mm chord in subcritical flows.

A considerable number of data were used to determine the interference field in some detail. For example, the load differences plotted in figure 14 indicated that the interference could be separated into its components due to downwash and to streamline curvature. Further data were used to establish the dependence of both components on the lift coefficient and on the square of the chord-to-height ratio. The interference field could then be expressed in general form as given by figure 15. It should be noted that the scales of figures 14 and 15 are higher expanded for analytical purposes.

Results from the supercritical models were essentially similar to those from the models of the O012. Figure 15 also shows that the chordwise interference load on the supercritical section was the same as that found on the O012.

For comparison purposes, the lift interference integrates to a correction on the attack angle of -0.16° per unit lift coefficient on a model having a chord of 152 mm.

CONCLUDING REMARKS

Interference generated by the proximity of the walls in the 6 in. by 22 in. airfoil tunnel has been evaluated as extremely small by means of data from three models of the NACA O012 profile and from two models of a supercritical section. Using a 152 mm model chord for reference, the net lift interference may be expressed as an attack angle error of -0.16° per unit lift coefficient and the blockage as negligible.

APPENDIX

SYMBOLS

C	model chord length (cm)
C_l	lift coefficient
C_p	pressure coefficient
h	wind-tunnel height
M	Mach number
p	pressure
p_o	stagnation pressure
p_∞	free-stream static pressure
p_c	pressure in plenum of wind tunnel
Re	Reynolds number
X	chordwise distance on airfoil (cm)
α	angle of attack (degrees)
δC_p	airfoil loading (C_p (lower surface)) - (C_p (upper surface))
$\Delta\alpha_{DW}$	angle of downwash induced by wind-tunnel interference (degrees)
$\Delta C_{l_{sc}}$	coefficient of lift from streamline curvature induced by wind-tunnel interference

REFERENCE

1. Vidal, R. J.; Catlin, P. A.; and Chudyk, D. W.: Two-Dimensional Subsonic Experiments With a NACA 0012 Airfoil. CALSPAN Rep. No. RK-5070-A-3, Dec. 1973.

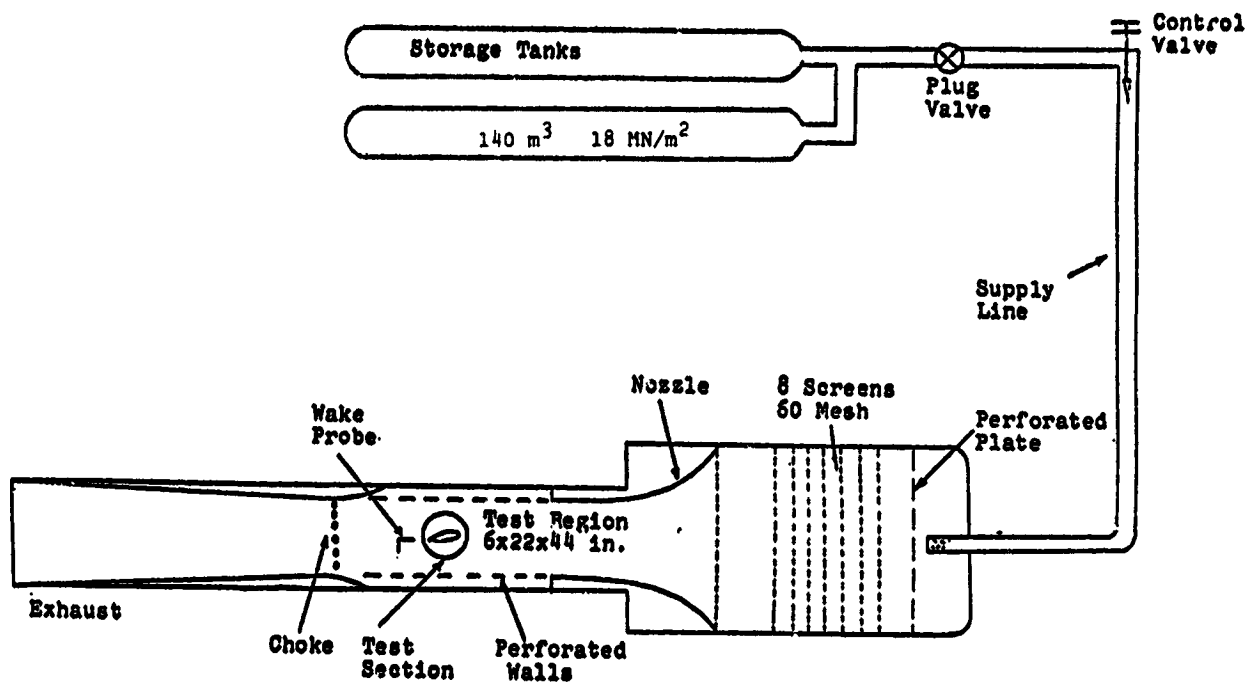


Figure 1.- Schematic layout of the 6 in. by 22 in. transonic airfoil tunnel system.

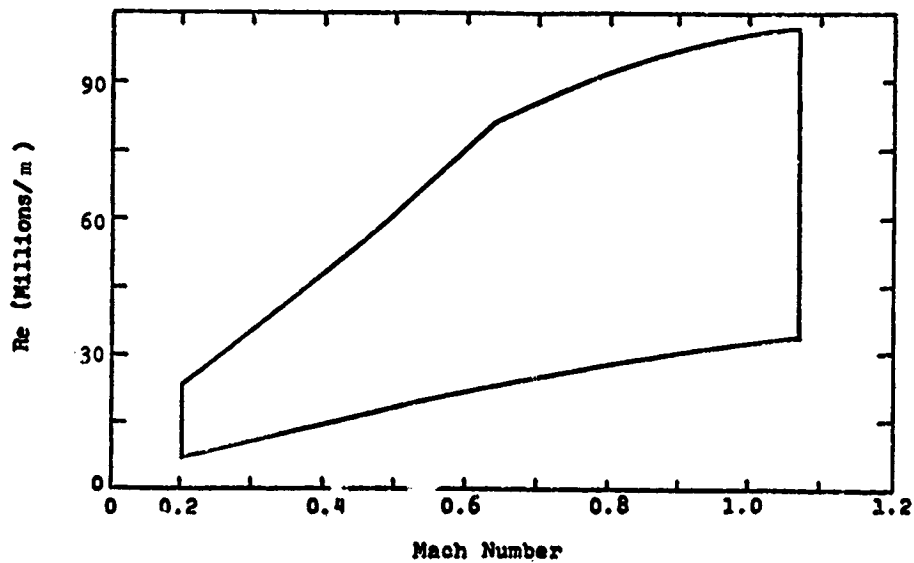


Figure 2.- Operating envelope for the 6 in. by 22 in. transonic tunnel.

ORIGINAL PAGE IS
OF POOR QUALITY

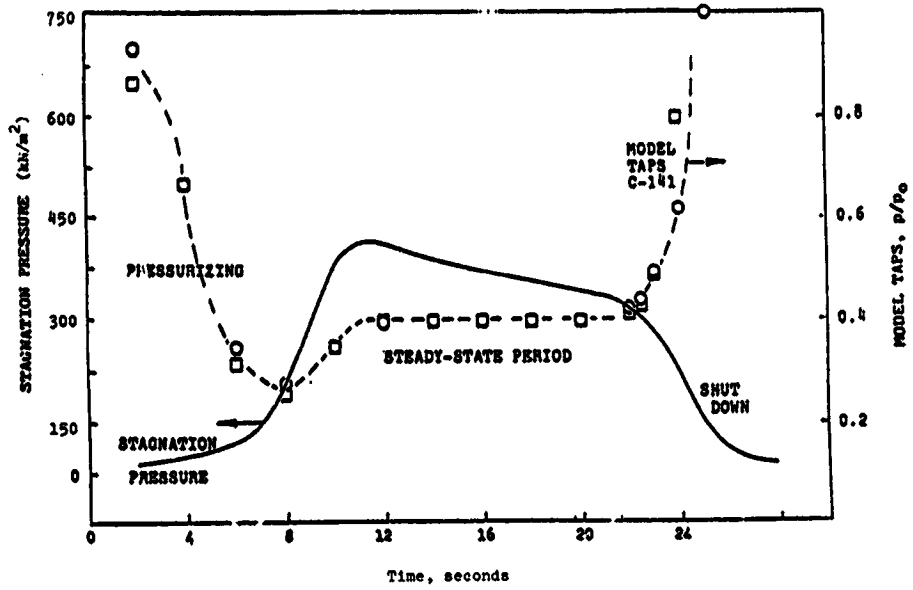


Figure 3.- Pressure-time history in a typical test.



Figure 4.- Some typical airfoil models.

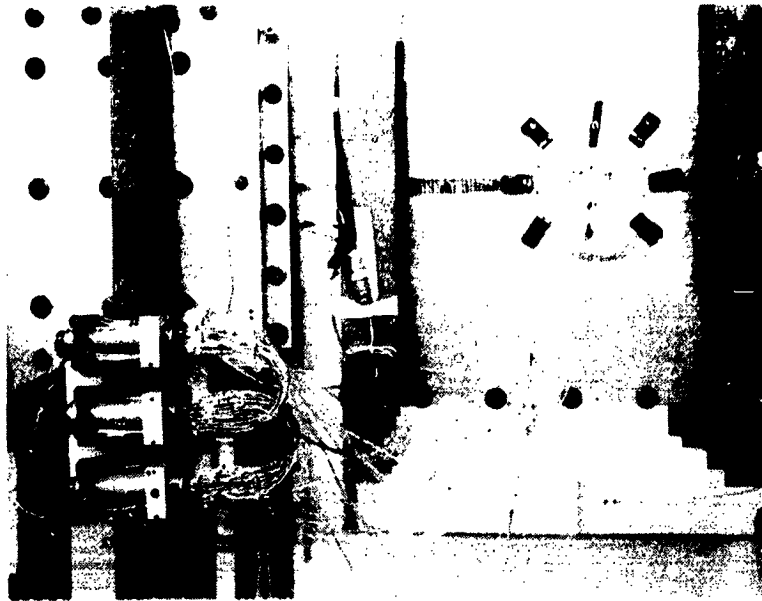


Figure 5.- View of the model mounting port and the scanivalve system.

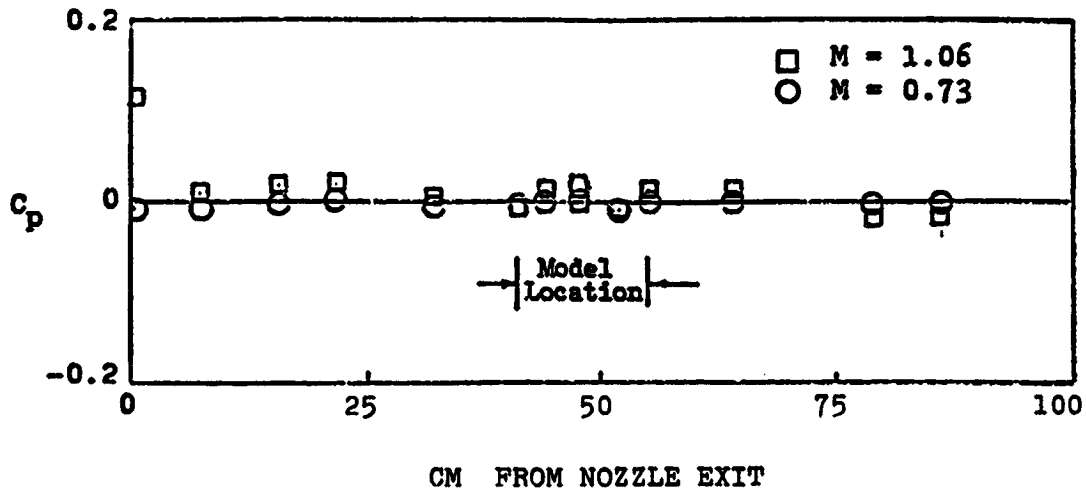


Figure 6.- Two typical pressure distributions through the test section from the calibration.

ORIGINAL PAGE IS
OF POOR QUALITY

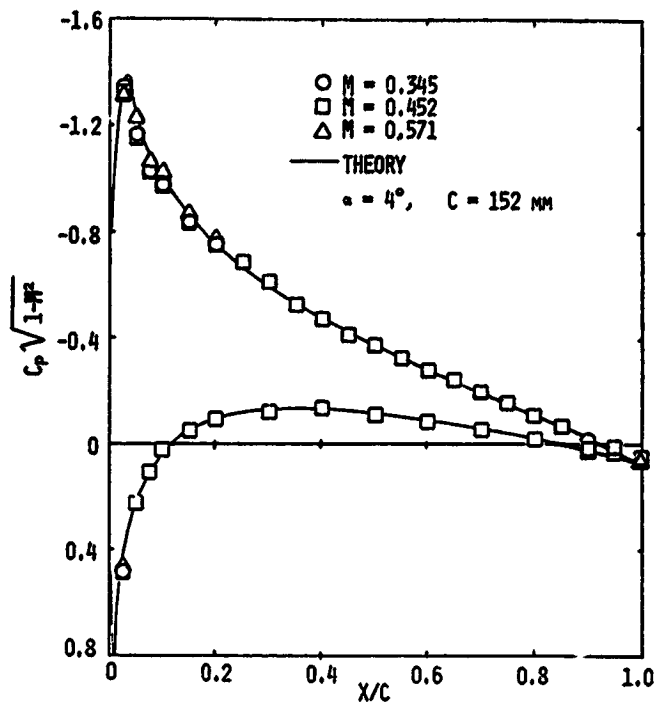


Figure 7.- Pressure distributions from the 152 mm 0012 model compared in a Prandtl-Glauert form.

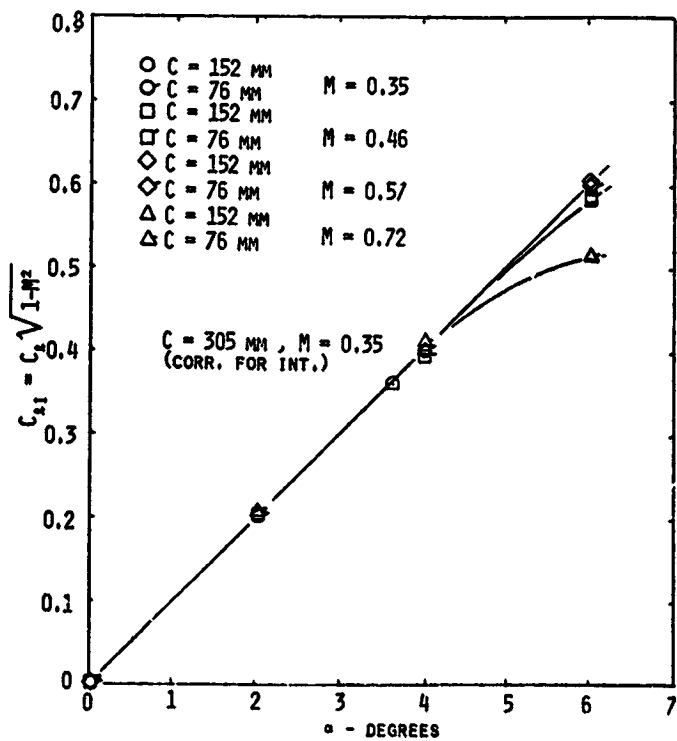


Figure 8.- Integrated lift coefficients for the 0012 models compared in a Prandtl-Glauert form.

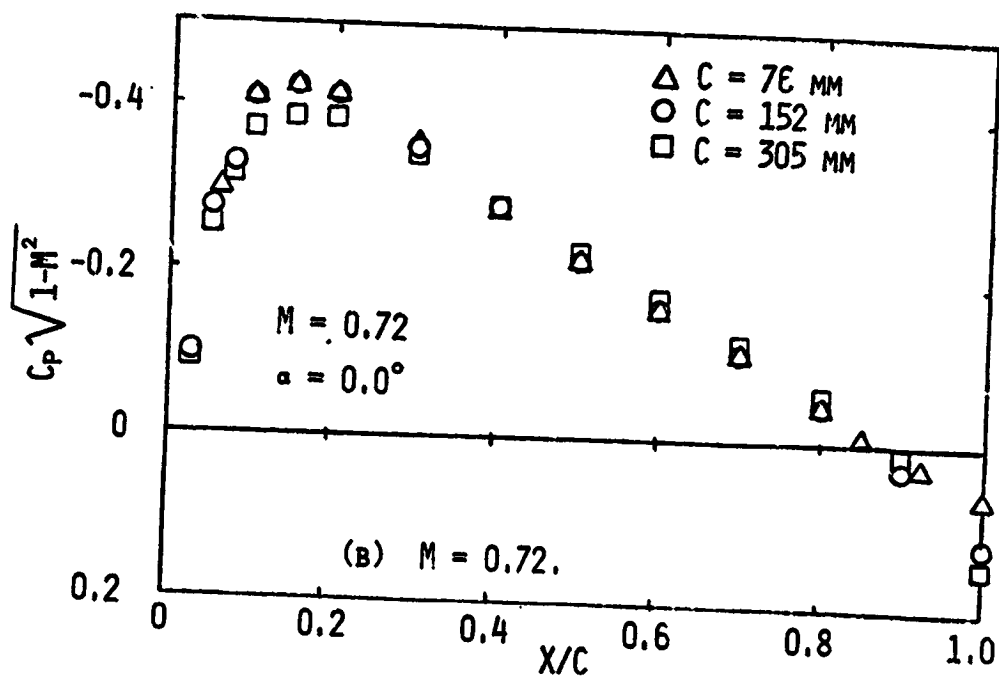
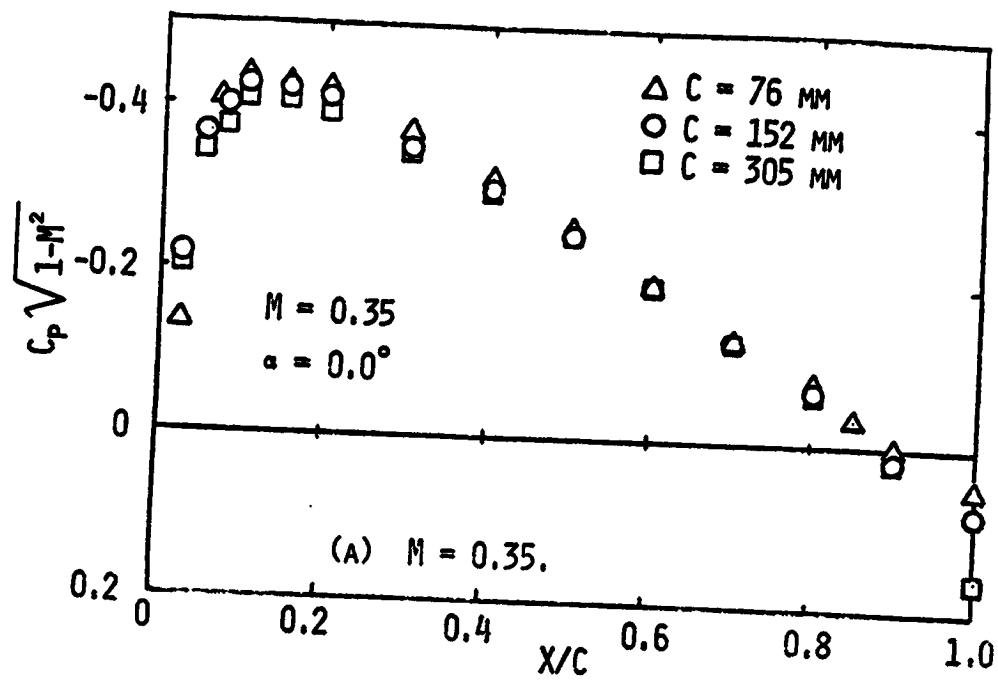


Figure 9.- Pressure distributions from the 0012 models showing blockage at zero angle of attack.

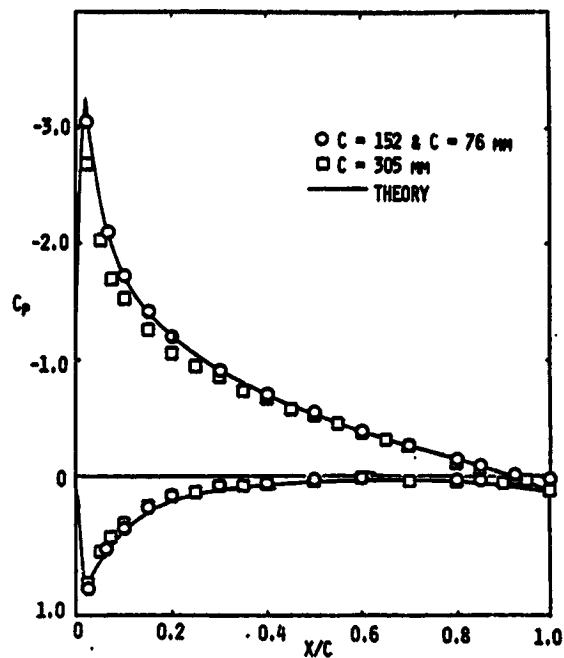


Figure 10.- Pressure distributions from the 0012 models compared to show interference at a subcritical condition. (Data from the 152 mm and 76 mm models fall within the same symbol on this scale.)

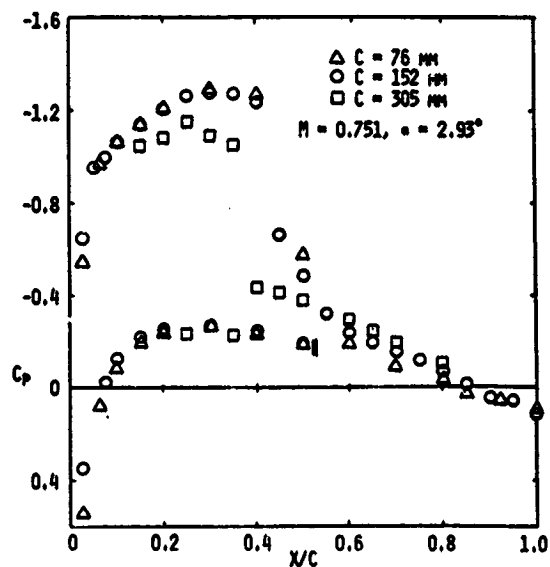


Figure 11.- Pressure distributions from the 0012 models compared to show interference at a supercritical condition.

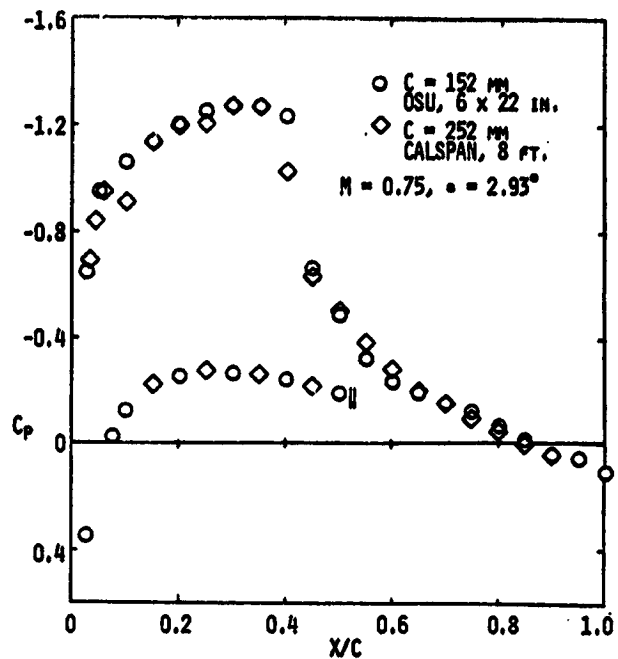


Figure 12.- Pressure distribution from the 152 mm 0012 model compared with that from a 152 mm model in the CALSPAN tunnel.

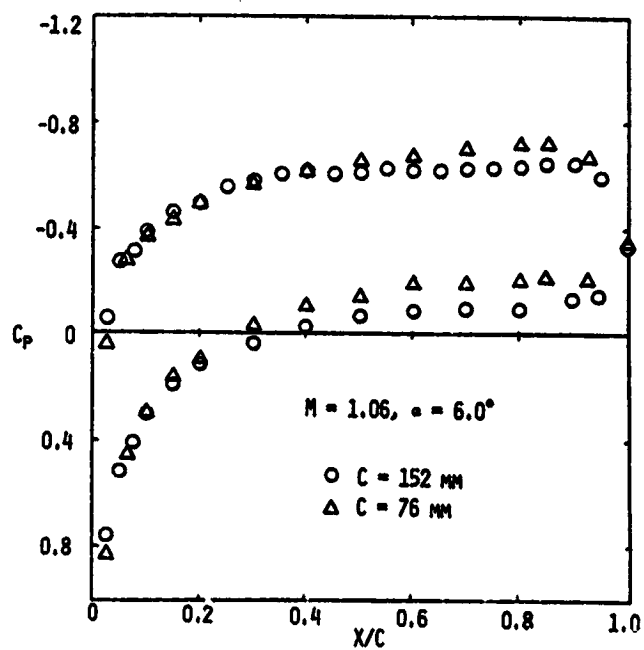


Figure 13.- Pressure distribution from the 0012 models compared at an extreme condition in the 6 in. by 22 in. tunnel.

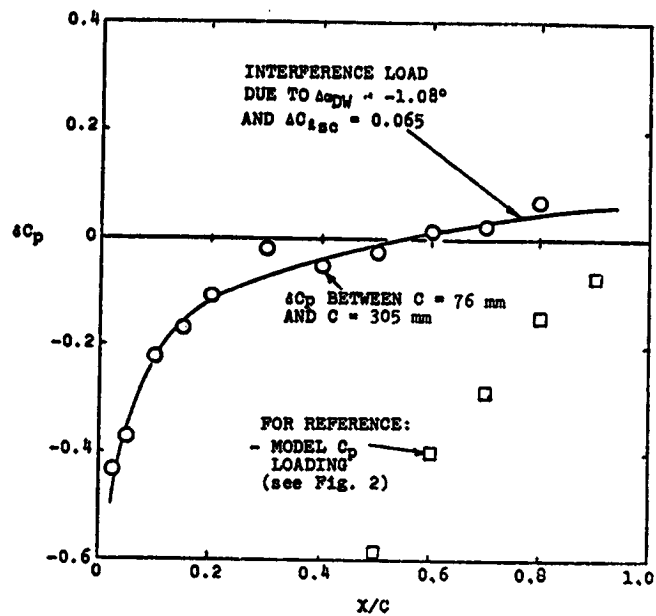


Figure 14.- Loading interference in the 6 in. by 22 in. tunnel on the 305 mm 0012 model compared with a superposition of downwash and streamline curvature.

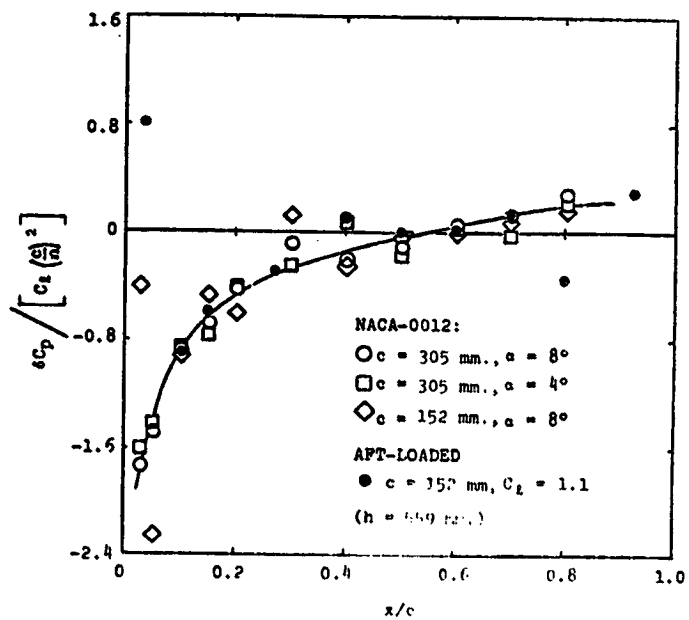


Figure 15.- Generalized loading interference compared for the various sets of models tested.

VISUALIZATION OF THE SEPARATION AND
SUBSEQUENT TRANSITION NEAR
THE LEADING EDGE OF AIRFOILS*

Anthony V. Arena and Thomas J. Mueller
University of Notre Dame

SUMMARY

A visual study was performed using the low speed smoke wind tunnels of the University of Notre Dame with the objective of obtaining a better understanding of the structure of leading edge separation bubbles on airfoils. The location of separation, transition and reattachment for a cylindrical nose constant-thickness airfoil model were obtained from smoke photographs and surface oil flow techniques. These data, together with static pressure distributions along the leading edge and upper surface of the model, produced the influence of Reynolds number, angle of attack and trailing edge flap angle on the size and characteristics of the bubble. Additional visual insight into the unsteady nature of the separation bubble was provided by high speed 16 mm movies. 8mm color movies taken of the surface oil flow supported the findings of the high speed movies and clearly showed the formation of a scalloped spanwise separation line at the higher Reynolds number ($Re_c = 450,000$). Results obtained from these experiments have improved our knowledge of the laminar separation bubble and the transition process.

INTRODUCTION

The next generation of business and commercial aircraft must not only have significant reductions in the noise and exhaust pollutants produced but must be fuel-conservative. One of the crucial areas where significant advances have been made in the past few years is in transonic and subsonic airfoil design. Although advances have been made, there are several areas which require careful investigation if further improvements are to be realized, especially in developing an airfoil with laminar flow over a substantial portion of its surface. One important area of concern is the occurrence and behavior of the leading edge separation bubble. The separation bubble plays an important part in determining the behavior of the boundary layer on the surface, including the stalling characteristics of the airfoil. In practical situations, this bubble may be partly laminar, with transition occurring after laminar separation, or completely turbulent (ref. 1). The primary objectives

* This research was supported by NASA Langley Research Center under Grant NSG 1419.

of this paper are to describe the unique low speed smoke wind tunnels and visualization techniques developed at Notre Dame and to use these techniques to obtain a better understanding of the structure of the leading edge separation bubble and the transition process.

SYMBOLS

Values are given in both SI and U.S. Customary Units. The measurements and calculations were made in U.S. Customary Units.

c	Chord
C_p	Pressure coefficient = $(P - P_\infty) / \frac{1}{2} \rho U_\infty^2$
P	Static pressure on model surface
P_∞	Freestream static pressure
Re_c	Chord Reynolds number = $\frac{c U_\infty \rho}{\mu}$
R	Reattachment location
S	Separation location
T	Beginning transition location
U_∞	Freestream velocity
X	Distance along airfoil chord
X^1	Distance from beginning of Test Section
α	Angle of attack
δ	Flap angle at centerline
θ	Diffuser angle, deg
μ	Absolute viscosity
ρ	Density

EXPERIMENTAL APPARATUS AND TECHNIQUE

A schematic drawing of one of the indraft low turbulence subsonic wind tunnels is shown in figure 1. The air passes through the twelve anti-turbulence screens before entering the 24:1 contraction section. The first seven screens are 14 x 18 mesh bronze and the last five are 25 x 35 mesh marquisette. Both the inlet and test sections are square and are mounted on rollers to provide an easy means of interchanging these components. In addition, each test section has removable rear panels, allowing ready access

to the test section. Downstream of the test section is the diffuser which is fixed into the wall of the laboratory and which transitions from the square cross-section of the test section to a circular cross-section at the fan. A four inch foam rubber section separates the test section and the diffuser to ensure no vibrations are transmitted to the working section from the fan. The fan is driven by an 11,185.5 W (15 hp) variable speed electric motor, located on a separate foundation outside the laboratory. The two-dimensional airfoil type model used in this investigation was the cylindrical leading edge constant-thickness model with a movable flap shown in figure 2. Thirty-four static pressure taps were placed along the leading edge and upper surface of the model as far as $x/c = 0.54$.

For smoke visualization, the smoke is introduced upstream of the first screen from a rake which can be moved and positioned horizontally or vertically so smoke lines may be placed anywhere in the test section. The smoke is generated by a device which allows deodorized kerosene to drip on to electrically heated plates; the smoke then proceeds to the smoke rake. The smoke rake has a filter bag and cooling coils which reduce the smoke temperature to approximately ambient before passing through the anti-turbulence screens and into the test section. Still photographs of the smoke flow were taken, using a Graflex 10 x 13 cm (4 x 5 inch) camera and several high intensity lights with a duration of about 20 micro-seconds. High speed movies were obtained with a Wollensak WF-3 Fastex 16 mm camera and several 1000 and 2000 watt quartz lights. Surface oil flow studies were also made, using time lapse and 8 mm color movie photography.

DISCUSSION OF RESULTS

Turbulence Intensity Measurements

It was necessary to measure the freestream turbulence in the wind tunnel to ascertain the effect of turbulence intensity on the flow over the airfoil model in this and future hot-wire studies. Two stations were chosen at which hot-wire measurements would be conducted. The first was near the entrance to the constant-area tunnel section ($X^1 = 37$ cm) and the second point was further downstream coincident to the location of the leading edge of the model ($X^1 = 76$ cm). The point $X^1 = 0$ signifies the point where the reduction cone ends and the test section begins. The model was removed from the tunnel while measurements were taken at the second station. Four different sets of measurements were taken at each station, varying the velocity from 6 m/sec to 25 m/sec. Three of the four runs utilized turbulence screens directly at the test section entrance ($X^1 = 0$). Results from these experiments are shown in figures 3 and 4. Turbulence intensities ranging from less than 0.2% (no turbulence screen) to less than 1.2% at station $X^1 = 37$ cm (i.e. fig. 3). These values dropped 0.1% and 0.7%, respectively, at $X^1 = 76$ cm, as shown in figure 4.

Static Pressure Distributions

Static pressure coefficient plots were obtained for angles of attack ranging from 6° to -4° , flap angles of 0° , $+30^\circ$ and -30° (positive chosen as downward), and chord Reynolds numbers from 150,000 to 460,000. Typical pressure coefficient versus percent chord results are shown in figure 5. These pressure coefficient plots for the shear layer flow may be divided into four distinct regions: (1) the laminar boundary layer extending along the airfoil surface from the leading edge to the point of separation, characterized by a marked decrease in pressure to a minimum peak, followed by an adverse pressure gradient causing the flow to separate; (2) the constant-pressure laminar shear layer, existing from the points of separation to transition; (3) the turbulent mixing region, between the onset of transition and the point of reattachment, characterized by a quick rise in pressure; (4) the turbulent boundary layer stretching from reattachment on downstream.

Smoke Pictures

For the smoke flow visualization portion of the experiments, several photographs were taken for each condition that pressure plots were available. The purpose was to freeze the action of the separated flow and identify points of separation and transition. Examples of these smoke photographs are shown in figures 6 and 7. Interestingly enough, even though several good photographs were taken at the same ambient and flow conditions, slightly different transition locations were obtained. High speed movies taken with the Wollensak Fastex camera confirmed this unsteady phenomenon in that the laminar portion of the separated flow was observed to grow and shrink in length during small time intervals. The still photographs show that the separation point is always within 1% of the top of the cylindrical leading edge. The angle at which the flow departs from the surface is between 9° and 22° , as measured from the photographs.

Oil Surface Flow

Before starting up the wind tunnel, the angle of attack and flap angle were chosen and a line of oil (approximately 1 cm x 10 cm) was placed on the center of the airfoil in a chord-wise direction. Once the tunnel was operating, the resulting airflow forced the oil to flow along the surface. Within one minute, the separation line along the leading edge was clearly visible. Behind this line were three different sections of oil: (1) oil flowing towards the leading edge, presumably part of the reverse flow inside the separation bubble; (2) a dark region where the turbulent flow is reattaching to the surface, forcing the oil to ooze in both directions; (3) oil flowing towards the trailing edge via the turbulent attached boundary layer (fig. 8a). In all these experiments, the point chosen as the reattachment point was the solid line separating the first light region and the dark region, because this line was clear, definite and always visible. Actually, it was reasoned that the real reattachment line is a few percent chord further downstream but the line chosen in this work is easily measured and is visibly affected by changes in

Reynolds number and angle of attack. The error is extremely small in cases of positive and zero angles of attack, as gravity will pull the oil as far towards the trailing edge (hence reattachment point) as possible. The error becomes a bit more significant, on the order of 3-4% chord, in the cases of negative angles of attack, as gravity forces the oil towards the leading edge, hence driving it slightly further away from the actual reattachment point.

Plots of the chord Reynolds number versus percent chord were obtained for each given angle of attack and flap angle, e.g. figures 9 and 10. Separation was virtually unaffected by increasing the Reynolds number, while the transition and reattachment points moved toward the leading edge in an exponential manner, as discussed by Huang and Hannan (ref. 2). As angle of attack increased, the region of turbulent mixing grew larger. At the highest Reynolds number used in this work (470,000), the position of reattachment was always within 14 to 18% chord, regardless of angles of attack and flap angle. At 6° angle of attack and 30° flap, reattachment was shown at 40% chord. Figure 9 shows at $Re_c = 140,000$ this point is moved to 25% chord, and figure 10 placed reattachment just beyond the 20% mark. Consequently, the slope of these curves is highly dependent on angle of attack.

While in the process of experimenting to obtain these reattachment points, an unexpected phenomenon occurred. With the angle of attack set at -4° , 0° flap angle and a chord Reynolds number equal to 469,000, the separation line no longer appeared to be merely straight, rather a scalloped wave-like pattern was formed. Figure 8 demonstrates the formation process of this pattern. Three distinct regions were observed in the chord-wise direction of this oil flow. From 10 to 12% chord a thick build-up of fluid occurred in an almost regular sinusoidal pattern along the upper surface of the model. Following this configuration was a region extending to the 14% chord-line containing a thinner, more dispersed layer of oil, which accounts for most of the pattern seen in figure 8d. The third zone exhibits a very small amount of fluid, again stretching about 2% of the chord, which assumes a shape similar to trailing vortices. This basic shape formed at the higher Reynolds numbers (above 400,000) for every angle of attack and flap angle tested. The scalloped line is a manifestation of the three-dimensionality of the transitional separated flow. The formation process was interesting in itself. The oil film was placed on the model and the tunnel was turned on to idling speed ($Re_c = 150,000$) and a very steady separation line formed at angle of attack -4° . An increase in Re_c to about 300,000 saw the separation line become somewhat unsteady, as it oscillated back and forth. Further increases in speed ($Re_c = 370,000$) resulted in the ceasing of the oscillatory motion in conjunction with the first appearance of the scalloped pattern. In this Reynolds number range, the line was very sensitive to velocity changes. An increase in tunnel speed resulted in the rebirth of the rapid oscillations for approximately 30 seconds before damping out; once again the oil assumed the wavy-like form. At maximum speed ($Re_c = 450,000$) the oil, in the scalloped pattern, was impervious to incremental velocity changes.

With the tunnel at peak velocity, it was desired to observe any changes evident in the surface oil pattern with respect to angle of attack increments. The angle was raised from -4° to -2° to 0° without any real alteration encount-

ered. However, once positive angles were introduced, a definite change in the wave pattern was noted, causing the frequency of the nodal points to increase in the sinusoidal wave. As before, just prior to the alteration of shape, an oscillatory motion was observed, eventually ceasing within 30 seconds. A similar physical situation was noted by Mattingly (ref.3) in 1962. His experiment involved the flow about a circular cylinder placed in a water tank. What he observed was an undulating separation line. He noted that the source of the separation line oscillation is related to the three-dimensional motion of the wake fluid directly behind the separation line. Mattingly calculated the frequency of these oscillations to be that of the prevailing shedding frequency. The frequency of the oscillatory motions observed in the oil flow line on the CLE-CT model was not determined. By visual observation, however, as in Mattingly's work, an increase in Reynolds number caused a corresponding increase in this frequency. These oscillations eventually damped out, however, and the oil flow line formed a steady, wavy pattern. Further experiments using hot-wire anemometry are planned to study this phenomenon in greater detail.

CONCLUDING REMARKS

Results from this study indicate that visual techniques can be used to increase our understanding of separated flow phenomenon. As adequate analytical methods are presently not available to predict the location and detailed structure of transition, the insight gained from these visual experiments is of significant importance.

Smoke flow photographs clearly visualized the free shear layer following separation from the leading edge. Also, due to the favorable thickness to length ratio of the bubble, the formation of Tollmein-Schlichting type waves in the laminar shear layer is quite distinct, as is the breakdown into a turbulent motion. These photographs will aid in the placement of the hot-wire probes in future investigations. The effect, if any, of the probe on the flow in and around the separation bubble can be easily determined. The unsteadiness of the transition process was clearly observed in the high speed movies.

An oil mixture placed along the upper surface of the model revealed the reattachment locations of the turbulent shear layer to the surface. These points, along with those taken from the smoke flow photographs, were plotted with the static pressure distributions. These plots indicate that the chosen parameters of chord Reynolds number, angle of attack and flap angle definitely affect the size and characteristics of leading edge separation bubbles. The surface oil flow produced a spanwise scalloped pattern at the higher Reynolds numbers. This oil flow pattern is a manifestation of the three-dimensional nature of the transition and separated flows. Hot-wire anemometer studies in progress will provide additional insight into this important but extremely complex flow problem.

REFERENCES

1. Tani, I., "Low Speed Flows Involving Bubble Separations", Aeronautical Research Institute, University of Tokyo, Progress in Aeronautical Sciences, Vol. 5, MacMillan Co., 1964.
2. Huang, T., and Hannan, D., "Pressure Fluctuations in the Regions of Flow Transition", David W. Taylor Naval Ship Research and Development Center, Bethesda, Md., Report 4723, December 1975.
3. Mattingly, G., "An Experimental Study of the Three-Dimensionality of the Flow Around a Circular Cylinder", MS Thesis, University of Maryland, 1962.

ORIGINAL PAGE IS
OF POOR QUALITY

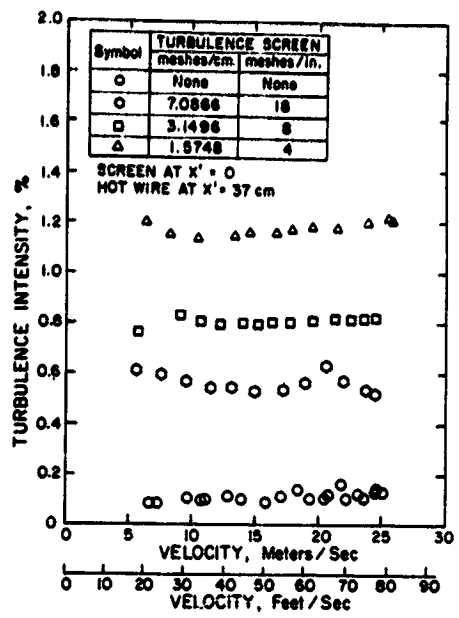


Figure 3.- Turbulence intensity at $X^1 = 37$ cm plotted against tunnel velocity.

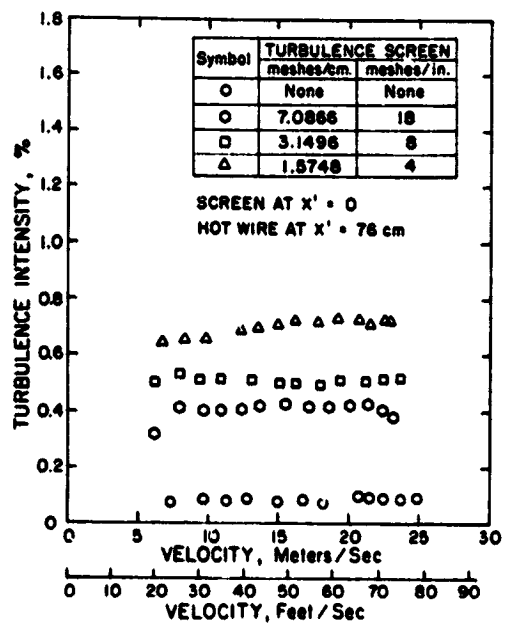


Figure 4.- Turbulence intensity at $X^1 = 76$ cm plotted against tunnel velocity.

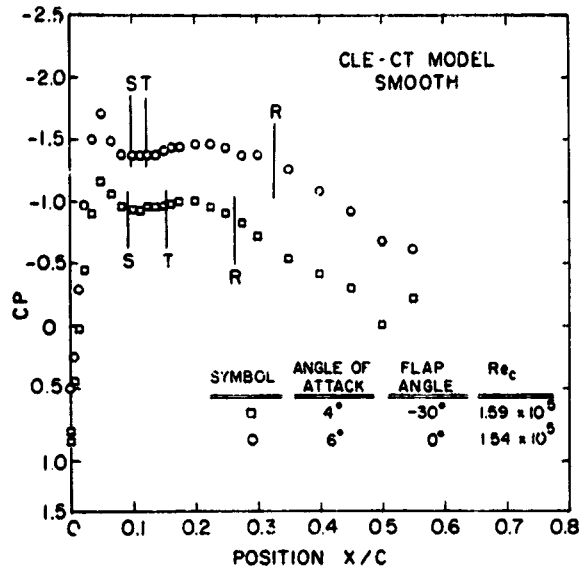


Figure 5.- Static-pressure coefficient along the chord of the CLE-CT model for $\alpha = 4^\circ$, $\delta = -30^\circ$, $Re_c = 1.59 \times 10^5$ and for $\alpha = 6^\circ$, $\delta = 0^\circ$, $Re_c = 1.54 \times 10^5$.

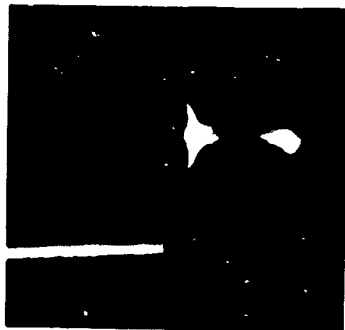


Figure 6.- Smoke-flow photograph at angle of attack of 4° , flap deflection of -30° , and $Re_c = 1.59 \times 10^5$.

ORIGINAL PAGE IS
OF POOR QUALITY



Figure 7.- Smoke-flow photograph at angle of attack of 6° with no flap deflection and $Re_c = 1.54 \times 10^5$.



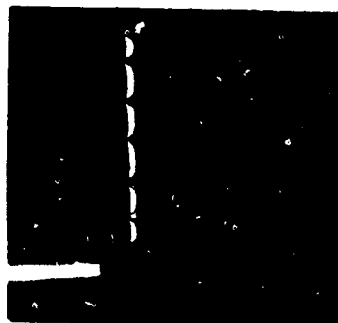
(a) $Re_c = 161,000$.



(b) $Re_c = 305,500$.



(c) $Re_c = 469,000$
(after 10 min).



(d) $Re_c = 469,000$
(after 50 min).

Figure 8.- Photographs of the surface oil flow for the CLE-CT model and for $\alpha = -4^\circ$ and $\delta = 0^\circ$.

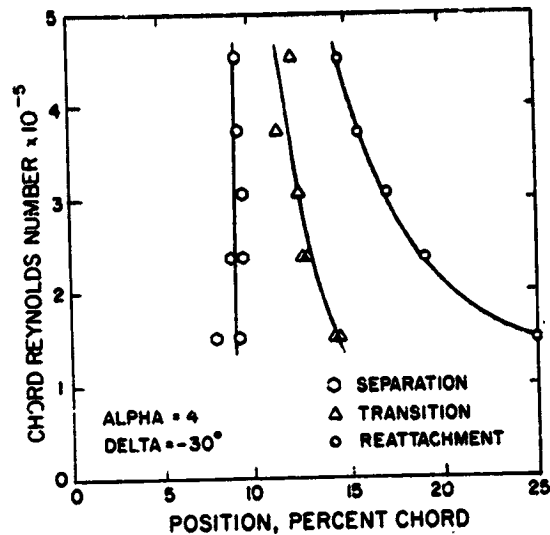


Figure 9.- Measured separation, beginning transition, and reattachment locations against chord Reynolds number for the CLE-CT model for $\alpha = 4^\circ$ and $\delta = -30^\circ$.

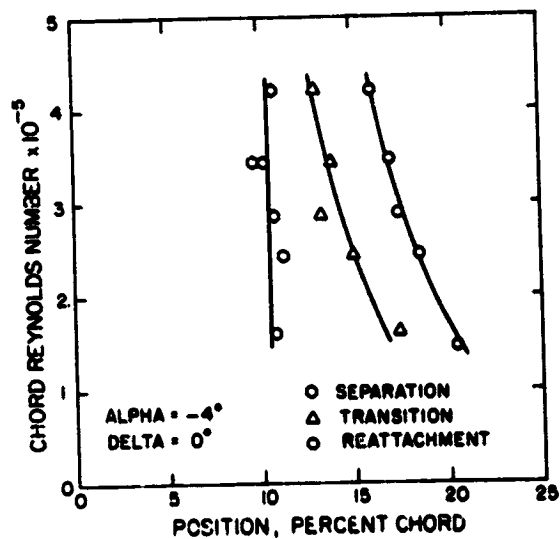


Figure 10.- Measured separation, beginning transition, and reattachment locations against chord Reynolds number for the CLE-CT model for $\alpha = -4^\circ$ and $\delta = 0^\circ$.

INSTRUMENTATION, TECHNIQUES AND DATA REDUCTION

ASSOCIATED WITH AIRFOIL TESTING PROGRAMS

AT WICHITA STATE UNIVERSITY

Edward J. Rodgers and William H. Wentz, Jr.
Wichita State University

H.C. Seetharam
Boeing Commercial Airplane Company

SUMMARY

Two-dimensional airfoil testing has been conducted at the Wichita State University Beech Wind Tunnel for a number of years. The instrumentation developed and adapted during this period of testing for determination of flow fields along with the traversing mechanisms for these probes are discussed. In addition, some of the techniques used to account for interference effects associated with the apparatus used for this two-dimensional testing are presented. The application of a mini-computer to the data reduction and presentation is discussed.

INTRODUCTION

During the wind tunnel testing program of two-dimensional airfoils at the Walter H. Beech Wind Tunnel at the Wichita State University during the last three years, certain instrumentation has been developed or adapted. These instruments include pressure probes for obtaining measurements near the surface of an airfoil and pressure probes for the determination of the velocity fields in reverse flow regions. Traversing mechanisms were also developed for positioning these probes. These probes and traversing mechanisms are described and samples of the data obtained are shown in this paper. In addition to the pressure probes, commercially available hot-film probes were adapted for measurement of velocity in the reverse flow regions. The hot-film probe came in two versions, a single-element probe and a split-film probe. These probes and their use are discussed and data obtained with the hot-film probes are shown.

Use of the probes and traversing mechanism in some regions and under some conditions introduced interference effects on the flow field about the model specimen. These interference effects are discussed along with modifications and techniques used to evaluate, minimize and correct for these interference effects. One of the effects discussed is that on the separation of the boundary layer and consequent changes to the pressure distribution.

Large amounts of data generated during wind tunnel programs can become unmanageable. A mini-computer has been implemented in the data acquisition and processing system at the Wichita State University wind tunnel. Use of the mini-computer system for data acquisition, reduction, analysis and display is described.

Symbol definitions are given in an appendix.

INSTRUMENTATION

The desired measurements are those required to determine and describe the flow field about the airfoil. For an incompressible flow, if one determines the velocity field both in magnitude and direction then one has all of the information necessary to understand the flow mechanism. The velocity field about the airfoil at the pre-stall through post-stall range of angles of attack of interest varies quite widely in character. The flow can be steady or unsteady with varying degrees of turbulence in different regions about the airfoil and also normal or reversed in direction. The regions of interest about the airfoil are those of the near-wall flow field, the far-field flow, and the wake flow field. It is difficult to get a single instrument that can operate under all of the conditions found in these different regions. A number of different instruments are therefore used. These instruments are discussed in the following sections, under two categories: 1) pressure probes, and 2) hot-film probes. In addition, the traversing mechanisms used to position these probes are also discussed.

Pressure Probes

The basic pressure probe used is the five-tube probe shown in figure 1. This probe consists of a total head tube and four static taps spaced about the circumference of the probe. The description, calibration and use of this probe have been documented in references 1 and 2. The probe is used to determine the magnitude and direction of the velocity in the far-field region over the airfoil and in the wake of the airfoil. In regions where the angularity of the local velocity with respect to the probe axis exceeds $\pm 40^\circ$, the probe cannot sense the direction or magnitude. Because of the physical dimensions of the tip it cannot be used for near-wall (< 0.2 mm) measurements. In order to obtain velocity measurements closer to the surface of the airfoil the flat-tube probe shown in figure 2 was developed (reference 1). This is a total head tube whose prime component is a flattened hypodermic tubing. This probe is capable of measurement as near as 0.15 mm from the local surface. The velocity magnitude is determined using the static pressure tap on the surface of the body for static pressure quantity. The flat-tube probe cannot sense the velocity angularity or direction, and like the other pressure probes, is insensitive to velocity fluctuations.

In an attempt to determine the separation and reattachment points over the airfoil in the near-wall region, the cylindrical-tube probe of figure 3 was developed (reference 1). This probe consisted of two hypodermic tubes, side-by-side, sealed at the extreme end with a small total pressure head opening drilled into each tube near its sealed end. During use, the tube was brought close to the surface of the airfoil and the flow direction and total pressure were obtained from the higher two pressures. The cylindrical-tube probe could not sense the flow angularity. The velocity magnitude was determined using the airfoil surface static pressure reading obtained simultaneously. This cylindrical-tube probe was found to be rather inaccurate for determining the separation and reattachment points, because of sensitivity to sidewash velocity near separation.

Another configuration developed for near-wall velocity measurements and also capable of determining flow reversal was the four-tube probe shown in figure 4. This probe has forward- and aft-facing flattened total tubes for near-wall flow direction and total pressure measurement. The pitot-type tubes are less sensitive to sidewash than the cylindrical-tube probe, and are capable of measurement nearer to the surface (down to 0.34 mm) than the cylindrical probe. The two static pressure tubes added to this probe give it the capability of direct static and total pressure measurement, and therefore velocity magnitude. The probe is not capable of determining flow angularity. Since flow direction near a wall is usually nearly parallel to the wall, the lack of flow angularity measurement capability is not a severe limitation. This probe was adapted as the secondary pressure device used in the flow measurement work supplementing the data from the five-tube probe. The four-tube probe is described in more detail in reference 3.

A comparison of typical velocity profiles measured over the airfoil using the cylindrical-tube, the five-tube, and the flat-tube probes are shown in figure 5. The differences in velocity as measured by the different probes are rather small. The five-tube probe data is probably the most accurate since it has been calibrated extensively as mentioned previously.

Another example of the data obtained for determining the flow field about the airfoil is the velocity field data shown in figure 6. The vectors are to scale and indicate both the magnitude and the direction of the flow over the airfoil and in the wake. As can be seen on the figure, the five-tube data does not supply any information in the reverse flow regions. The four-tube data shown by the dashed lines is used to supplement the five-tube data although the velocity angularity in this reverse flow region is not determined.

Another pressure probe developed and used was the boundary layer mouse shown in figure 7 and discussed more fully in reference 4. This probe or rake consists of a number of total head tubes stacked closely and attached tangent to the surface of the airfoil. The total pressures determined were used with the surface static pressures to obtain the velocity magnitudes near the wall. Velocity magnitudes in the reversed flow regions cannot be determined with this rake. A typical total pressure measurement survey over the flap and the flap cove of an airfoil is shown in figure 8.

Hot-Film Probes

In the course of the present research program, a hot-film sensor and associated control signal conditioning equipment were obtained (reference 4). The first probe obtained was a single hot-film sensor shown in figure 9. The sensor consists of a small cylindrical wire, .050 mm in diameter, mounted between two supports. The cylindrical sensor is made of a quartz material coated with a thin film of platinum. The film is heated by proper circuitry and the rate of heat transfer depends on the velocity of the flow past the wire. The hot-film probe is sensitive to unsteady flow velocities and is calibrated to measure the magnitude of the velocity. However, it cannot sense the direction of the flow if reversed. One can speculate from the data obtained whether the flow does reverse since in this region the velocity would intermittently become zero.

Recently, split-film sensors have become available which eliminate the flow direction ambiguity associated with single-film sensors (reference 5). Figure 10 is a schematic of the split-film sensor. The thin film of platinum is deposited on the fore and aft portion of the cylindrical sensor of this probe which is .15 mm in diameter. The electronic circuitry of the equipment allows the determination of the flow direction and its magnitude. Although the flow angle is not determined, the probe does determine the magnitude and whether the flow is in the fore or aft direction. The split-film and single-film sensors are described more thoroughly in reference 5.

Figure 11 shows how the output of the split-film [a voltage] and the four-tube pressure probe [a pressure differential] vary with the velocity.

Figure 12 shows how the output of the split-film equipment appears on an oscilloscope for different levels of turbulence and percentage of time of reversal of flow.

A temporal sample of a calibrated velocity trace obtained by the split-film equipment is shown in figure 13. This temporal data can be analyzed to obtain statistical information regarding the flow. Programs are being written at WSU for this analysis.

One of the present ways of presenting the data is that shown in figure 14, a typical split-film survey result. This data shows distinct regions about the airfoil and in its wake where certain characteristics of the flow exist.

TRAVERSING MECHANISMS

The probes discussed in the previous section were mounted onto a traversing mechanism shown schematically in figure 15. The probe positioning could be controlled from outside the wind tunnel both in the vertical and axial direction. While trying to repeat previous data of a high angle of attack case, it was observed that the surface static pressures obtained on the model without the probe differed significantly from that when the probe was present. This

difference was thought to be an interference effect due to the strut and the probe travel track. The strut was therefore modified from a circular section to an airfoil section and the probe travel track was modified and relocated outside of the wind tunnel. The remodified probe traversing mechanism is shown in figure 16. This modification resulted in an improvement in the data as seen from figure 17. The changes in the pressure coefficient under the different conditions along with other data and visual observations led the authors to conclude that the introduction of the probe effected the separation point at the large (near stall) angles of attack (reference 3). The modified strut and track resulted in lesser interference on the separation point location than the unmodified versions. As seen from figure 17, some interference still exists but it is minimal. At the lower angles of attack the pressure data shows insignificant interference.

The traversing mechanism shown in figure 18 has recently been constructed to allow close measurements near the wall while eliminating some of the vibrational problems that exist between the probe and the model. The probe is mounted in the mechanism shown. The shaft holding the probe rotates within the housing, changing the vertical location of the probe from the model. This device permits repeatable positioning of the probe as close as 0.15 mm to the model surface. The entire housing with the shaft and probe is mounted to the side plate of the two-dimensional section walls. Holes are drilled so that the probe can be located at various axial positions along the model chord. The entire device rotates with the model during an angle of attack change.

INTERFERENCE ON INSTRUMENTATION

In the course of the testing the static pressure used to determine the free-stream velocity of the test section was re-located on the two-dimensional section walls. In trying to repeat data from previous tests it was found that at the high angles of attack with flaps deflected the data was somewhat in error from that obtained in earlier tests (reference 6). Investigation of various possibilities showed that the dynamic pressure determined using the new location of the static taps was in error. The error was due to the fact that the velocity at the static tap location was now higher because of the velocity field about the airfoil.

Further investigations showed that a correction could be made to the static pressure tap reading and therefore to the measured dynamic pressure which was dependent on the lift coefficient of the airfoil. As shown in figure 19, the velocity induced by the airfoil at the static tap location is determined by the circulation about the airfoil and the vortex image system representing the location of the walls. It was found that not only the image system shown but a set of image vortices had to be used for the correction to be adequate. The resulting correction to the measured dynamic pressure for the airfoil and wind tunnel set up used was given by the relationship shown on figure 19 which depends on the square of the lift coefficient. This correction is discussed more fully in reference 6.

DATA ACQUISITION, REDUCTION AND DISPLAY SYSTEM

The components of the force data reduction and display system are shown in figures 20 and 21. The system is described fully in reference 7. A mini-computer serves as the central element of this system.

Figure 21 shows the complete elements of the configuration with the mini-computer at the center. Various input and output devices are associated with the mini-computer. This has allowed more refined treatment of the data and improved the efficiency of the data acquisition and reduction. The engineer now has results available almost instantaneously and can determine whether the data point is satisfactory or whether it should be re-run.

Data can also be plotted on line using the digital plotter. Typical results are shown in figures 22 and 23. The first of these shows a sample of velocity field plot. The airfoil and velocity vectors are plotted about 6 seconds after the data points had been obtained. A sample pressure distribution plot of an airfoil with flaps is shown in figure 23.

Computer programs are being formulated and written to obtain statistical information from the histograms obtained by the split-film probes. This should allow more information to be obtained from the data presently generated during the wind tunnel tests.

APPENDIX

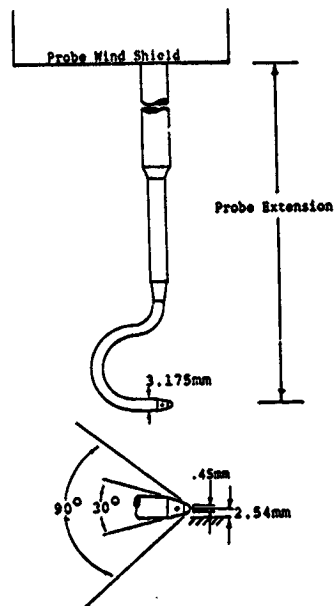
SYMBOLS

Values are given in both SI and U.S. Customary Units. The measurements and calculations were made in the U.S. Customary Units.

C	Airfoil chord
C_L	Airfoil section lift coefficient, $\frac{\text{section lift}}{QC}$
C_p	Static pressure coefficient, $\frac{p_s - p_\infty}{Q}$
C_{p_t}	Total pressure coefficient, $\frac{p_t - p_\infty}{Q}$
h	Wind tunnel test section height
x_0	Location of wall static pressure tap from airfoil quarter chord
p_s	Local static pressure
p_t	Local total pressure
p_∞	Free stream static pressure
Q	Free stream dynamic pressure
Re	Reynolds number based on wing chord and free stream conditions
U	Free stream velocity
U^*	Dimensionalized component of local velocity in the free stream
V_0	Axial component of velocity at wall static pressure tap
V_R	Resultant velocity at wall static pressure tap
x	Streamwise coordinate
z	Vertical coordinate
Γ	Airfoil circulation

REFERENCES

1. Seetharam, H.C. and Wentz, W.H. Jr.: Experimental Studies of Flow Separation and Stalling on a Two-Dimensional Airfoil at Low Speeds. NASA CR-2560, July 1975.
2. Walker, J.K.: Calibration of a Five-Tube Probe. Wichita State University AR 74-1, April 1974.
3. Seetharam, H.C., Rodgers, E.J. and Wentz, W.H. Jr.: Experimental Studies of Flow Separation of the NACA 2412 Airfoil at Low Speeds. Wichita State University AR 77-3, 1977.
4. Seetharam, H.C. and Wentz, W.H. Jr.: A Low Speed Two-Dimensional Study of Flow Separation on the GA(W)-1 Airfoil with 30-Percent Chord Fowler Flap. NASA CR-2844, May 1977.
5. Wentz, W.H. Jr., and Seetharam, H.C.: Split-Film Anemometer Measurements on an Airfoil with Turbulent Separated Flow. Proceedings of Fifth Biennial Symposium on Turbulence, University of Missouri-Rolla, Oct. 2-4, 1977.
6. Wentz, W.H. Jr. and Fisco, K.A.: Wind Tunnel Force and Pressure Tests of a 21% Thick General Aviation Airfoil with 20% Aileron, 25% Slotted Flap and 10% Slot-Lip Spoiler. Wichita State University AR 77-6, Nov. 1977.
7. Howe, Donald and Fisco, K.A.: Minicomputer Utilization as a Method of Data Reduction in a Low Speed Wind Tunnel. Paper #78-313, AIAA 14th Annual Meeting and Technical Display, Washington, DC, February 7-9, 1978.



USE

- TOTAL PRESSURE: FAR WALL & WAKE
- STATIC PRESSURE: FAR WALL & WAKE
- VELOCITY MAGNITUDE: FAR WALL & WAKE

SHORTCOMINGS

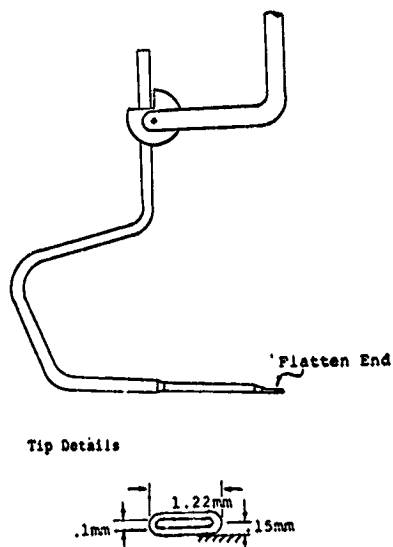
- ACCURACY DECREASES AT HIGH ANGLES OF FLOW

- INSENSITIVE TO FLUCTUATIONS
- CANNOT GET NEAR WALL DATA

COMMENTS

- PROBE CALIBRATED FOR DETERMINATION OF VELOCITY MAGNITUDE AND ANGLE ($\pm 50^\circ$)
- CORRECTION FOR IMAGE EFFECT NEAR WALL
- CORRECTION FOR MODEL DEFLECTION
- ALIGNED PARALLEL TO AIRFOIL
- REFERENCE (1), (2)

Figure 1.- Five-tube probe.



USE

- TOTAL PRESSURE: NEAR & FAR WALL
- VELOCITY MAGNITUDE: NEAR & FAR WALL

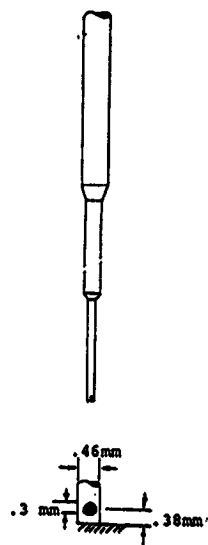
SHORTCOMINGS

- REVERSED FLOW NOT SENSED
- INSENSITIVE TO FLUCTUATIONS
- STATIC PRESSURE NOT MEASURED
- FLOW ANGLES NOT DETERMINED

COMMENTS

- WALL STATIC PRESSURE FOR VELOCITY MEASUREMENTS
- CORRECTIONS FOR MODEL DEFLECTIONS
- ALIGNED PARALLEL TO AIRFOIL SURFACE
- REFERENCE (1)

Figure 2.- Flat-tube probe.



USE

- TOTAL PRESSURE: NEAR & FAR WALL
- VELOCITY MAGNITUDE: NEAR & FAR WALL
- REVERSED FLOW REGIONS

SHORTCOMINGS

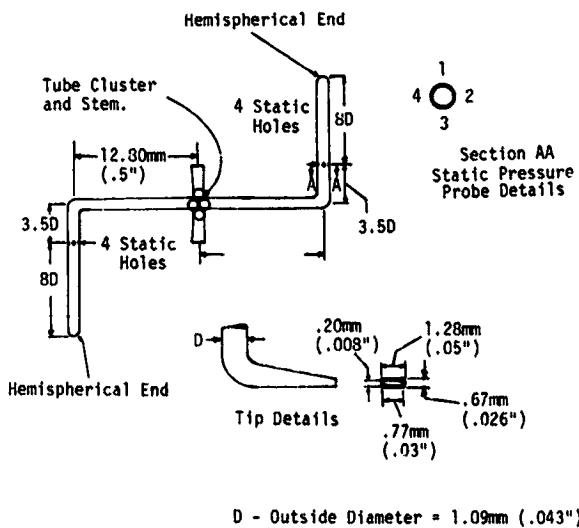
- SEPARATION & REATTACHMENT POINT NOT SENSED ACCURATELY
- INSENSITIVE TO FLUCTUATIONS
- STATIC PRESSURE NOT MEASURED
- FLOW ANGLES NOT DETERMINED

COMMENTS

- ALIGNED PARALLEL TO AIRFOIL SURFACE
- CORRECTIONS FOR MODEL DEFLECTIONS
- WALL STATIC PRESSURE FOR VELOCITY MEASUREMENTS
- REFERENCE (1)

Figure 3.- Cylindrical-tube probe.

FOUR TUBE PROBE



USE

- FLOW REVERSAL REGIONS
- NEAR WALL MEASUREMENTS
- STATIC PRESSURE
- TOTAL PRESSURE
- VELOCITY MAGNITUDE

SHORTCOMINGS

- INSENSITIVE TO FLUCTUATIONS
- FLOW ANGLES NOT DETERMINED
- ACCURACY DECREASES WITH LARGE FLOW ANGLES

COMMENTS

- USED IN PARALLEL WITH 5-TUBE PROBE
- ALIGNED PARALLEL TO SURFACE
- ALIGNED PARALLEL TO FREE STREAM FLOW IN WAKE
- DATA REDUCTION PROGRAM DETERMINES FLOW DIRECTION IN REVERSED FLOW
- REFERENCE (3)

Figure 4.- Four-tube probe.

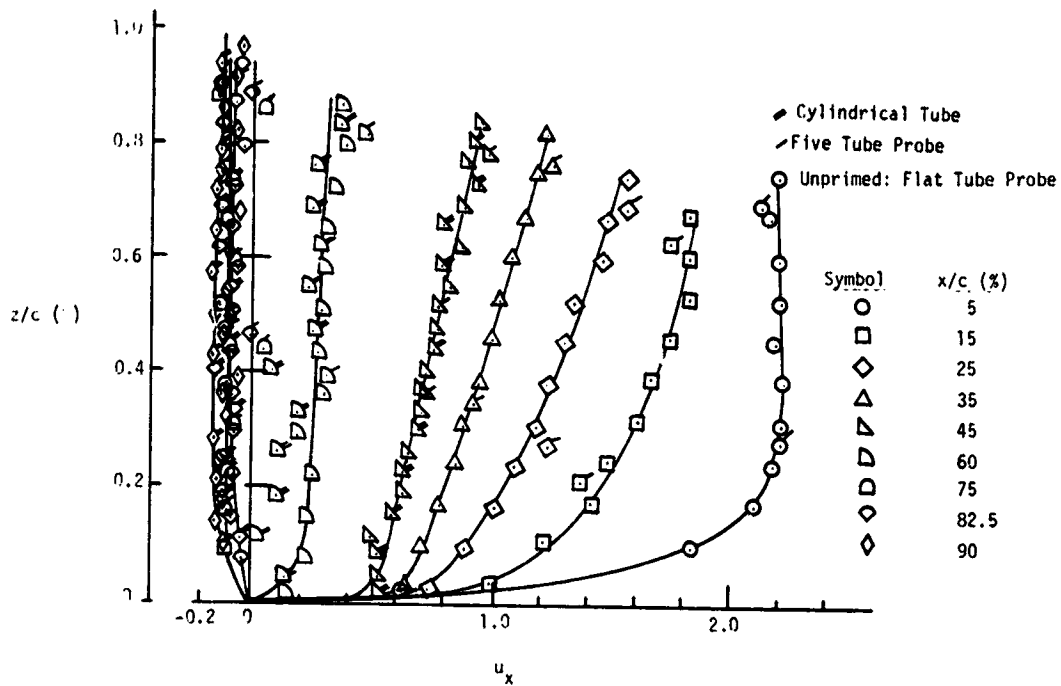


Figure 5.- Typical velocity profiles over an airfoil.

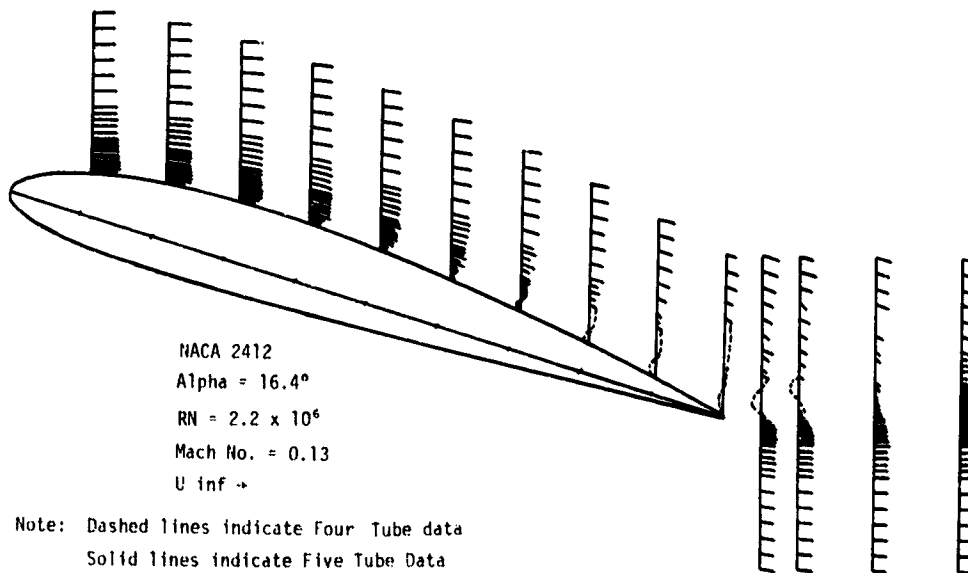
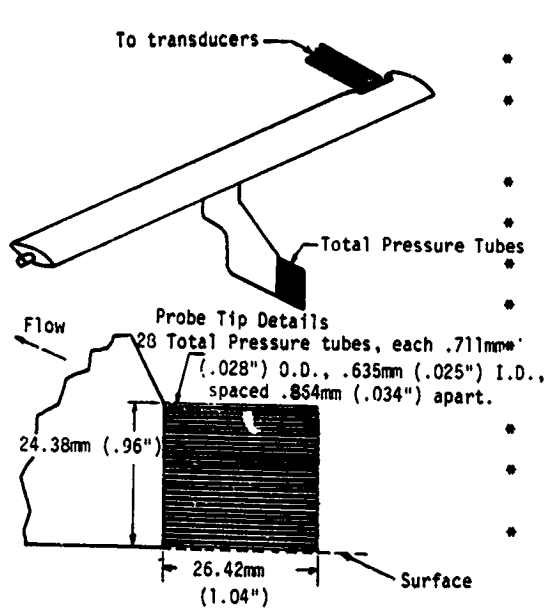


Figure 6.- Velocity field data.



USE

- * TOTAL PRESSURE NEAR WALL
- * VELOCITY MAGNITUDE NEAR WALL

SHORTCOMINGS

- * NON-TRAVERSING
- * REVERSED FLOW NOT SENSED
- * INSENSITIVE TO FLUCTUATIONS
- * STATIC PRESSURE NOT MEASURED
- * FLOW ANGLES NOT DETERMINED

COMMENTS

- * ALIGNED PARALLEL TO AIRFOIL SURFACE
- * WALL STATIC PRESSURES FOR VELOCITY MEASUREMENTS
- * REFERENCE (4)

Figure 7.- Boundary-layer mouse.

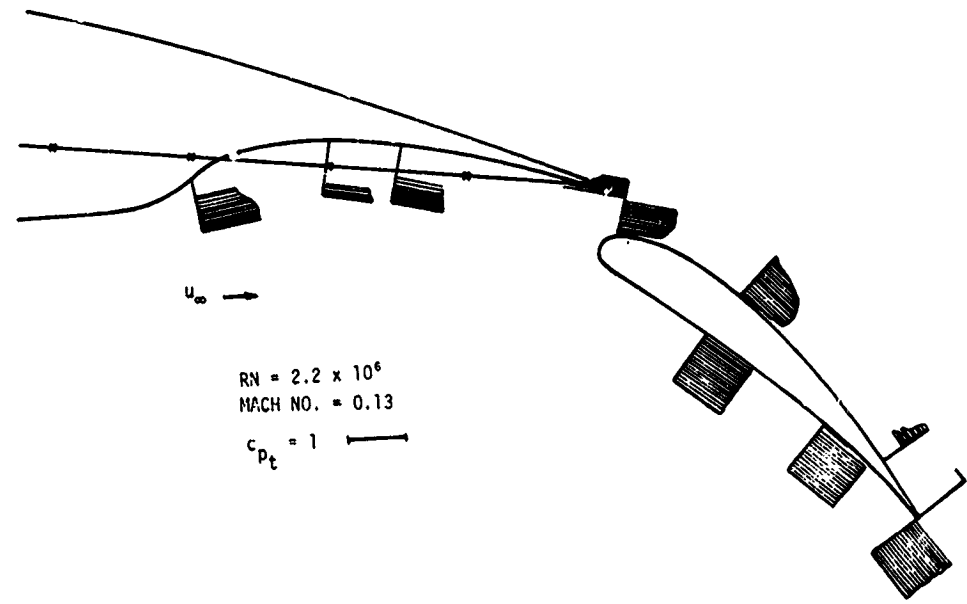


Figure 8.- Mouse total-pressure measurements.

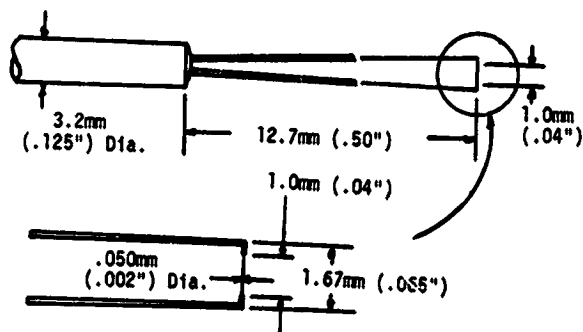


Figure 9.- Single hot-film sensor.

USE

- REVERSED FLOW SENSING
- UNSTEADY VELOCITIES

SHORTCOMINGS

- REVERSED FLOW NOT MEASURED
- PRESSURES NOT MEASURED
- FLOW ANGLES NOT DETERMINED

COMMENTS

- REQUIRES FREQUENT CALIBRATION
- REQUIRES MORE SIGNAL PROCESSING THAN PRESSURE PROBES
- REFERENCES (4,5)

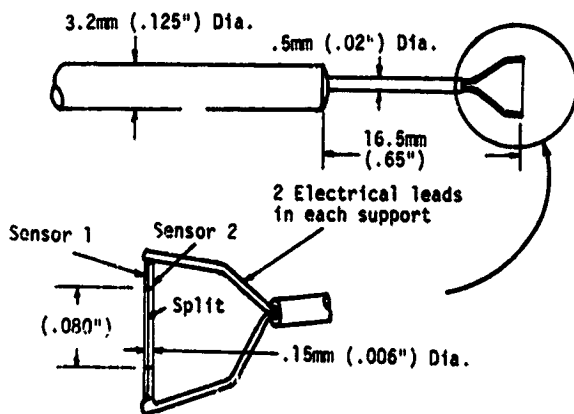


Figure 10.- Split-film sensor.

USE

- REVERSED FLOW
- UNSTEADY VELOCITIES

SHORTCOMINGS

- PRESSURES NOT MEASURED
- FLOW ANGLES NOT DETERMINED

COMMENTS

- REQUIRES FREQUENT CALIBRATION
- REQUIRES MORE SIGNAL PROCESSING THAN PRESSURE PROBES
- REFERENCE (5)

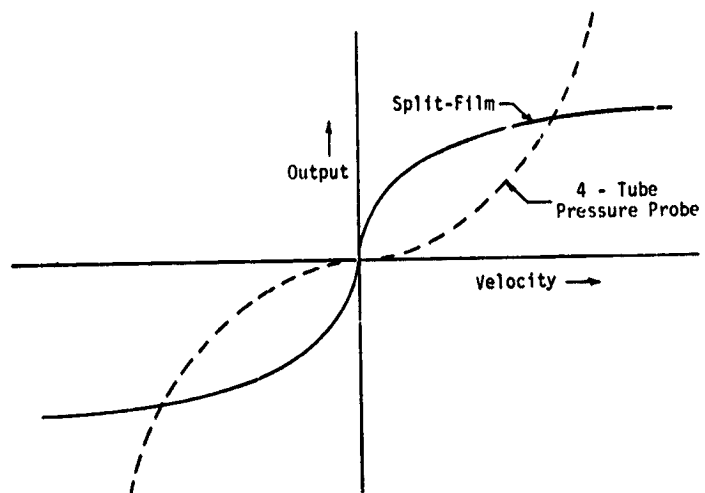


Figure 11.- Comparison of pressure and split-film probes.

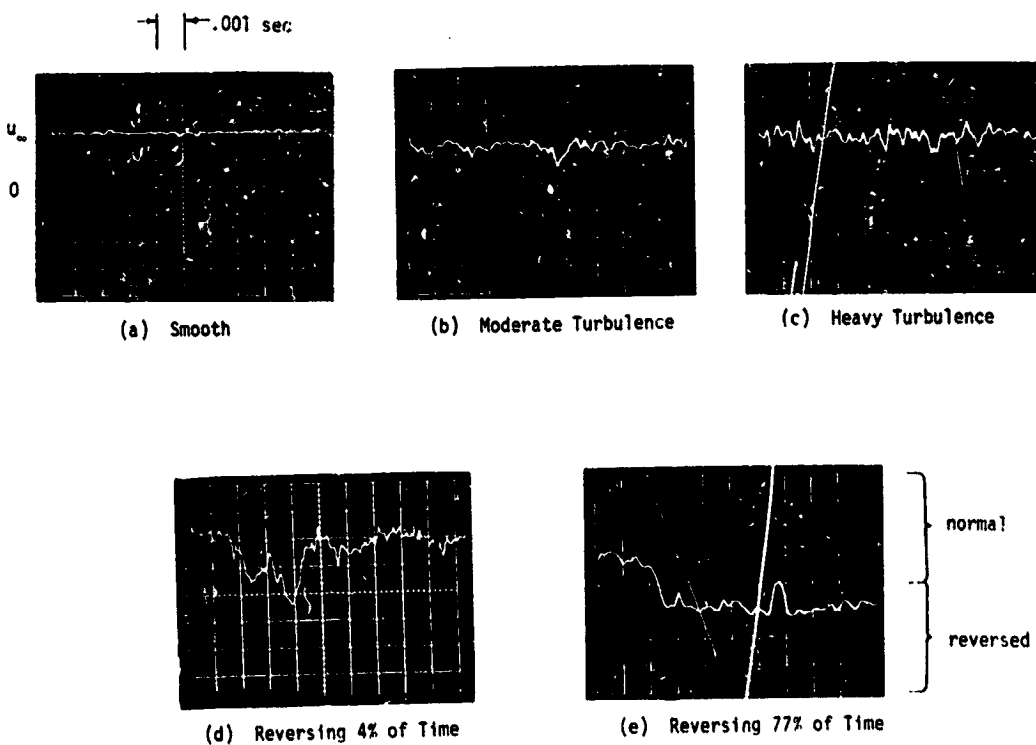


Figure 12.- Split-film oscilloscope traces.

ORIGINAL PAGE IS
OF POOR QUALITY

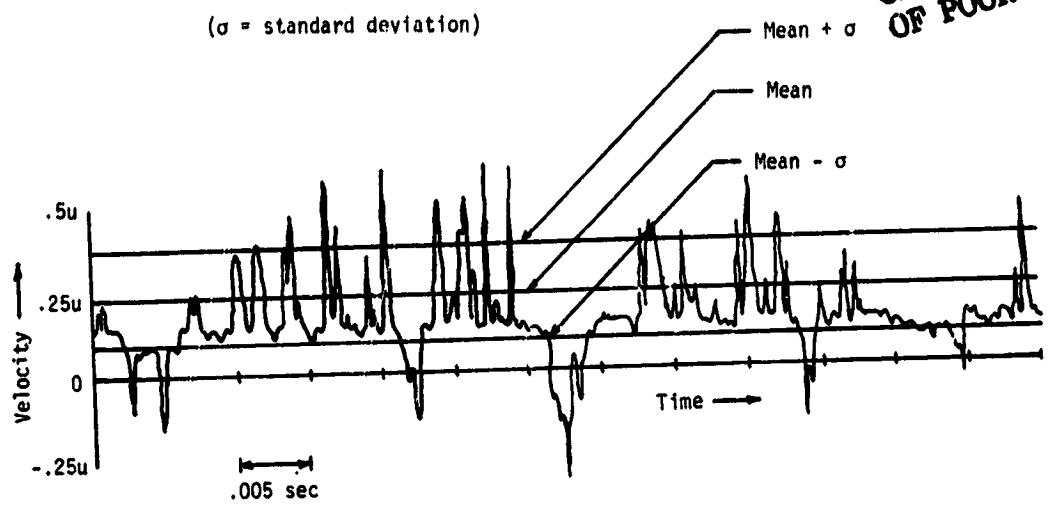


Figure 13.- Sample split-film probe velocity trace.

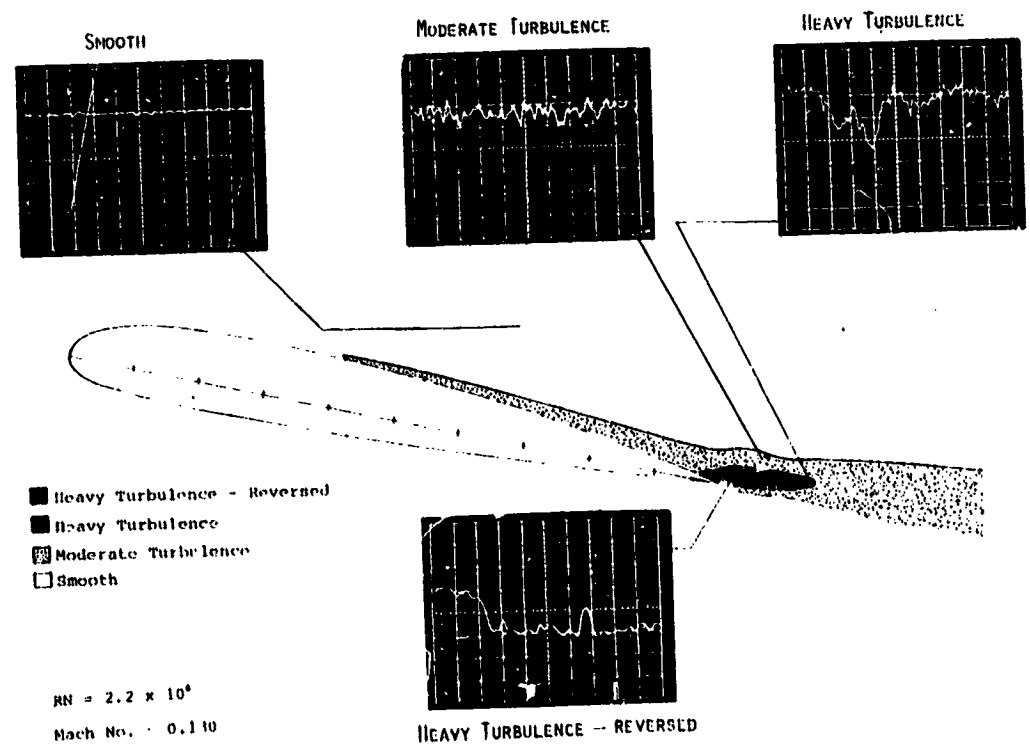


Figure 14.- Typical split-film survey.

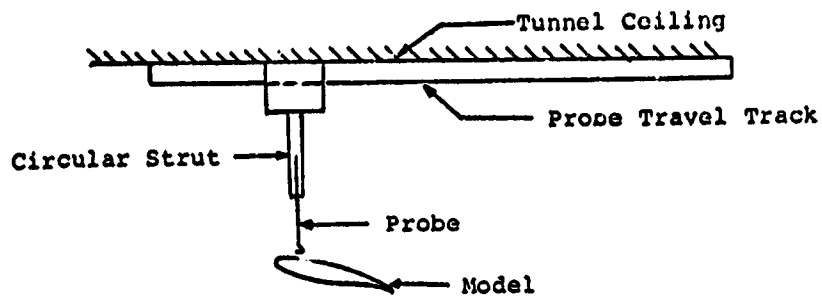


Figure 15.- Probe traversing mechanism before modification.

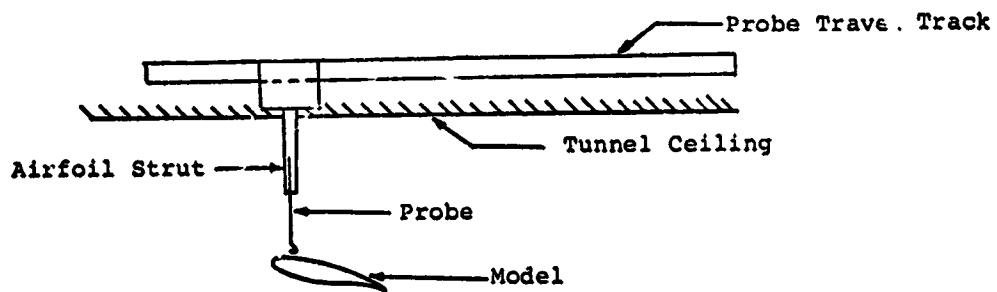
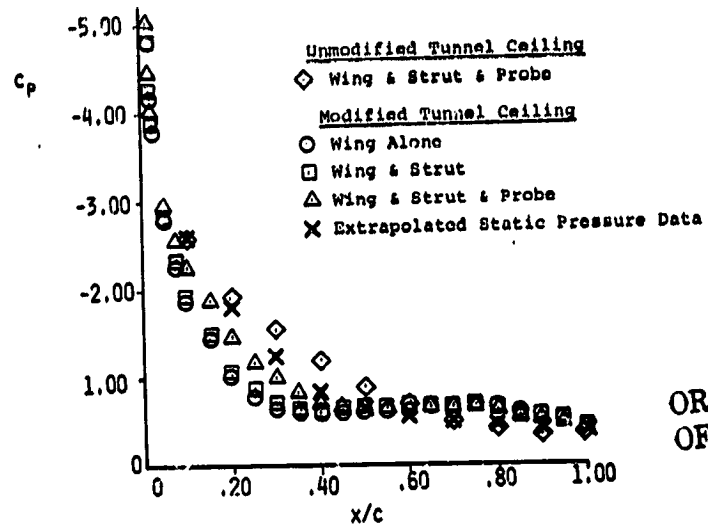


Figure 16.- Probe traversing mechanism after modification.



ORIGINAL PAGE IS
OF POOR QUALITY

Figure 17.- Surface static-pressure interference.

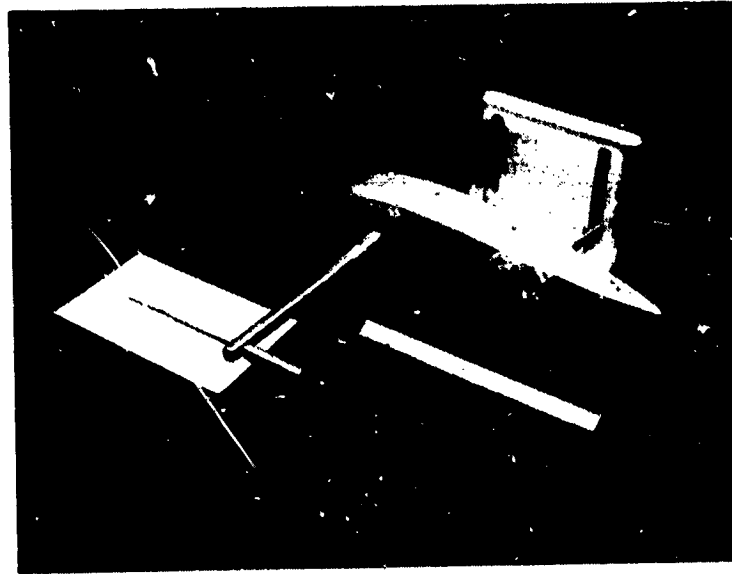


Figure 18.- Probe traversing mechanism.

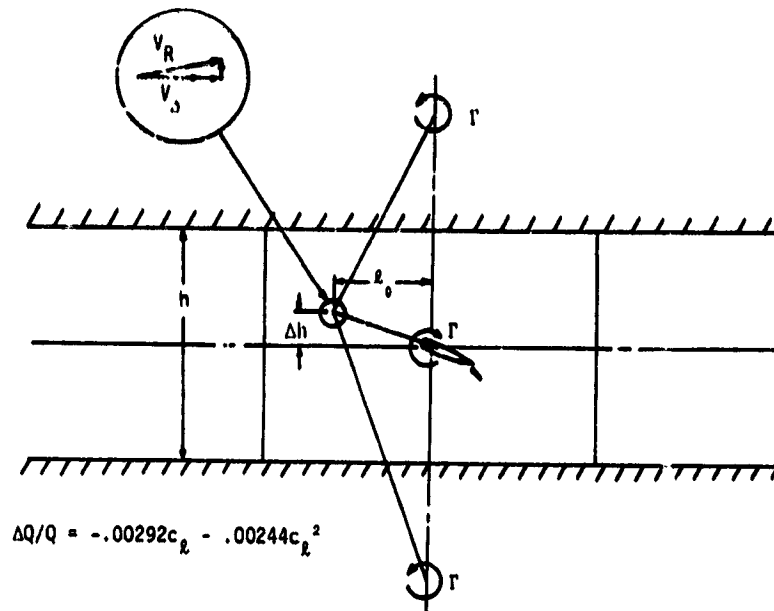


Figure 19.- Dynamic-pressure correction for wall static-pressure error.

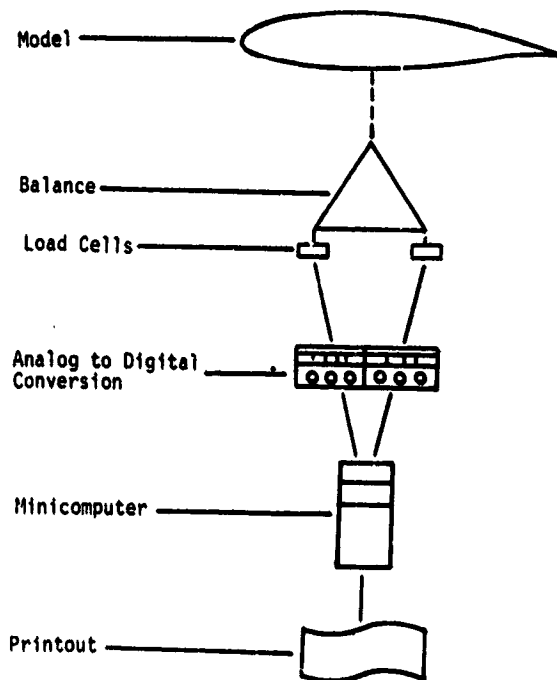


Figure 20.- Force data-reduction system.

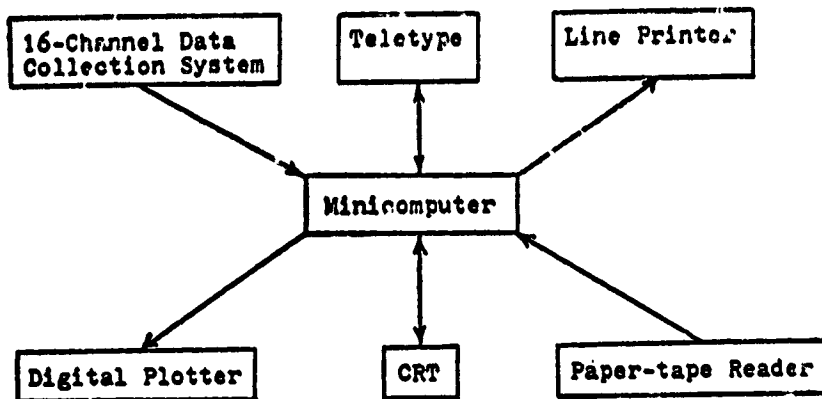


Figure 21.- Elements of the configure !

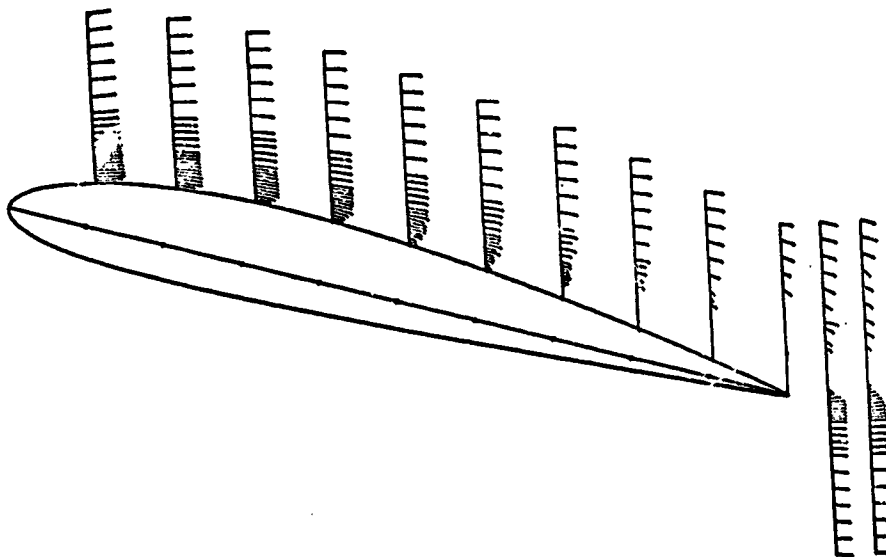


Figure 22.- Sample velocity field plot.

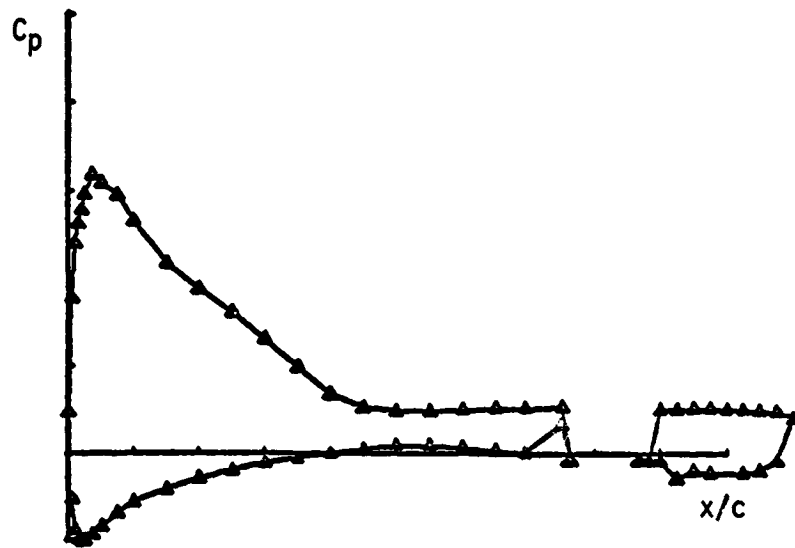


Figure 23.- Sample pressure-distribution plot.

APPLICATION OF THE LASER VELOCIMETER TO
AIRFOIL RESEARCH

Danny R. Hoad*
NASA Langley Research Center

SUMMARY

A laser velocimeter (LV) was installed in the Langley V/STOL tunnel to measure the velocity field about a wing with a NACA 0012 airfoil section. These measurements were compared at low angle of attack with a two-dimensional viscous-flow prediction program. The velocity field over the wing in a fully stalled condition was also measured by the LV. The unique ability of the LV to measure absolute flow magnitude and direction without prior knowledge of general flow direction was demonstrated in the complex separated reverse flows near the wing upper surface at the high angle of attack.

The general characteristics of the flow field over the stalled wing were substantiated by a vapor screen flow visualization technique.

INTRODUCTION

The laser velocimeter (LV) is a relatively new device to measure fluid velocities. It is unique with its capabilities of obtaining these measurements in flow conditions where conventional devices either cannot obtain measurements or would seriously influence the measurement due to the presence of the device. This fact indicates that it is a viable tool to determine velocity field conditions about an airfoil, and is particularly important near the surface where a conventional probe's presence would induce velocity components, thereby biasing the measured data.

The performance of an airfoil is typically judged by body force measurements or surface pressure measurements. In fact, two-dimensional prediction techniques are designed to estimate the local surface pressures as a prime objective. One such prediction technique is described in reference 1. It has been shown to accurately predict the surface pressures on a single element airfoil at low angles of attack.

The performance characteristics of the NACA 0012 airfoil are well-defined. It is not the intent of this paper to present anything new about the airfoil. Because of its application in the aerospace industries, particularly on helicopters, it was chosen as the baseline model to demonstrate the application of the LV to airfoil flow-field research.

* Structures Laboratory, AVRADCOM Research and Technology Laboratories

SYMBOLS

The axes used for this investigation are presented in figure 1. The velocity measurement position was referenced to the airfoil chord line, and the velocity measurement magnitude was referenced to the free-stream direction. The units for the physical quantities defined in this paper are the International System of Units. Most quantities were measured in this system; however, some were measured in the U. S. Customary Units and converted by using factors given in reference 2.

c	wing chord, 0.3048 m
U_f	local velocity component, in direction of free-stream velocity, m/sec
U_R	local total velocity, $\sqrt{U_f^2 + V_f^2}$, m/sec
U_T	free-stream velocity determined from pitot-static probe, m/sec
V_f	local velocity component, perpendicular to direction of free-stream velocity, m/sec
X_c, Y_c	coordinate axis relative to wing chord
x_c	distance downstream from airfoil leading edge along chord, m
y_c	distance above and perpendicular to wing chord, m
α	wing angle of attack, deg

APPARATUS

A fringe-type LV optics system operating in the backscatter mode was used for these tests. A sketch of the optics system is presented in figure 2 and a photograph is presented in figure 3. A high-speed burst counter was used to measure the period of the high-frequency signal contained in the burst from a particle traversing the sample volume. LV system control, data acquisition, and data reduction were handled by a minicomputer. A complete description of the LV optical system, electronics system, and data acquisition and reduction is available in reference 3.

The model used in this investigation was a simple straight wing. It had a span of 2.438 m, a chord of 0.3048 m, and a NACA 0012 airfoil section. Velocity measurements were made at center span to obtain two-dimensional characteristics. The wing was supported by struts from the floor near the tunnel center line with no balance measurements taken. The location of the strut mount to the wing was chosen as far outboard as structurally feasible to minimize flow disturbance at the wing center line. A photograph of the model with crossing laser beams is presented in figure 4.

This investigation was conducted in the Langley V/STOL tunnel at a nominal free-stream Mach number of 0.15. The Reynolds number based on the wing chord was approximately 1×10^6 . Local flow velocities were measured about the center line at two geometric angles of attack: (1) at $\alpha = 0^\circ$ in order to compare with a two-dimensional theoretical prediction technique at a condition for which the flow is two-dimensional and the theory is appropriate, and (2) at $\alpha = 19.40^\circ$ in order to investigate the flow-field characteristics over the separated airfoil at a constant angle of attack. A pitot-static probe was mounted 2.5 m below and 1 m ahead of the wing center line to provide accurate reference of the free-stream tunnel dynamic pressure. A hygrometer was used to obtain wet-bulb temperatures, and total temperature was measured in the settling chamber. Thus, the tunnel air density could be calculated and, with dynamic pressure measurements, the tunnel velocity could be accurately calculated.

DISCUSSION

The velocity measurements at each measurement location were first reduced to histogram form. These data for the wing at $\alpha = 0^\circ$ (relative to tunnel geometric center line) along with a description of data reduction technique, histogram interpretation, and complete error analysis can be found in reference 3.

Free-stream velocity measurements were obtained with the LV with no wing in place at the location of the wing center line. These data indicated an average upwash angle of 0.6° (relative to tunnel geometric center line). The wing was installed with the chord line parallel to the test-section center line; therefore, the effective angle of attack was assumed to be 0.6° .

Prediction Technique

The external forces generated on a body in a fluid are manifested in the velocity distribution of the fluid about the body. In developing a prediction technique, the calculations at the surface of the body are verified with conventional pressure and force measurements. Reference 1 presents an excellent comparison with measured surface pressures for this viscous-flow prediction. Since the local surface pressures are computed from predicted local surface velocities, it is justifiable to question the validity of the predicted velocities away from the surface. The need to verify these predicted velocities is evident. The use of conventional probes near the surface raises questions about the accuracy of the measurement with interferences caused by the presence of the probe. It was determined that the LV was a device capable of measuring this flow field without inducing any interference since nothing was present in the field but the wing and light beams.

The theory for this prediction technique (ref. 1) involves an iterative procedure which first obtains an inviscid-flow solution for the basic airfoil. It computes a boundary-layer solution based on the inviscid-flow solution and constructs a modified airfoil by adding the boundary-layer displacement

thickness to the original airfoil. It obtains the inviscid solution for the modified airfoil and repeats these steps until appropriate convergence criteria are satisfied. The field point velocities away from the surface are then computed from the basic vorticity distribution along the modified airfoil.

Experiment-Theory Comparison at $\alpha = 0^\circ$

The velocity vectors as measured by the LV for the wing at a geometric angle of attack of 0° are presented in figure 5. Each velocity vector (arrow) is an average of an ensemble of measurements taken over a short period of time at the desired location. This arrow plot indicates the relative location of the velocity measurements, magnitude, and angle of the velocity vector. The velocity magnitude and direction are indicated by the length and orientation of the arrow. The tunnel free-stream magnitude and direction reference are provided in the lower left corner of the figure. The position of the velocity measurement is marked by the tail end of the arrow.

The velocity measurements were obtained by positioning the sample volume at a desired chordwise station (x/c) and incrementing the entire optics package downward along this chordwise station. This was accomplished remotely and was completely controlled by the minicomputer. Four of these series of measurements (scans A, B, C, and D from fig. 5) are presented in more detail in figure 6. This figure presents a comparison between LV-measured velocities and the two-dimensional viscous-flow prediction. The comparison is presented with the resultant velocity nondimensionalized by tunnel free-stream velocity as a function of the vertical position of the measurement nondimensionalized by the wing chord. The scans near the leading edge have velocity gradients which are the most difficult to predict. The free-stream upwash angle without wing or supports was measured at 0.6° at this Mach number. Typically, flow angularity is affected by a model's presence. It is normally determined by model upright and inverted angle-of-attack ranges. Comparison of balance data from these two conditions provides the total flow angularity. It is very difficult to obtain this type of measurement with discrete velocity measurements in the presence of the model. Since no balance measurements were obtained on this investigation, there is some uncertainty in the effective angle of attack of the wing. Predicted velocities were calculated first using the measured 0.6° tunnel flow angle without the wing. These are presented as dashed lines with maximum discrepancies on the order of 6 percent. Calculations were repeated with a 1-degree shift in angle of attack to provide an assessment of the effect of uncertainty in this measurement. These calculations are presented as solid lines with $\alpha = -0.4^\circ$ and indicated better agreement with theory. It is obvious in these comparisons that the precise measurement of these velocities depended on the precise determination of the effective angle of attack of the wing. It is justified to say, however, that these data provide a quantitative and qualitative measure of the accuracy and applicability of LV measurements about a surface submerged in a fluid flow situation.

Airfoil at $\alpha = 19.4^\circ$

An arrow plot of the mean velocity field about the airfoil at $\alpha = 19.4^\circ$ is presented in figure 7. Each velocity vector is presented with the length of the arrow indicating magnitude and direction of vector relative to the airfoil. It is obvious from this figure that the airfoil is in a fully separated condition from leading edge to trailing edge. The shear layer region between the free-stream and the separated turbulent area over the wing is broad, but easily discernible. The velocity field in the separated region indicates the existence of a large recirculating eddy with reverse flow near the airfoil surface. The velocity fluctuations within the shear layer were large; however, in the reverse flow region the velocity fluctuations were smaller. A dashed line is provided indicating the approximate location of zero velocity in the separated region. At the trailing edge (see fig. 8), a very sharp shear layer is evident with low, reverse flow velocities generated near the airfoil upper surface and with nearly free-stream velocity from the lower surface. The spatial distance across this shear layer is on the order of $0.005 y_c/c$. The reverse flow in the wake region above the airfoil is also evident.

These velocity measurements were obtained without prior knowledge of the direction of the flow at each measurement point. The LV is unique in this capability unlike conventional probes, which require this information to reduce ambiguity primarily caused by support structure interference.

Flow Visualization of Airfoil at $\alpha = 19.4^\circ$

To visualize the flow patterns over the airfoil, a thin plane of light (approximately 2 cm thick), perpendicular to the wing trailing edge and parallel to the free-stream direction, was projected from behind the wing along the centerspan. The only flow patterns visible were those depicted by smoke traversing this plane. The patterns were recorded on video tape with still pictures taken later from a television monitor. The reversed recirculating flow in the separated region was observed, thus confirming the directions and general flow patterns as measured by the laser velocimeter.

One of the pictures taken from the television monitor of the flow is presented in figure 9. The television camera which recorded this frame was not positioned orthogonal to the wing chord due to difficulties in locating the camera mount. The view is from the left rear. The airfoil section evident is the tip and not the airfoil section at the location of the vapor screen. The leading edge of the airfoil at the location of the vapor screen is near the leading edge of the separated region. The trailing edge of the airfoil at this location is at the trailing edge of the bright streak. This streak is the reflection of the sheet of light from the wing upper surface.

The separated region is evident in this figure, although the reverse flow just above the airfoil is not. The sharp shear layer at the trailing edge can be seen. With better photographic techniques, the vapor screen technique with the laser as a powerful light source can be a very useful research tool in

assessing the character of the flow field as measured by the laser velocimeter.

CONCLUSIONS

A laser velocimeter was installed in the Langley V/STOL tunnel to measure the velocity field about a straight wing with a NACA 0012 airfoil section. The wing was installed at zero angle of attack to provide data to compare with a well-accepted two-dimensional viscous-flow prediction program. These results provide a qualitative confidence level in the accuracy of the LV measurements. The wing was also installed at a fully stalled condition ($\alpha = 19.4^\circ$) to characterize the flow field in the separated region.

The results of the investigation indicated that

1. The laser velocimeter is an effective and accurate instrument for measuring the velocity field about a surface.
2. The precision of the laser velocimeter for the low angle-of-attack data in this case depended on the precise determination of the effective angle of attack of the wing in the tunnel.
3. The separated region over the wing in the fully stalled condition was well-defined. The shear layer between this region and the free stream was broad and highly turbulent; however, in the reverse flow region the measurements indicated relatively lower turbulent characteristics.
4. The measurements in the reversed flow region demonstrated the unique capability of the laser velocimeter for measuring velocity magnitude and direction without prior knowledge of the flow direction.
5. The trailing-edge measurements demonstrated the capability of the laser velocimeter to measure the velocity characteristics across a very sharp velocity gradient.
6. The vapor-screen technique with the laser as a powerful light source was demonstrated to be effective in assessing the character of the laser velocimeter measured flow characteristics.

REFERENCES

1. Smetana, Frederick O.; Summey, Delbert C.; Smith, Neill S.; and Carden, Ronald K.: Light Aircraft Lift, Drag, and Moment Prediction - A Review and Analysis. NASA CR-2523, 1975.
2. Mechtly, E. A.: The International System of Units - Physical Constants and Conversion Factors (Second Revision). NASA SP-7012, 1973.
3. Hoad, Danny R.; Meyers, James F.; Young, Warren H., Jr.; and Hepner, Timothy E.: Laser Velocimeter Survey About a NACA 0012 Wing at Low Angles of Attack. NASA TM-74040, 1978.
4. Hoad, Danny R.; Meyers, James F.; Young, Warren H., Jr.; and Hepner, Timothy E.: Correlation of Laser Velocimeter Measurements Over a Wing With Results of Two Prediction Techniques . NASA TP-1168, 1978.

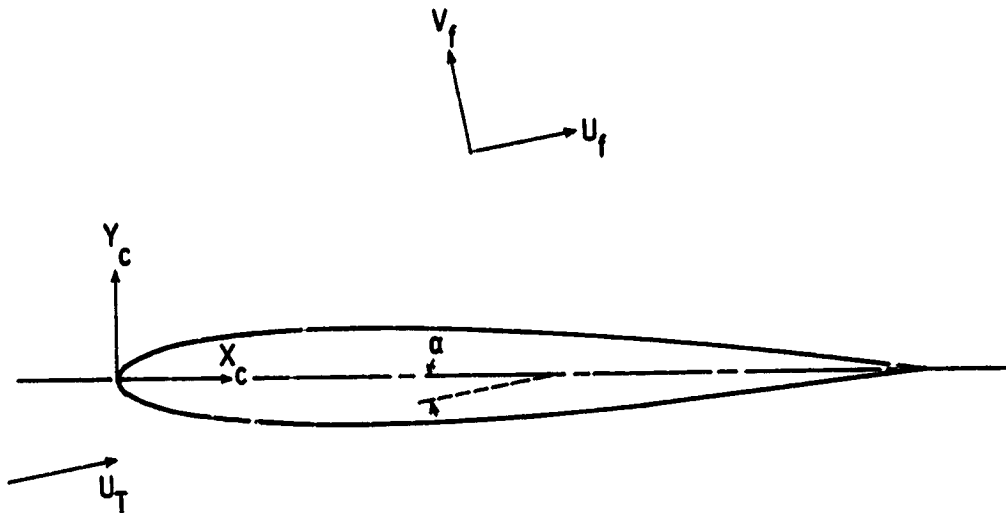


Figure 1.- Sketch of axis system used including direction of velocity components computed.

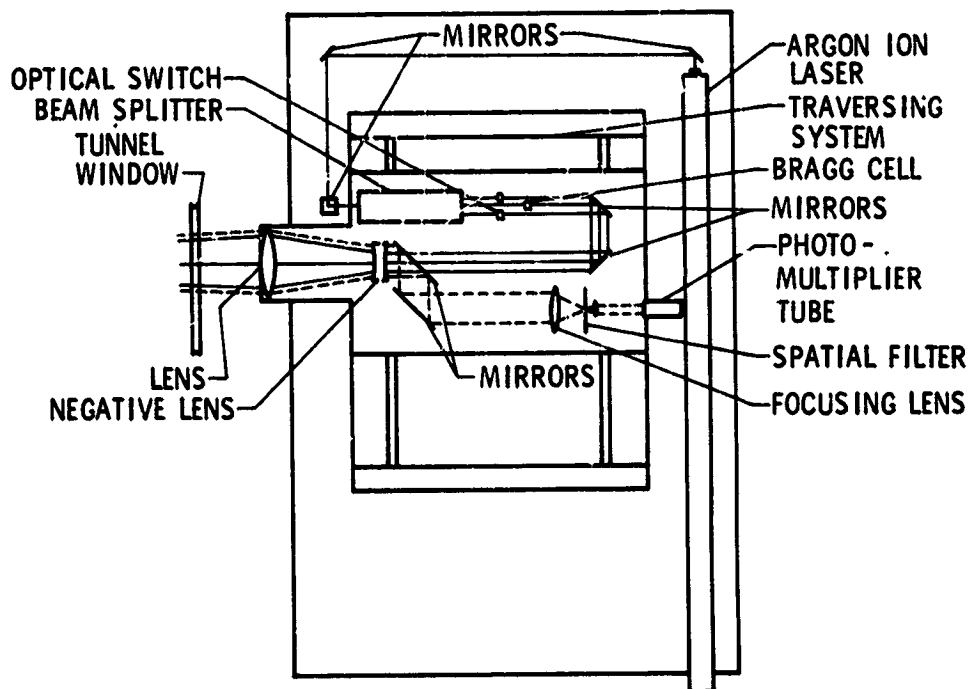


Figure 2.- Schematic of laser velocimeter optics.

ORIGINAL PAGE
OF POOR QUALITY

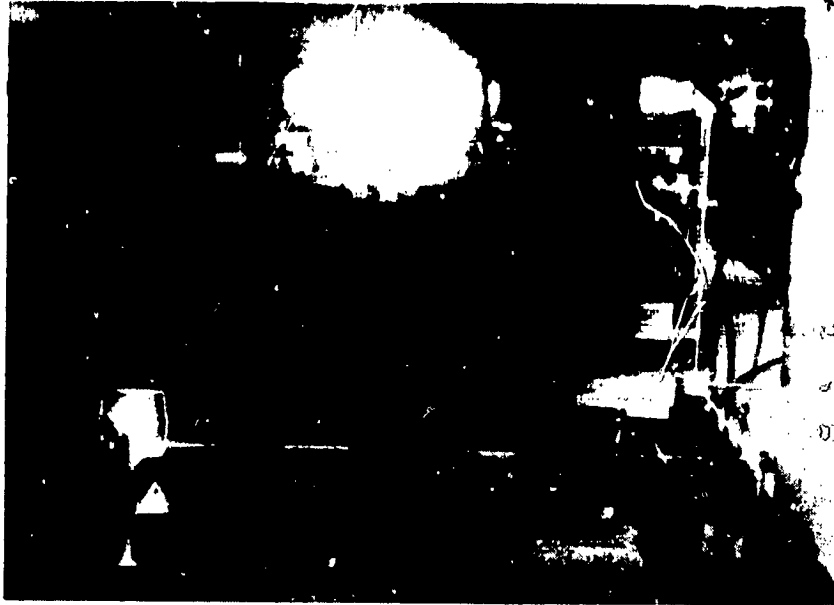


Figure 3.- Photograph of laser velocimeter optics.

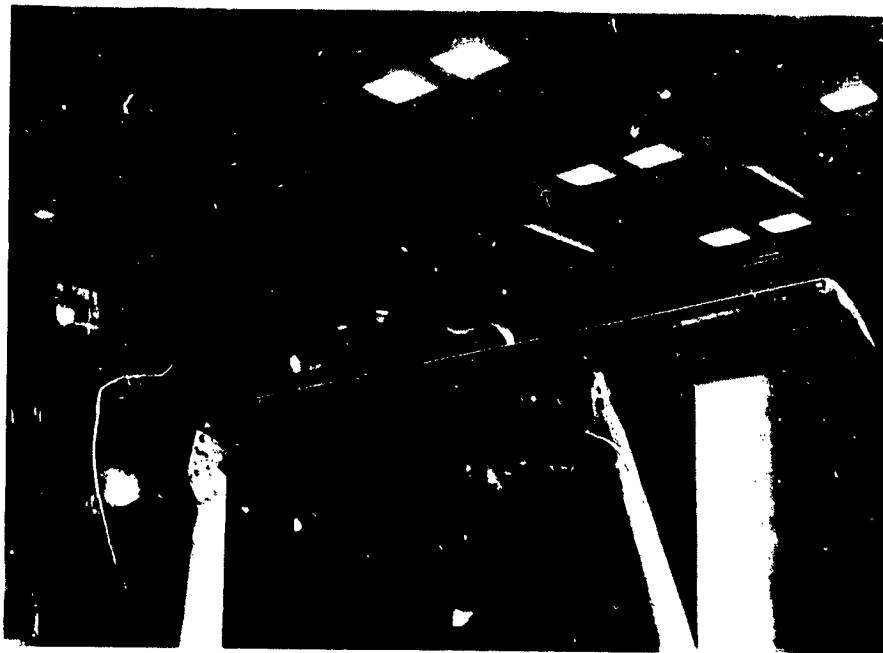


Figure 4.- Straight wing with NACA 0012 airfoil section installed in Langley V/STOL tunnel with crossing laser beams.

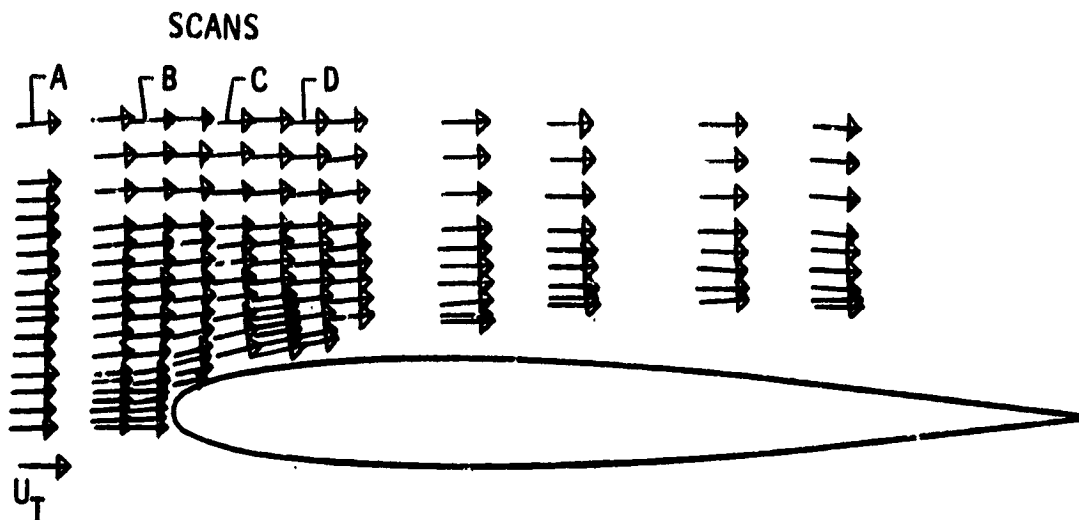


Figure 5.- Velocity vectors computed from measurements over wing.

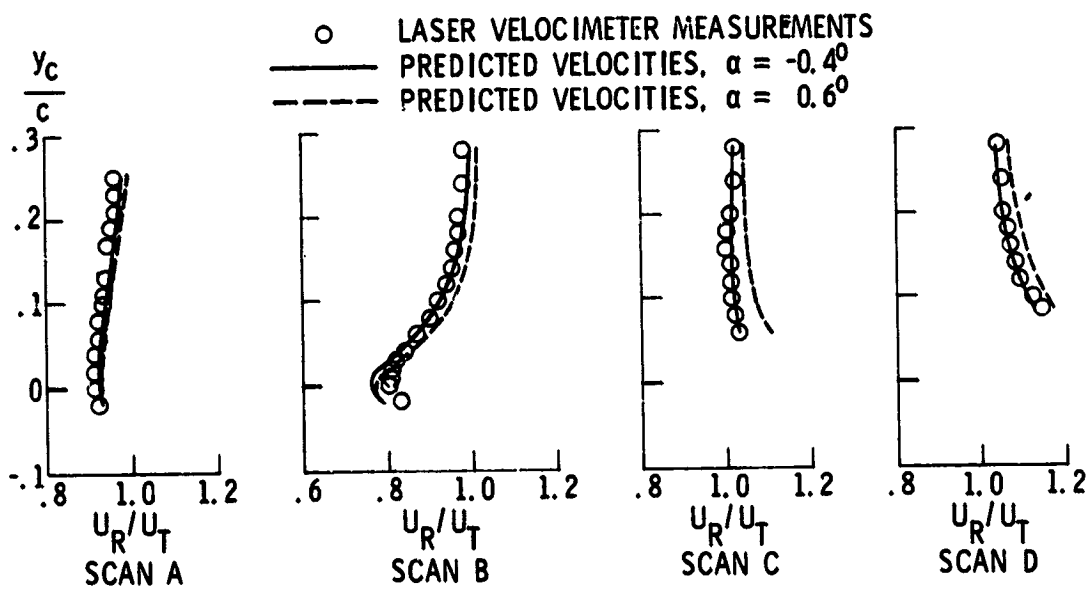


Figure 6.- Comparison of laser velocimeter flow-field velocity measurements with a two-dimensional viscous-flow prediction program.

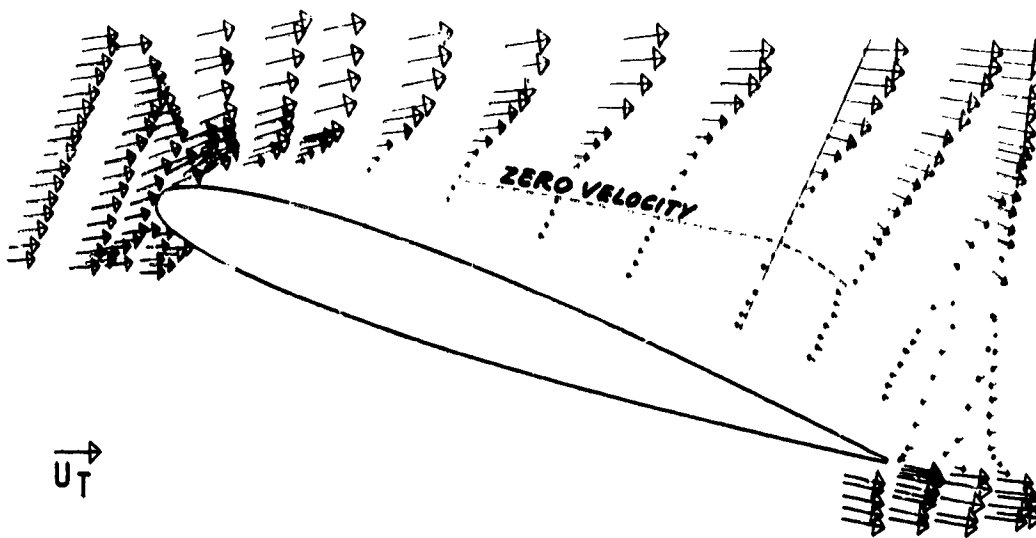


Figure 7.- Velocity measurements over the stalled wing ($\alpha = 19.4^\circ$), free-stream Mach number = 0.13.

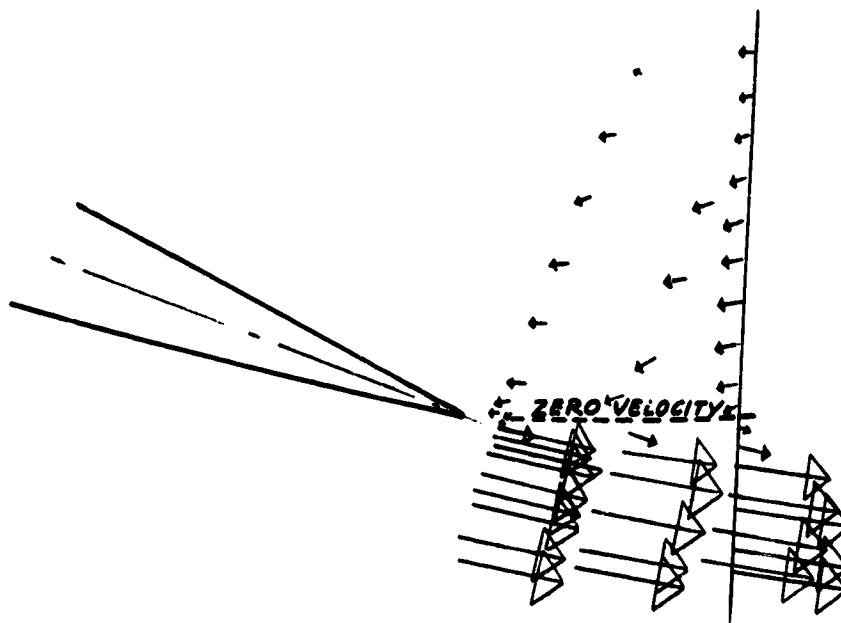


Figure 8.- Velocity measurements at trailing edge of wing at $\alpha = 19.4^\circ$.



Figure 9.- Flow patterns over wing depicted by vapor-screen flow-visualization technique.

ORIGINAL PAGE IS
OF POOR QUALITY

APPLICATIONS OF DYNAMIC MEASUREMENT TECHNIQUES
TO WIND-TUNNEL TESTING

F. K. Owen*
Consultant

SUMMARY

The uses of laser doppler velocimeter, hot wire and surface hot film techniques in the study of turbulent flows are described and data obtained in compressible flows are discussed. Applications are illustrated with measurements of wind-tunnel freestream turbulence characteristics and with data obtained in transitional, turbulent and separated shear flows. A new method which has been developed for the study of time dependent and unsteady turbulent flows is also presented.

INTRODUCTION

Although the title of my paper suggests a broad subject area, in the interest of conciseness, I have decided to restrict my comments to the areas in which I have had direct experience and to stress measurements which I feel are particularly relevant to laminar flow and unsteady aerodynamic research. Thus, the paper will be restricted to applications of hot wire and hot film anemometer and dynamic pressure measurements and to laser velocimeter measurements of unsteady flowfields.

At the present time little is known about the influence of freestream flow turbulence on steady and dynamic measurements on models in wind tunnels at transonic speeds. Indeed, few measurements have been made of the characteristics of freestream unsteadiness in transonic wind tunnels. The result is that information on velocity, pressure and temperature fluctuations, their amplitude, frequency, phase relation and space-time correlation, is lacking. This information is needed if we are to accurately assess the relationship between wind-tunnel and flight behaviour.

Perhaps the major open question is the influence of freestream disturbances on model boundary-layer transition. Recent developments in boundary-layer transition research, particularly those of the NASA Transition Study Group, have stressed the dominant role freestream fluctuations have on model boundary-layer stability at transonic and supersonic speeds. Not only do the external fluctuation amplitudes dominate transition but their spectral characteristics are particularly significant. This importance of the spectrum of the external

*P.O. Box 1697, Palo Alto, CA 94302.

disturbances was first demonstrated by Spangler and Wells at subsonic speeds. They found a much higher transition Reynolds number on a flat plate than did Schubauer and Skramstad even though the freestream disturbance amplitudes were similar in the two experiments. However, the spectra of the freestream disturbances were radically different.

The influence of flow unsteadiness on shock-wave—boundary-layer interaction is also determined by the connection between boundary-layer development and transition location. For example, freestream turbulence can determine whether the shock causes laminar boundary-layer separation with or without transition or whether the interaction is with a turbulent boundary layer. Freestream flow unsteadiness may also induce shock-wave oscillations.

Experiments on flat plates with turbulent boundary layers at zero pressure gradient have shown the influence of freestream turbulence on boundary-layer development. An increase in freestream turbulence level leads to an increase in skin friction coefficient, a fuller velocity profile and a thicker boundary layer. Measurements show that a small increase in free-stream turbulence has the same effect on the shape of the boundary-layer velocity profile as a fractional increase in Reynolds number roughly 60 times as great. Calculations suggest that similar effects occur in flows with moderate pressure gradients, with an increase in turbulence level delaying separation onset.

However, the flow around the wing of a wind-tunnel model goes through regions of high acceleration and deceleration which distort the turbulence, the further from freestream conditions the more anisotropic it becomes. It is possible that the interaction between the distorted turbulence and the shear layer could well be quite different from flat plate observations. In the case of dynamic measurements of wing buffeting, turbulent pressure fluctuations can mask the data and can, therefore, be difficult to detect. There are also indications that buffet boundaries change with changing turbulence level, presumably due to a movement of the mean shock position.

It should be borne in mind that the object of wind-tunnel testing is to simulate atmospheric flight so that the key question remains whether the levels and scales of turbulence in the atmosphere have any significant effect on boundary-layer structure. Since it is to be expected that the most energetic scales will be many times the boundary-layer thickness even on large transport aircraft, the primary influence on boundary layers in flight will probably be on the large-scale unsteadiness of the flow.

Thus, it is essential that the freestream characteristics of wind tunnels used in advanced aerodynamic testing be thoroughly documented. In this way, disturbance levels and scales can be assessed in relationship to those thought likely to be encountered in flight.

Symbols are defined in an appendix.

DISCUSSION

Facility Disturbance Characteristics

Since there is very little information available on the structure of the freestream turbulence, the scales involved, their magnitude and how they vary from tunnel to tunnel, an investigation was undertaken (ref. 1) in which transition data and hot wire turbulence and pressure fluctuation levels were measured in two wind-tunnel facilities namely the NASA Ames 3.5 ft. and the Langley 18 in. Variable Density Wind Tunnels.

Fig. 1 shows rms values of the mass flow and total temperature fluctuations in the Ames 3.5 ft. wind tunnel calculated assuming a correlation coefficient of -1.0 . Due to the scatter in the data, no trends in turbulence level with operating pressure could be established. However, the mean values indicated in Fig. 1, i.e., mass-flow and total-temperature fluctuations of 2.65 and 0.83 per cent, respectively, should be representative of the freestream turbulence levels over the unit Reynolds range.

These data show the types of measurements that can be obtained in supersonic flow. Although data interpretation is a little more complex, similar techniques can be applied to transonic flows. However, it must be borne in mind that rms intensities give little if any indication of the turbulent scales involved. This information can be obtained from power spectra and space-time correlation measurements of the turbulent fluctuations. The pressure disturbance spectra, presented in Fig. 2, show that, although most of the energy is concentrated at low frequencies, the spectra levels are quite different at high frequencies, reflecting expected differences in fluctuation scale due to wind-tunnel size.

Some interesting features of the freestream disturbances have been determined from two-wire, space-time correlation measurements. Streamwise disturbance convection velocities were measured in both facilities and found to be independent of scale and equal to 70% of the freestream velocity. This result is in good agreement with an extrapolation of Laufer's lower Mach number data. Fig. 3 shows the variation of the optimum spatial correlation functions in the streamwise and lateral directions as measured on the tunnel centerline in the Ames facility. These results, which indicate that the disturbance length scales (calculated for $R_{xx} = 1/e$) are several times their width, are consistent with the concept of radiated sound from the sidewall turbulent boundary layer; i.e., the indicated ratio of streamwise scale to lateral length scale of approximately 3.0 agrees with that predicted assuming wall boundary-layer source propagation angles originating upstream of the test section where the source Mach number was approximately 3.0. These streamwise fluctuation scales correspond to overall wind-tunnel wall boundary-layer source lifetimes of several boundary-layer thicknesses.

Recent cross-correlation measurements have also been made of the test section and diffuser static pressure fluctuations in the Ames 12 ft. wind tunnel. Since the probe separation was sufficient (approximately 8 metres)

to make the correlation of the background turbulence negligibly small, correlations of the acoustic modes could be directly measured. With the diffuser probe output delayed, it is apparent that there is a coherent acoustic mode which propagates upstream. The propagation speed is determined to be approximately equal to the speed of sound minus the wind-tunnel freestream velocity.

Boundary-Layer Transition

Apart from the complex coupling of the usually unknown freestream turbulence spectra and model boundary-layer transition a major source of scatter in transition data can be attributed to inconsistent choice of transition "point" indicated by different techniques, mostly locating positions near the end of transition, which generally have a strong Mach number and unit Reynolds number dependence. A more complete picture of transition dependence on these parameters can be obtained from experiments in which the positions of the beginning and end of transition are accurately determined. It is of interest to note that transition data reported for supersonic and hypersonic flows are not generally based on observations of turbulent spots but rather some macroscopic quantity such as skin friction, heat transfer, or surface pitot pressure, whose departure from laminar values can be detected only when the turbulent intermittency is appreciably greater than zero.

Because of the importance of correctly determining the onset and extent of boundary-layer transition, techniques which do not disturb the flowfield and which respond to microscopic changes must be used. Such a technique, i.e., one that detects turbulent bursts at the model surface, is the surface hot film gauge. An example of the variation of the rms thin film gauge output over a range of unit Reynolds numbers on a cone model in the Ames 3.5 ft. wind tunnel is shown in Fig. 4: The curve clearly shows a rise from the laminar to the turbulent level, with an intermediate peak. These curves enable three distinct points in the transition region to be accurately and consistently determined: namely, the onset of transition, defined as the point where the rms signal begins to increase from its laminar value (this onset of intermittency can be clearly seen on the oscilloscope traces); the peak rms signal, which coincides with the point of maximum turbulent burst frequency (ref. 2); and the end of transition. Examples of the characteristics of the film voltage fluctuations through the transition region are also shown on Fig. 4.

Measurements of this type enable the effects of Mach number and unit Reynolds number on the beginning and length of transition to be established more precisely than with previously used methods. Examples are given in refs. 1 and 2.

Turbulence Structure Measurements

As in the freestream, turbulence intensity measurements of the mode fluctuations can also be obtained across compressible turbulent shear layers. Once again, however, this time from the turbulence modelling viewpoint, information on the turbulence scales and lifetimes are of crucial importance.

Since turbulent flows vary not only in time but also in space, their investigation must involve an examination of both the spatial and temporal statistical structure. Space-time correlations can make a contribution to this study since they give evidence of the heredity and structure of turbulence, as well as values of the convection velocities of the vorticity and entropy modes compared with the average mass transport velocities.

Examples of both auto and space-time correlations in a compressible turbulent boundary layer (ref. 3) are given in Figs. 5 and 6. These data were obtained on a cone-ogive-cylinder model in the Ames 3.5 ft. wind tunnel.

Fig. 5 shows the autocorrelation of the fluctuating signals on the cylindrical portion of the model 176 cm from the cone apex, at two positions in the boundary layer and in the far field. It can be seen that there is a marked variation of energy distribution with frequency across the boundary layer and that, as expected, the far field contains proportionately much less energy in the high wave number range than the wall region.

The results of a series of filtered (4 kHz) cross-correlation measurements at several separations in the boundary layer are shown in Fig. 6. It can be seen that each cross-correlation curve reaches a maximum at a non-zero value of the time delay, clearly indicating the presence of convection. The amplitude of this maximum is a function of the wire separation distance. A convection velocity of these disturbances may be determined from the time delay at which the maximum of a particular cross-correlation occurs.

The peaks of the cross-correlations obtained for various values of wire separation distance represent the autocorrelation in a reference frame moving with the disturbances. They are, therefore, a measure of the lifetime of the disturbance pattern as it is swept along with the mean flow. The long turbulence lifetimes which can be inferred from these space-time correlation measurements (refs. 3 and 4) illustrate a major objection to turbulence models based on local flow conditions. It cannot be assumed that turbulence is uniquely related to local conditions, and flow history must be considered, especially when attempting to calculate non-equilibrium flows.

Turbulent Boundary-Layer Separation

Turbulent separated flows occur in many types of engineering configurations. They may be unintentional features of some classes of equipment or they may be deliberately introduced. But in all cases such flows can have a significant effect on engineering performance. Furthermore, additional complications are added by the unsteady aspects of the turbulent boundary-layer separation and reattachment processes. Despite the fact that these flows have been extensively studied, detailed information regarding the unsteady nature of turbulent separation is practically nonexistent for high-speed compressible flows. Conventional "time averaged" measurements such as surface pressure, skin friction, heat transfer, and pitot pressure surveys cannot supply this information. However, once again thin platinum films mounted flush with the model surface provide basic information on the significant

unsteady character of turbulent boundary-layer separation. The fluctuating voltages from these films provide measurements related to the flow character above the film.

Two typical variations of the rms thin film voltage fluctuations through a shock-wave—boundary-layer interaction region (ref. 5) are shown in Fig. 7. Also indicated are the measured pressure distributions for the two cases. Data are shown for an attached flow (shock-wave generator wedge angle of 7.5°) and a separated flow (wedge angle of 15°). For both flows detailed pitot pressure surveys, surface skin friction and surface oil flow data were obtained. These mean measurements indicated attached flow for the 7.5° wedge angle and a substantial region of separated flow for the 15° wedge angle. (The region of measured negative wall shear, as determined from a floating element skin friction balance, is indicated on the figure.) The thin film results show a marked difference between the attached and separated flows. Normalized power spectra of the fluctuations in the turbulent separated region and after reattachment are shown in Fig. 8 where it can be seen that the energy increase in the separated region is confined to a narrow band around 15 kHz while the increased energy due to the pressure rise after reattachment is broad band. Power spectra containing this energy peak were obtained at measuring stations between 183 and 194 cm from the model tip. Similar measurements were also obtained for the turbulent attached flow and for a laminar separated flow (at reduced wind-tunnel total pressure). These results showed a smooth power spectra with no energy peak. Since such an energy peak was not evident in these cases, it is felt this peak is associated with turbulent separation unsteadiness. The scale of this unsteadiness, based on measured convection velocities and the measured peak frequency, is of the order of the length of the separated region.

The decrease and subsequent increase in rms voltage after the first peak for the separated flow (Fig. 7) can also be explained by this unsteadiness. This minimum rms region, which is where the measured skin friction was most negative, corresponds to the region where the flow remains separated most of the time and least affected by the increased voltage fluctuations due to the unsteadiness of the separation onset and reattachment regions.

Similar observations of shock induced separation unsteadiness have also been made during transonic airfoil testing. An example, provided by D. A. Johnson of NASA Ames, Fig. 9, shows a shadowgraph of a 64A010 airfoil section at an angle of attack of 6 degrees and freestream Mach number of 0.6 in the Ames 2 x 2 ft. wind tunnel. Included in Fig. 9 is a power spectrum of the output from a transverse laser schlieren system in the region of the shock wave. The peak around 1400 Hz is thought to be associated with similar, larger scale motions of the separation zone.

Thus, from the turbulence modelling viewpoint, it is important to determine details of the small- and large-scale contributions to the total turbulent field.

Measurement of Unsteady Flowfields

Considerable attention and effort have been directed to the area of conditional sampling as a means of revealing flow features which appear intermittently rather than continuously yet still have an important influence on flow structure and development. However, these efforts have all been restricted to experiments in which the flowfield sensor has a continuous output which itself can be used to generate the criteria for the conditional averages; so that, to date, measurements have of necessity been restricted to unidirectional shear flows in which, for example, standard hot wire anemometry techniques can be used. Whole classes of flows, namely recirculating and unsteady wake flows have, therefore, been neglected. In these flows, it is extremely difficult to generate reliable analog or digital outputs with conventional flow instrumentation, since they are extremely sensitive to probe interference and since linearized data interpretations are not accurate in such highly turbulent flows. Thus, reliable quantitative information can only be obtained using nonintrusive linear techniques.

In ref. 6 a combined nonintrusive surface thin film gauge and laser velocimeter technique was described which can be used to obtain new information on the phase averaged and turbulent structure of time-dependent flowfields.

The experiments were conducted in the Ames 2 x 2 ft. wind tunnel on a circular cylinder of aspect ratio 24:1 in crossflow over a range of Reynolds numbers in the subsonic and transonic regime. The cylinder was instrumented with constant temperature surface hot film gauges of the type used in ref. 2. The dynamic gauge response (greater than 60 kHz with negligible phase distortion) was sufficient to determine the time history of the vortex shedding. These gauge outputs were used to trigger a forward scatter laser velocimeter which generated conditionally sampled axial and vertical velocity distributions in the unsteady vortex flow behind the cylinder. Detailed information obtained by this new sampling technique on the time-dependent mean flowfield behind a circular cylinder and of the large- and small-scale turbulent structure of its wake were presented.

To illustrate some of these measurements, data taken in the wake 2.5 diameters downstream of the cylinder ($x/d = 2.5$) are shown in Fig. 10. On the axis, positive and negative vertical velocities are equally probable. Thus, conventional averaging would give a time-averaged velocity close to zero and a large rms velocity fluctuation level which is, of course, due to instantaneous changes in induced mean flow velocity caused by alternate vortex shedding. Any time-dependent information would be lost. Above the centerline ($y/d = 0.5$), the probability density function is still bimodal, although negative vertical velocities predominate, as here the local flow is determined more by vortex shedding from the upper surface. In this case, conventional averaging would indicate a small negative vertical velocity, a large rms and, once again, time-dependent information would be lost. Below the axis ($y/d = -0.5$), positive vertical velocities induced by vortex shedding from the lower surface are more likely, but again, conventional averaging would lose the true nature

of the time-dependent local flowfield. However, outside the wake (e.g., $y/d = -1.75$), where single-peaked probability distributions occur, the averaged data are now valid.

To determine the time-dependent nature of the wake, the bimodal velocity distributions must be conditionally sampled using the thin film gauge output. Since the flow repeats itself periodically, we can sample the velocity when the shedding vortices are at some given position in the flow as determined by the time-dependent thin film gauge voltage signature. One cycle later we can sample again, and thus, over many cycles, build up an ensemble average at constant phase. These velocities represent the regular- and small-scale random behavior of the flow at a fixed point in the flowfield with the vortices frozen in some average position. Data obtained throughout the shedding cycle are shown in Fig. 11 where it can be seen that the conditionally sampled vertical velocity variations are approximately sinusoidal, their period corresponding to that of the Strouhal shedding frequency.

Fig. 12 shows a comparison of the axial and vertical rms velocity fluctuation levels measured across the wake at $x/d = 2.5$. As mentioned previously, the apparent vertical velocity fluctuations are extremely high in the center of the wake. However, when phase-sampled, the small-scale turbulence data fall below the axial centerline turbulence measurements. Assuming isotropic small-scale turbulence in the wake, we can infer that there is a vortex-induced contribution to the axial turbulence on the wake centerline. The large differences in the rms vertical velocity data also show the dominance of the large-scale structures in the vertical wake turbulence. It is clearly incorrect to attempt to model these large rms fluctuation levels with techniques that are only valid for small-scale turbulence. In general, it is equally insufficient to attempt to use current turbulence models scaled to match rms velocities measured in the conventional manner in any flow where unsteady phenomena are likely to be encountered, separated flows being a prime example.

CONCLUDING REMARKS

Hot wire, surface hot film, dynamic pressure and laser doppler measurement techniques have been described and their applications in the areas of freestream turbulence, transition, turbulent separated and unsteady flow measurement have been discussed.

With regard to freestream turbulence measurements, it is particularly important that the spectra and length scales of the mode fluctuations be documented in addition to their rms values. Only then can the suitability of wind-tunnel test environments for specific model testing be determined and their relationship to environments likely to be encountered in particular flight envelopes be assessed.

In studies of boundary-layer transition it has been found that a more complete picture of transition dependence on Mach and unit Reynolds numbers

can be obtained by measuring the change in the root mean square of the voltage fluctuation across surface thin film gauges operated at constant temperature. This nonintrusive technique not only enables the beginning and end of the transition region to be located, but also enables the turbulent intermittency distribution through the transition region to be determined in both low- and high-speed flows.

Compressible turbulent boundary-layer measurements have also shown the importance of spectra and length scale measurements of the mode fluctuations. In compressible flows large differences were detected between the mass-flow and total-temperature fluctuations. Not only were the scales different, but their probability densities and skewness were significantly different across most of the boundary layer. Long turbulence lifetimes suggest that future turbulence models must account for flow history especially when calculating non-equilibrium flowfields.

In turbulent separated flows surface thin film gauges have been shown to provide basic information on the significant unsteady character of these flows. Conventional "time averaged" techniques cannot supply this information. The thin film gauges also indicate a greater extent of the separated region since the onset and reattachment locations of separation are intermittent. Time-averaged techniques can only locate regions where the flow is reversed at least 50 per cent of the time while the instantaneous thin film measurements are sensitive to regions which are separated for only a small fraction of time.

A combined surface hot film and laser velocimeter measurement technique which can be used to obtain new information on the structure of time-dependent flowfields has also been described. The data obtained in a cylinder wake show that mean and constant phase-averaged velocities can be determined. In addition, turbulence data can be obtained by conventional and conditional averaging of the velocity fluctuations. These data provide initial details of the small- and large-scale contributions to the total turbulent field.

APPENDIX

SYMBOLS

D	diameter of wind tunnel
d	diameter of cylinder
$e'^2(f), e'^2(o)$	mean square fluctuation levels
f	frequency
P_w	wall static pressure
P_o	stagnation pressure
R_{xx}, R_{zz}	correlation coefficient
Re/m	Reynolds number per meter
rms	root mean square
T_o	stagnation temperature
U, u	streamwise velocity
U_c	convection velocity
x, y	streamwise and vertical coordinates
$\Delta x, \Delta z$	streamwise and lateral separation distances
δ	boundary-layer thickness
ρ	density
τ	time delay
$\langle ' \rangle$	rms value

REFERENCES

1. Stainback, P.C., Wagner, R.D., Owen, F.K., and Horstman, C.C.
"Experimental Studies of Hypersonic Boundary-Layer Transition and Effects of Wind-Tunnel Disturbances." NASA TN D-7453, March 1974.
2. Owen, F.K. "Transition Experiments on a Flat Plate at Subsonic and Supersonic Speeds." AIAA J., Vol. 8, No. 3, p. 518, March 1970.
3. Owen, F.K. and Horstman, C.C. "On the Structure of Hypersonic Turbulent Boundary Layers." J. Fluid Mech., Vol. 53, pt. 4, pp. 611-636, June 1972.
4. Owen, F.K., Horstman, C.C., and Kussoy, M.I. "Mean and Fluctuating Flow Measurements of a Fully-Developed, Non-adiabatic, Hypersonic Boundary Layer." J. Fluid Mech., Vol. 70, pt. 2, pp. 393-413, 1975.
5. Horstman, C.C. and Owen, F.K. "New Diagnostic Technique for the Study of Turbulent Boundary Layer Separation." AIAA J., Vol. 12, No. 10, p. 1436, 1974.
6. Owen, F.K. and Johnson, D.A. "Measurement of Unsteady Vortex Flowfields". AIAA paper no. 78-18, AIAA 16th Aerospace Sciences Meeting, Jan. 1978.

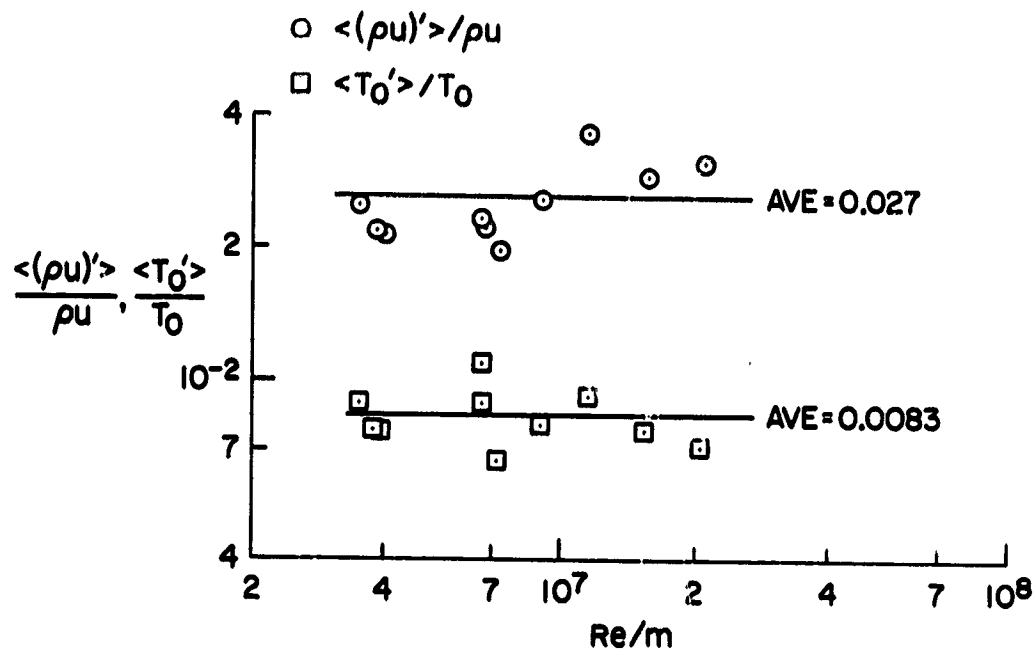


Figure 1.- Freestream turbulence measurements in the Ames 3.5 ft wind tunnel.

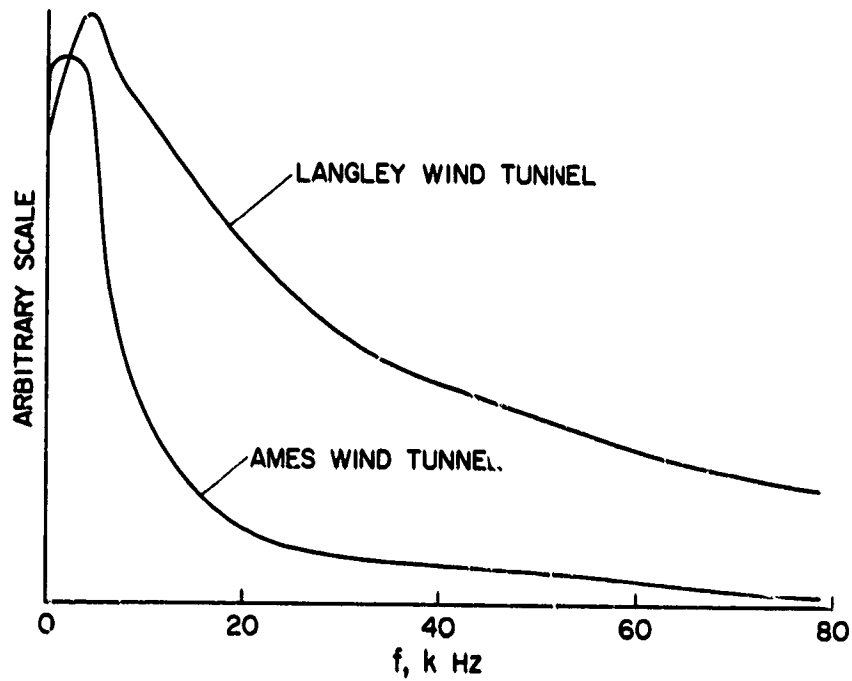


Figure 2.- Comparison of wind tunnel freestream spectra.

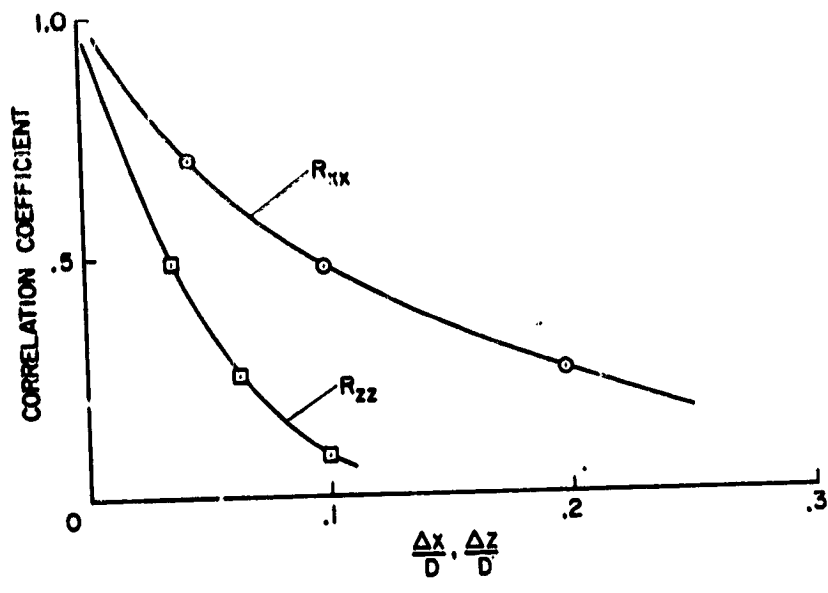


Figure 3.- Longitudinal and lateral mass flux correlations.

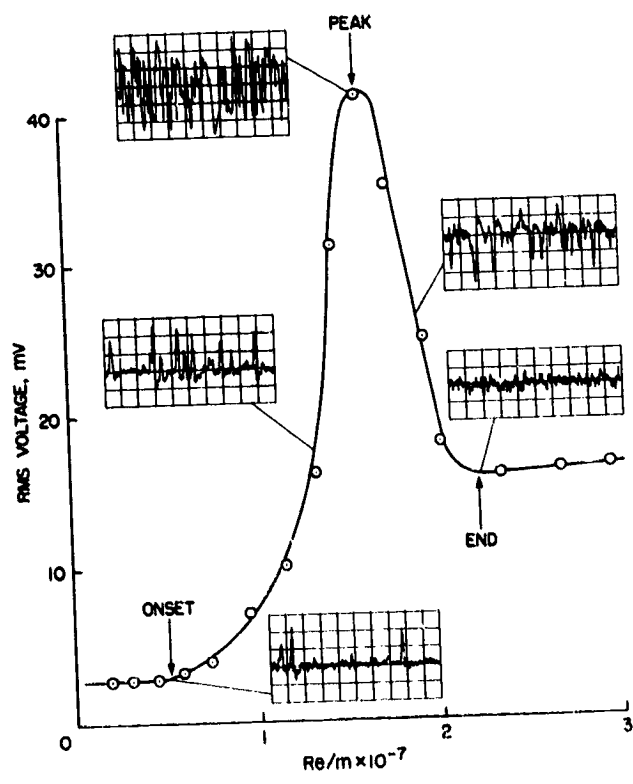


Figure 4.- Thin film gauge output through transition.

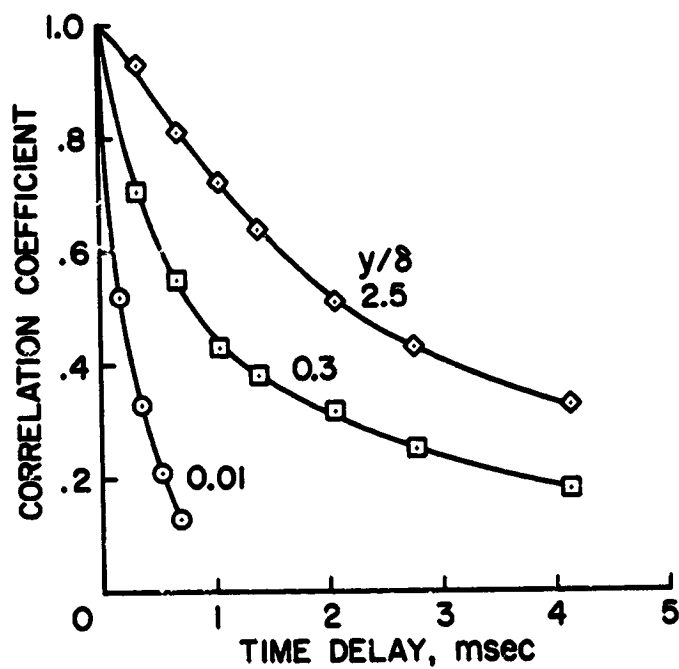


Figure 5.- Autocorrelations in a turbulent boundary layer.

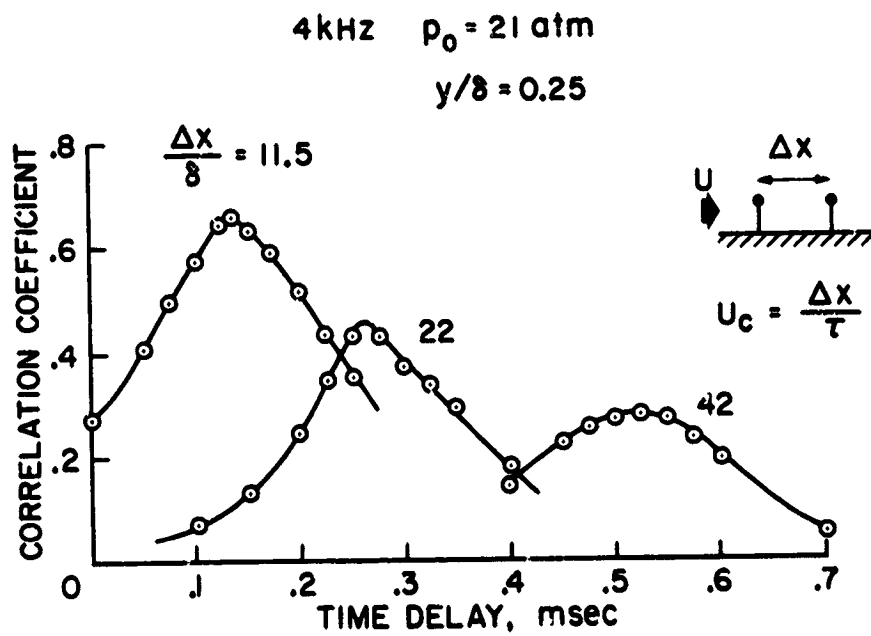


Figure 6.- Longitudinal cross-correlations in a turbulent boundary layer.

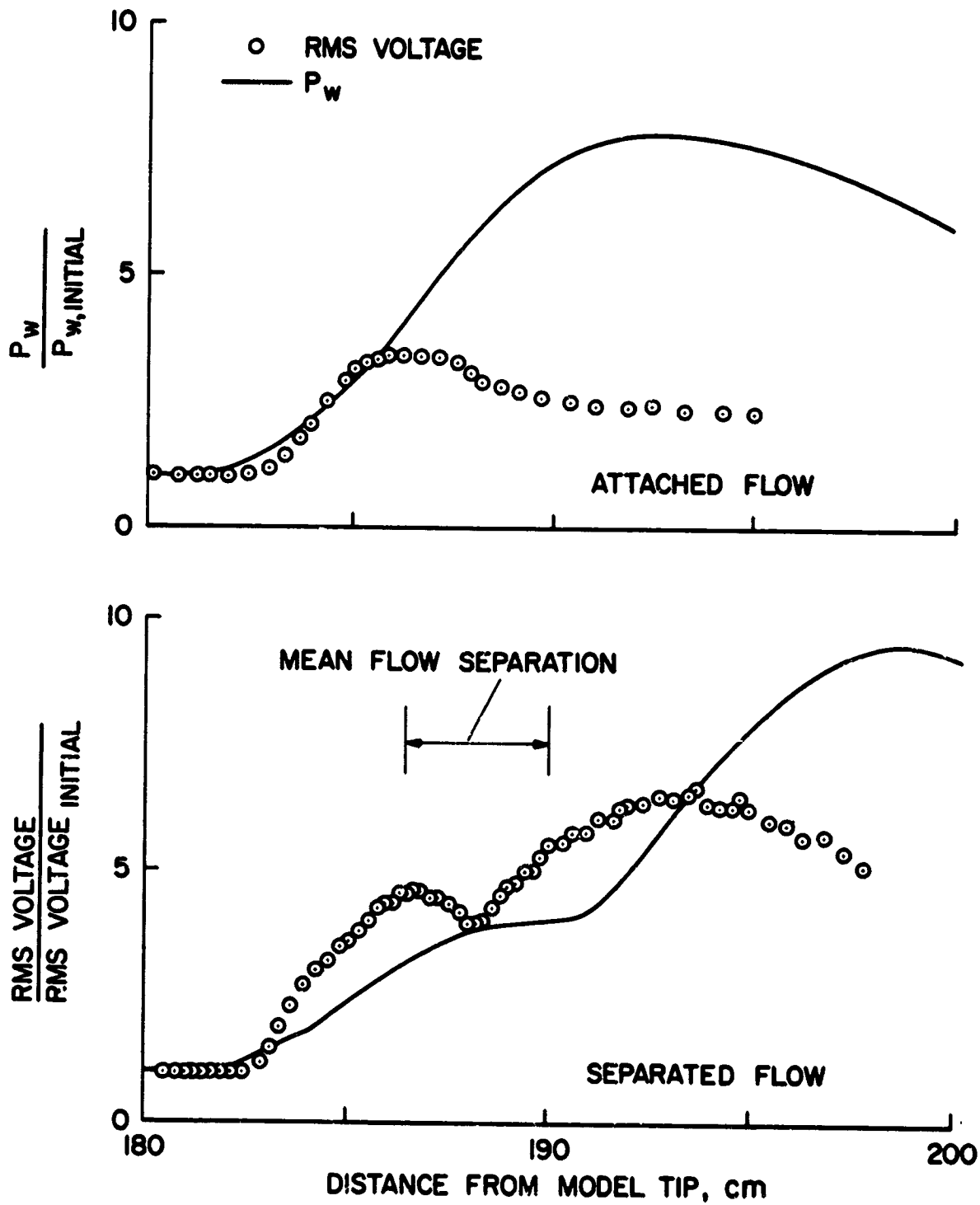


Figure 7.- Shock induced separation in the Ames 3.5 ft wind tunnel.

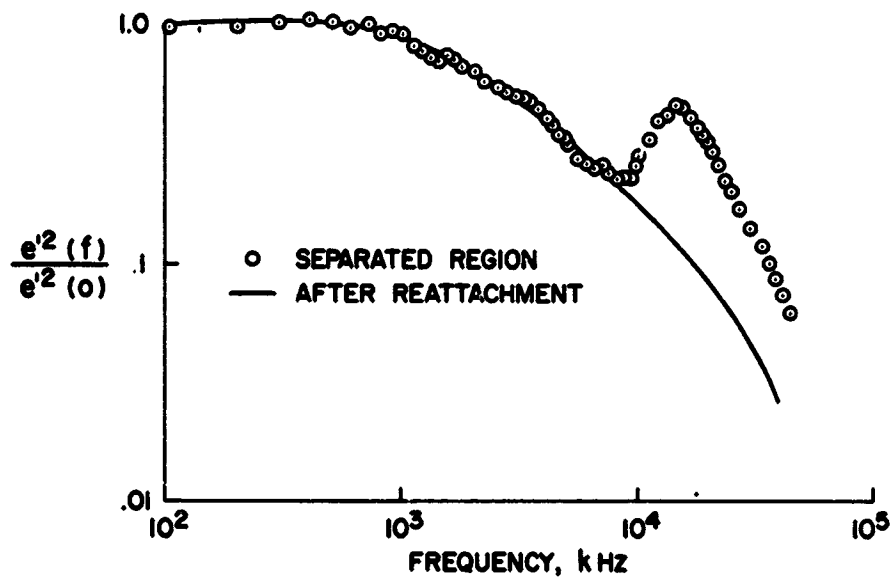


Figure 8.- Hot film spectra through separation.

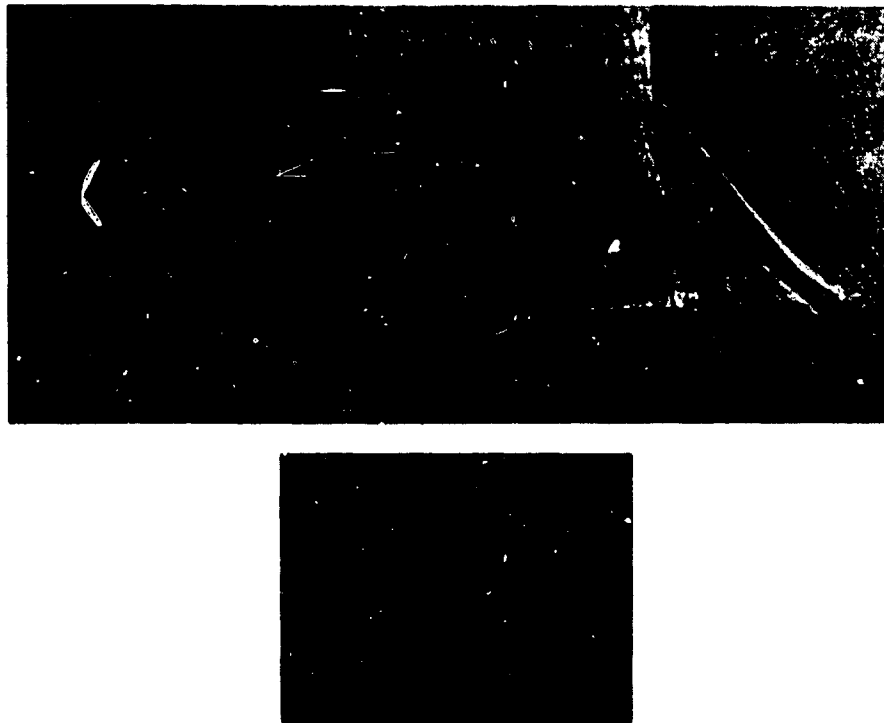


Figure 9.- Shadowgraph and laser schlieren spectra in the Ames 2 × 2 ft wind tunnel.

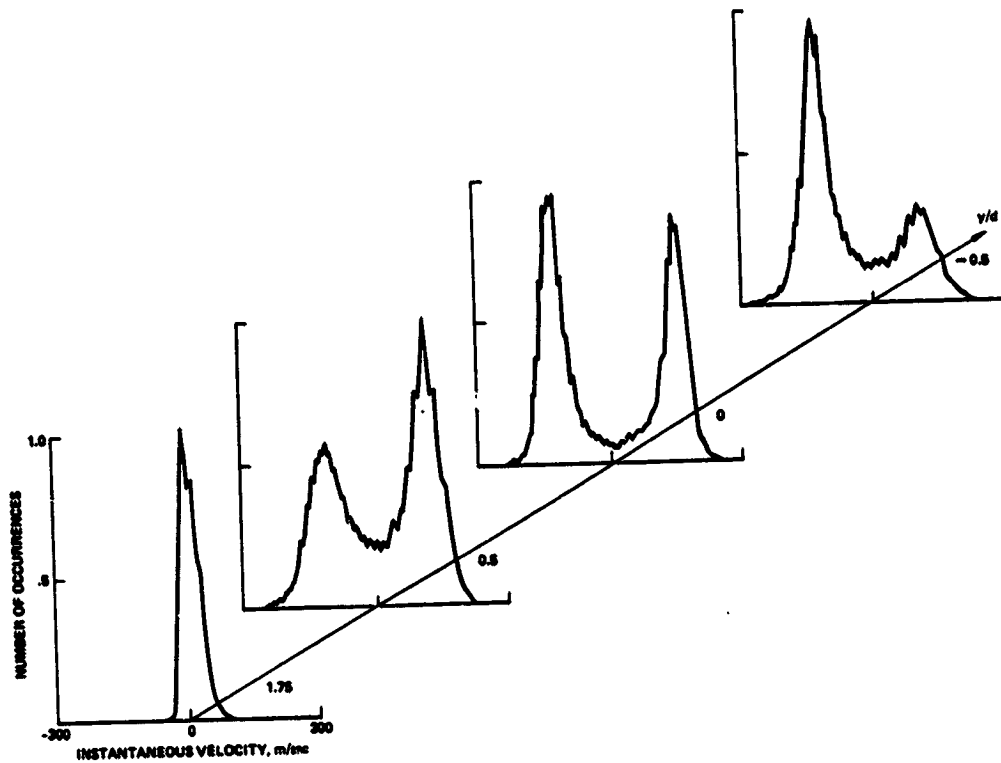


Figure 10.- Velocity probability densities in a cylinder wake.

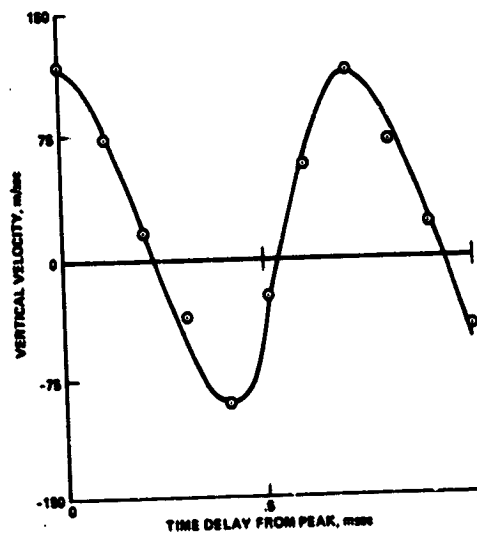


Figure 11.- Conditionally sampled velocities in a cylinder wake.

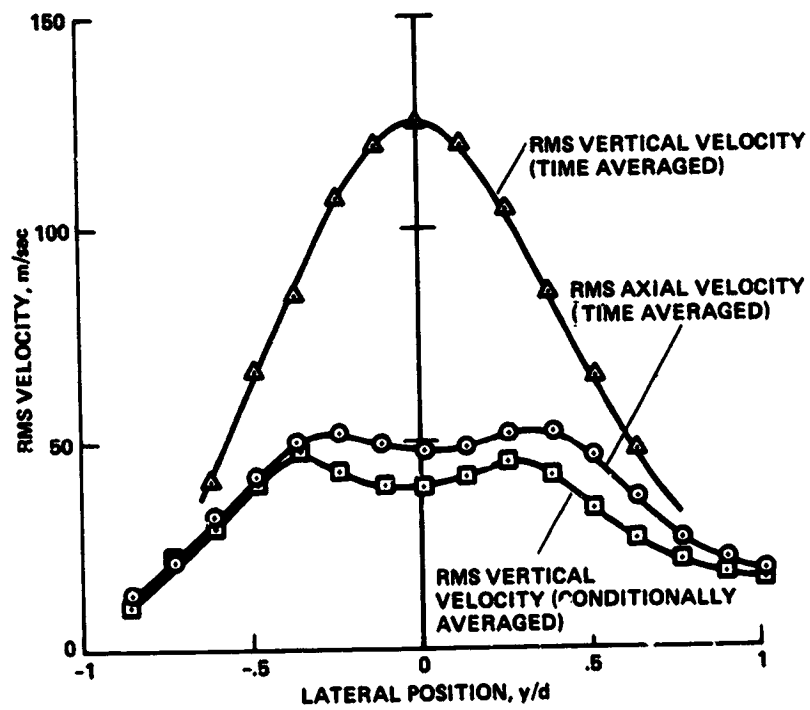


Figure 12.- Root mean square velocity profiles across a cylinder wake.

HOLOGRAPHY AND LDV TECHNIQUES, THEIR STATUS
AND USE IN AIRFOIL RESEARCH

D. A. Johnson
NASA Ames Research Center
and
W. D. Bachalo
Spectron Development Laboratories, Inc.

SUMMARY

In recent experiments conducted in the NASA-Ames 2- by 2-Foot Transonic Wind Tunnel, the measurement capabilities of laser velocimetry and holographic interferometry in transonic airfoil testing were demonstrated. Presented in this paper are representative results obtained with these two nonintrusive techniques on a 15.24-cm (6-in.) chord 64A010 airfoil section. These results include the density field about the airfoil, flow angles in the inviscid flow and viscous flow properties including the turbulent Reynolds stresses. The accuracies of the density fields obtained by interferometry were verified from comparisons with surface pressure and laser velocimeter measurements.

INTRODUCTION

Considerable advances have been made toward the numerical solution of the transonic flow past two-dimensional airfoil sections (e.g., refs. 1-5). However, these numerical methods currently have a limited range of applicability either because they ignore viscous effects altogether or because they inadequately predict the viscous effects as the shock wave strengthens on the airfoil's upper surface. Accurate predictions are especially difficult to obtain once shock-induced separation occurs. The poor agreement with experiment in this case is believed due to deficiencies in the models employed for the turbulent Reynolds stresses (ref. 4).

Although, it is the airfoil surface pressures, for which experimental data are plentiful, that the computational methods attempt to predict (the prediction of skin friction drag is much more elusive), quantitative measurements of the external flow are needed to truly assess the ability of the methods to describe the flow behavior and to provide insight into how to improve upon these methods. In view of this, there has been an effort within the Aerodynamics Research Branch at NASA Ames Research Center to establish measurement capabilities for the study of the flow past airfoils at transonic speeds. Two nonintrusive techniques applicable to airfoil research that have been under development are laser velocimetry and holographic interferometry. In this paper, the measurement capabilities of these two techniques in two-dimensional airfoil testing are described. The data presented are from experi-

of data obtainable with these two optical methods, a few representative results are presented. A more complete presentation of results with emphasis on fluid mechanical interpretation can be found in a paper presented at the 11th AIAA Fluid and Plasma Dynamics Conference, Seattle, Washington, July 10-12, 1978. (See ref. 6.)

The symbols used herein are defined in an appendix.

MEASUREMENT TECHNIQUES

Laser Velocimetry

Figure 1 is a schematic of the laser velocimeter system for the NASA Ames 2- by 2-Foot Transonic Wind Tunnel. This fringe-mode velocimeter is a dual-color system utilizing the 4880 Å and 5145 Å lines of an argon-ion laser. One color is used to measure the streamwise velocity component; the other to measure the vertical velocity component. Bragg cell frequency shifting necessary for probing highly turbulent and separated flow regions is incorporated in both colors. It also facilitates the measurement of the vertical velocity component (i.e., $\pm 45^\circ$ beam orientations to resolve the vertical velocity are unnecessary).

As seen in figure 1, most of the optical components are located outside the tunnel plenum chamber. There, color separation, Bragg cell frequency shifting, and the establishment of the four beam matrix are accomplished. Only the transmitting lens, collecting lens, and photo detectors are mounted inside the plenum chamber. Two traversing systems are shown inside the plenum chamber. The one on the opposite side of the test section from the laser holds the collecting lens and photo detectors when forward-scatter light collection is used. This is the case in airfoil testing since there is no problem with the model blocking the field of view. The traversing system on the laser side of the test section supports the transmitting lens and the light collection optics when backscatter light collection is used. Mirrors affixed to this traversing system permit three-dimensional scanning of the velocimeter's sensing volume; the optics outside the plenum chamber remain stationary. Both traversing systems are driven with computer controlled stepper motors.

Signal processing is accomplished with single-particle, burst counters and the individual realizations from the two channels are simultaneously recorded with a digital computer. Hence, the velocity correlation $\overline{u'v'}$ can be obtained straightforwardly by multiplying and averaging rather than by the less accurate method of subtracting the variances of the two signals obtained from $\pm 45^\circ$ beam orientations.

Naturally occurring particles are sufficiently abundant in this facility to obtain data rates approaching several thousand per second. These particles arise from vaporized lubricating oil in the drive system which recondenses in the nozzle section of the tunnel. Flow response measurements across a normal shock wave have shown these particles to be 1 μm in diameter and smaller.

However, rates as high as $50,000 \text{ sec}^{-1}$ can be realized by injecting a DOP aerosol downstream of the test section wherein the entire tunnel is seeded. This aerosol produced by an ultrasonic generator has a mean diameter of $0.7 \text{ }\mu\text{m}$.

Holographic Interferometry

Figure 2 is a schematic of the holographic interferometer setup used in the Ames 2- by 2-Foot Transonic Wind Tunnel. As seen in figure 2, the holography system is designed to utilize the existing tunnel Schlieren mirrors. This allows a field of view equal to the dimensions of the tunnel test section windows (41 cm in diameter). The light source for this system is a Q-switched ruby laser with a pulse duration of a few nanoseconds which is more than sufficiently short to freeze any mechanical motions. A series of mirrors shown on the opposite side of the test section from the laser are used to match path lengths between the reference and object beams. The dual-plate method is employed wherein only one reference shot is needed, thereby eliminating the need to shut the tunnel down for each new test condition. Due to the relatively large span of the tunnel, the sensitivity of the system to density changes is quite good in two-dimensional testing. For $M_\infty = 0.8$, for example, one fringe shift corresponds to only about a 0.5% change in density and a corresponding change in Mach number of about 1%. This and the high aspect ratio of the wings tested in this facility (typically four), which improves the two-dimensionality of the flow, both contribute to the accuracies obtainable with this optical method.

DISCUSSION

A representative infinite-fringe interferogram taken on a 15.24-cm (6-in.) chord 64A010 airfoil section at $M_\infty = 0.8$ and an angle of attack, $\alpha = 0^\circ$, is shown in figure 3. The fringes of the interferogram represent lines of constant density. As noted earlier, the change in density between adjacent fringes is approximately 0.5%.

Holographic interferometry, unfortunately, does have the disadvantage of being sensitive to flow disturbances along the total optical path. For most practical applications, this limits quantitative measurements to two-dimensional and axisymmetric flows. Its range of applicability becomes even more questionable when one considers that most two-dimensional experiments exhibit some three-dimensional effects. Where applicable though, one hologram as illustrated in figure 3 can provide detailed density information which would be very laborious to realize with a point density measurement device if it existed. A means for determining whether minor three dimensionalities in the flow severely degrade the accuracy of the interferograms is available through comparison with laser velocimeter and surface pressure results. Where the flow can be considered to be isentropic (a good assumption due to the small total pressure losses across the shock wave at transonic conditions), the density results obtained by holographic interferometry can be compared to velocity and pressure results.

ORIGINAL PAGE IS
OF POOR QUALITY

Figure 4 shows a comparison between direct surface pressure measurements and surface pressures inferred from an interferogram assuming isentropic flow and constant pressure across the airfoil boundary layer for $\alpha = 3.5^\circ$. At this angle of attack, the boundary layer is separated at the foot of the shock wave, but the airfoil is not near a stall condition. As seen from figure 4, the agreement with on-centerline surface pressure measurements is very good. What three dimensionalities are present in the flow appear to have a negligible effect on the accuracy of the interferogram. There is a difference, however, in the peak suction ahead of the shock wave recorded by the pressure transducers and the interferogram. This may be due to differences in the averaging times of the two techniques. Further investigation wherein a number of holograms are taken for the same test condition are needed to resolve this point.

An even more thorough evaluation of the accuracy of the interferograms can be made by making comparisons with localized laser velocimeter measurements. Figure 5 shows such a comparison for $\alpha = 0^\circ$, $M_\infty = 0.8$. In this figure, Mach contours were obtained by linearly interpolating between stations where point velocity measurements were obtained with the velocimeter. Away from the airfoil, the agreement is seen to be excellent. Close to the airfoil at the midchord position where the shock wave is located, the agreement is not as good. The explanation for these differences may be the same as with the pressure measurements since the velocimeter results are obtained over a much longer time period. Overall, the comparisons of figures 4 and 5 demonstrate that the interferometer can provide quantitative information of sufficient accuracy to give new insight into the character of the flow past airfoil sections at transonic conditions.

Interferometry, although a very powerful technique, cannot provide information, for example, on flow direction or local turbulence properties. To obtain these quantities, the laser velocimeter technique must be utilized.

Flow direction measurements in the inviscid flow regions become extremely important when tunnel wall effects on the flow field need to be considered. Flow angle measurements obtainable with the laser velocimeter are illustrated in figure 6 for a scan at a fixed height ($y/c = 0.167$) above the chord line at $\alpha = 0^\circ$. At this condition, both tunnel wall and viscous effects are minimal and agreement with theory should be expected as is seen in figure 6. However, as the angle of attack is increased, this has not been the case, primarily due to tunnel wall effects (the Ames 2- by 2-Foot Transonic Wind Tunnel has slotted upper and lower walls). To totally account for any wall effects in comparisons with theory when slotted upper and lower walls are used, it appears that far-field flow angle measurements with the velocimeter will be needed to establish valid boundary conditions.

The pacing item in advancing our ability to predict the transonic flow past airfoil sections is the development of improved turbulence models. The realization of this does not appear forthcoming by numerical experimentation on large-scale computers devoid of any new physical insights about the flows. If a solution to the turbulence modelling problem for transonic airfoils is to be realized, it seems that this will come about from measurements of the quantities that need to be modeled. Until recently, the fluid dynamicist did

ORIGINAL PAGE IS
OF POOR QUALITY

not have the means to measure these flow quantities (i.e., the turbulent Reynolds stresses) on a transonic airfoil even when the flow was attached. Now, in principle, with the laser velocimeter, this measurement capability has become a reality even in regions of separated flow. An illustration of the laser velocimeter's capabilities in measuring the turbulent flow properties is given in figure 7. The profile data shown were obtained in the separated flow region for an angle of attack close to C_{Lmax} . Measurements were realized within 0.5 mm of the wing's surface. Note the smoothness in the Reynolds shear stress ($\overline{\rho u'v'}$) distribution (the mean density has not been added). A check on the correlation coefficient, $R_{uv} = \overline{u'v'}/\overline{u'v'}$, at the point of maximum shear shows it to be nearly -0.5. Also, the mixing length, $l/\delta = (\overline{u'v'})^{1/2}/[(\partial u/\partial y)\delta]$, at this point is approximately 0.09. The self-consistency of these two results, which indicate the flow to be in near-equilibrium in this part of the layer, supports the validity of the shear-stress measurements. From data like that shown in figure 7, obtained along the airfoil and in the wake, improved turbulence models can be formulated for airfoil flow field predictions.

CONCLUDING REMARKS

Laser velocimetry and holographic interferometry have been known to offer great promise in the study of the transonic flow past two-dimensional airfoils. In recent experiments in the NASA Ames 2- by 2-Foot Transonic Wind Tunnel, the measurement capabilities of these two techniques in transonic airfoil testing were demonstrated. A sample of the results obtained for a 15.24-cm (6-in.) chord 64A010 airfoil section has been presented in this paper. The detailed flow field information that can be realized by these measurement techniques should provide the understanding needed to formulate improved turbulence models for airfoil flow field prediction methods.

ORIGINAL PAGE IS
OF POOR QUALITY

APPENDIX

SYMBOLS

Measurements and calculations were made in the U.S. Customary Units. They are presented herein in the International System of Units (SI) with the equivalent values given parenthetically in the U.S. Customary Units.

c	airfoil chord
C_p	pressure coefficient, $\frac{p - p_\infty}{q}$
p	local static pressure
p_∞	free-stream static pressure
M_∞	free-stream Mach number
R_{uv}	velocity correlation coefficient
x	streamwise coordinate
y	normal coordinate
u_∞	free-stream streamwise velocity component
\bar{u}	mean streamwise velocity component
\bar{v}	mean normal velocity component
u'	r.m.s. value of streamwise velocity component
v'	r.m.s. value of normal velocity component
$\overline{u'v'}$	velocity correlation
α	angle of attack
δ	boundary-layer thickness
l	mixing length
$\bar{\rho}$	mean local density

ORIGINAL PAGE IS
OF POOR QUALITY

ORIGINAL PAGE IS
OF POOR QUALITY

REFERENCES

1. Jameson, A.: Transonic Flow Calculations for Airfoils and Bodies of Revolution. Rept. 390-71-1, Grumman Aerospace Corp., 1971.
2. Bauer, F.; Garabedian, P.; and Korn, D.: A Theory of Supercritical Wing Sections, with Computer Programs and Examples. Lecture Notes in Economics and Mathematical Systems, Vol. 66, M. Beckman and H. P. Kunzi, eds., Springer-Verlag, N.Y., 1972.
3. Murman, E. M.; and Cole, J. D.: Calculation of Plane Steady Transonic Flow. AIAA J., vol. 9, no. 1, Jan. 1971, pp. 114-121.
4. Deiwert, G. S.: Computation of Separated Transonic Turbulent Flows. AIAA J., vol. 14, June 1976.
5. Seg'ner, A.; and Rose, W. C.: A Numerical Solution of the Flow Field Over a Transonic Airfoil Including Strong-Shock-Induced Flow Separation. AIAA Paper 76-330, 1976.
6. Johnson, D. A.; and Bachalo, W. D.: Transonic Flow About a Two-Dimensional Airfoil - Inviscid and Turbulent Flow Properties. AIAA Paper 78-117, 1978.

ORIGINAL PAGE IS
OF POOR QUALITY

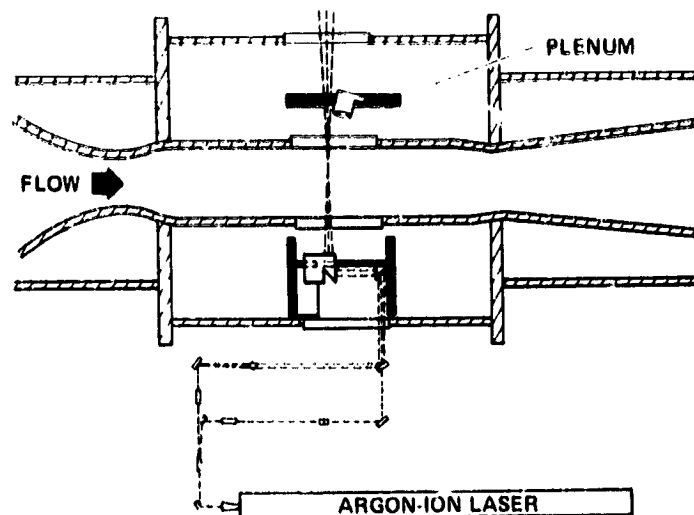


Figure 1.- Schematic diagram of laser velocimeter system for the Ames 2- by 2-foot transonic wind tunnel.

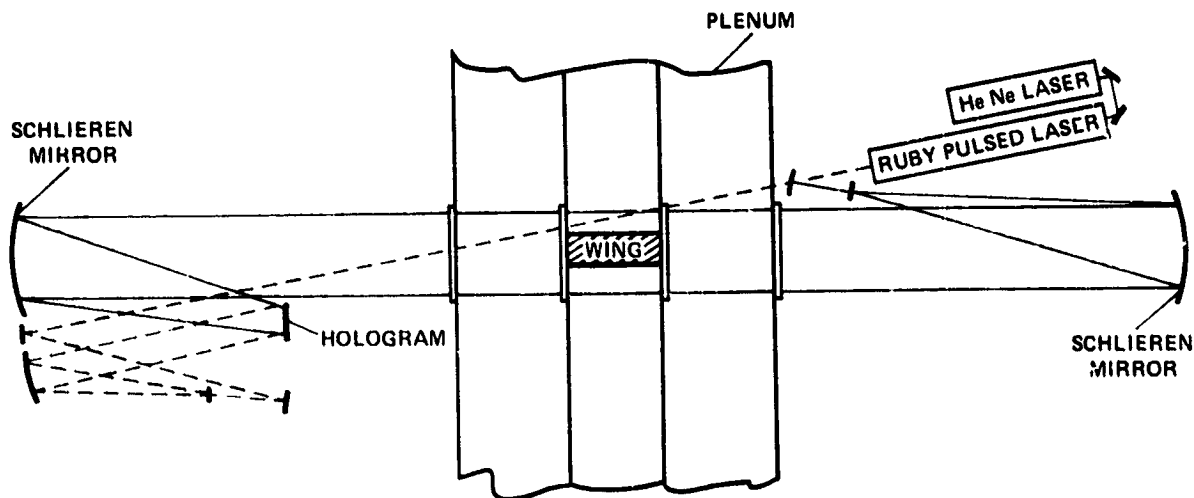


Figure 2.- Schematic diagram of holographic interferometer installation in the Ames 2- by 2-foot transonic wind tunnel.

ORIGINAL PAGE 1.
OF POOR QUALITY

ORIGINAL PAGE IS
OF POOR QUALITY

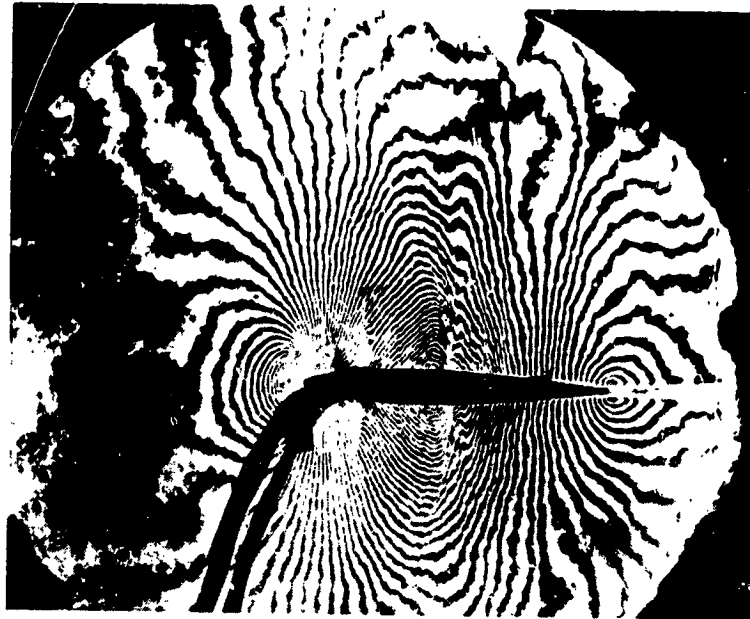


Figure 3.- Representative holographic interferogram for a 15.24-cm (6-in.) chord 64A010 airfoil section. $M_\infty = 0.8$; $\alpha = 0^\circ$.

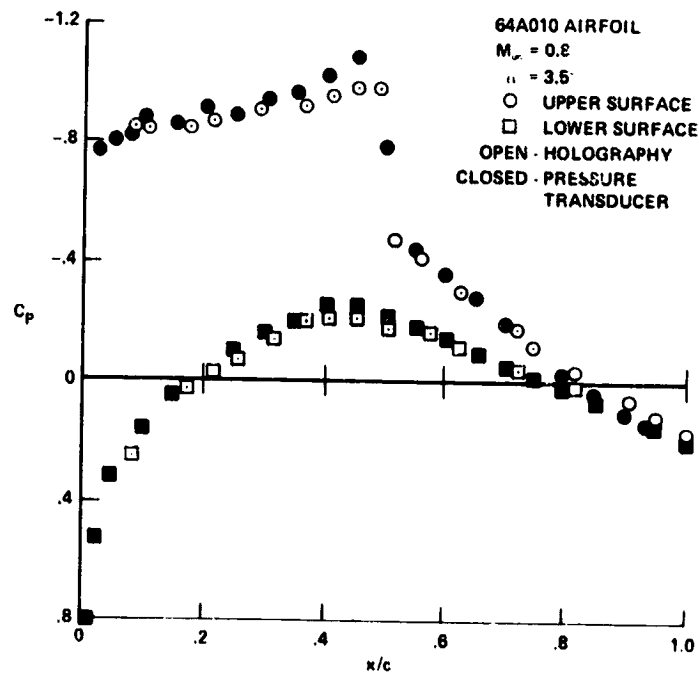


Figure 4.- Comparison of surface pressures inferred from an interferogram with surface pressures measured directly.

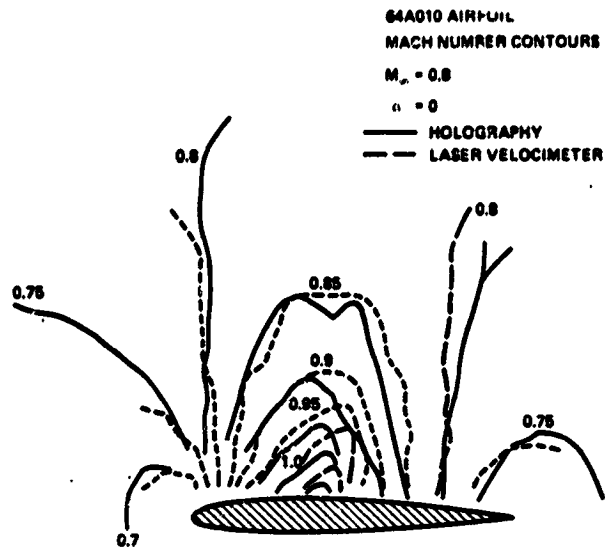


Figure 5.- Comparison of interferometer and laser velocimeter results.

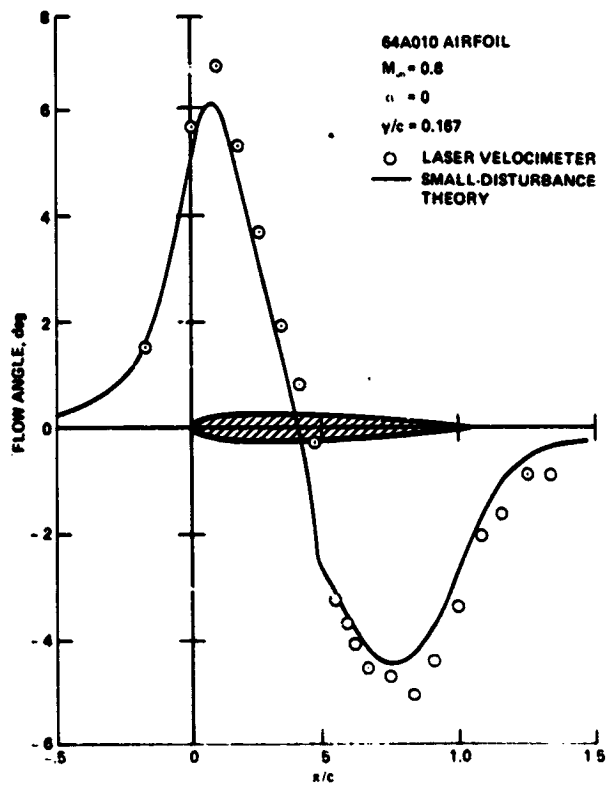


Figure 6.- Flow-angle determinations with laser velocimeter.

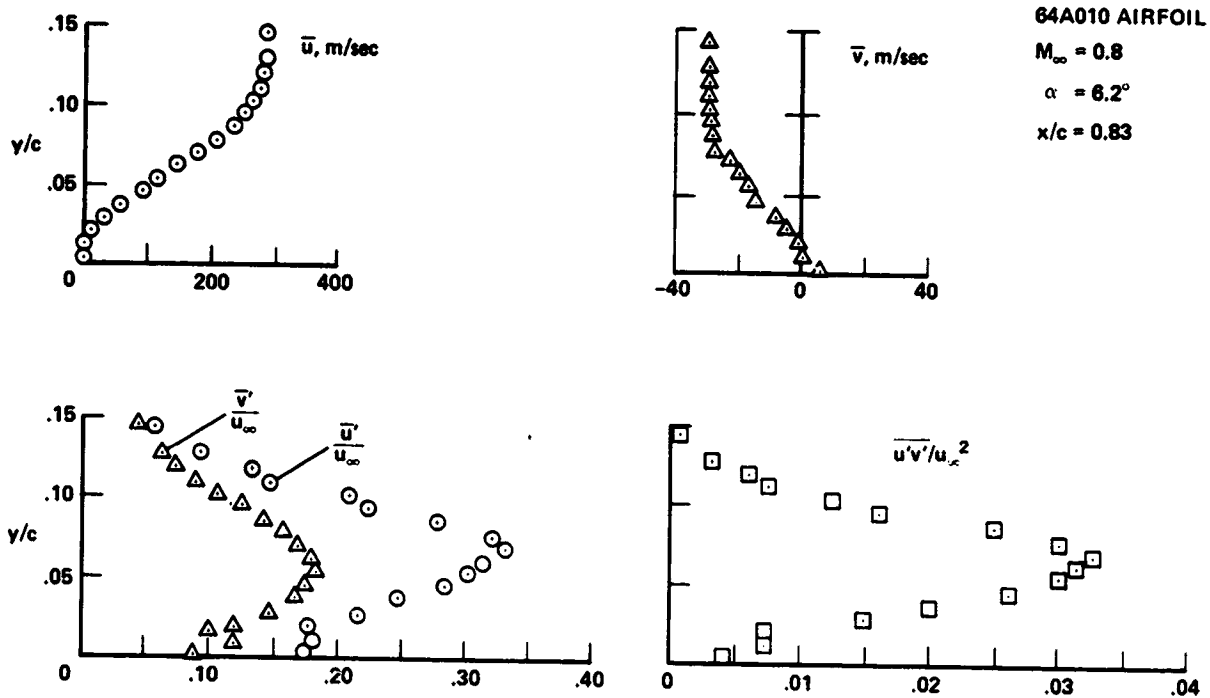


Figure 7.- Representative laser velocimeter turbulent-flow measurements.

SECTION DRAG COEFFICIENTS FROM PRESSURE PROBE
TRAVERSES OF A WING WAKE AT LOW SPEEDSLawrence C. Montoya, Paul F. Bikle*, and Richard D. Banner
NASA Dryden Flight Research Center

SUMMARY

An in-flight wing wake section drag investigation was conducted using traversing pitot and static probes. The primary objective of this investigation was to develop measurement techniques and improve the accuracy of in-flight wing profile drag measurements for low values of dynamic pressure and Reynolds number. Data were obtained on a sailplane for speeds from about 40 knots to 125 knots at chord Reynolds numbers between 1×10^6 and 3×10^6 . Tests were conducted with zero flap deflection, deflected flaps, and various degrees of surface roughness, and for smooth and rough atmospheric conditions.

Several techniques were used to increase data reliability and to minimize certain bias errors. A discussion of the effects of a total pressure probe in a pressure gradient, and the effects of discrete turbulence levels, on the data presented herein and other experimental results is also included.

INTRODUCTION

In the fall of 1973 a joint NASA-SSA (Soaring Society of America) flight experiment was initiated to define the wake characteristics of a low speed airfoil section. The primary objective of the investigation was to develop measurement techniques and improve the accuracy of in-flight wing profile drag measurements for low values of dynamic pressure and Reynolds number. This improvement in accuracy is necessary if small airfoil performance differences due to such things as airfoil surface, ambient air turbulence, or Reynolds number are to be measured. The accuracy effort was prompted by the desire for aerodynamic efficiency, which improves fuel consumption, and the desire of the designer to choose the optimum airfoil for a given mission.

This paper reviews the techniques used to increase data reliability and to minimize certain bias errors during a series of wing profile drag measurements performed in flight on a sailplane airfoil. The pitot-traverse method developed by Jones (ref. 1) was used in this study. Jones' equation was rearranged so that incremental pressure measurements rather than absolute pressures in the wake region could be used to determine section drag. This was done so that (1) only one transducer could be used to measure both the total and static pressures in the wake, thereby eliminating errors from additional transducers; (2) differential pressure measurements could be used instead of the difference in absolute pressure measurements (which made it easier to

*Soaring Society of America.

scale the transducer to the pressure measurement range); (3) in-flight transducer tare readings could be routinely obtained; and (4) the wake edges were well defined.

Unresolved questions concerning errors in the use of total pressure probes in this and other studies are discussed.

SYMBOLS

Physical quantities in this report are given in the International System of Units (SI) and parenthetically in U.S. Customary Units. The measurements were taken in Customary Units. Factors relating the two systems are presented in reference 2.

c	chord at test station, cm (in.)
c_d	section drag coefficient
D	external diameter of circular pitot probe or external height of rectangular pitot probe
p_0	free-stream static pressure, kN/m^2 (lb/ft^2)
p_{t_0}	free-stream total pressure, kN/m^2 (lb/ft^2)
p_{t_w}	wake total pressure, kN/m^2 (lb/ft^2)
p_w	wake static pressure, kN/m^2 (lb/ft^2)
q_0	free-stream dynamic pressure, $p_{t_0} - p_0$, kN/m^2 (lb/ft^2)
q_w	wake dynamic pressure, $p_{t_w} - p_w$, kN/m^2 (lb/ft^2)
x	distance along chord, cm (in.)
y	vertical wake width, cm (in.)
β	pitot probe displacement
δ	boundary layer thickness
Δp	$= p_w - p_0$, kN/m^2 (lb/ft^2)
Δp_t	$= p_{t_0} - p_{t_w}$, kN/m^2 (lb/ft^2)

Δy vertical wake width increment, cm (in.)

Λ turbulence scale

AIRPLANE AND TEST CONDITIONS

The test vehicle was a T-6 sailplane with a modified Wortmann FX61-163 airfoil (fig. 1). The airfoil modification consisted of straightening the aft lower surface cusp region and incorporating a 17-percent flap hinged on the lower surface (insert, fig. 1). The coordinates of the airfoil are presented in table I. A more complete description of the test vehicle is given in reference 3.

The wing surface finish was smooth, with a maximum waviness for the test region near the midsemispan of about 0.008 centimeter (0.003 inch) in a 5.08-centimeter (2-inch) section of surface.

Data were obtained for calibrated airspeeds from about 40 knots to 125 knots, which provided in-flight test section chord Reynolds numbers between 1×10^6 and 3×10^6 , respectively. Tests were performed on a physically clean wing (for flap deflections measured at the test sections from 3° to -10°), for smooth and rough atmospheric conditions, and for various wing surface conditions (which included 600 and 220 grit sandpaper finish, dusty wing, simulated insect impacts near the leading edge, and boundary-layer trips at the 5-percent chord).

INSTRUMENTATION AND TECHNIQUE

The pitot-traverse method developed by Jones (ref. 1) was used to convert the wake data into section drag coefficients. Some rearrangement of Jones' equation was made to take advantage of the differential pressure measurement scheme, which is described below. Details of the way in which Jones' equation was used are given in the appendix.

The wake measurements were made 24.4 centimeters (9.6 inches) behind the wing trailing edge, a distance corresponding to about 32 percent of the 75.9-centimeter (29.9-inch) local chord.

The wake probe had both total and static pressure heads, as shown in figure 2. Also shown are the sources for the reference total pressure (a Kiel tube) and reference static pressure (a trailing boom). The Kiel tube and trailing boom were mounted on the wing near the probe to remove lag effects. The probe traversed about 20.32 centimeters (8 inches) above and below the wing's trailing edge at a rate of about 7.62 centimeters (3 inches) per second.

An important part of the wake probe unit was the switching function provided by the valve (fig. 3). Pneumatic lag was minimized by incorporating a design that

resulted in a small internal volume. The design also minimized the possibility of pneumatic leaks. In the incremental total pressure (Δp_t) mode, the difference between the reference total pressure sensed by the Kiel tube and the wake total pressure was measured. Thus, the probe transducer sensed the total pressure defect (Δp_t) in the wake. When the probe moved outside the wake, both sides of the transducer's sensing element were exposed to free-stream total pressure, thereby providing in-flight tare readings for the transducer. This feature minimized the bias error for the transducer and provided well-defined wake edges.

In the incremental static pressure (Δp) mode, the difference between the wake static pressure and the reference static pressure sensed by the trailing boom was measured. Therefore, the difference between wake static pressure and the free-stream static pressure was obtained from a direct measurement and from the application of the position error correction. The position error calibration for the trailing boom source was obtained from the airplane static pressure source. The airplane airspeed system is discussed in reference 4.

Through the switching valve feature just described, the same transducer provided both Δp_t and Δp . As a result, the wake static pressure bias errors were also minimized through the in-flight tare measurements, which were made before and after the incremental static pressure measurements when the switching mechanism was in the Δp_t mode. A $\pm 1.72 \text{ kN/m}^2$ ($\pm 0.25 \text{ psid}$) low range pressure transducer, which had an infinite resolution and natural frequency of 5000 hertz, was used.

Six Δp_t traverses and several Δp traverses were made in succession, while indicated airspeed, and consequently q_0 , was held constant. Individual wake probe traverses were made alternately in the upward and downward directions and were averaged for determining the section drag coefficients for each test point (see appendix). The incremental static pressures through the wakes are not presented herein, but they were obtained with the same accuracy as the incremental total pressures.

Probe position and the pressures were recorded on tape by utilizing a system mounted on a shelf behind the pilot's headrest. Aircraft dynamic pressure, q_0 , was determined from a calibrated airspeed system and also measured with a transducer housed in the recorder package. Pressure altitude, air temperature, indicated airspeed, general atmospheric conditions (smooth or rough air), and pilot comments were hand recorded by the pilot for each test point.

Lift coefficient values at the test section were not measured directly but were determined from known aircraft lift coefficients (± 1 percent) adjusted for measured tail loads (from pressure distributions) and nonuniform span lift distributions. The nonuniform span lift distribution was determined from measured flap and aileron deflections at a number of spanwise stations.

RESULTS AND DISCUSSION

The data presented herein illustrate some of the results of the experiment. The section drag data presented (flight, computed, and wind tunnel) are for chord Reynolds numbers corresponding to those obtained in flight, which varied from 1×10^6 at the lowest speed to 3×10^6 at the highest speed.

Examples of the wake profiles obtained by using this method are shown in figure 4. Data beyond the wake edges are not included, since the total pressure differences were zero using the measurement method described previously. These profiles were obtained at a calibrated velocity of 44 knots. Note the low pressures (0.10 kN/m^2 (2.1 lb/ft^2)) that the instrumentation must measure at these speeds. The very low random scatter illustrates the good repeatability and low magnitude of the random errors. The fact that the shapes and displacements are the same for alternate upward and downward traverses indicates that lag effects were essentially absent.

The ability of the wake probe measurements to reflect the effects of small changes in dynamic pressure is clearly demonstrated in figure 5 by the magnitude of the increase in separation as speed decreases from 42.0 knots to 41.5 knots. All of the increased separation occurs on the upper surface; the wake from the lower surface remains essentially unchanged. In-flight tuft photos (fig. 6) confirm these results. Drag polars were defined for each of five incremental flap settings from 3° to -10° as measured at the test section. The flap results were cross plotted and adjusted to zero flap deflection and are summarized in figure 7. These data represent approximately 360 wake traverses and were obtained from seven flights over a period of 6 months. The line represents a fairing of the data. Most data fall within about 3 percent of the fairing, which gives another indication of the repeatability of the results. A few data points fall outside this 3-percent band. The four isolated points between lift coefficients of 0.4 and 0.7 represent the largest scatter (approximately 14 percent). The reason for the large scatter of these four points is not known.

Figure 8 shows section drag coefficients from the test airfoil with boundary layer transition strips, which were 0.63 centimeter (0.25 inch) wide, had 0.089-centimeter (0.035-inch) grit, and were located at the 5-percent chord. The figure also shows the fairing of the clean wing data from figure 7. The artificially fixed transition increased section drag to approximately double the level measured for natural transition, indicating that there was some laminar flow on the clean wing. This finding is consistent with wind-tunnel results for this class of airfoil.

With the flaps deflected 6° , the mean camber line and the maximum lift coefficient were essentially the same as for the unmodified airfoil (airfoil without flaps). Flight data for both 0° and 6° flap deflections are shown in figure 9. This comparison shows the effects of the modifications on measured airfoil performance.

The flight data for the 6° flap setting is compared with wind-tunnel and computed data for the unmodified airfoil (without flaps) in figure 10. One set of wind-tunnel data is reported in reference 5; the other wind-tunnel data are reported

in reference 6. The average difference in drag between these sets of data is about 12 percent, although both sets of data were derived from the same type of tests and airfoil model. The only changes were in instrumentation. The 1972 (ref. 6) data are believed to be the more accurate. This assumption appears to be confirmed by the comparison in figure 10, which shows that the flight and computed data tend to support the 1972 wind-tunnel data. The computed data are based on Squire-Young computational methods. As figure 10 shows, the agreement between the flight data, computed data, and 1972 wind-tunnel data is generally good.

Section drag coefficients obtained during flight in rough air which was typical of turbulent convection are presented in figure 11. Even though the data are somewhat limited (37 wake traverses from seven flights), they indicate that the rough air did not increase the drag until stall speeds were approached, and then only because the lift coefficient extended into the higher section drag coefficient regions.

Figure 12 shows the effects of several surface conditions on the airfoil section lift-drag polar. The clean wing results (solid line) which were shown previously (fig. 7) are for a standard 600 grit sandpaper finish. The artificially tripped boundary layer results (dashed line, shown previously in fig. 8) are also included. The circle symbols are for a dusty wing (the wing was not cleaned after the sailplane was tied down for 3 weeks), and the triangular symbols represent a standard 220 grit sandpaper finish. The square symbols represent the drag coefficients that resulted when roughness particles simulating insect impacts were placed near the leading edge. As expected, the insect impact simulation appreciably increased the section drag (the increase was roughly 40 percent of the increase caused by the transition strips), while the other surface conditions had no detectable effects. The effects of insect impacts, as is well known, depend on the number and size of the insects and their distribution near the leading edge of the wing.

DATA UNCERTAINTY

As shown in data presented previously in this paper, the low level of scatter indicates that random errors were quite small. Systematic errors such as bias errors and lag errors were also essentially eliminated.

Error in the section lift coefficients resulting from the adjustments mentioned in the Instrumentation and Technique section are systematic in nature and may approach 4 percent at high lift coefficients and 10 percent at low lift coefficients. These errors are not felt to be of concern because of the insensitivity of the drag levels to lift coefficient through the lift coefficient range of greatest interest (section lift coefficients less than or equal to 1.0).

The systematic error which remains of concern is that associated with the total pressure obtained from a total pressure probe in the environment of a wake or boundary layer where (1) there is a pressure gradient across the face of the probe, (2) there is a discrete turbulence scale factor, (3) there are viscosity effects, or (4) the streamlines are deflected by the presence of the probe. Literature on the subject (refs. 7 to 20) acknowledges these problems; a summary of the findings is listed in table II, which was adapted from reference 7. The findings shown in

table II are expressed in terms of an equivalent displacement of the probe centerline required to obtain correct total pressure values.

As table II shows, the displacement values are inconsistent, even where test conditions overlap. The differences can probably be attributed to the varying influence of the four factors mentioned previously. The reference 8 results are for test conditions essentially identical to those used in acquiring the flight data reported in this paper. Use of the probe displacement corrections advocated in reference 8 increases the section drag coefficients (for the data from this experiment) by 0.0004, or about 6 percent, over the entire range of section lift coefficients.

A survey of flight and ground facility results indicates that such errors also existed in the data from those experiments. However, these errors have generally not been accounted for or even acknowledged. It is probable that the probe effects vary from one airfoil to another under identical conditions or from identical airfoils in different facilities. The designer may have difficulty in selecting an airfoil from such performance experiments, which are subject to significant errors. The current energy situation is such that small performance differences can be significant when extrapolated to long distances or large numbers of aircraft. It is therefore incumbent upon experimenters to investigate and attempt to reduce the impact of the four items previously identified. As a first step, measurement techniques could be standardized, such as probe configuration and size relative to the wake or boundary layer being measured. An attempt should also be made to determine some form of turbulence criterion at the probe measuring station; alternatively, an attempt could be made to eliminate this problem with new remote measurement techniques or equipment such as lasers.

In any event, experimenters and authors should acknowledge the four factors listed, indicate which are unaccounted for, and provide some estimate of the resulting uncertainties, so that the readers are aware of the limitations of the subject data.

It is commonly assumed that published airfoil data are accurate at least to within a few percent. Designers sometimes make airfoil selections on the basis of performance differences of a few percent. Published data are not necessarily accurate, however. An error in the 1963 data for the FX61-163 airfoil resulted in the selection of this airfoil for several aircraft designs, a selection which led to deficient aircraft performance. Further, the error in the data has not been called to the attention of potential data users.

CONCLUDING REMARKS

An in-flight wing wake section drag investigation was conducted using traversing total and static pressure probes. The primary objective of the investigation was to develop measurement techniques and to improve the accuracy of in-flight wing profile drag measurements for low values of dynamic pressure and Reynolds number so that small differences in airfoil performance could be determined.

The results showed that repeatable in-flight wing section drag measurements could be obtained using traversing total and static pressure probes with the techniques described. Small drag differences resulting from varying wing surface conditions and ambient air turbulence were well defined. Of the surface conditions evaluated (other than transition strips), only simulated insect impacts affected the drag. Data obtained in rough (turbulent) air showed that the drag was only affected at conditions near the wing stall speeds and then only because the variation in lift coefficient extended into the high drag regions.

The absolute level of the measurements in this and other experiments utilizing wake surveys is questionable because of undefined total pressure errors. These errors, which are not adequately understood, have not been accounted for or even acknowledged in similar experiments, whether conducted in flight or in wind tunnels. This has made meaningful comparisons between various experiments difficult and has caused users to be misled in interpreting the data in terms of airfoil performance.

**APPENDIX — METHOD USED TO OBTAIN
SECTION DRAG COEFFICIENTS FROM MEASURED INCREMENTAL PRESSURES**

Jones' equation (ref. 1) is as follows:

$$c_d = \frac{2}{c} \int \sqrt{\frac{p_{t_w} - p_w}{q_0}} \left(1 - \sqrt{\frac{p_{t_w} - p_0}{q_0}} \right) dy$$

Since

$$p_{t_w} - p_0 = q_w + \Delta p$$

Jones' equation can be rewritten as

$$c_d = \frac{2}{c} \int \sqrt{\frac{q_w}{q_0}} \left(1 - \sqrt{\frac{q_w + \Delta p}{q_0}} \right) dy$$

The procedure used in this study for a given number of Δy increments across the wake may be described as follows.

Step 1: Determine q_0 (a direct measurement from the aircraft system. Includes a position error correction).

Step 2: Determine Δp_t (a direct measurement (see Instrumentation and Technique section)).

Step 3: Determine Δp (a direct measurement (see Instrumentation and Technique section)).

Step 4:

$$q_w + \Delta p = (\text{Step 1}) - (\text{Step 2})$$

Step 5:

$$q_w = (\text{Step 4}) - (\text{Step 3})$$

Step 6:

$$\left(q_w / q_0 \right)^{\frac{1}{2}} = \sqrt{(\text{Step 5}) / (\text{Step 1})}$$

Step 7:

$$\left(\frac{q_w + \Delta p}{q_0}\right)^{\frac{1}{2}} = \sqrt{(\text{Step 4}) / (\text{Step 1})}$$

Step 8:

$$1 - (\text{Step 7})$$

Step 9:

$$(\text{Step 6}) \times (\text{Step 8}) \Delta y$$

Step 10:

$$\Sigma (\text{Step 9})$$

Step 11:

$$c_d = (\text{Step 9}) \times \frac{2}{c}$$

REFERENCES

1. Jones, B. Melvill: The Measurement of Profile Drag by the Pitot-Traverse Method. Reports and Memoranda No. 1688, Brit. A.R.C., Jan. 1963.
2. Mechtly, E. A.: The International System of Units — Physical Constants and Conversion Factors. Second Revision. NASA SP-7012, 1973.
3. Bikle, Paul: Description of the T-6 Sailplane. Soaring, vol. 34, no. 8, Aug. 1970, pp. 12-15.
4. Bikle, Paul: Airspeed Calibration. Soaring, vol. 35, no. 1, Jan. 1971, pp. 22-28.
5. Wortmann, F. X.: Some Laminar Profiles for Sailplanes. Soaring, Jan. 1964, pp. 14-18. (Primary source - Wortmann, F. X.; and Schwoerer, K.: Einfluss der Profilpolaren auf die Flugleistungen von Segelflugzeugen. Aero Revue, Sept. 1963.)
6. Althaus, D.: Stuttgarter Profilkatalog I. Messergebnisse aus dem Laminarwindkanal des Instituts fuer Aerodynamik und Gasdynamik der Universitaet Stuttgart 1962-1972. Institut fuer Aerodynamik und Gasdynamik, Universitaet Stuttgart, c.1972.
7. Allen, Jerry M.: Pitot-Probe Displacement in a Supersonic Turbulent Boundary Layer. NASA TN D-6759, 1972.
8. Young, A. D.; and Maas, J. N.: The Behaviour of a Pitot Tube in a Transverse Total-Pressure Gradient. R. & M. No. 1770, Brit. A.R.C., 1937.
9. Johannesen, N. H.; and Mair, W. A.: Experiments With Large Pitot Tubes in a Narrow Supersonic Wake. J. Aeronaut. Sci., vol. 19, no. 11, Nov. 1952, pp. 785-787.
10. Marson, G. B.; and Lilley, G. M.: The Displacement Effect of Pitot Tubes in Narrow Wakes at Subsonic and Supersonic Speeds. Rep. No. 107, Coll. of Aeronaut., Cranfield (Engl.), Oct. 1956.
11. Davies, P. O. A. L.: The Behaviour of a Pitot Tube in Transverse Shear. J. Fluid Mech., vol. 3, pt. 5, Feb. 1958, pp. 441-456.
12. Sami, Sedat: The Pitot Tube in Turbulent Shear Flow. Developments in Mechanics, Vol. 5, H. J. Weiss, D. F. Young, W. F. Riley, and T. R. Rogge, eds., Iowa State Univ Press, 1969, pp. 191-200.
13. Davies, F. V.: Some Effects of Pitot Size on the Measurement of Boundary Layers in Supersonic Flow. Tech. Note No. Aero. 2179, Brit. R.A.E., Aug. 1952.

14. Blue, Robert E.; and Low, George M.: Factors Affecting Laminar Boundary Layer Measurements in a Supersonic Stream. NACA TN 2891, 1953.
15. Cole, J. A.; and Cope, W. F.: Boundary Layer Measurements at a Mach Number of $2\frac{1}{2}$ in the Presence of Pressure Gradients. NPL Eng. Div. No. 420/49, Brit. A.R.C., May 1949.
16. Preston, J. H.: The Determination of Turbulent Skin Friction by Means of Pitot Tubes. J. Roy. Aeronaut. Soc., vol. 58, no. 518, Feb. 1954, pp. 109-121.
17. MacMillan, F. A.: Experiments on Pitot-Tubes in Shear Flow. R. & M. No. 3028, Brit. A.R.C., 1957.
18. Livesey, J. L.: Behavior of Transverse Cylindrical and Forward Facing Total Pressure Probes in Transverse Total Pressure Gradients. J. Aeronaut. Sci., vol. 23, no. 10, Oct. 1956, pp. 949-955.
19. Quarmby, Alan; and Das, H. K.: Displacement Effects on Pitot Tubes With Rectangular Mouths. Aeronaut. Quart., vol. XX, pt. 2, May 1969, pp. 129-139.
20. Becker, H. A.; and Brown, A. P. G.: Response of Pitot probes in turbulent streams. J. Fluid Mech., vol. 62, pt. 1, 1974, pp. 85-114.

TABLE I.—COORDINATES OF TEST SECTION

[0° flap deflection]

x/c	Coordinates for —	
	Upper surface, cm (in.)	Lower surface, cm (in.)
0	0 (0)	0 (0)
0.00102	0.3556 (0.14)	-0.3302 (-0.13)
0.00422	0.8128 (0.32)	-0.6350 (-0.25)
0.00960	1.2954 (0.51)	-0.8890 (-0.35)
0.01702	1.8288 (0.72)	-1.1684 (-0.46)
0.02650	2.3622 (0.93)	-1.4732 (-0.58)
0.03602	2.9464 (1.16)	-1.7526 (-0.69)
0.05158	3.5052 (1.38)	-2.0574 (-0.81)
0.06694	4.0894 (1.61)	-2.3628 (-0.93)
0.08422	4.6482 (1.83)	-2.6416 (-1.04)
0.10330	5.1816 (2.04)	-2.9210 (-1.15)
0.12403	5.6642 (2.23)	-3.2004 (-1.26)
0.14643	6.1468 (2.42)	-3.4544 (-1.36)
0.17037	6.5532 (2.58)	-3.7084 (-1.46)
0.19558	6.9342 (2.73)	-3.9370 (-1.55)
0.22221	7.2390 (2.85)	-4.1402 (-1.63)
0.24998	7.4930 (2.95)	-4.3180 (-1.70)
0.27891	7.6708 (3.02)	-4.4704 (-1.76)
0.30861	7.8232 (3.08)	-4.5720 (-1.80)
0.33923	7.8740 (3.10)	-4.6228 (-1.82)
0.37056	7.8740 (3.10)	-4.6482 (-1.83)
0.40243	7.7724 (3.06)	-4.6482 (-1.83)
0.43469	7.5946 (2.99)	-4.5720 (-1.80)
0.46733	7.3152 (2.88)	-4.4450 (-1.75)
0.49997	6.9850 (2.75)	-4.2672 (-1.68)
0.53274	6.6040 (2.60)	-4.0132 (-1.58)
0.56525	6.1722 (2.43)	-3.7592 (-1.48)
0.59750	5.7404 (2.26)	-3.5052 (-1.38)
0.62938	5.2832 (2.08)	-3.2766 (-1.29)
0.66074	4.8006 (1.89)	2.9718 (1.17)
0.69133	4.3688 (1.72)	2.6924 (1.06)
0.72115	3.9116 (1.54)	2.4384 (0.96)
0.74995	3.5052 (1.38)	2.1844 (0.86)
0.77773	3.0734 (1.21)	1.9304 (0.76)
0.80435	2.6924 (1.06)	1.7272 (0.68)
0.82970	2.3622 (0.93)	1.4478 (0.57)
0.85350	1.9558 (0.77)	1.2192 (0.48)
0.87590	1.6256 (0.64)	0.9906 (0.39)
0.89604	1.3208 (0.52)	0.7620 (0.30)
0.91571	1.0922 (0.43)	0.5334 (0.21)
0.93299	0.8890 (0.35)	0.3302 (0.13)
0.94848	0.6858 (0.27)	0.2032 (0.08)
0.96192	0.5080 (0.20)	0.1524 (0.06)
0.98291	0.3048 (0.12)	0.1016 (0.04)
1.00000	0.0508 (0.02)	0.0508 (0.02)

TABLE II.—PROBE DISPLACEMENT LITERATURE
 [Adapted from ref. 7]

Reference	Probe shape	D/δ	Mach number	Reynolds number, per meter (per foot)	General results
Free shear flow (wakes)					
8	Circular	0.02 to 0.27	0	1.3×10^6 (0.396×10^6)	$\beta/D \approx 0.18$
9	Circular	0.3 to 6.0	1.96	13.0 (3.96)	No displacement
10	Circular	0.62 to 14.2	0 to 3.2	1.0 to 13.7 (0.3 to 4.18)	$\beta/D \approx 0.18$, but decreasing for large D
11	Circular	0.01 to 3.2	0	1.5 (0.46)	Positive displacement
12	Circular	<0.04	0	0.6 to 1.1 (0.18 to 0.335)	Positive displacement
Laminar boundary layers					
13	Circular	0.18 to 1.18	2.30	10.0 to 12.0×10^6 (3.05 to 3.66×10^6)	$\beta/D \approx -0.15$
14	Rectangular	0.06 to 0.32	2 and 3	5.0 to 9.9 (1.52 to 3.02)	Negative displacement
Turbulent boundary layers or pipe flow					
13, 15	Circular	0.08	2.5	3.3×10^6 (1.0×10^6)	Positive displacement near wall
13, 15	Rectangular	0.02 to 0.16	2.5	3.3 (1.0)	Negative displacement for probes touching wall
16	Circular	0.03 to 0.12	0	0.6 to 2.4 (0.18 to 0.732)	$0.12 < \beta/D < 0.18$ for probes touching wall
16	Rectangular	0.003	0	3.0 (0.91)	Negative displacement near wall
17	Circular	0.02 to 0.12	0	0.5 to 2.3 (0.15 to 0.7)	$\beta/D \approx 0.15$, but decreases near wall
18	Circular	0.01 to 0.13	0	0.5 (0.15)	$\beta/D \approx 0.09$
11	Circular	0.04 to 0.68	0	1.5 (0.46)	No displacement
19	Rectangular	0.02 to 0.09	0	0.6 to 1.3 (0.18 to 0.40)	$\beta/D \approx 0.19$, but decreases near wall
7	Circular	0.2 to 0.7	2	8.0 (2.44)	Positive displacement
20	Square	0.4	<0.5	1.5 (0.46)	$\Lambda < 5D$

ORIGINAL PAGE IS
OF POOR QUALITY

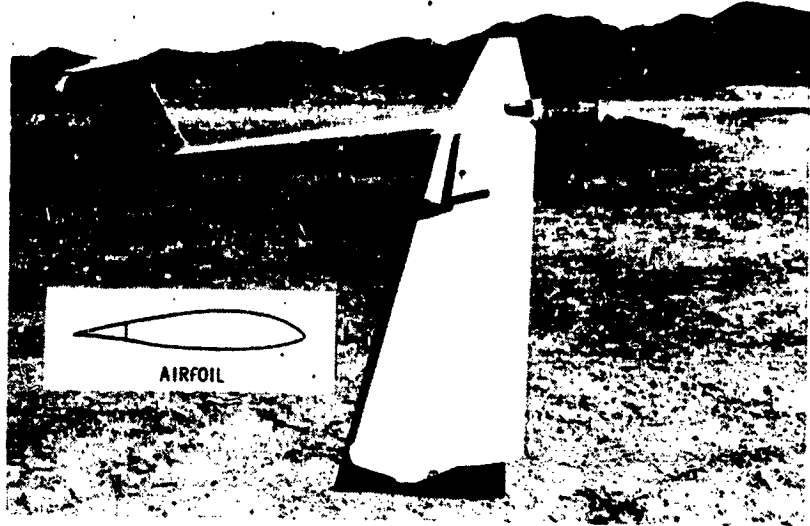


Figure 1.- Test vehicle and airfoil section.

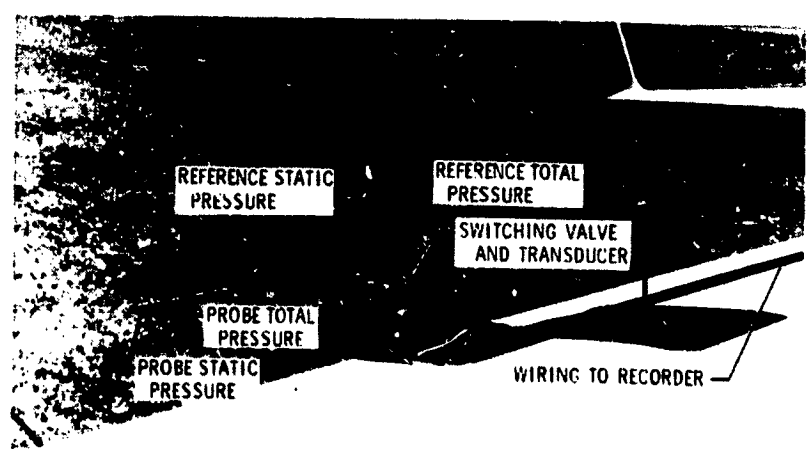


Figure 2.- Traversing-probe mechanism, reference pressure sources, and related equipment on the wing.

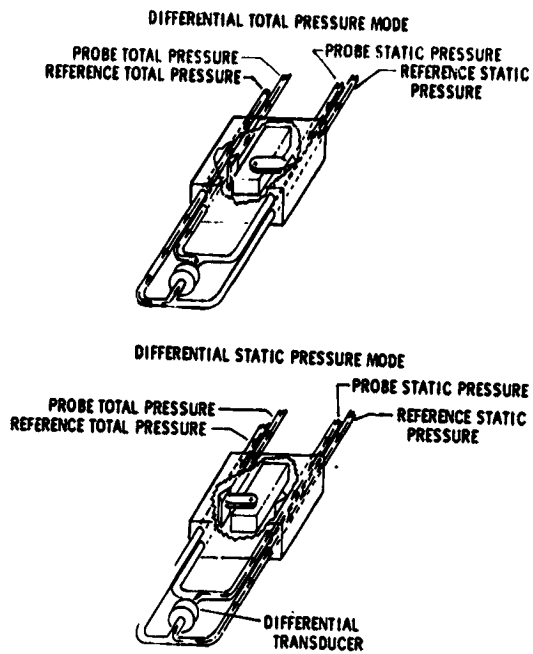


Figure 3.- Schematic drawing of switching valve in the incremental total and incremental static-pressure modes. All lines show continuous flexible tubing.

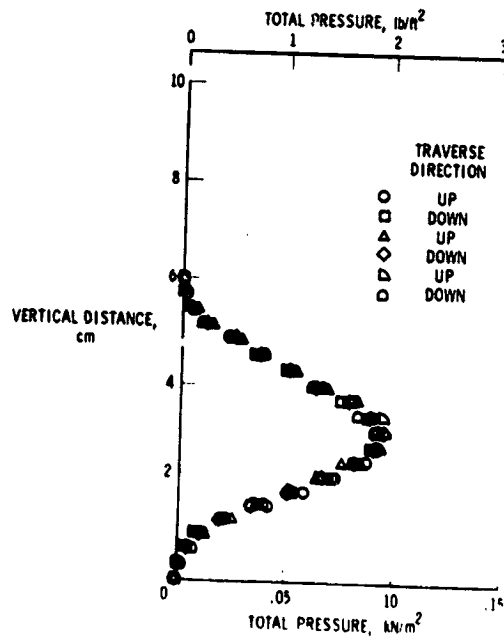


Figure 4.- Typical total-pressure wake profiles. Six consecutive wakes; flap deflection, 0° ; velocity, 44.0 knots; q_0 , 0.31 kN/m^2 (6.5 lb/ft^2).

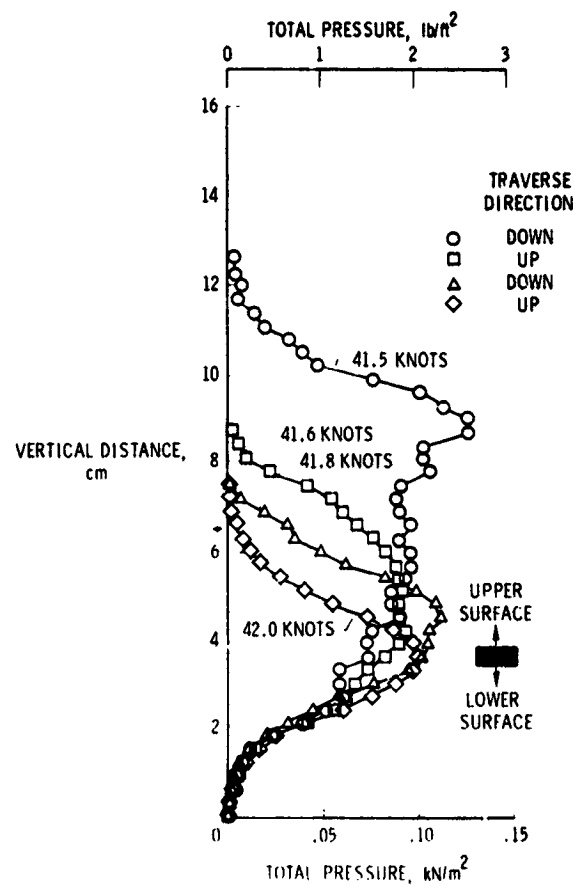
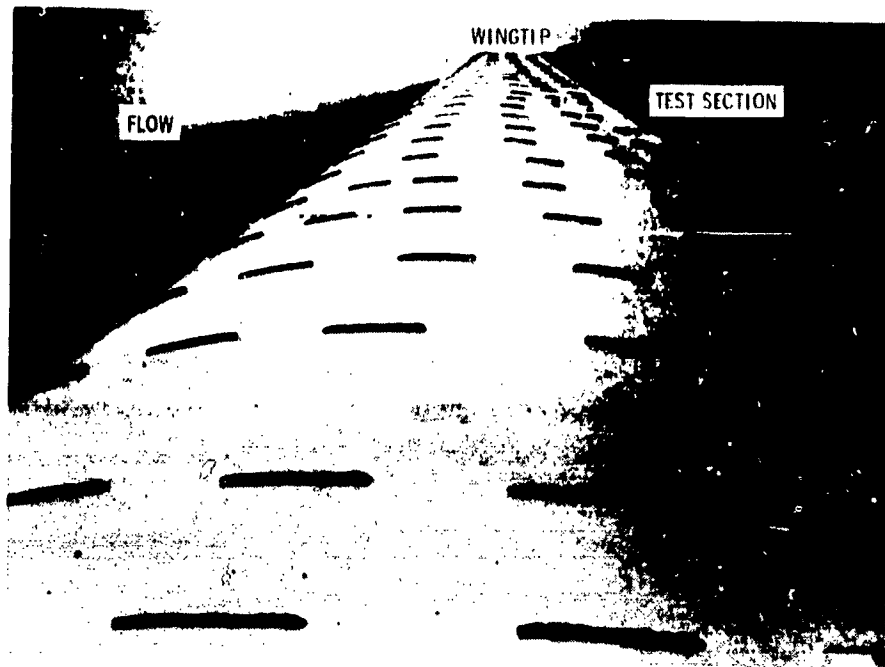
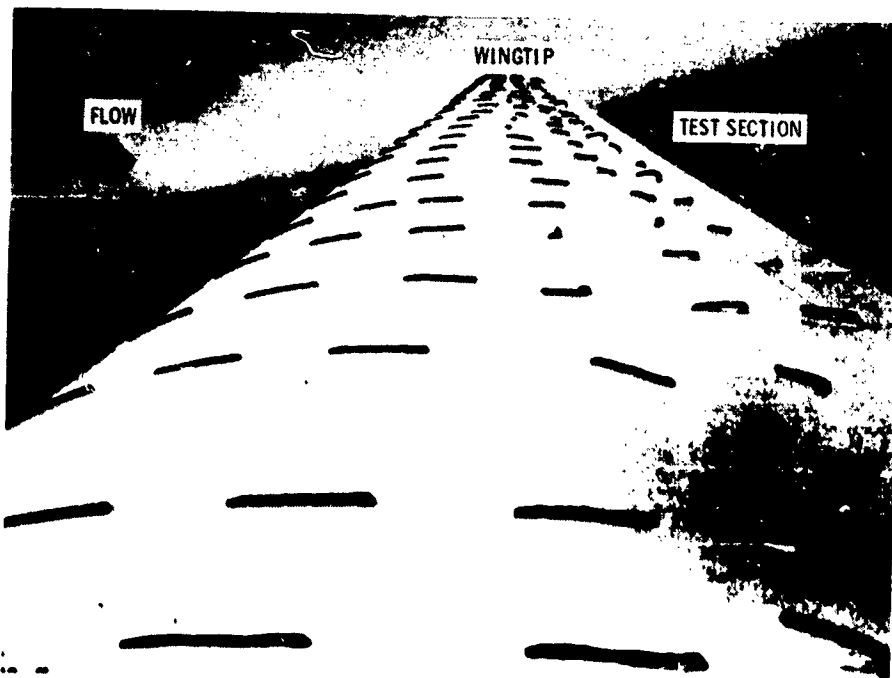


Figure 5.- Total-pressure wake profiles showing the development of flow separation. Flap deflection, 0°.



(a) Test conditions similar to the 42.0-knot wake in figure 5.



(b) Test conditions similar to the 41.5-knot wake in figure 5.

Figure 6.- Tuft photographs on the right wing upper surface.

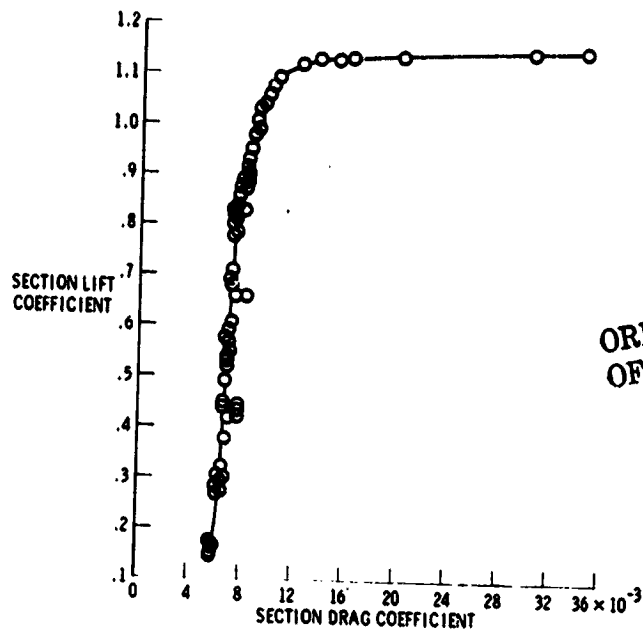


Figure 7.- Variation of section drag coefficient with section lift coefficient. Flap deflection, 0° ; seven flights over 6 months.

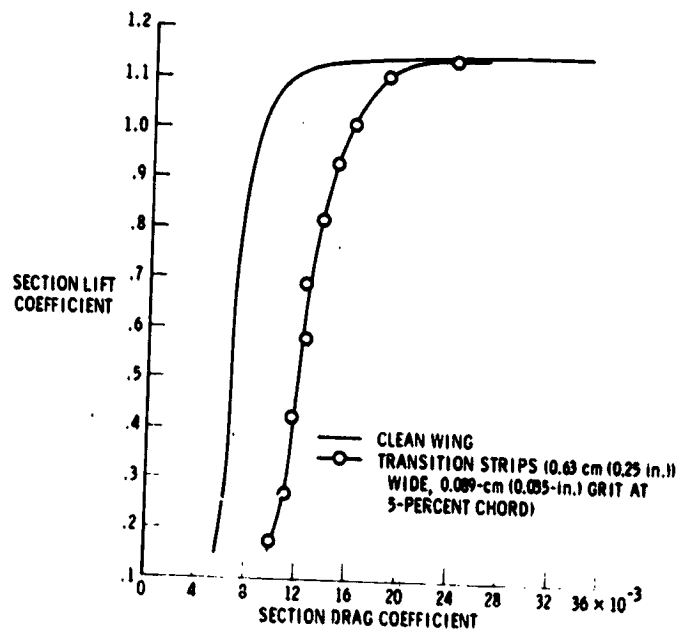


Figure 8.- Section drag coefficients with and without transition strips. Flap deflection, 0° .

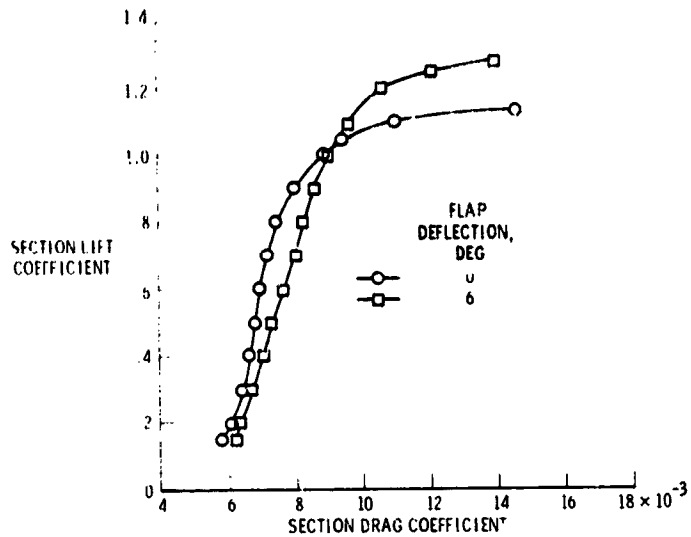


Figure 9.- Comparison of section drag coefficients between 0° and 6° flap-deflection data.

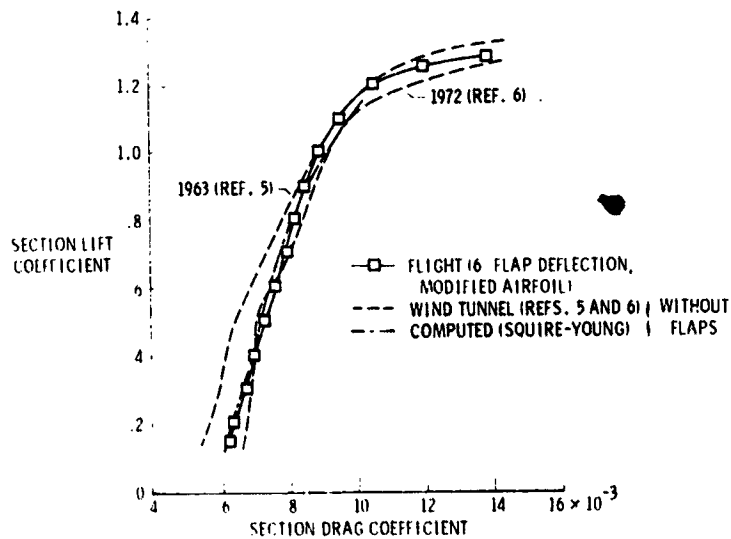


Figure 10.- Comparisons of section drag coefficients between flight, wind tunnel, and computed results for the FX61-163 airfoil.

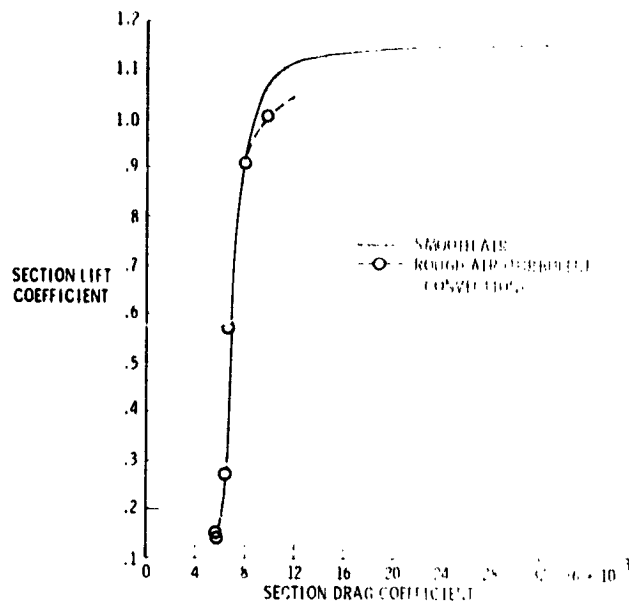


Figure 11.- Comparison of smooth and rough air section drag coefficients. 0° flap deflection.

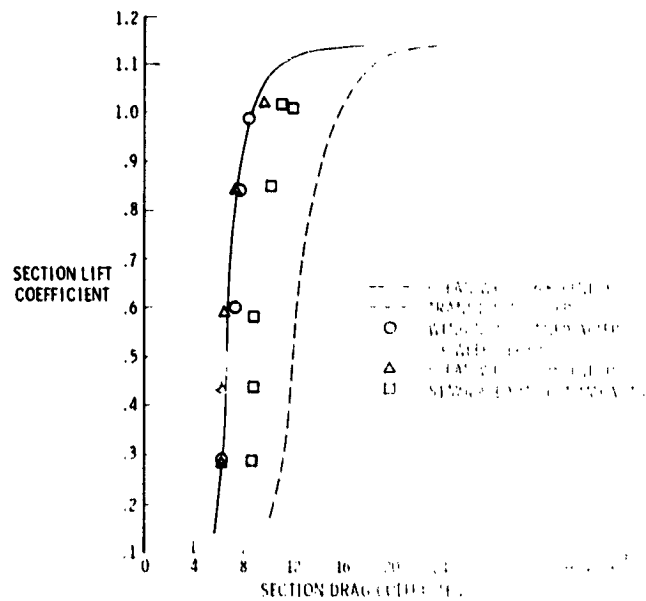


Figure 12.- Section drag coefficient for various surface conditions. 0° flap deflection.

FLIGHT TEST TECHNIQUES

FOR LOW SPEED AIRFOIL EVALUATION*

M. J. Hoffmann, G. M. Gregorek, and G. S. Weislogel
The Aeronautical and Astronautical Research Laboratory
The Ohio State University

SUMMARY

Techniques for in-flight evaluation of new airfoils by modifying a single engine general aviation aircraft and measuring and recording airfoil surface pressures, airfoil wake pressures, and aircraft angle of attack and airspeed are presented. Included are descriptions of the aircraft modifications, instrumentation, data reduction techniques, illustrations of typical results and comments on new equipment for flight test applications.

INTRODUCTION

The NASA LS(1)-0413 airfoil section characteristics have been evaluated in a flight test program (ref. 1). A single engine aircraft was modified, instrumented and flown, and pressure data was acquired, reduced and summarized. The program was successfully accomplished by implementing certain effective techniques. The existing wing of a "Beech Sundowner" testbed was "gloved" over the existing full-span to the contour of the LS(1)-0413 airfoil by the Beech Aircraft Corporation, an active participant in the flight program, thereby saving the expense of construction of an entirely new wing. The aircraft was instrumented with existing equipment supplemented by specially developed pressure measuring systems. A sophisticated and efficient data processing scheme was developed to handle the large quantities of data.

The purpose of this paper is to summarize the details of the techniques used to effectively complete the flight test program and to comment on some new instrumentation systems that could enhance future flight test efforts.

The symbols used herein are defined in an appendix.

*Some of the techniques described herein were developed and implemented while under contract to NASA Langley Research Center.

AIRCRAFT MODIFICATION

Background

To satisfy the objective of determining the section characteristics of the LS(1)-0413 airfoil in flight, it was first necessary to change the wing of a testbed aircraft, shown in figure 1, to the appropriate contour. Two options were available; build an entirely new wing, or modify the existing wing. Designing, building and proving a new wing is, unfortunately, time consuming and expensive. Modifying the existing wing by bonding on a new surface seemed attractive for this particular program for various reasons:

- 1) budget constraints favored the relatively inexpensive nature of this modification approach,
- 2) structural integrity of the existing wing structure could be utilized,
- 3) cable and tubing routing could be easily facilitated,
- 4) total time to modify the aircraft wing was a fraction of the time of the former alternative,
- 5) by use of bonding, a smooth finished surface could be obtained without extensive structural proving.

Based on these observations the "gloving" approach to wing modification was adopted. This simply meant that the new contour would be obtained by bonding formers to the old wing surface and bonding a new skin to those formers.

Design and Fabrication

The LS(1)-0413 was a 13% thickness ratio airfoil while the existing 632415 airfoil of the Sundowner was 15%. Figure 2 shows the modified wing with the larger chord. In order to accommodate the modification in the easiest manner, the leading edge was extended by 17.5 cm (7 in.) and the trailing edge by 7.5 cm (3 in.) to obtain a "good" range of center of pressure relative to the aircraft center of gravity (CG). The new gloved wing had an incidence angle 1.4 degrees larger than the existing wing, and the original linear wing twist of 2 degrees washout from root to tip was preserved. Also, an internal channel was incorporated into the modification for running cables and tubing from the wing without significantly disturbing the airflow.

The modification was begun by stripping the painted surfaces of the existing wing and ailerons. Balsa formers of 2.5 cm (1 in.) thickness were then bonded to the "old" skin on 20.3 cm (8 in.) centers with an epoxy type adhesive. Spanwise stringers were used for contour uniformity with wing results as shown

in figure 3 and aileron results in figure 4. These formers were wrapped with 0.5 mm (0.020 in.) sheet aluminum which was also bonded, thereby leaving a smooth, uniform rivetless surface. Also, external mass balances were used to statically balance the now modified ailerons.

INSTRUMENTATION SYSTEM

Overview

Once modified, the aircraft was instrumented as shown schematically in figure 5. Aircraft angle of attack was monitored as was dynamic pressure (not pictured). A scanivalve/cut-off valve system, operated by a remote controller, was used to acquire surface pressure data. A wake survey probe, sensing total and static pressure and a rotary drive mechanism were used to obtain momentum deficit information, ultimately resulting in drag coefficients. All these systems were powered from an instrument rack equipped with power supplies and signal conditioning equipment.

Sensors

The angle of attack sensor (vane) pictured in figure 6 consisted of a 15.2 cm (6 in.) stem fitted with a 3.8 cm (1.5 in.) fin, driving a one turn potentiometer. A collar was used to limit the sensor travel to 5 degrees nose up and 40 degrees nose down relative to the mounting boom. The vane was located 0.75 chord ahead of the quarter chord point. To correlate the vane reading to local section, a deck angle inclinometer (bubble level, figure 7) was used. This added piece of instrumentation allowed for the determination of local geometric angle of attack.

To sense surface pressures along the chord a strip-a-tube belt was used. The belt was formed from 5.1 mm (0.2 in.) plastic tube arranged in a group of twenty. Each tube was plugged appropriately to obtain forty active lines from the twenty tubes. Orifices were located once the belt was fastened to the aircraft wing surface with double sided tape. Lead in lines were run from the belt sensor, through the wing channel, into the cabin and connected to the scanivalve/cut-off valve system. Figure 8 shows a typical belt installation.

The wake survey probe was actually two sensors - one total pressure and one static pressure sensor - which was rotated through the wake of the wing at one of two spanwise stations during a given flight. The sensors were separated from each other by 5.1 cm (2 in.) in the wing spanwise direction, thus allowing total and static pressures to be measured at the same chordwise station (0.14 chord aft of trailing edge). By properly locating the wake probe, either a baseline (basic airfoil) or aileron station could be surveyed. Figure 9 illustrates this wake survey probe.

Supporting Equipment

To provide excitation voltages and signal conditioning an instrument rack (figure 10) was constructed. The rack contained all necessary power supplies, amplifiers, bridge balance units and carrier demodulators. Also, the scanivalve/cut-off valve system was mounted to the rack, and the 7 channel FM analog tape recorder used for data recording was mounted atop the rack. The total weight of the rack fully equipped was 351 N (79 lbs.) with approximate dimensions of 48 cm W x 53 cm H x 41 cm D (19 in. W x 21 in. H x 16 in. D).

For ease in operating all the instrumentation systems a remote controller was designed and built. The controller allowed full manual or automatic control of the systems from the flight test engineer position. The controller had an internal clock used to sequence the scanivalve/cut-off system and the "pitch-pause" motion (described later) of the wake survey probe. Once the engineer selected a data point, he did not have to intervene until all data from that test point was fully acquired and recorded. The systems would then be reset for another test condition. Figure 11 is a photograph of this controller.

DATA PROCESSING

A typical test flight would produce twelve test points resulting in large quantities of raw data. A special data processing scheme was developed to efficiently handle these data. Upon completion of a flight, the FM recorder (figure 12) would be taken to the ground based digital computer system (figure 13) and would be "patched" into the computer, thereby allowing the computer to digitize the analog signals played back by the recorder. Timing pulses provided by the instrumentation controller greatly assisted in the digitizing sequence. FORTRAN coded programs were used to manipulate the now digitized data and also allowed the operator to select options as to how the data should be reduced and presented. For instance, plots and printouts could be immediately generated for each test condition and/or summary plots could be made. In typical cases, fully reduced and plotted data could be "in-hand" within 3 hours of aircraft landing.

TYPICAL RESULTS

Surface Pressures

Typical of the partially reduced surface pressure data were pressure coefficient-chordwise location plots shown in figure 14. Two flight test angles of attack are shown by symbols and the corresponding analytic computations (ref. 2) are shown by the solid lines. These comparisons are at matched angle of attack, not matched lift. The two-dimensional angle of attack was obtained by subtracting an induced angle calculated by a three dimensional analytic code of Beech Aircraft Corporation. At the lower angle the scatter in the flight test data is seen to be low and compares well with analytic calculations. At

the higher angle (lower dynamic pressure for the case at hand) the scatter is slightly more due to the pressure belt itself and the decreasing accuracy of the pressure measurements at low dynamic pressure. Overall, however, these results are highly acceptable.

Wake Surveys

Partial reduction of the raw data from wake surveys lead to pressure-position plots similar to those shown in figure 15. The first plot shows a continuously scanned survey while the second plot shows the stepped or "pitch-pause" method of surveying. The latter method was generally used to eliminate any potential response problems. The result of the method was a physical averaging of the data due to a finite number of points through the wake (shown by the relative smoothness of the plot). Both total and static pressures were measured and presented and the static pressure variation is seen as significantly different from free stream static (the reference pressure). Based on these kinds of plots, limits of integration were chosen and drag coefficients produced.

Baseline Lift and Moment

Carrying the surface pressure data reduction to completion by integration of pressure distribution resulted in lift and moment coefficients as functions of angle of attack (figure 16). Lift data from three spanwise stations are shown to coincide very well by applying the three-dimensional analytic induced angle correction and compares well with the faired wind tunnel data (solid line) of McGhee, et al. (ref. 3). The lift coefficient data becomes somewhat scattered at low dynamic pressures again due to the lower accuracy of the transducers in that regime. A small error in the dynamic pressure measurement unfortunately comes through strongly in the final reduction. The moment coefficients are scattered and are generally more positive than wind tunnel measurements. The significant deviation could be due to slight trailing edge differences between the LS(1)-0413 modified aircraft wing and the wind tunnel model used for comparison.

Drag Polars

Full reduction of the wake pressures lead to the baseline drag polar shown in figure 17. The symbols represent two test flights taken almost one year apart. The wind tunnel data is again that of McGhee. The cases shown are for smooth wing surface and smooth model. Due to the varying Reynolds number in the flight data two bracketing wind tunnel cases are presented and the proper trend of the flight data can be seen. A similar drag polar is shown in figure 18. Here, however, the wind tunnel model boundary layer was tripped at 7.5% chord as was the flight test airfoil. The baseline drag polar is also shown for reference as a solid line. Very good agreement can be seen as the flight test data trends from almost exact agreement at lower lift/higher Reynolds number to good agreement at higher lift/lower Reynolds number.

Pressure Station Data

Pressure beam and potentiometer surveys were also taken at aileron stations. Figure 19 shows a typical pressure distribution at an aileron station with the solid line being a typical test data for clarity. The "pinched in" (reduced lift) nature of the airfoil due to gap flow is evident. No attempt was made to apply the more theoretical analytic induced angle computations at these stations because of the "distorted" type of flow phenomenon. Figure 20 shows the rather serious drag increase incurred by having gap flow. The comparison is with either a standard airfoil (solid line) and represents a 45% increase in drag coefficient.

NEW SYSTEMS

The additional data obtained by developing and using the aforementioned instruments led to the design and construction of at least two new methods of probes. Figure 21 shows a rotating type probe mechanism which is able to be adjustable in the chordwise direction. The rotating nature of the probe allows two spanwise stations to be surveyed. The drive itself is approximately 10 cm wide and high and 30.5 cm (12 in.) long. Overall length including support platform is 55.9 cm (22 in.) while the total weight including probe and foam formers (streamlining) is 26.7 N (6 lbs.).

To enhance the data reduction capability while in flight, a Digital Data Acquisition and Reduction System (DDARS) has been developed in-house (ref. 3). A block diagram of the main components of this system, the main-frame (on left), the microprocessor, and the ground based disc drives (on right). The microprocessor is an Intel microprocessor, 32K words of memory, all necessary interface logic, and disc type drives and a 32 channel analog-to-digital converter (with a throughput using all channels). Also included are several relays for on/off type controls. Contained in a separate rack (not shown) are 6 bridge balance units and 6 differential amplifiers for signal conditioning. The components used in a flight of either the probe or the signal conditioner rack and the small console terminal are contained in the airborne package is 600 N (135 lbs.) and the maximum power consumption is 400 watts. The total volume required to locate the system is approximately 2.4 cubic meters (8.8 cubic ft.).

CONCLUSIONS AND OBSERVATIONS

Effective results have been obtained to evaluate the performance of an airfoil in a flight condition. Aircraft modification and instrumentation have been discussed and a data processing scheme and typical results. The data along with the results seem to indicate the system was acceptable over most of the aircraft's operating regime, questionable only at the very low dynamic pressure conditions. A transducer replacement could cure that problem. Also discussed are the new systems which can be effectively applied

In future flight test efforts - a wake survey drive mechanism and a new digital data acquisition and reduction system. The DDARS system seems to offer a quantum improvement in flight test data acquisition and reduction by implementation of its microprocessor-based mainframe and real time peripherals while the wake survey mechanism offers good probe motion in a small, light package

REFERENCES

1. Gregorek, G. M., Hoffmann, M. J., Weislogel, G. S., and Vogel, G. M., "In-Flight Measurements of the GA(W)-2 Aerodynamic Characteristics", Paper 770461 presented at the SAE Business Aircraft Meeting, Wichita, Kansas, March 1977.
2. Stevens, W. H., Goradia, S. H., Branden, J. A., "Mathematical Model For Two-Dimensional Multi-Component Airfoils in Viscous Flow", NACA CR 1843, 1971.
3. McGhee, R. J., Beasley, W. D., Somers, D. M., "Low Speed Aerodynamic Characteristics of a 13 Percent Thick Airfoil Section Designed for General Aviation Applications", NASA TM X-72697, 1975.
4. Freuler, R. J., Hoffmann, M. J., "Digital Data Acquisition and Reduction System for Flight Testing General Aviation Aircraft", AIAA Paper No. 77-1216 presented at the AIAA Aircraft Systems and Technology Meeting, Seattle, Washington, August 1977.

APPENDIX

SYMBOLS

Measurements and calculations were made in the U.S. Customary Units. They are presented herein in the International System of Units (SI) with the equivalent values given parenthetically in the U.S. Customary Units.

c	chord of an airfoil
C_d	section drag coefficient, $\frac{\text{Section drag}}{q_\infty c}$
C_l	section lift coefficient, $\frac{\text{Section lift}}{q_\infty c}$
C_m	section pitching moment coefficient with respect to 0.25 chord, $\frac{\text{Section moment}}{q_\infty c^2}$
C_p	static pressure coefficient, $\frac{p - p_\infty}{q_\infty}$
p	measured local pressure
p_∞	free stream static pressure
q_∞	free stream dynamic pressure
R_e	Reynolds number based on chord
$x, x/c$	distance along chord, non-dimensional distance along chord
α, α_{2D}	angle of attack in two-dimensional flow



Figure 1.- Testbed aircraft in flight.

— LS (1)-0413 MOD
- - - EXISTING 63₂⁴¹⁵



Figure 2.- Airfoil-modification cross section.

ORIGINAL PAGE IS
OF POOR QUALITY

ORIGINAL PAGE IS
OF POOR QUALITY

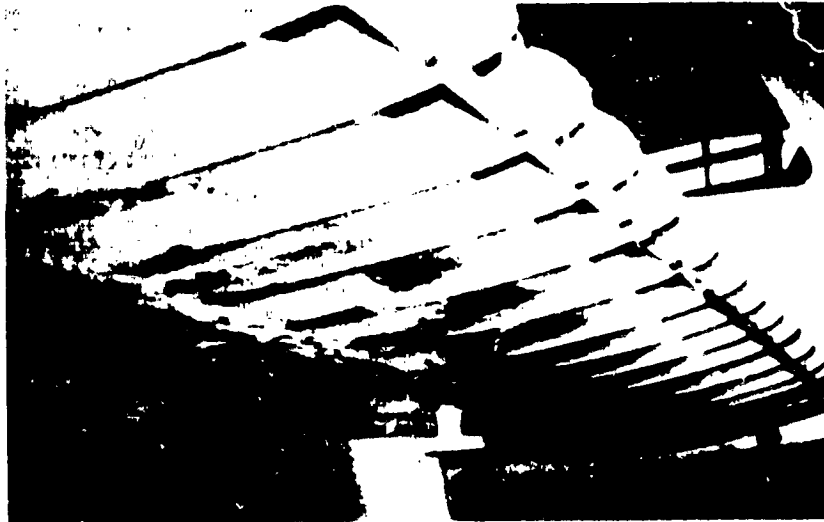


Figure 3.- Balsa-wood wing formers.



Figure 4.- Aileron modification.

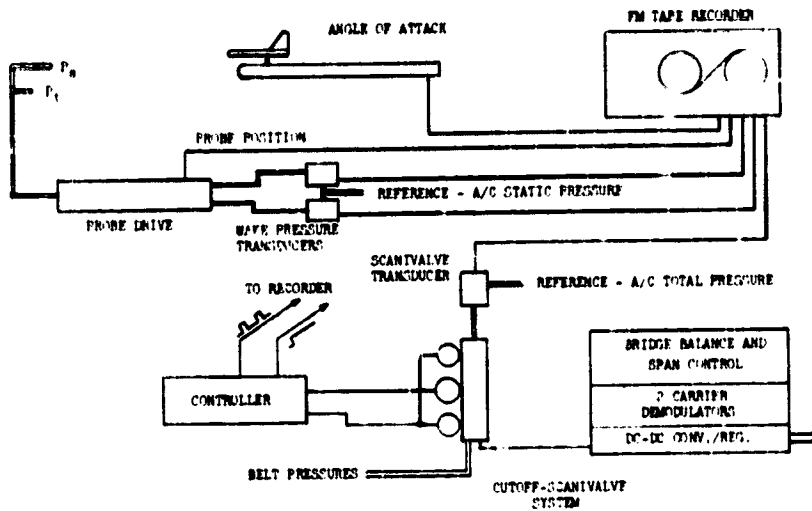


Figure 5.- Data-acquisition schematic diagram.

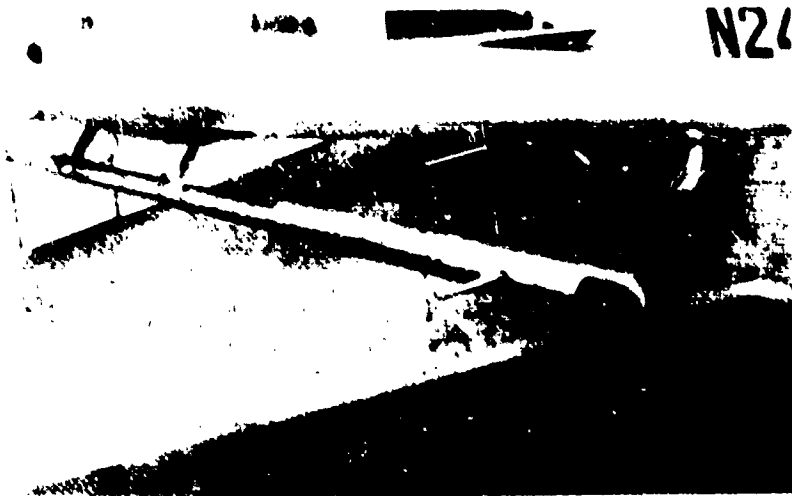


Figure 6.- Angle-of-attack sensor.

ORIGINAL PAGE IS
OF POOR QUALITY

ORIGINAL PAGE IS
OF POOR QUALITY



Figure 7.- Deck-angle inclinometer.

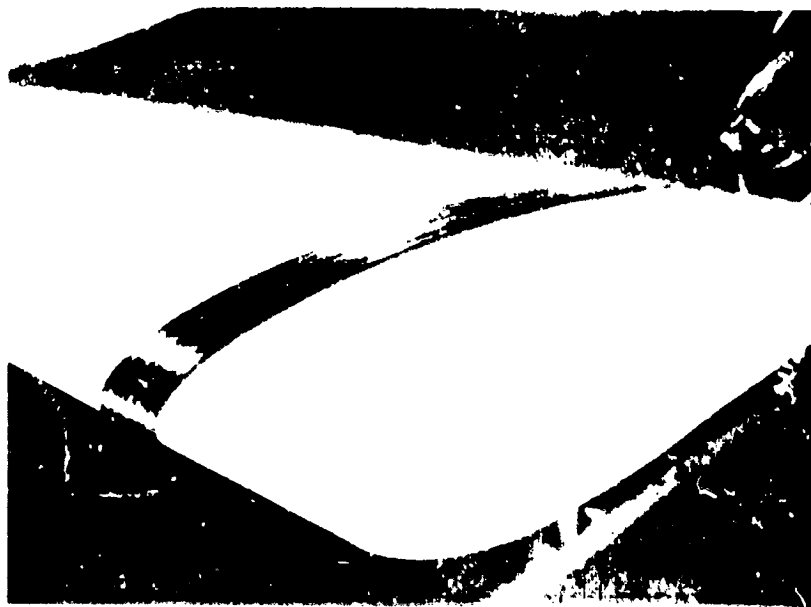


Figure 8.- Pressure-belt sensor.



Figure 9.- Wake-survey probe.

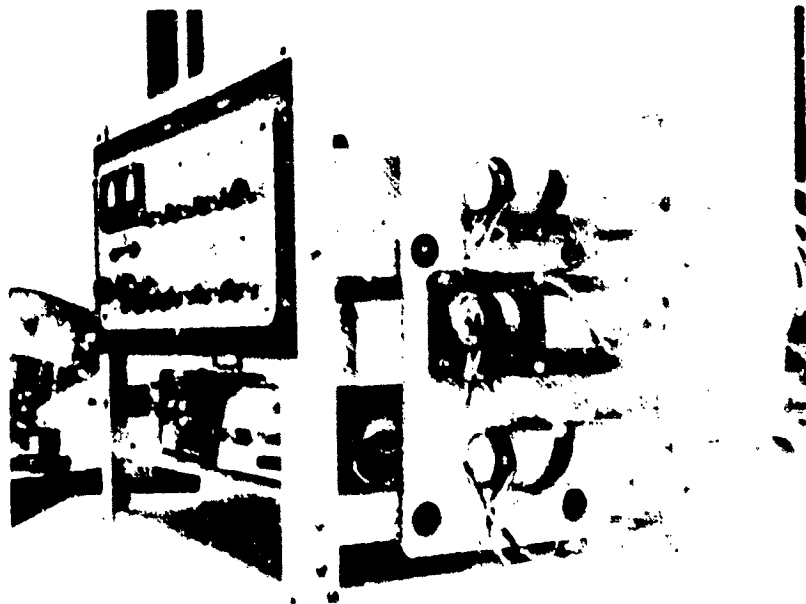


Figure 10.- Instrument rack.

ORIGINAL P.L.
OF POOR QUALITY

ORIGINAL PAGE IS
OF POOR QUALITY

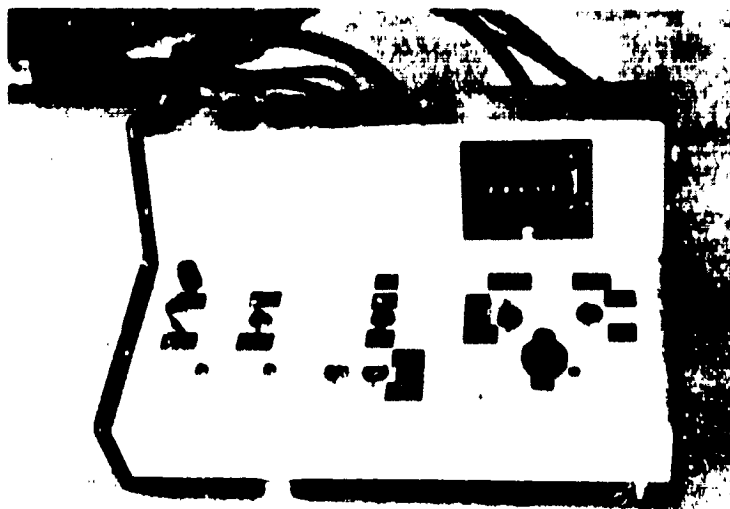


Figure 11.- Remote-control panel.

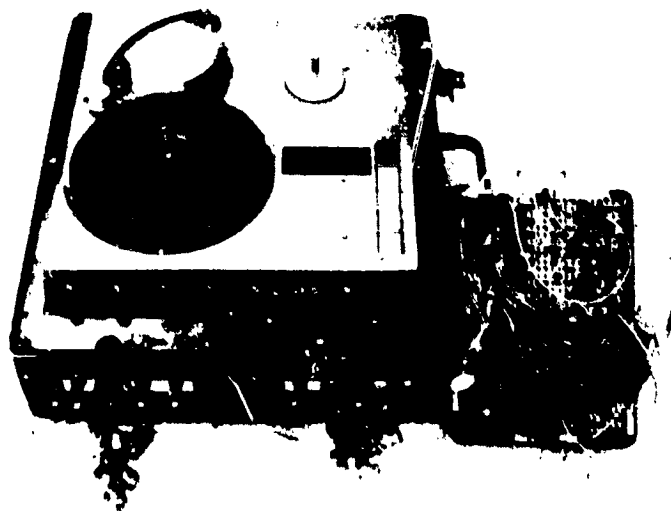


Figure 12.- FM analog recorder with patch panel.



Figure 13.- Ground-based digital computer system.

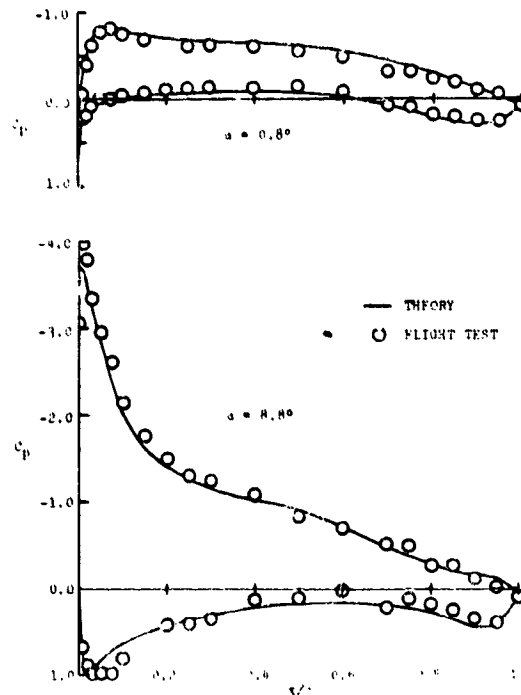


Figure 14.- Comparison of pressure distributions.

ORIGINAL PAGE IS
 OF POOR QUALITY

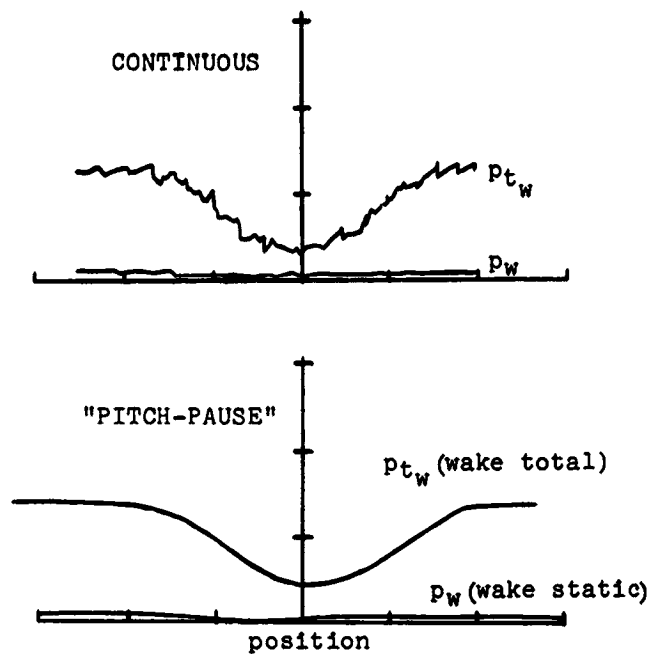


Figure 15.- Typical wake-survey profiles.

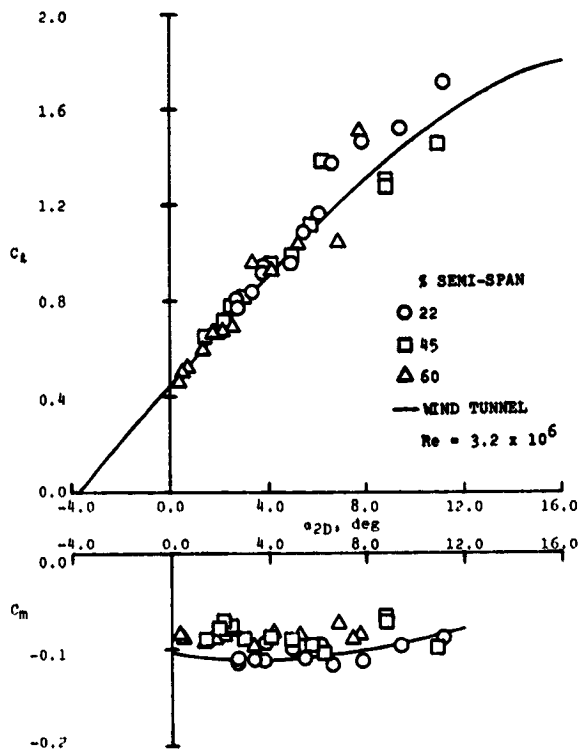


Figure 16.- Lift and moment coefficients.

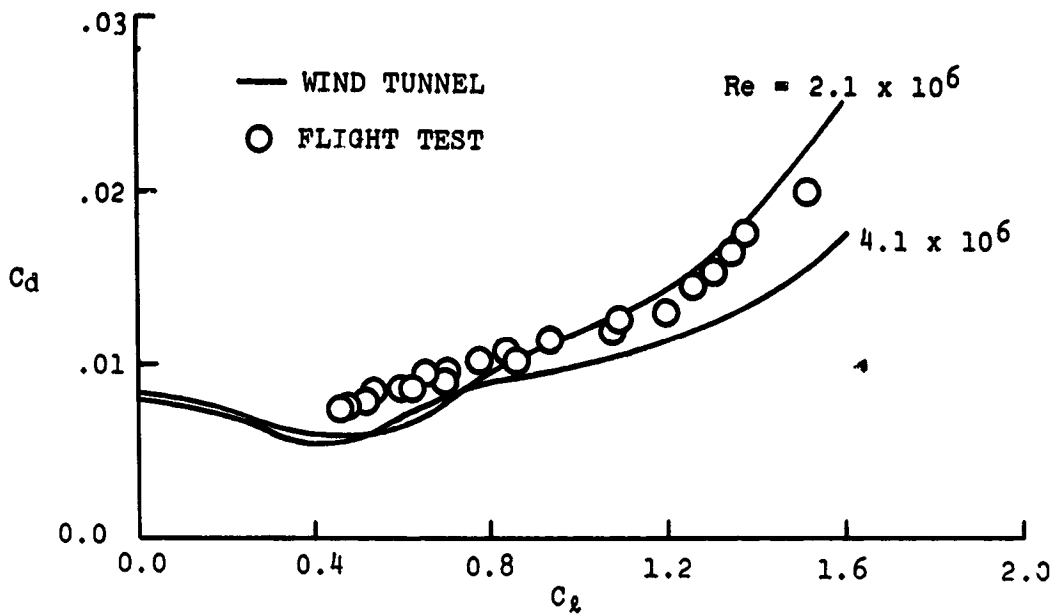


Figure 17.- Baseline drag polar.

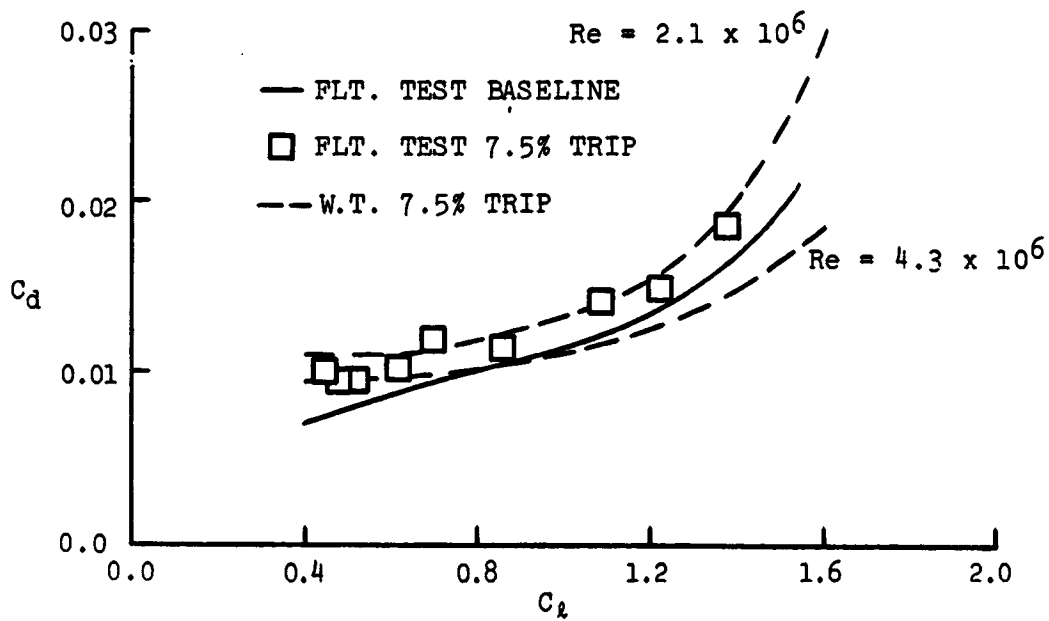


Figure 18.- 7.5% trip drag polar.

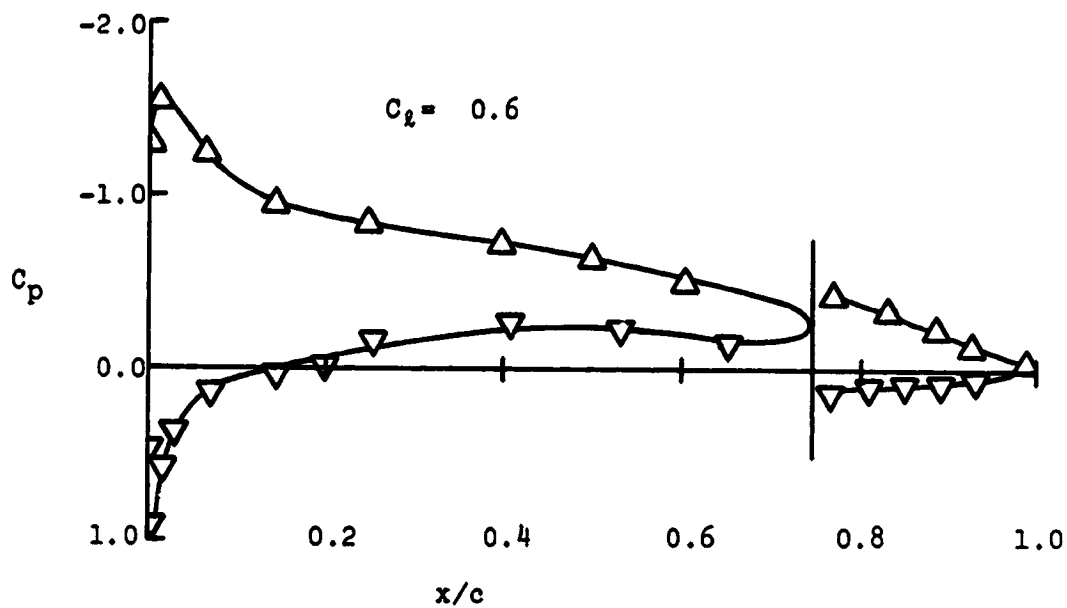


Figure 19.- Aileron-station pressure distribution.

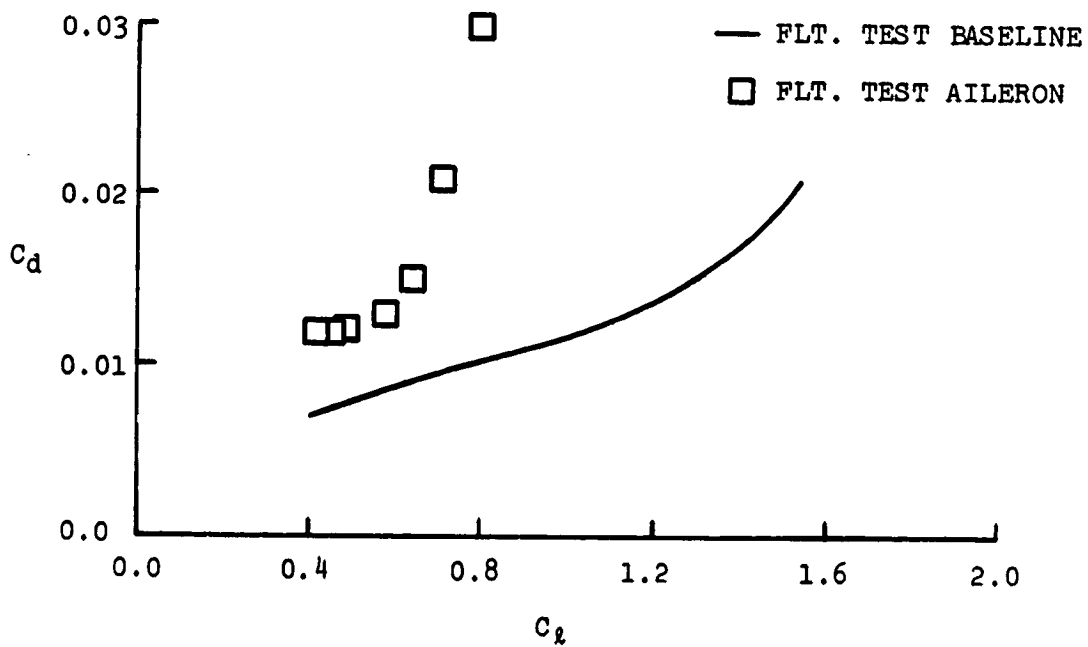


Figure 20.- Aileron-station drag polar.

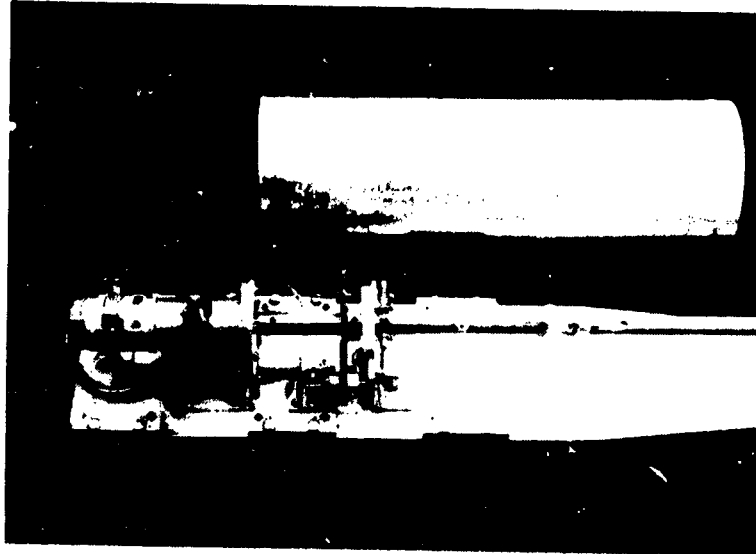


Figure 21.- New wake survey mechanism.

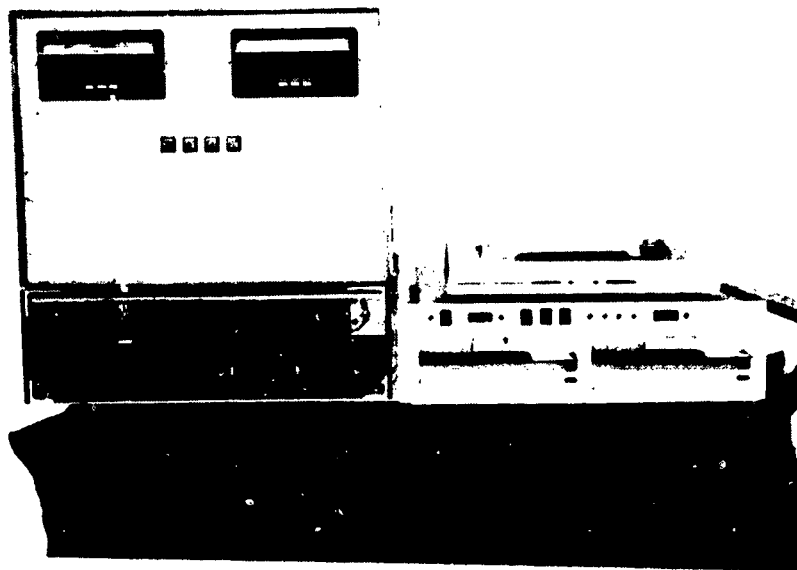


Figure 22.- Digital-data acquisition and reduction system.

IN-1. (GHT THREE-DIMENSIONAL BOUNDARY LAYER AND WAKE
MEASUREMENTS FROM A SWEEP SUPERCRITICAL WING

David P. Lux
NASA Dryden Flight Research Center

SUMMARY

Three-dimensional boundary layer and wake velocity profiles were measured in flight on the supercritical wing of the F-111 transonic aircraft technology (TACT) aircraft. These data, along with pressure distributions, were obtained to establish a data base with which data obtained by three-dimensional analytical techniques could be correlated. Only a brief summary of the total data base is given in this paper.

The data presented represent one chord station at a wing leading-edge sweep angle of 26° . They cover an angle of attack range from 6° to 9° at free-stream Mach numbers from 0.85 to 0.90. A brief discussion of the techniques used to obtain the boundary layer and wake profiles is included.

INTRODUCTION

A recurring problem during the initial design of transonic aircraft is the lack of proven analytical methods to reliably predict three-dimensional, viscous flow effects. Many analytical methods have been or are being developed to predict these effects. A few of these methods are described in references 1 to 3. However, there is a lack of adequate full-scale Reynolds number, three-dimensional data with which to compare and verify these analytical methods.

Therefore, an investigation of the three-dimensional boundary layer and wake flow characteristics was conducted at one semispan station on the F-111 transonic aircraft technology (TACT) aircraft. The purpose was to establish a data base with which three-dimensional analytical techniques could be correlated.

The three-dimensional upper-surface boundary layer measurements were obtained at 96 percent chord and the wake measurements at 108 percent chord of the TACT wing for a leading-edge sweep angle of 26° . The data presented are for a range of airplane angles of attack from 6° to 9° at Mach numbers from 0.85 to 0.90. The chord Reynolds number of these data is approximately 20 million. These data provide examples of boundary layer and wake flow characteristics at, above, and below the optimum airfoil design conditions. A brief discussion of the techniques used in obtaining the three-dimensional data is included.

SYMBOLS

The angle of attack used in this paper is the aircraft angle of attack referenced to the wing reference plane. However, because of wing twist and aeroelastic effects, the angle of attack for the section characteristics is 4° lower than that for the airplane.

B	aircraft span at wing sweep angle of 26° , cm
C_L	lift coefficient, Lift/qS
C_p	pressure coefficient, $(p - p_\infty)/q$
h	distance above or below wing trailing edge, cm
M	Mach number
p	local static pressure, kN/m^2
p_∞	free-stream static pressure, kN/m^2
q	free-stream dynamic pressure, kN/m^2
S	wing area, m^2
V_x/V_∞	ratio of chordwise velocity to free-stream velocity
V_y/V_∞	ratio of spanwise velocity to free-stream velocity
x/c	ratio of distance from leading edge to local chord length
Y	distance from aircraft centerline, cm
z	distance above and perpendicular to wing upper surface, cm
α	aircraft angle of attack referenced to wing reference plane
η	semispan station, $2Y/B$

EXPERIMENT DESCRIPTION AND TECHNIQUE

The TACT test-bed airplane is a modified F-111A airplane (fig. 1). The modification consisted of the installation of a new wing incorporating an earlier NASA

supercritical airfoil. Although the aircraft's maximum speed is in excess of Mach 2.0 the supercritical wing was designed for transonic speeds and represents a compromise between cruise conditions ($M = 0.85$, $C_L = 0.47$) and maneuver conditions ($M = 0.90$, $C_L = 0.67$) at a wing sweep angle of 26° (ref. 4).

For the boundary layer and wake data presented in this paper, the wing leading-edge sweep angle was fixed at 26° where chordwise pressures were previously obtained. The boundary layer, wake, and surface pressure measurements were made at semispan station 0.705, as shown in figure 2. The boundary layer measurements were made on the upper surface using the fixed, trailing-edge rake, which is shown in figure 3. This rake was approximately 11 centimeters high with 12 multi-orifice probes to sense local flow velocity and direction (fig. 4). The calibration technique used to determine total pressure and flow direction angles for this probe is described in reference 5. For the present experiment, the rake calibration was checked with tests conducted in Ames Research Center's 2- by 2-Foot Wind Tunnel. These results agreed with the results of reference 5. Airfoil wake measurements were made using the rotating probe shown in figure 5. The drive motor, position transducer, and pressure manifold were mounted under the trailing edge of the wing, and the probe head rotated behind the wing at 108 percent chord. Details of the probe head are shown in figure 6. The calibration used to determine total pressure and flow angles for this probe head is described in reference 5. Velocity profiles of the wake relative to the trailing edge of the airfoil were obtained by applying an axis transformation to the local flow angles at the probe head as it rotated behind the wing.

The rake and rotating probes described above and the associated sensors were found to perform adequately, exhibiting good repeatability for all flight conditions where attached flow existed. However, the 10-second rotation time limited the amount of wake data that could be obtained with the rotating probe. For some applications, a fixed wake rake may be more desirable.

All pressures from the boundary layer rake and wake probe were measured by differential pressure transducers located in temperature-controlled transducer boxes within the wing. The transducer boxes were interconnected by a common reference line with the reference pressure being measured by a precision, variable-capacitance, absolute transducer. The pressures and air data parameters were recorded on an onboard aircraft data tape.

The boundary layer data were gathered by flying the aircraft at a quasi-stabilized Mach-altitude condition. Then, to obtain data for a range of angles of attack, the aircraft was flown into a pushover-pullup maneuver followed by a slow-rate windup turn. This series of maneuvers generated an angle of attack range from approximately 2° to 10° during a time interval of about 20 seconds. The wake data were obtained at the same nominal conditions with one exception. During the windup turn maneuver, the pilot would incrementally hold each angle of attack for 30 seconds. This allowed rotating probe data to be obtained for a minimum of three complete probe cycles for each angle of attack.

RESULTS AND DISCUSSION

Representative three-dimensional boundary layer and wake data from the experiment are shown in figures 7 to 10. Each boundary layer and wake velocity profile is presented with the corresponding wing upper-surface pressure distribution. All velocity distributions are nondimensionalized with respect to the free-stream velocity obtained from the aircraft's onboard air data system. A complete description of this system is given in reference 6.

The pressure distribution and boundary layer velocity profiles for a Mach number of 0.85 and an angle of attack of 8° at a dynamic pressure of 14.36 kN/m^2 are shown in figure 7(a). Wake velocity profiles are presented in figure 7(b) for the same flight condition. The chordwise pressure distribution data suggest that this flight condition is nearly optimum for upper-surface flow. There is a long chordwise region of supercritical flow that terminates in an aft shock wave. The aft shock may cause a separation bubble at its base, but the pressure makes a complete recovery at the trailing edge and there is no second velocity peak. This flight condition is the basis for all other data comparisons in this paper.

Note that in figure 7(b) the chordwise wake edge velocity ratio exceeds 1.0. This is attributed to a static pressure error induced by the location of the static pressure orifices only two diameters behind the shoulder of the probe head (fig. 5). While this error does not affect the total pressure measurements, it causes the absolute values of the calculated velocities to be incorrect. This static pressure position error is evident in all the wake data presented.

It is of interest to compare the semispanwise flow characteristics for the wing upper surface at an x/c of 0.96 with the corresponding results at an x/c of 1.08 (figs. 7(a) and 7(b)). Note that at an x/c of 0.96, the spanwise flow component is inboard ($V_y/V_\infty = -0.1$) throughout most of the boundary layer. In the wake, at a distance of more than 8 centimeters above the surface of the wing, the flow turns outboard. This general trend can also be seen in the data for the other flight conditions considered in this paper.

Figures 8(a) and 8(b) show a comparison of the data for the optimum upper-surface flow condition (figs. 7(a) and 7(b)) with those obtained at an angle of attack of 6° . At this angle of attack, the shock wave is farther forward and a strong second velocity peak is followed by recompression to the trailing edge. Relative to the data for an angle of attack of 8° , the boundary layer velocity distribution for an angle of attack of 6° shows a thinning of the boundary layer and the wake velocity profiles show a similar thinning of the wake. This is, of course, indicative of lower section profile drag. While this lower section profile drag may seem more desirable, it should be remembered that less section lift is generated at an angle of attack of 6° , and airfoil efficiency is determined by the ratio of maximum lift to drag.

It is of interest to relate these results to corresponding wing boundary layer and wake data from the F-8 supercritical wing airplane (ref. 7). The F-8 data showed that the boundary layer and wake were thinnest at the airfoil design condition. This difference between the results of the present experiment and those obtained with the F-8 supercritical wing airplane is attributed to the fact that the F-8 supercritical

wing was designed for a specific flight condition ($M = 0.99$, $C_L = 0.40$), whereas the F-111 TACT wing represents a compromise between a Mach 0.85 cruise condition and a Mach 0.90 maneuver condition.

A comparison of the boundary layers and wakes for the optimum flow condition and an off-design condition of 9° angle of attack is shown in figures 9(a) and 9(b). Figure 9(a) shows that at the off-design condition, the wing shock has moved forward and the flow at the trailing edge is separated. The boundary layer velocity profiles (fig. 9(a)) show that the boundary layer has thickened considerably. Reverse flow occurred over the lower half of the profile, for which the data are not presented. Note that the boundary layer rake was not large enough to determine an edge condition in the chordwise velocity distribution. In addition, it can be seen that the spanwise velocity distribution had less inboard flow.

The wake velocity profiles show a similar thickening of the wake and, in addition, indicate a trend toward less inboard (that is, more outboard) flow. These results are not surprising when one considers the fact that the upper-surface flow has separated as indicated by the pressure distribution.

Figure 10 compares the data for the optimum flow angle of attack at a Mach number of 0.85 to data obtained at a Mach number of 0.90. Again, the pressure distribution obtained at a Mach number of 0.90 shows trailing-edge separation. The boundary layer velocity distributions show that the boundary layer has again thickened and an edge condition has not been reached. The lower half of the boundary layer is in reverse flow. The spanwise velocity distribution shows the flow to be less inboard than that for the profile at a Mach number of 0.85. No wake velocity profiles are given for this flight condition because the separated flow in the wake enveloped the wake probe in a reverse flow condition throughout the wake region. However, as shown in the pressure distributions, the separated flow region extends only a short distance forward to the base of the shock wave and does not envelop the entire upper surface of the wing. This unique feature of the supercritical wing provides improved maneuver performance at the higher transonic speeds (ref. 4).

CONCLUDING REMARKS

Three-dimensional upper surface boundary layer and total wake characteristics have been obtained from a supercritical airfoil at design and off-design conditions. The results of this experiment show that, in general, for this wing section at a Mach number of 0.85 and angles of attack from 5° to 9° , the boundary layer and wake thicknesses increase with increasing angle of attack.

In general, the data also indicate that there is little change in the three-dimensional characteristics of the boundary layer and wake until flight conditions are reached where trailing-edge separation occurs.

The boundary layer rake and rotating wake probe used in this study were found to satisfactorily measure boundary layer and wake flow angles where attached flow conditions exist.

REFERENCES

1. Bushnell, Dennis M.; Cary, Aubrey M., Jr.; and Harris, Julius E.: Calculation Methods for Compressible Turbulent Boundary Layers—1976. NASA SP-422, 1977.
2. Wortman, A.: Three-Dimensional Turbulent Boundary Layer Calculations - Exact and Simplified Solutions. AIAA Paper 75-854, June 1975.
3. Baker, A. J.: Finite Element Computational Theory for Three-Dimensional Boundary Layer Flow. AIAA Paper 72-108, Jan. 1972.
4. Hallissy, James B.; and Ayers, Theodore G.: Transonic Wind-Tunnel Investigation of the Maneuver Potential of the NASA Supercritical Wing Concept. Phase I. NASA TM X-3534, 1977.
5. Dudzinski, Thomas J.; and Krause, Lloyd N.: Flow-Direction Measurement With Fixed-Position Probes. NASA TM X-1904, 1969.
6. Cooper, James M., Jr.; Hughes, Donald L.; and Rawlings, Kenneth III: Transonic Aircraft Technology - Flight-Derived Lift and Drag Characteristics. Volume I. AFFTC-TR-77-12, Air Force Flight Test Center, Edwards, Calif., July 1977.
7. Montoya, Lawrence C.; and Banner, Richard D.: F-8 Supercritical Wing Flight Pressure, Boundary-Layer, and Wake Measurements and Comparisons With Wind Tunnel Data. NASA TM X-3544, 1977.

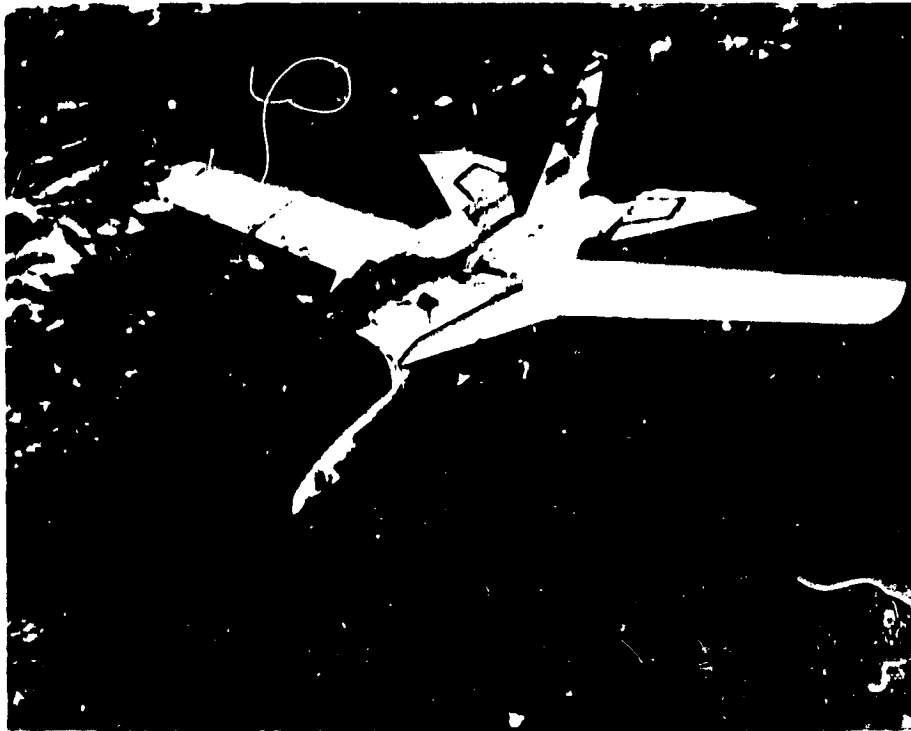


Figure 1.- F-111 TACT aircraft. Wing sweep angle, 26°.

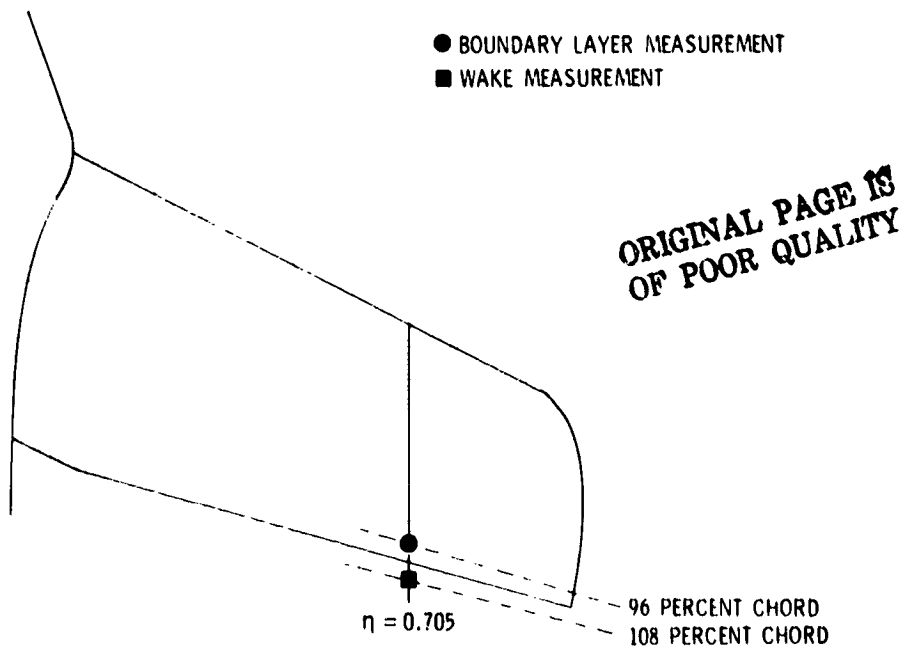


Figure 2.- Location of boundary layer, wake, and pressure-distribution measurements on the F-111 TACT wing.

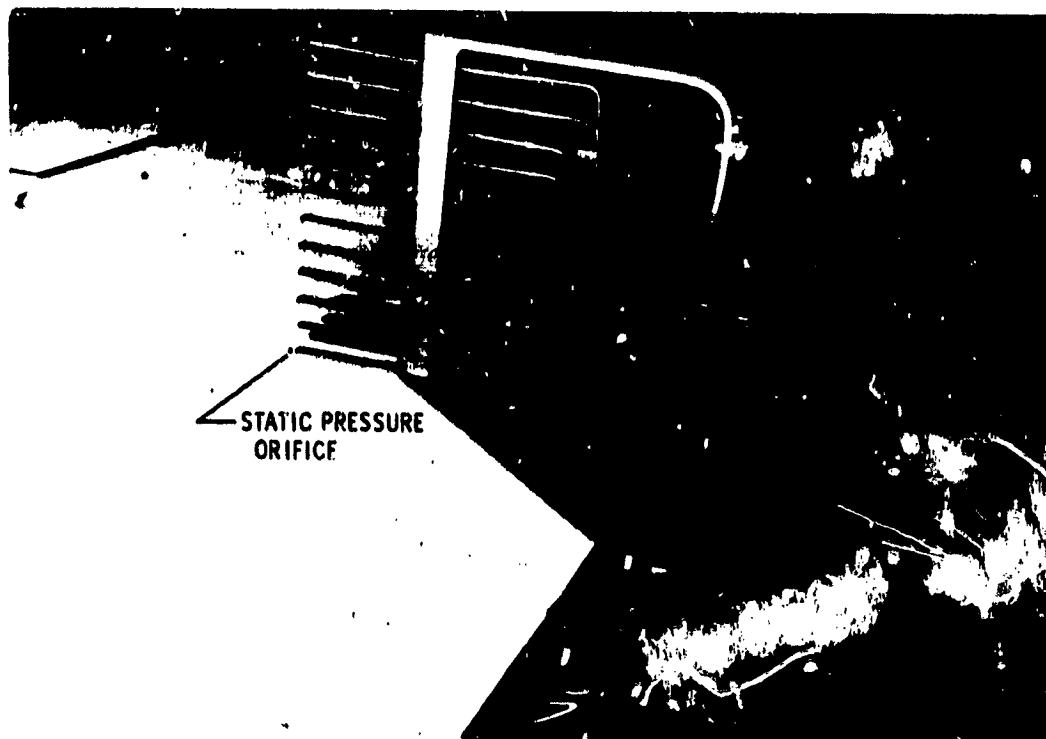


Figure 3.- Boundary-layer rake installed on wing of F-111 TACT aircraft.

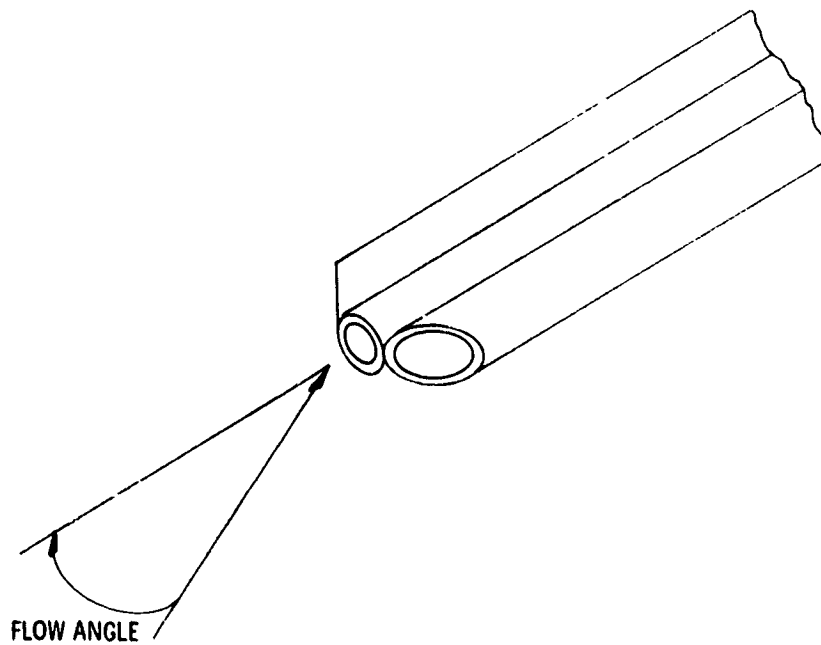


Figure 4.- Directional probe head for defining flow angle within the boundary layer.

ORIGINAL PAGE IS
OF POOR QUALITY

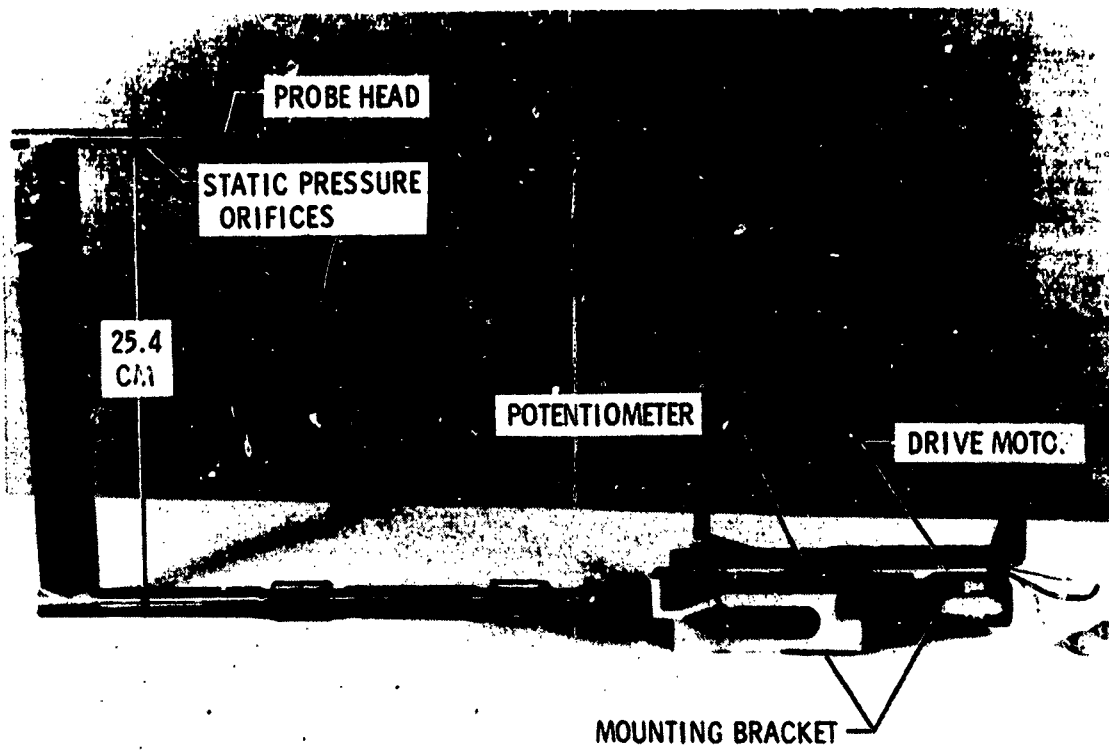


Figure 5.- Wake probe and drive mechanism.

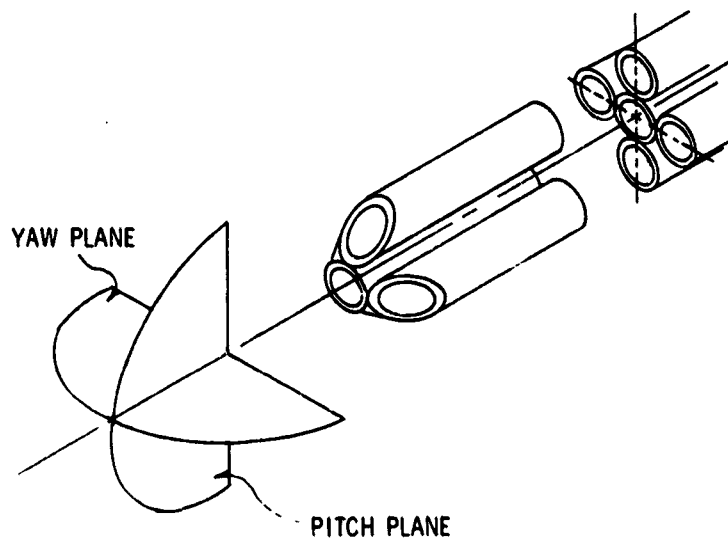
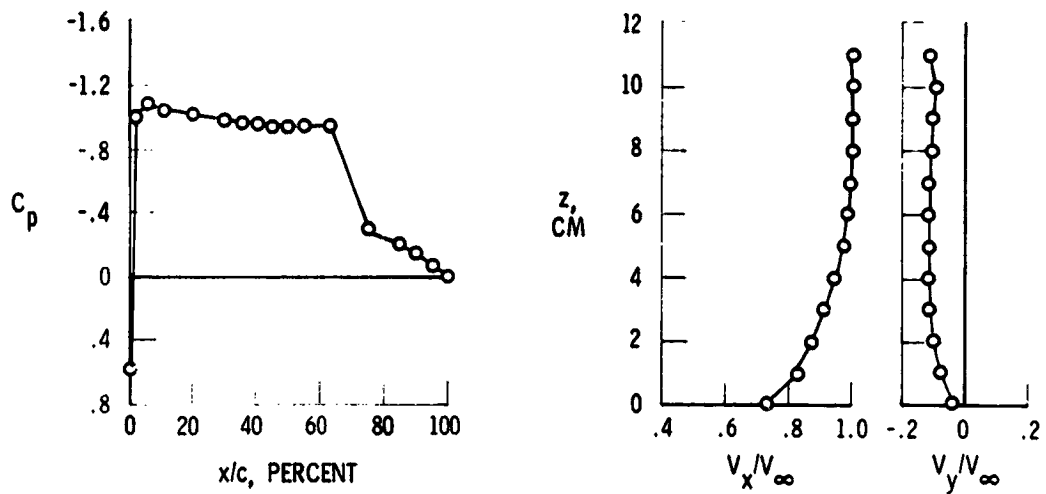
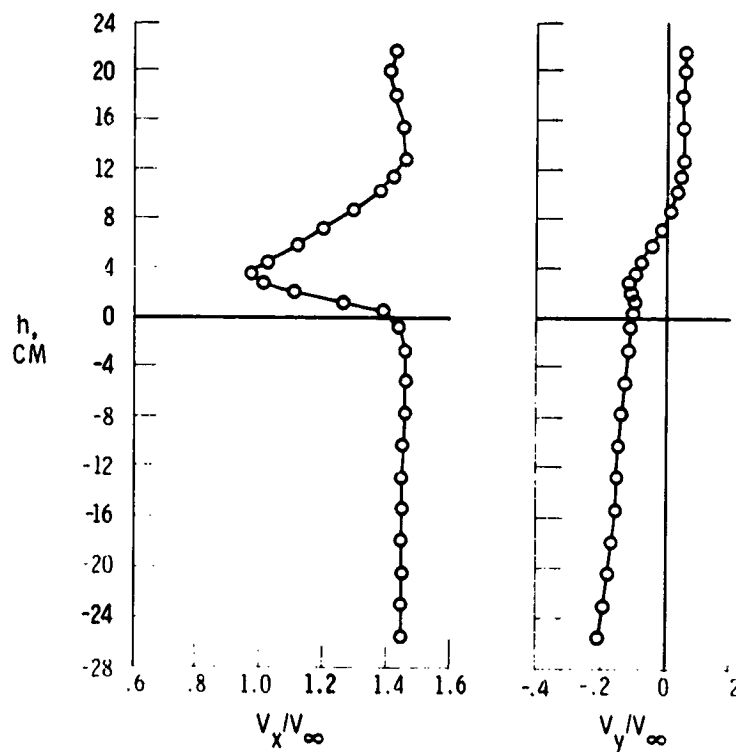


Figure 6.- Three-dimensional wake-probe head.



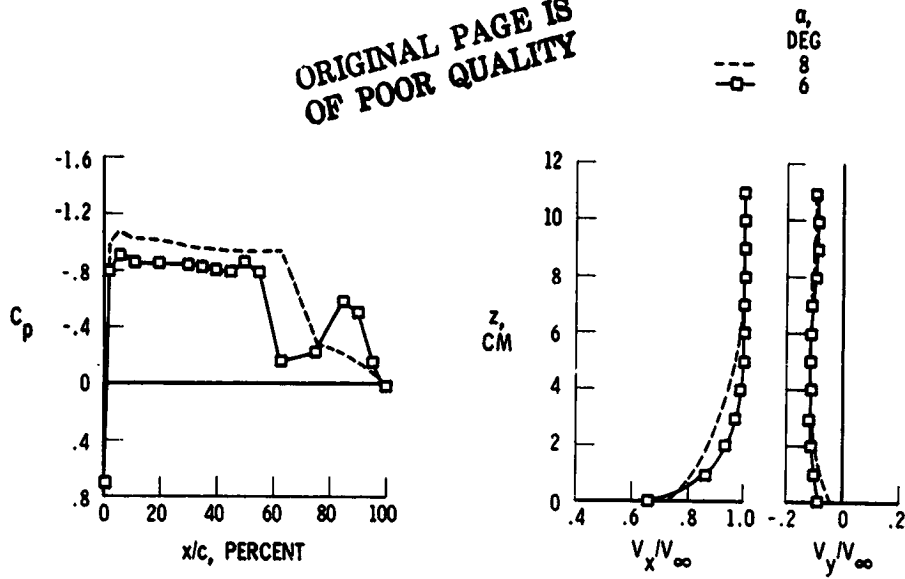
(a) Pressure distribution and boundary-layer velocity profiles.



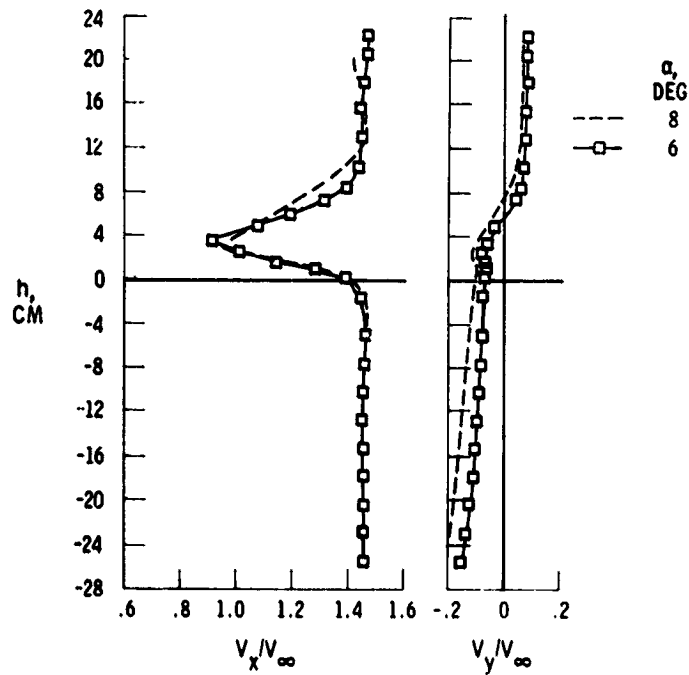
(b) Wake-velocity profiles.

Figure 7.- Section flow characteristics. $M = 0.85$; $q = 14.36 \text{ kN/m}^2$; $\alpha = 8^\circ$.

ORIGINAL PAGE IS
OF POOR QUALITY

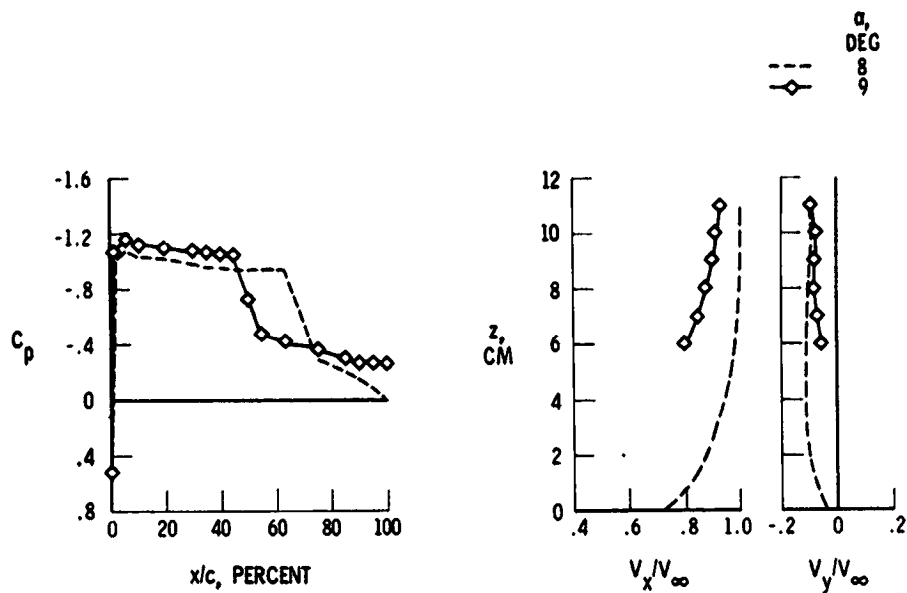


(a) Pressure distribution and boundary-layer velocity profiles.

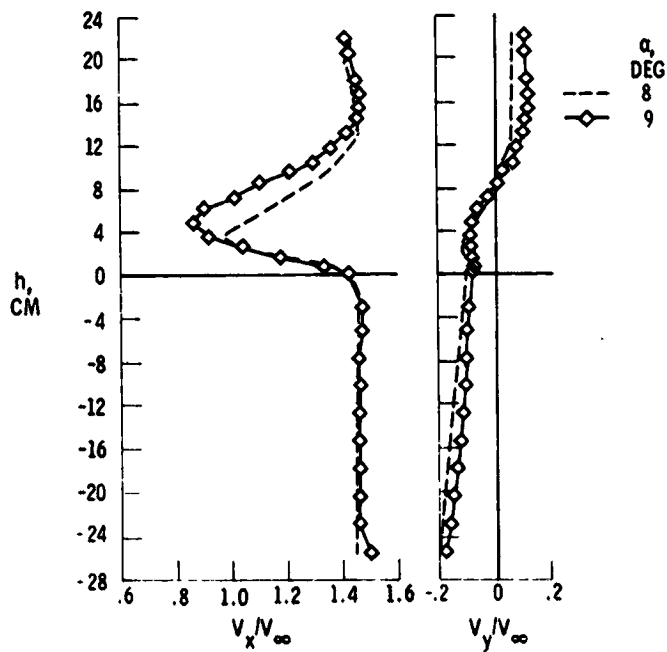


(b) Wake-velocity profiles.

Figure 8.- Section flow characteristics. $M = 0.85$; $q = 14.36 \text{ kN/m}^2$; $\alpha = 6^\circ$.



(a) Pressure distribution and boundary-layer velocity profiles.



(b) Wake-velocity profiles.

Figure 9.- Section flow characteristics. $M = 0.85$; $q = 14.36 \text{ kN/m}^2$; $\alpha = 9^\circ$.

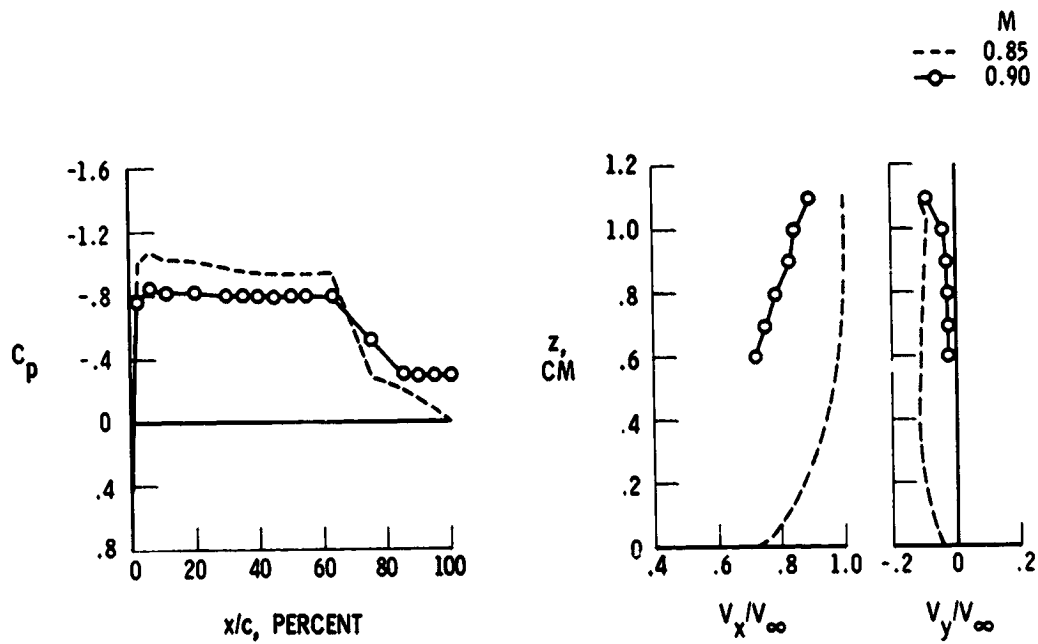


Figure 10.- Section flow characteristics. $q = 14.36 \text{ kN/m}^2$; $\alpha = 8^\circ$.

A PROCEDURE FOR ANALYZING TRANSONIC FLOW OVER
HARMONICALLY OSCILLATING AIRFOILS*

43

Warren H. Weatherill, F. Edward Ehlers, and
James D. Sebastian
The Boeing Company

SUMMARY

Finite difference procedures have been successfully used to solve the steady transonic flow about airfoils and appear to provide a practical means for calculating the corresponding unsteady flow. The purpose of the current paper is to describe a finite difference procedure derived from the equations for the potential flow by assuming small perturbations and harmonic motion. The velocity potential is divided into steady and unsteady parts, and the resulting unsteady equation is linearized on the basis of small amplitudes of oscillation. The steady velocity potential, which must be calculated first, is described by the classical nonlinear transonic differential equation. The initial research on this procedure was presented by Ehlers in reference 1, and is a direct extension of the steady state difference procedure of Murman, Cole, and Krupp (refs. 2, 3, and 4). The current authors have described further research pertaining to the procedure in references 5 and 6.

INTRODUCTION

The intent of the research described in this paper has been to develop a means for calculating air forces for use in the analysis of flutter and other aeroelastic phenomena. Thus, there is a need for developing a relatively efficient computational procedure as well as, of course, providing adequate accuracy in the representation of the physical phenomenon.

The procedure of this paper is intended to be intermediate in terms of computer machine resource usage and is based on a finite difference method. The assumption of small perturbations from a uniform stream near the speed of sound retains the necessary complexity for describing flows with local supersonic regions. The application of the perturbation velocity potential restricts the solution to weak shocks, which, for thin wings of reasonably good design, is not too limiting an assumption. When the flow is steady, the resulting nonlinear differential equation reduces to the well-known transonic small perturbation equation. The unsteady differential equation is simplified by considering the flow as consisting of the sum of two separate potentials representing the steady and unsteady effects. The assumption of small amplitudes of harmonic oscillation leads to a linear differential equation for the unsteady potential with variable coefficients depending on the steady flow. The resulting air forces are thus superposable and may be directly used in conventional flutter analysis formulations.

The effect of thickness is included in the steady flow analysis. The unsteady analysis is carried out for a wing of vanishing thickness but submerged in a velocity potential distribution resulting from the steady analysis. As formulated, the shock is fixed by the steady flow, and it does not move with the wing motion. It is noted that shock motion could be included in a linear fashion; see, for example, reference 7.

This work was jointly sponsored by the NASA Langley Research Center and The Boeing Commercial Airplane Company.

FORMULATION AND SOLUTION

The complete nonlinear differential equation for the velocity potential was simplified by assuming the flow to be a small perturbation from a uniform stream near the speed of sound. The resulting equation for unsteady flow is

$$[K - (\gamma - 1)\varphi_t - (\gamma + 1)\varphi_x]\varphi_{xx} + \varphi_{yy} - (2\varphi_{xt} + \varphi_{tt})/\epsilon = 0 \quad (1)$$

where $K = (1 - M^2)/M^2\epsilon$. M is the freestream Mach number of velocity U_0 in the x -direction, x and y are made dimensionless to the semichord b of the airfoil and the time t to the ratio b/U_0 , γ is the ratio of specific heats and ϵ is defined in terms of thickness ratio δ as $\epsilon = (\delta/M)^{2/3}$.

The potential is separated into steady and harmonic parts and written as:

$$\varphi = \varphi_0(x,y) + \varphi_1(x,y)e^{i\omega t} \quad (2)$$

For the steady potential, φ_0 , we obtain the usual nonlinear differential equation:

$$[K - (\gamma + 1)\varphi_{0x}]\varphi_{0xx} + \varphi_{0yy} = 0 \quad (3)$$

While the unsteady potential, φ_1 , is given by a linear equation of the form:

$$\left\{ [K - (\gamma - 1)\varphi_{0x}]\varphi_{1x} \right\}_x + \varphi_{1yy} - (2i\omega/\epsilon)\varphi_{1x} + q\varphi_1 = 0 \quad (4)$$

where:

$$q = \omega^2/\epsilon - i\omega(\gamma - 1)\varphi_{0xx} \quad (5)$$

Linear boundary conditions are applied on the slit in the plane of the wing for both equations.

A computer program for solving the steady-state transonic flow about lifting airfoils based on equation (3) was developed by Krupp and Murman (refs. 3 and 4). The output of this or a similar program can be used in computing the coefficients for the differential equation of the unsteady potential. The similarity of the unsteady differential equation to the steady-state equation suggests that the method of column relaxation used by Krupp for the nonlinear steady-state problem should be an effective way to solve equation (4) for φ_1 . Note that equation (4) is of a mixed type, being elliptic or hyperbolic whenever equation (3) is elliptic or hyperbolic. Central differencing was used at all points for the y derivative and at all subsonic or elliptic points for the x derivatives. Backward (or upstream) differences were used for the x derivatives at all hyperbolic points.

For the set of difference equations to be determinate, the boundary conditions on the outer edges of the mesh must be specified. In the original unsteady formulation, these boundary conditions were derived from asymptotic integral relations in a manner parallel to that used by Klunker (ref. 8) for steady flow. A later formulation in reference 6 applies an outgoing wave boundary condition to the outer edges of the mesh. This boundary condition is numerically simpler to apply and, on the basis of limited experience, appears to provide better correlation (see the following section on numerical accuracy).

The preferred numerical solution approach to the resulting large order set of difference equations is a relaxation procedure, which permits the calculation to be made as a sequence of relatively small problems. The initial solutions were obtained using a line relaxation procedure. Convergence is determined by monitoring ERROR, the maximum change in the velocity potential between iteration steps. ERROR is defined as the maximum value over all i and j of

$$\frac{|\varphi_{1ij}^{(n)} - \varphi_{1ij}^{(n-1)}|}{r} \quad (6)$$

where $\varphi_1^{(n)}$ is the unsteady velocity potential for the n 'th iteration, $\varphi_1^{(n-1)}$ is the corresponding potential for the preceding iteration, and r is the relaxation factor. The solution was considered converged when $\text{ERROR} \leq 10^{-5}$. In some cases, particularly for finer meshes and for the pitch mode, convergence was considered complete when $\text{ERROR} \leq 10^{-4}$.

RESULTS

The above procedure has been used for problems with mixed flow and low reduced frequencies with generally satisfactory results. In this section, results, as calculated with this procedure, are compared (1), with linear theory appropriate to a flat plate of vanishing thickness and (2), with experimental results for a NACA 64A006 airfoil with an oscillating quarter-chord flap.

The flat plate results are shown in figures 1 and 2. Figure 1 shows the jump in pressure coefficient across a flat plate oscillating in pitch. Figure 2 shows the same distribution across a flat plate with a harmonically oscillating quarter-chord control surface. In each figure, results obtained using the finite difference procedure are compared with corresponding results obtained using a kernel function program. For these calculations, the program is the subsonic routine generated for NASA-Langley by Rowe, Winther, and Redman (refs. 9 and 10). For the flat plate, the results from the two theories should match exactly. The differences may be attributed to the finite difference representation together with the limited solution region.

Corresponding results for a wing with thickness are shown in figures 3, 4, and 5. Here results from the finite difference theory are compared directly with experimental data from Tijdeman and Schippers (ref. 11). Figure 3 shows the jump in pressure distribution for the airfoil at $M = 0.80$ with a reduced frequency of 0.25. At this Mach number, the pressure distribution does not have a shock and the singularity in the pressure distribution is solely due to the presence of the control surface hingeline. Generally, the pattern of the calculated pressure distribution matches that of the measured values very well. The calculated amplitude of the real part exceeds the measured value near the leading edge for the real part and over the front 75% of the chord for the imaginary part. Parallel results at $M = 0.875$ and $\omega = 0.06$ are shown in figure 4. Here, the flow is mixed with the shock appearing just aft of midchord. The characteristic pressure rise due to the shock and the pressure singularity due to the presence of the hingeline are clearly reflected in both measured and calculated distributions. Figure 5 presents corresponding results at $M = 0.9$. The shock has moved aft to a position just in front of the hingeline, but the two pressure rises still appear as separate peaks. Also, the amplitudes are in better agreement than in the preceding two examples.

These examples are typical of results obtained for low reduced frequencies (e.g., refs. 1, 5, 6, 12, 13, and 14). The reason for the discrepancy between theory and experiment is not known, but

may be due to boundary layer or separation effects, or both, or to unknown problems with the theory or with the pressure measurements. The qualification "for low reduced frequencies" is made for the following reason. As previously noted, the preferred solution procedure is a sequential row relaxation which permits the efficient numerical solution of the large set of simultaneous equations. This solution procedure becomes unstable, in the sense that successive iterates diverge, above certain values of $\lambda_1 = \omega M / (1 - M^2)$. At a given Mach number, this is essentially a frequency limitation. However, the "low reduced frequency" qualification should really be a "low λ_1 " qualification. Means of getting around this limitation are still under investigation. For example, where this limitation has been avoided we have encountered accuracy problems. This point is discussed in more detail in the next two sections.

RELAXATION SOLUTION STABILITY

As has been discussed in a preceding NASA report by the authors (refs. 5 and 6), significant stability problems were encountered with the relaxation procedures used to solve the finite difference equations. Generally, these procedures paralleled those successfully used for the steady-state problem.

The characteristics of the solution instability are as follows:

1. It occurs when the flow is purely subsonic as well as mixed, and thus is not involved with the presence or absence of transonic shock flow.
2. It appears to be a function of λ_1 and the dimensions of the finite difference region. An analysis of the flat plate with a uniform mesh yields, for the critical value of λ_1 , the value of λ_1 above which the relaxation solution is unstable:

$$\lambda_{1\text{CRITICAL}} = \pi \left[\frac{1}{a^2} + \frac{1}{Kb^2} \right]^{1/2} \quad (7)$$

where a is the streamwise dimension of the mesh region, b is the height.

3. The rate of convergence decreases as the frequency approaches the critical value, and hence, the region of convergence is not actually well defined, although it is generally in the neighborhood of the value given by the preceding formula.

Some insight into the causes of the instability may be obtained by considering the Helmholtz equation into which the difference equation for the oscillating flow over a flat plate may be transformed, namely,

$$\chi_{xx} + \chi_{yy} + \lambda_1^2 \chi = 0 \quad (8)$$

Solutions to the Helmholtz equation may not be unique for given types of boundary conditions on a closed region since eigenfunctions corresponding to real eigenvalues can occur: i.e., functions representing standing waves for which homogeneous boundary conditions occur on the boundary. For the rectangular mesh area of length a and width b , the first eigenvalue associated with numerical solutions of the Helmholtz equation with Dirichlet boundary conditions is the critical value of λ_1 just presented. In terms of the relaxation procedure, it was noted in reference 5 that solutions of a relaxation problem of the form

$$[A]\{\varphi_1\} = \{R\} \quad (9)$$

with certain conditions on the structure of A , converge only when $[A]$ is positive definite, and this holds for the model unsteady problem of eq. (8) when λ_1 is less than $\lambda_{1\text{CRITICAL}}$.

Several concepts have been studied in hopes of moderating or removing the relaxation solution stability problem. For example, integral equation formulations currently in use for the linearized subsonic unsteady problems employ only the outgoing wave solution for the Green's function. Boundary conditions designed to do this in the finite difference formulation do not appear to be adequate. An investigation of a variety of different kinds of boundary conditions has not resulted in any significant improvement in solution stability. Other concepts that we have tried include (1) using a coordinate transformation so that the boundary conditions in the physical plane at infinity could be applied to the outer boundaries of a finite mesh region, (2) replacing the iterative relaxation solution with a full direct solution, (3) using an overlapping subregion concept, (4) artificial manipulation of the elements in $[A]$ in order to provide a better conditioned matrix, (5) using a sequential mesh refinement system, and (6) applying a mathematical technique for making $[A]$ positive definite for values of λ_1 above $\lambda_{1\text{CRITICAL}}$ by premultiplication by the conjugate transpose of $[A]$ (see ref. 7).

The studies performed on these concepts are described in reference 6. Only the full direct solution appears promising. Recently, we have been investigating the effect of adding a small amount of viscosity by including a ν_{1xxx} term in a one-dimensional formulation. Although this study is not complete, results to date show little reason for optimism.

In the full direct solution, the problem is solved "all at once" rather than "sequentially." Mathematically, this involves inverting $[A]$, a process that should be possible except at values of λ_1 for which A is singular; that is for values of λ_1 that are eigenvalues. This procedure has been explored with very mixed results.

In light of the original formulation, it was natural to try a semidirect solution of the form

$$[A(\lambda_1)] \{\varphi_1^{(n)}\} = \{R(\varphi_1^{(n-1)})\} \quad (10)$$

where $\{\varphi_1^{(n)}\}$ contains an element for each interior mesh point and the right-hand side, which applies the boundary conditions, is a function of the φ_1 distribution of the preceding (iterative) solution. The vector of unknown φ_1 's is found directly but iteration is required to update the boundary conditions. Although this procedure was very efficient for small meshes for which it was used (i.e., permitted by an available in-core solution routine), it was subject to the same type of solution instability as the relaxation solutions. However, it is possible to rewrite the equations so that all unknowns are on the left-hand side of the equation and the solution may then be obtained without iteration, i.e., a full direct solution procedure.

The full direct solution procedure has been tested with both one- and two-dimensional problems, and no difficulty was encountered in obtaining solutions for values of λ_1 well above the critical values. However, the accuracy of these solutions, as measured against analytic calculations, is good for values of λ_1 smaller than $\lambda_{1\text{CRITICAL}}$ but it deteriorates rapidly as λ_1 is increased. This point is discussed in the next section. However, the full direct solution does provide a means of obtaining solutions where the relaxation procedure does not work.

NUMERICAL ACCURACY

The discussion of accuracy for this paper will be very limited, but there are several points that should be made. First, as noted above, for certain values of Mach number and reduced frequency, generally satisfactory results have been obtained when correlated with linear theory and with available experimental data. Second, it appears that the use of outgoing wave boundary conditions, together with a coordinate transformation, provides better correlation with linear theory than Klunker-type boundary conditions. This is demonstrated in figure 6. Note that two different mesh patterns have been used.

The problems of accuracy noted in connection with the direct solution have been studied with both one- and two-dimensional formulations. First, the one-dimensional analysis shows the difference between an exact analytic analysis and the finite difference solution may be a function of the form of the boundary conditions used. The nature of the eigenvalues (i.e., values of λ_1) of $[A]$ are determined by the kind of boundary conditions used to formulate the problem. If the boundary conditions result in eigenvalues that are real values of λ_1 then the error distribution (the difference between the analytic and finite difference solution) is singular for the values of λ_1 corresponding to these eigenvalues. If the eigenvalues of $[A]$ are complex values λ_1 then this singular behavior in error curve is suppressed since λ_1 take on only real values. This is shown very clearly in figure 7 where Dirichlet boundary conditions were used in the first case and Dirichlet and Cauchy boundary conditions were combined in the second case.

The error between analytic and finite difference solutions can be shown to be generally proportional to $h^2 \lambda_1^3$. This is illustrated in figure 8 and it is noted that a conventional truncation analysis would indicate that the error was proportional to ω^4 .

The distribution of the jump in the pressure coefficient across a flat plate oscillating in pitch is shown for a freestream Mach number of 0.4 and two reduced frequencies in figures 9 and 10. The point of these figures is to show the accuracy problem encountered when solutions are calculated at values of λ_1 above $\lambda_{1\text{CRITICAL}}$ using the full direct solution. Since pivoting was used in the solution routine, it is currently thought that this problem is related to the limited number of mesh points used in the calculation, due to use of in-core matrix inversion routine. The effect of increasing the number of mesh points will be investigated with the completion of an out-of-core routine currently under development.

REFERENCES

1. Ehlers, F. Edward: A Finite Difference Method for the Solution of the Transonic Flow Around Harmonically Oscillating Wings. NASA CR-2257, January 1974.
2. Murman, E. M.; and Cole, J. D.: Calculation of Plane Steady Transonic Flow. AIAA Paper 70-188, January 1970.
3. Krupp, J. A.; and Murman, E. M.: Computation of Transonic Flows Past Lifting Airfoils and Slender Bodies. AIAA Journal, vol. 10, pp. 880-887, July 1972.

4. Krupp, J. A.: The Numerical Calculation of Plane Steady Transonic Flows Past Thin Lifting Airfoils. Doctor of Philosophy Thesis, University of Washington, 1971; also Scientific Research Laboratories, Boeing document D180-12958-1, June 1971.
5. Weatherill, W. H.; Ehlers, F. E.; and Sebastian, J. D.: Computation of the Transonic Perturbation Flow Fields Around Two- and Three-Dimensional Oscillating Wings. NASA CR-2599, December 1975.
6. Weatherill, W. H.; Sebastian, J. D.; and Ehlers, F. E.: The Practical Application of a Finite Difference Method to the Analysis of Transonic Flow Over Oscillating Airfoils and Wings. NASA CR-2933, December 1977.
7. Hafez, M. M.; Rizk, M. H.; and Murman, E. M.: Numerical Solution of the Unsteady Transonic Small-Disturbance Equations. Paper presented at the 44th meeting of the Structures and Materials Panel of AGARD, Lisbon, Portugal, 17-22 April 1977.
8. Klunker, E. B.: Contributions to Methods for Calculating the Flow About Thin Lifting Wings at Transonic Speeds. NASA TN D-6530, November 1971.
9. Rowe, W. S.; Winther, B. A.; and Redman, M. C.: Prediction of Unsteady Aerodynamic Loadings Caused by Trailing Edge Control Surface Motions in Subsonic Compressible Flow-Analysis and Results. NASA CR-2003, March 1972.
10. Redman, M. C.; Rowe, W. S.; and Winther, B. A.: Prediction of Unsteady Aerodynamic Loadings Caused by Trailing Edge Control Surface Motions in Subsonic Compressible Flow-Computer Program Description. NASA CR-112015, March 1972.
11. Tijdeman, H.; and Schippers, P.: Results of Pressure Measurements on an Airfoil With Oscillating Flap in Two-Dimensional High Subsonic and Transonic Flow (Zero Incidence and Zero Mean Flap Positions). NRL report TR 73078U, August 1973.
12. Traci, R. M.; Albano, E. D.; Farr, J. L., Jr.; and Cheng, H. K.: Small Disturbance Transonic Flows About Oscillating Airfoils. TR-AFFDL-TR-74-37, June 1974.
13. Traci, R. M.; Farr, J. L.; and Albano, E. D.: Perturbation Method for Transonic Flows About Oscillating Airfoils. AIAA paper 75-877, presented at the AIAA 8th Fluid and Plasma Dynamics Conference, Hartford, Connecticut, 16-18 June 1975.
14. Traci, R. M.; Albano, E. D.; and Farr, J. L., Jr.: Small Disturbance Transonic Flows About Oscillating Airfoils and Planar Wings. AFFDL-TR-75-100, August 1975.

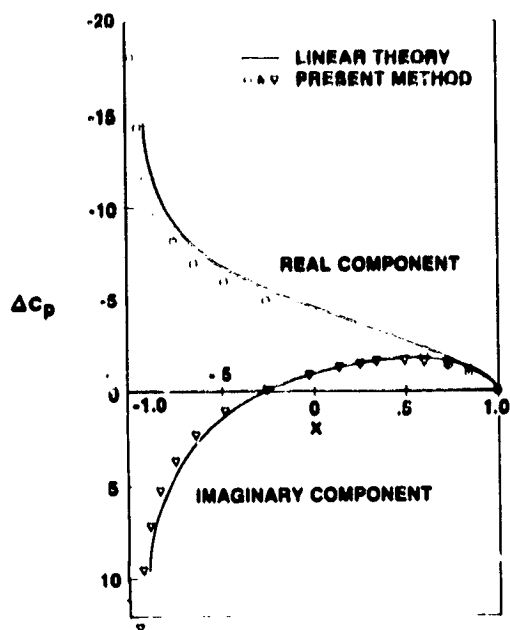


Figure 1.- Jump in pressure coefficient C_p across a flat plate oscillating in harmonic pitch. $M = 0.85$; $\omega = 0.18$.

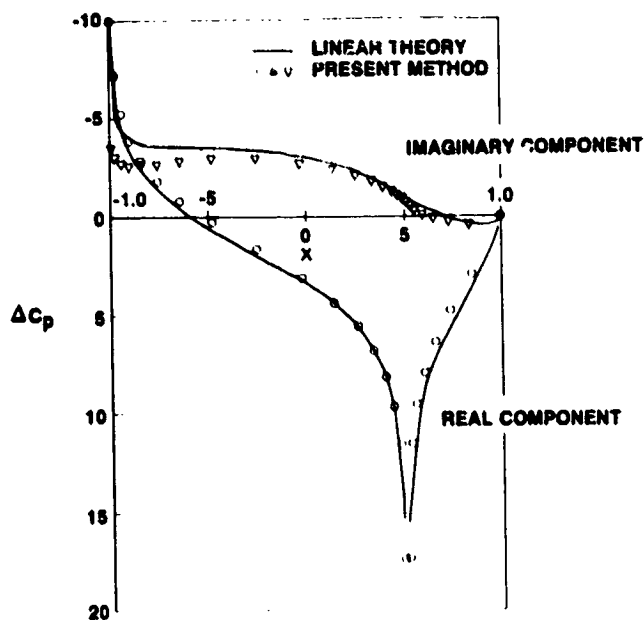
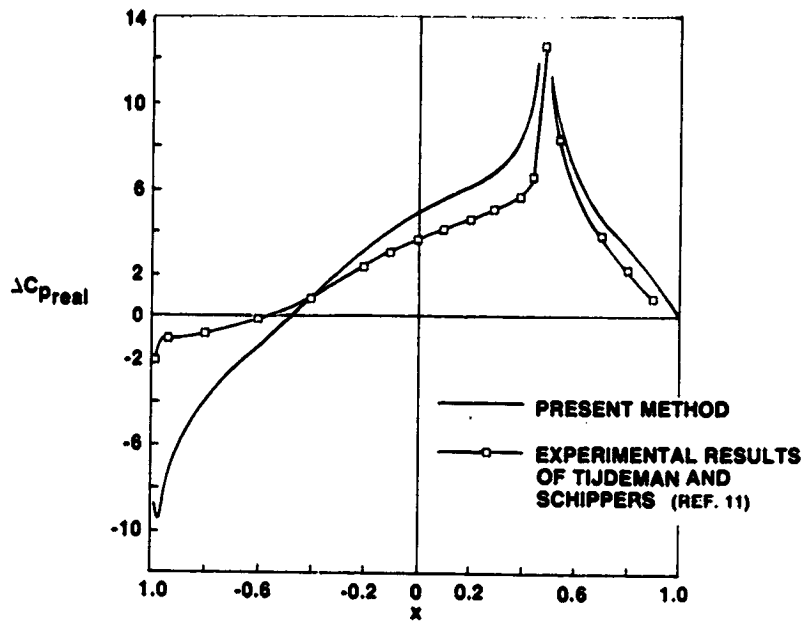
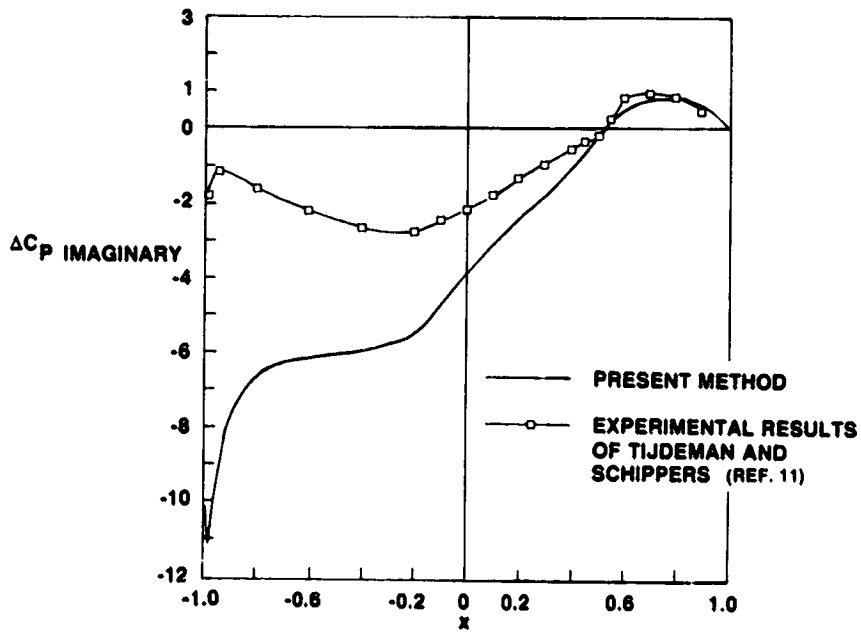


Figure 2.- Jump in pressure coefficient across a flat plate with harmonically oscillating quarter-chord control surface. $M = 0.9$; $\omega = 0.120$.

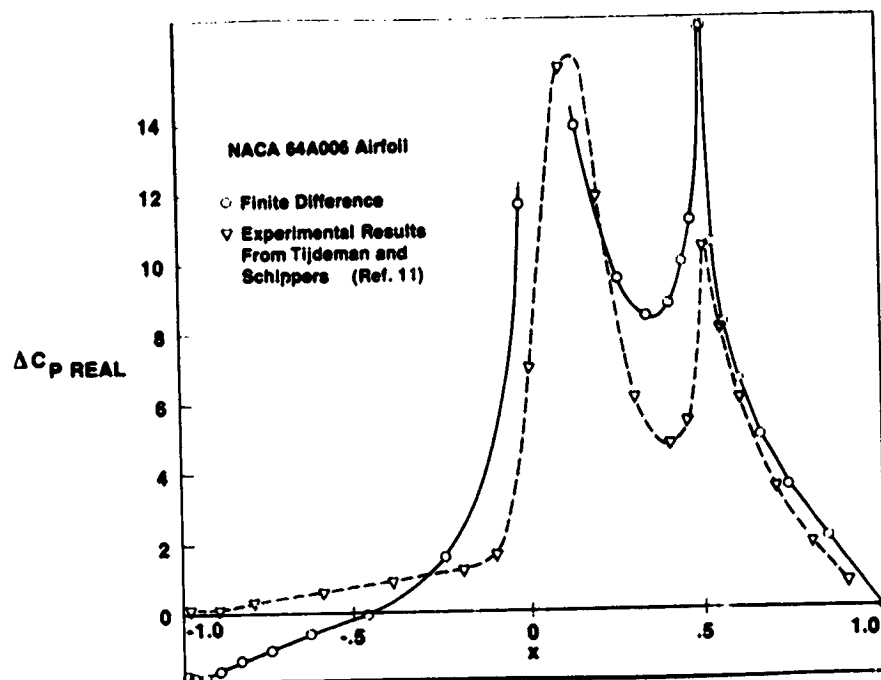


(a) Real pressure distribution.

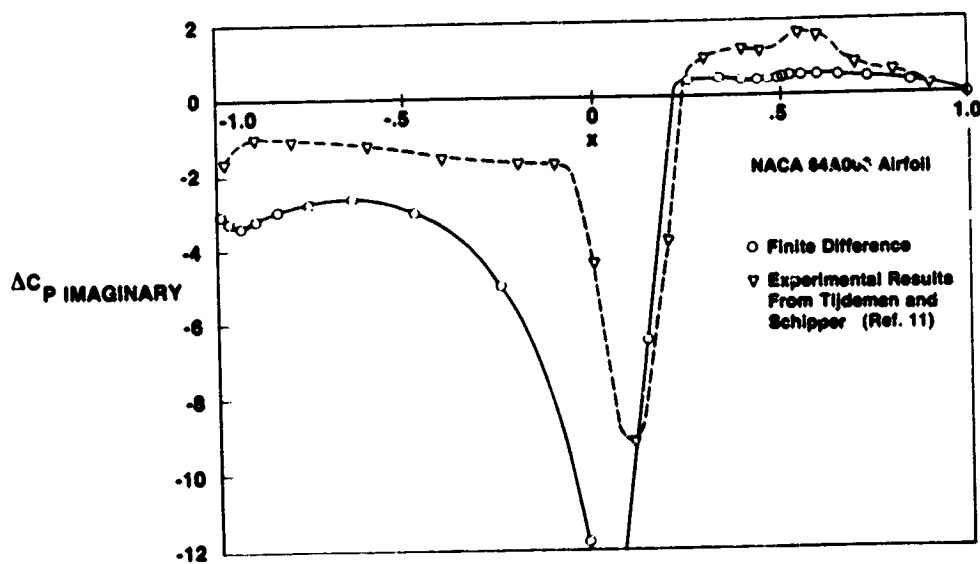


(b) Imaginary pressure distribution.

Figure 3.- Jump in pressure coefficient across an airfoil with a harmonically oscillating quarter-chord control surface. $M = 0.804$; $\omega = 0.253$.

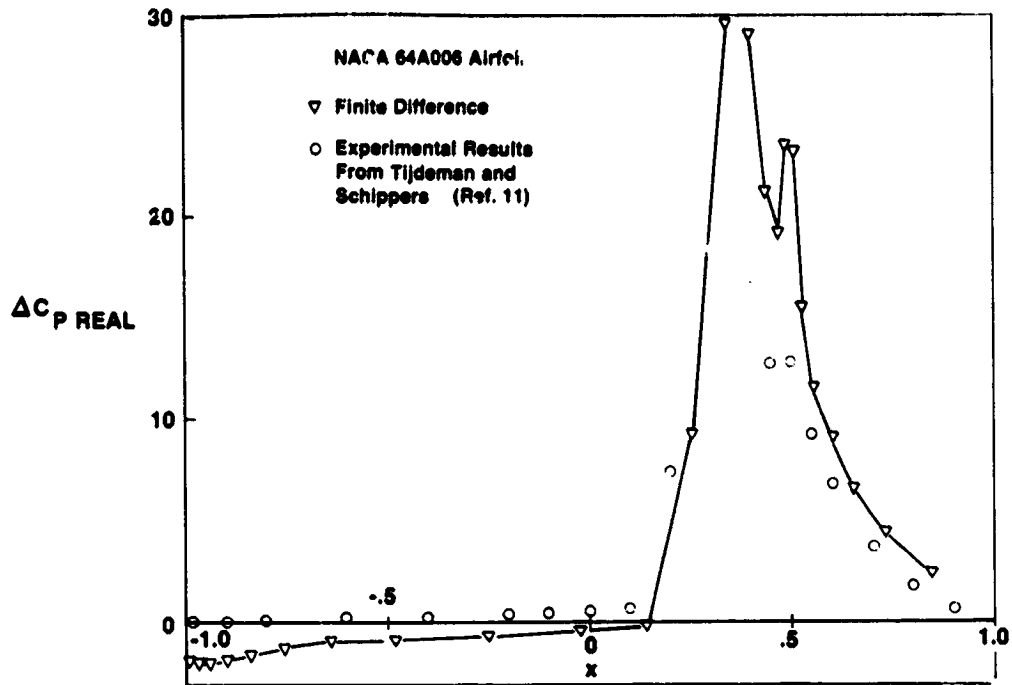


(a) Real pressure distribution.

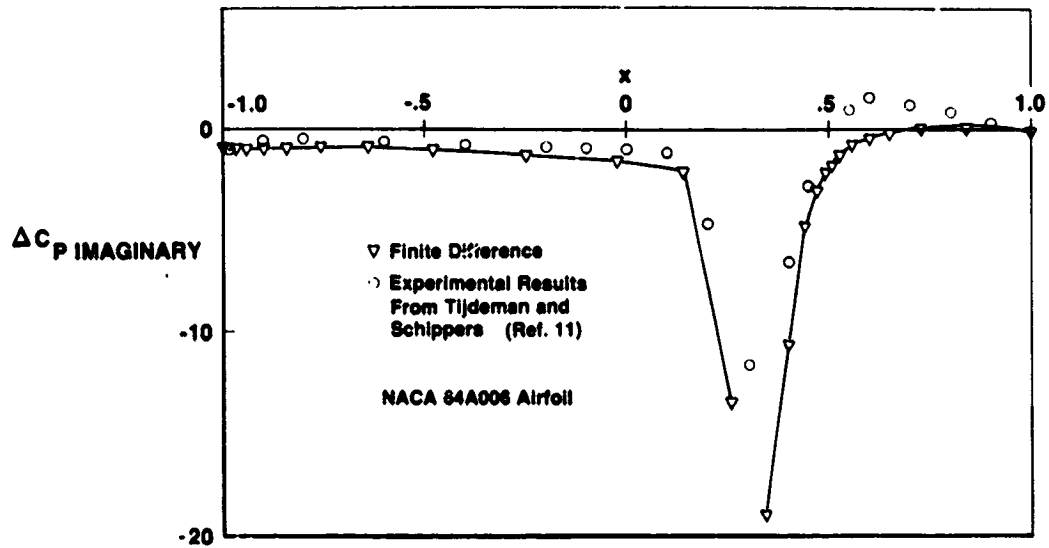


(b) Imaginary pressure distribution.

Figure 4.- Jump in pressure coefficient across an airfoil with harmonically oscillating quarter-chord control surface. $M = 0.875$; $\omega = 0.06$.



(a) Real pressure distribution.



(b) Imaginary pressure distribution.

Figure 5.- Jump in pressure coefficient across an airfoil with harmonically oscillating quarter-chord control surface. $M = 0.9$; $\omega = 0.06$.

MACH NUMBER = 0.9
 REDUCED FREQUENCY = 0.06
 PITCH ABOUT LEADING EDGE

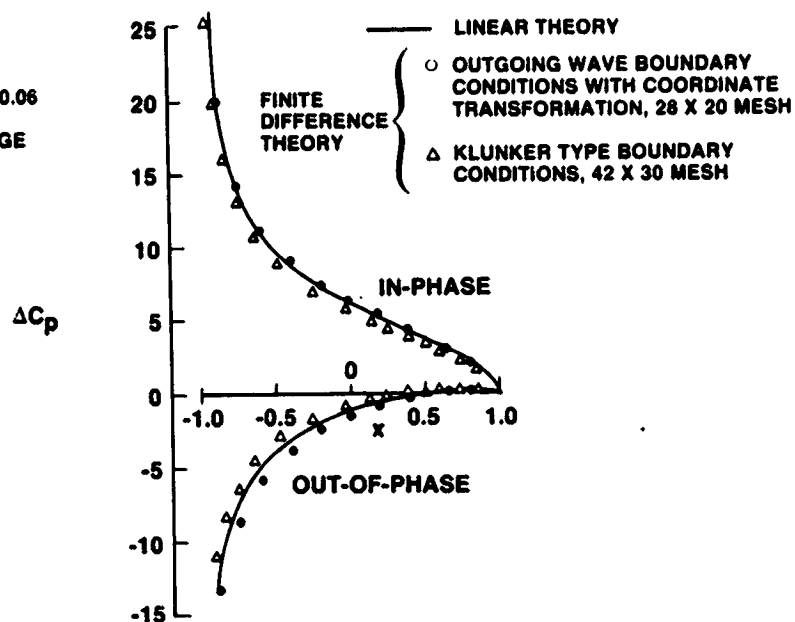


Figure 6.- Jump in pressure coefficient across a flat plate oscillating in pitch. $M = 0.9$; $\omega = 0.06$.

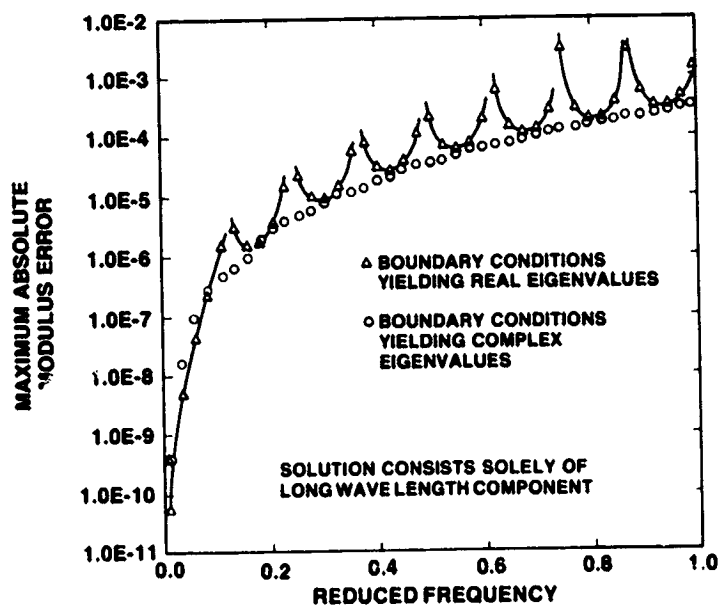


Figure 7.- Comparison of error curves for boundary conditions yielding all real and complex eigenvalues.

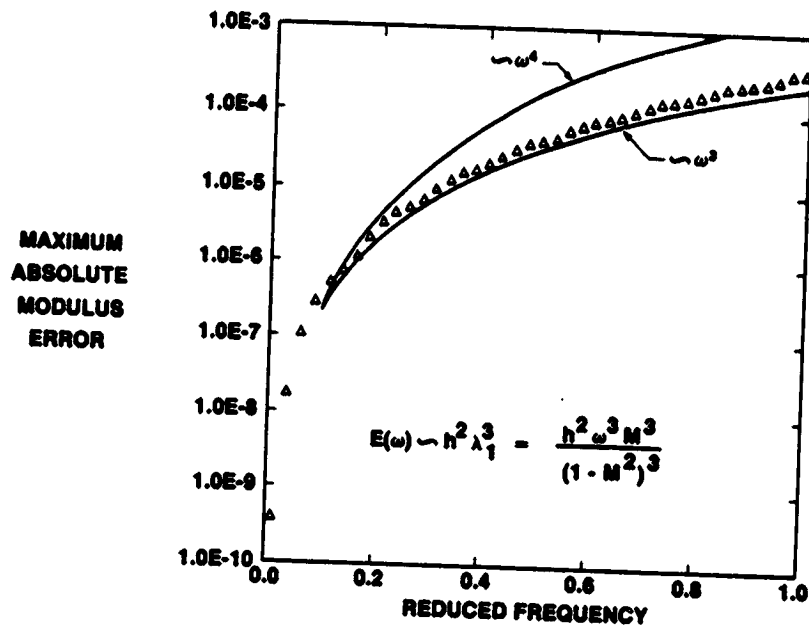


Figure 8.- Variation of error curve with reduced frequency.

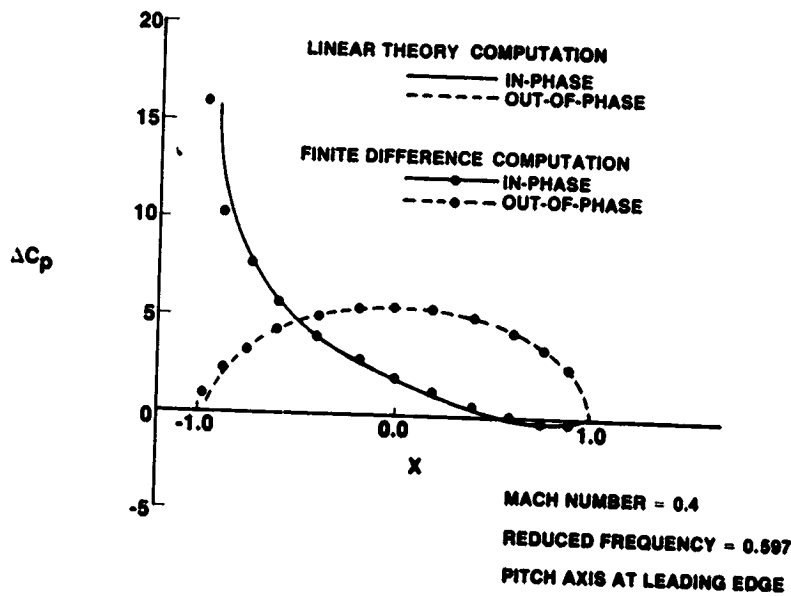


Figure 9.- Jump in pressure coefficient across a flat plate oscillating in pitch. $M = 0.4$; $\omega = 0.597$.

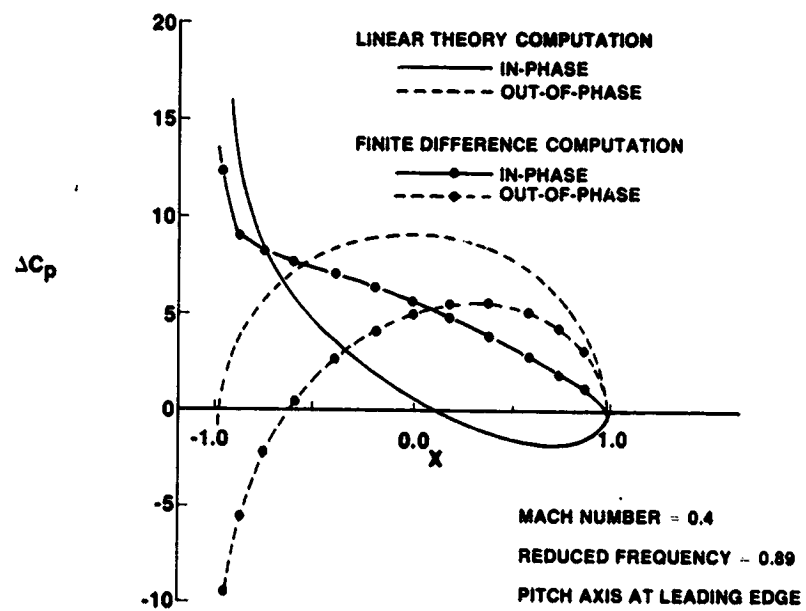


Figure 10.- Jump in pressure coefficient across a flat plate oscillating in pitch. $M = 0.4$; $\omega = 0.89$.

A NEW TWO-DIMENSIONAL OSCILLATING WING APPARATUS FOR

UNSTEADY AERODYNAMICS RESEARCH

Sanford S. Davis and Gerald N. Malcolm
NASA Ames Research Center

SUMMARY

A new apparatus for experimental research into unsteady transonic flows is described in this paper. The apparatus, as installed in the NASA-Ames 11- by 11-Foot Transonic Wind Tunnel, can impart full two-degree-of-freedom motions at reduced frequencies to 0.3, oscillatory amplitudes to $\pm 2^\circ$, mean angles to 12° , Mach numbers to 1.4 and Reynolds numbers to 12×10^6 . The test wing is fully instrumented for dynamic waveform measurements and the data can be acquired, processed, and displayed in real-time with a new computational data acquisition system. Following a description of the apparatus, sample data from a recently completed test program will be presented.

INTRODUCTION

Rapid advances in computational techniques have made it possible to compute the unsteady aerodynamics of oscillating airfoils using a variety of governing equations. Until recently, analytical and numerical solutions were only available for incompressible flows (analytical solutions based on the Theodorsen Function) and linearized compressible flows (numerical solutions based on the Possio Integral Equation). Today, solutions are available for a relatively complete spectrum of equations including the Euler Equations, the full Potential Equation, the Small Disturbance Transonic Equation (low-frequency approximation) and the linearized Small Disturbance Transonic Equation. For two-dimensional flows, only the effects of viscosity are lacking. It is important to have experimental data to compare with these computations.

The only detailed experimental data which are available are the results of the recent NLR (National Laboratory for Research, Netherlands) investigations (ref. 1). These tests proved to be invaluable for their physical insights into the complex flow fields surrounding oscillating airfoils. For subsequent investigations, however, it would be desirable to obtain data at higher Reynolds numbers, more favorable ratios of chord/wind-tunnel height and more general airfoil motions than were possible with the NLR investigations. Due to the wide operating range of the NASA-Ames 11- by 11-Foot Transonic Wind Tunnel, this facility was chosen for the installation of a new two-dimensional pitch-plunge apparatus for the study of oscillating airfoils. The results of the first test series with the new apparatus will be used to validate transonic theories, to compare with recent NLR tests, and to develop a data base for unsteady transonic flows.

GENERAL DESCRIPTION OF APPARATUS HARDWARE

Arbitrary pitch-plunge motions require a more complicated wing support mechanism than for a simple pitching wing. The final design uses two splitter plates to form a two-dimensional channel in the tunnel. Figure 1 shows a sketch of the wing-splitter-actuator system as installed in the wind-tunnel test section. The normal 3.4 m × 3.4 m test section is augmented with two splitter plates which are 3.4 m high × 2.8 m long × 0.025 m thick. In order to preclude excessive deflections of the splitters, side struts provide lateral support at mid-span. The splitters extend into the tunnel's plenum area at the top and bottom where they are bolted to I-beam anchors. Access panels for the instrumentation cables and four slots for the push-pull drive rods are included in the splitter plate.

Four 0.0412-m- (1.625 in.) diam carbon-epoxy push-pull rods connect the four corners of the wing to independently controlled hydraulic actuators. The hydraulic actuators, located in the lower plenum area, are supported by flexures and bear directly onto a massive concrete foundation through the four support columns. With this design, the tunnel pressure shell does not have to support the oscillatory reaction loads due to the actuator's motion.

The wing model itself is free to pitch and plunge in response to the actuator's command signal. It is restrained in the fore-aft direction by a pair of carbon-epoxy drag rods, and in the lateral, roll, and yaw directions by sliding cover plates which move with the wing on the inner surface of the splitter plates. The 1.35-m-span × 0.5-m-chord graphite-epoxy wing is extensively instrumented near the mid-span station.

The capabilities of the test apparatus include sinusoidal oscillations over a frequency range of 0 to 60 Hz. The maximum angle-of-attack oscillation varies from $\pm 2^\circ$ at low frequencies to $\pm 0.8^\circ$ at 60 Hz around any point along the chord axis from $-\infty$ to $+\infty$, and a vertical displacement in heaving motion up to ± 5 cm (2 in.). The mean angle of attack is manually adjustable from -5° to $+15^\circ$.

The various components that make up the system just discussed will now be described in more detail, since the basic performance requirements dictated state-of-the-art design in many cases. Many of the components that will be described can be seen in the photograph in figure 2 which shows the system installed in the tunnel, and in the photograph in figure 3 which shows the basic system set up on a test stand to be described later. In the following description it may be helpful to refer to these photographs to visualize the various components and their interrelationship.

DETAILED DESCRIPTION OF APPARATUS COMPONENTS

Motion Generators

The servo-hydraulic actuator system is driven by two 11 kW (150 hp) hydraulic pump units rated at $4.1 \times 10^{-3} \text{ m}^3/\text{s}$ (65 gal/min) at $21 \times 10^6 \text{ N/m}^2$ (3000 psi). Each of the four actuators consists of two separate pistons on a single rod enclosed in a dual chamber cylinder. The upper piston is used for generating dynamic forces, the lower piston for load biasing. The load-bias system is necessary to support the mean aerodynamic lift load, thereby reducing the power required to drive the dynamic piston. As static bias requirements change, the servo-valve system responds accordingly to maintain the required force output. Velocity and position transducers are combined into a single physical unit with coils and cores axially aligned for mounting in the center of the actuator.

Wing and Push-Pull Rods

The wing model is connected to the push-pull rods through flexure bearings, and the rods are in turn screwed directly into the actuator pistons. The wing, as well as the push-pull rods, is a lightweight graphite-epoxy structure. It is designed to withstand a 2300 m/s^2 (230 g) acceleration and a 44,000 N (10,000 lb) aerodynamic load. The push-pull rods are each capable of withstanding a 22,000 N (5000 lb) tension load. The flexures, which are mounted between the push-pull rods and the wing, are also designed for a 22,000 N (5000 lb) load. The flexures are also strain-gauged to provide a direct measure of the lift load on the wing. A pair of graphite-epoxy rods, mounted to the wing with a flexure support and attached forward of the wing to the splitter plates, provides a means of holding the wing in place in the splitter plate to counteract drag loads. These are capable of 6700 N (1500 lb) each.

The wing is instrumented with both static pressure orifices and dynamic pressure transducers. As many as 41 channels of static and dynamic data can be accommodated. These are all located approximately at midspan. Static pressure tubes are routed from the end of the wing (see fig. 4, which also shows the drag restraints discussed earlier), down through a cavity in the splitter plate to the tunnel plenum chamber, and out an access port to scanivalve/transducer units located outside of the tunnel shell. Dynamic transducers are mounted in the wing by inserting the transducer (2.36 mm in diam) in the end of a long plastic sleeve, which is in turn inserted into a cylindrical channel molded into the interior of the wing. The channel terminates at the center of the wing to an orifice communicating to the wing surface. The transducer wires are then routed out the end of the wing (see fig. 5), through the splitter plates and out through the tunnel walls to the data acquisition equipment in the tunnel control room. A single reference pressure tube from each dynamic transducer is also inserted into the plastic sleeve and routed through the splitter plate to the scanivalve/transducer assembly outside the tunnel. The dynamic reference pressure can be selected to

be the static pressure of the adjacent static orifice on the wing or any other convenient pressure (such as the tunnel static pressure). Six accelerometers have also been mounted inside the wing, one at each of the attachment points of the four push-pull rods near the corners of the wing, and two at the mid-span near the leading and trailing edges. The actual motion of the wing can be determined from the accelerometer output and compared to the output of the motion transducers located in the actuator piston rods.

Two airfoil sections have been tested in this series. An NACA 64A010 laminar-flow symmetrical airfoil (shown installed in the splitter plates in fig. 6) was tested to obtain unsteady aerodynamic data to compare with the numerical computation of Magnus and Yoshihara based on the Euler equations of motion, which is being performed under contract to the Air Force Flight Dynamics Laboratory. A NLR 7301 supercritical airfoil section was tested to obtain unsteady aerodynamic data to compare with experiments at NLR.

Splitter Plates

Vertical splitter plates with trailing-edge flaps and horizontal side struts form the support structure within the test section for the wing and connected apparatus (see fig. 2). They each have a sharp leading edge and a movable trailing-edge flap which is manually adjustable between $\pm 2^\circ$ from the plane of the splitter plate. All testing has been done with the flaps at 0° . Horizontal side struts (see fig. 4) attach to the outside of the splitter plates just below the vertical center, and protrude through the test-section wall to the exterior tunnel structure. These provide stabilization to the splitter plates and eliminate any excessive deflection in the lateral direction due to aerodynamic loads. The splitter plates are installed with a 0.1° diverging angle from tunnel centerline to account for boundary-layer growth. There are openings (figs. 4 and 5) in the splitter plate to attach the wing to the top of the push-pull rods which are centered in the four channels cut in the splitter plates. In order to seal these openings when the wing is oscillating, sliding covers (fig. 6) are attached to the wing end plates and slide with the wing on the inside surface of the splitter plate. These are also made from graphite-epoxy to reduce weight and are teflon lined in order to slide freely on the surface.

The splitter plates and trailing-edge flaps contain a total of 130 pressure orifices distributed over the inside and outside surfaces of both plates. The inside orifices are utilized to select the proper channel Mach number, and the outer ones, in conjunction with the inner ones, are used to monitor the loading on the splitter plates. While testing, accelerometers are mounted on the trailing-edge flaps to monitor any large or potentially destructive flutter motions on the flaps or main splitter plates, such as might be produced from the oscillating flow behind the wing or naturally induced from the channel air flow. Previous testing in the NASA-Ames 2- by 2-Foot Transonic Wind Tunnel (ref. 2) have demonstrated the viability of the splitter-plate concept.

Pretest Setup

Since every part of this system was new and there was no test information available to judge the performance and reliability of the system as a whole, a special pretest facility was built to permit a detailed checkout program. Many of the components, including the wing, push-pull rods, drag restraints and the hydraulic actuator motion generator system are new designs and would not be a satisfactory risk in the wind tunnel without pretest experiments. Figure 3 is a photograph of the assembly in the test area. A support structure was constructed to which the various components were attached. The hydraulic actuators are mounted at the base with the push-pull rods screwed in to the top of the pistons. The wing is then mounted on the push-pull rods with flexures and angle-of-attack blocks between the rod end and the wing end cap. The drag restraint is fastened on top of the rear flexures and the other end tied to the support frame. Lift loads were simulated by an inflatable bag between the lower surface of the wing and a support cradle fastened to the support stand. Drag loads were simulated by a pneumatic cylinder coupled to cables and straps looped over the wing. A nearly complete envelope of test conditions could be evaluated on the test stand. In the early stages of the test checkout, a dummy wing constructed of fiberglass (shown in fig. 3) was used before risking the graphite-epoxy test wing. This proved to be an extremely valuable and low-risk method of evaluating the performance of the entire system. The only real limitations were that the fiberglass wing was not stiff enough to prevent large deflections at the mid-span, particularly in heaving, at the higher frequencies (above 30 Hz), and was not strong enough to accept the maximum lift loads. A limited amount of testing was done with the carbon-epoxy wing before installation in the wind tunnel.

DATA ACQUISITION SYSTEM

In the past, multichannel unsteady aerodynamic data were acquired with analog tape recorders. Raw data were recorded and stored for future analysis. On-line analysis was restricted to a few selected channels using special purpose "boxes" to extract limited usable data from the great mass of incoming data. These systems suffered from long-time lags between acquisition and analysis and the high probability of unknowingly recording spurious data. In the present test a new computational data acquisition and analysis system was developed for on-line display of steady and unsteady aerodynamic data. Figure 7 depicts the main elements of the new system. It has the capability of graphically displaying the first-harmonic, pressure distribution (both magnitude and phase) due to arbitrary pitch-plunge motions of the airfoil, along with the conventional static pressure distribution. At the user's option, an overlay of selected theoretical or experimental pressure distributions from computer-resident codes or from a dedicated data bank can be accessed.

The system is centered about a Data General Eclipse minicomputer, a high-speed (500 kHz) multichannel analog-to-digital converter, a large capacity (92 Mbyte) storage device, and a graphics terminal. The software

system consists of approximately 50 independent Fortran-coded programs which are controlled by two executive programs: one for dynamic data, the other for static data.

Dynamic Data Acquisition

A sinusoidal signal generator drives the four-channel hydraulic actuator, which in turn drives the four push-pull rods attached to the four corners of the wing. The actuator's control system is adjusted to impart the desired pitching and/or heaving motion to the wing. The motion of the four push-pull rods is continuously monitored and is acquired along with the unsteady pressure data. The signal generator is also used to trigger a pulse to initiate the unsteady data acquisition process.

The dynamic signals from 41 miniature pressure transducers are amplified and filtered before entering the analog-to-digital converter. Since the signal is periodic, it is possible to obtain good waveform samples with minimum storage per data point by signal-averaging the data. Theoretically, a periodic signal is completely defined by just one cycle of data (e.g., a 40 ms record is all that is necessary to characterize a 25 Hz periodic oscillation). However, the experimental signal is usually so contaminated by random pressure fluctuations due to wind-tunnel turbulence and model vibrations that one cycle of data is not very useful.

The signal-averaging technique is implemented as follows: we have a sample waveform and a pulse train which is triggered at the same phase position for each cycle of the airfoil's motion. These timing relations are shown in figure 8. At time t_0 , the sample waveform is recorded for τ seconds. At time $t_0 + nT$, the waveform is recorded again for τ seconds, where T denotes the period. The process is repeated M times. These M samples, each being initiated by the phase-locked pulse, are then ensemble averaged to obtain the averaged signal. In the current experiment τ is chosen to be slightly greater than one period; $n = 2$, and $M = 100$ is sufficient for a good average. At the user's option, the signal averaged waveform and the M th realization for any selected channel can be displayed on the graphics unit.

For on-line analysis, the first harmonic of the response is most useful. A simple Fourier analysis algorithm is implemented to extract the magnitude and phase information at the fundamental frequency. This data is displayed in tabular form on the graphics unit within 30 sec of the termination of data acquisition. This data is sufficient to determine if the unsteady data acquisition process was successful. If more on-line analysis is required, the first harmonic data may be displayed graphically in pressure coefficient form. The magnitude and phase of the chordwise pressure distributions on the upper and lower surfaces of the airfoil are displayed along with certain theoretical curves. The software package currently includes two theoretical options: (1) linear, incompressible small disturbance theory (Theodorsen function) and (2) linear, compressible small disturbance theory (Possio Integral Equation). For time-efficient on-line analysis it does not seem feasible to include unsteady transonic codes on the current generation of minicomputers.

Also available for comparison are the results of other investigations (theoretical and/or experimental) which have been stored in the data bank. For comparing with NACA 64A010 data, the theoretical investigations of Magnus-Yoshihara are available. For the NLR 7301 wing, experimental data obtained at NLR-Amsterdam are available. It is possible to obtain a comparison between the current data and the selected theoretical/experimental overlay in approximately 45 sec after the termination of data acquisition.

Static Data Acquisition

The static pressures are sensed with a conventional system using pneumatic tubing connected to a pressure scanning valve. The electrical output of the pressure cell to which the unknown pressures are multiplexed are read with a digital voltmeter whose BCD output feeds directly into the minicomputer.

Setting Test Conditions

The splitter-plate arrangement used for the oscillatory airfoil test requires special attention with regard to the free-stream Mach number (M_∞). As discussed in a previous report (ref. 2), the Mach number in the channel between the plates is not the same as computed from a static tap in the plenum chamber. In order to obtain the approach Mach number, the splitter plates are equipped with approximately 150 static pressure orifices which are distributed among 10 rows above and below the plane of the wing on the inner and outer walls of the splitter plates. These pressures are also sensed by the scanning system. The computed Mach numbers on the splitters are displayed on the graphics unit, and the approach Mach number is selected interactively by fairing the horizontal cursor of the graphics unit to the data. Using this procedure, the velocity can be selected to ± 0.002 in Mach number. Once the Mach number has been chosen, the static pressure distribution is displayed along with selected overlays. A static pressure distribution with overlays can be displayed in approximately 30 sec after the raw data have been acquired.

REPRESENTATIVE DATA FROM THE OSCILLATING AIRFOIL TEST

Steady and unsteady pressure distributions were measured on two airfoils: (1) an NACA 64A010 and (2) a NLR 7301 supercritical. The purpose of the NACA 64A010 tests is to compare the measurements with numerical solutions to the inviscid Euler equations obtained by Magnus and Yoshihara. These calculations were made under AFFDL (U.S. Air Force Flight Dynamics Laboratory, Wright-Patterson AFB, Ohio) sponsorship and were made available to NASA-Ames under the terms of a joint NASA-AFFDL cooperative program on the measurement and analysis of unsteady transonic flows.¹ The measurements on the supercritical

¹J. Olsen of the AFFDL coordinated these calculations with our testing program.

airfoil will be compared to similar measurements on an 18-cm-chord model that was recently tested at NLR-Amsterdam (ref. 1). The NLR data was supplied to NASA-Ames under a cooperative program between NASA-Ames and the NLR.² Both the NACA 64A010 and NLR 7301 comparison data were stored in the data bank for on-line comparisons with the experimental data.

For the purpose of indicating the capability of the new testing technique, some results will be shown which indicate the versatility and economy of the on-line data acquisition scheme. A comparison between the steady and unsteady (first harmonic) calculations of Magnus and Yoshihara with the experimental data will be shown for the NACA 64A010 airfoil. The usefulness of the on-line analysis technique will be demonstrated by comparing the NLR experiments with the current experiment for the condition of shockless flow on the supercritical airfoil.

The data to be presented in figures 9 through 12 are copies made directly from the graphics terminal. These unedited results contain some spurious data points from plugged tubes, broken transducers, etc., but the value of these displays for on-line analysis will be evident.

Figure 9 depicts the measured and computed static pressure distribution for the NACA 64A010 airfoil. The strength of the shock wave is predicted quite well by the inviscid theory. However, the measured shock position is slightly upstream of the computed position. Further analysis of the viscous effects will be made using measured data at other Reynolds numbers. The calculations do not include the effect of wind-tunnel walls, and the measurements indicate that the ratio of airfoil chord to test-section height for the current experiment was sufficiently small to preclude large interference effects due to blockage.

Figure 10 shows a comparison between the experimental and calculated first harmonic unsteady pressure distribution. The mean conditions are those shown in figure 9. The model was oscillated at 33 Hz about the 0.25 chord location with an amplitude of $\pm 1^\circ$. The first harmonic response can be expressed as the first term of a Fourier series:

$$p(x/c,t) = a_1 \cos(\omega t) + b_1 \sin(\omega t)$$

where p is the unsteady pressure, x/c is the fraction of chord, ω is the radian frequency, and a_1 and b_1 are Fourier coefficients. The data in figure 10 show the magnitude and phase of the pressure normalized by the dynamic pressure q_∞ :

$$\text{mag } C_p = \frac{1}{q_\infty} (\sqrt{a_1^2 + b_1^2})$$

$$\text{phase } C_p = \tan^{-1}(-b_1/a_1) \quad -\pi < \text{phase} \leq \pi$$

²H. Tijdeman supplied the NLR experimental data.

The phase reference for the C_p data is arbitrary. The phase reference for the C_p calculations is the α motion. The phase angle for the experimental data (x) has been shifted (\otimes) so that both experimental and calculated results are keyed to the same reference.

Upstream of the shock wave (indicated by a bump in the magnitude and a large phase shift), the magnitudes agree very well. This is probably due to the fact that the mean flows agree with one another and the unsteady response is tied so closely to the mean flow. At the shock, the measured peak lies somewhat below the calculated one due to viscous effects. Downstream agreement is again quite good. The phase agrees quite well upstream of the shock. As mentioned above, the Euler equation calculations were made for free-field conditions. The good agreement shown here indicates that wall interference is probably not a problem. These results are typical of other comparison data between the experiment and calculations. Data have also been obtained at conditions beyond the capabilities of current computer codes (e.g., where strong shock wave boundary-layer effects exist). Comparisons such as those in figure 10 serve as valuable baseline data for confirming the correctness of both the calculations and the experiments.

Figures 11 and 12 depict the mean pressure distribution on the NLR 7301 airfoil for two different angles of attack α . The NLR data were obtained at an angle of attack of 0.85° . This was the experimentally determined shockless condition in their facility. In figure 11, data from the NASA-Ames facility at this condition is shown in comparison with the NLR data. The presence or absence of a shock wave on the upper surface is hard to perceive, but the agreement is not very good. After some trial and error, best agreement was found at $\alpha = 0.37^\circ$ as shown in figure 12. As shown by the data key, the on-line analysis enabled the experiment to be successfully compared with the NLR data in approximately 4 min. Due to the time constraints, the unsteady data from the supercritical airfoil has not been examined very closely. A complete off-line analysis of all the data is currently underway.

CONCLUDING REMARKS

A new dynamic oscillation apparatus, capable of testing two-dimensional wing sections in transonic flow with motions ranging from a pure rotational oscillation to a pure heaving motion, has been developed for operation in the NASA-Ames 11- by 11-Foot Transonic Wind Tunnel. It provides unsteady pressure measurements at Reynolds numbers and reduced frequencies previously unobtainable. Two airfoil sections have recently been tested, an NACA 64A010 and an NLR 7301 supercritical. Preliminary comparisons between theory and experiment show good agreement. A more complete analysis of the steady and unsteady data is underway.

REFERENCES

1. Tijdeman, H.: Investigations of the Transonic Flow Around Oscillating Airfoils. NLR TR 77090 u, 1977.
2. Davis, S. S.; and Satyanarayana, B.: Two-Dimensional Transonic Testing with Splitter Plates. NASA TP 1153, 1978.

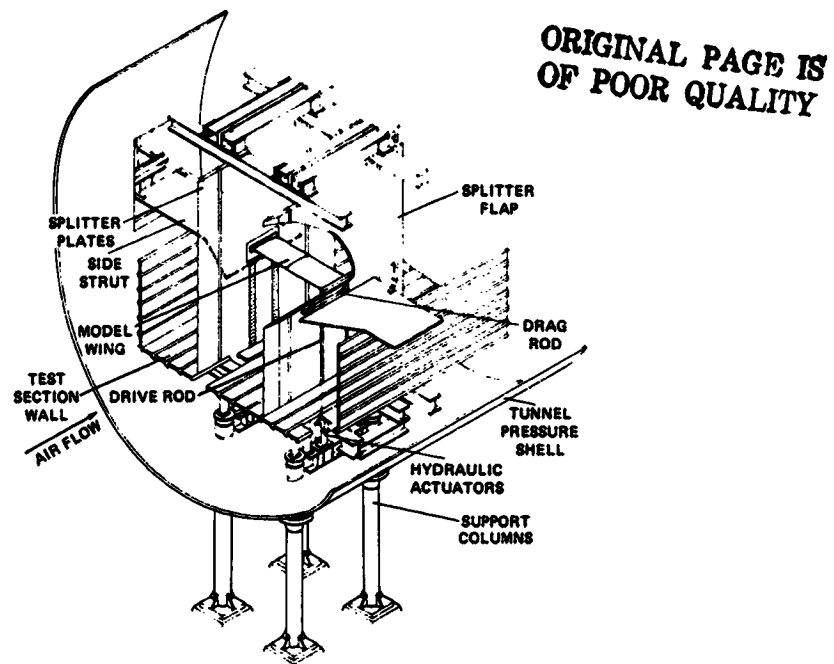


Figure 1.- Two-dimensional oscillating airfoil test apparatus installed in NASA Ames 11- by 11-foot transonic wind tunnel.



Figure 2.- Photograph of two-dimensional oscillating airfoil apparatus installed in the NASA Ames 11- by 11-foot transonic wind tunnel.

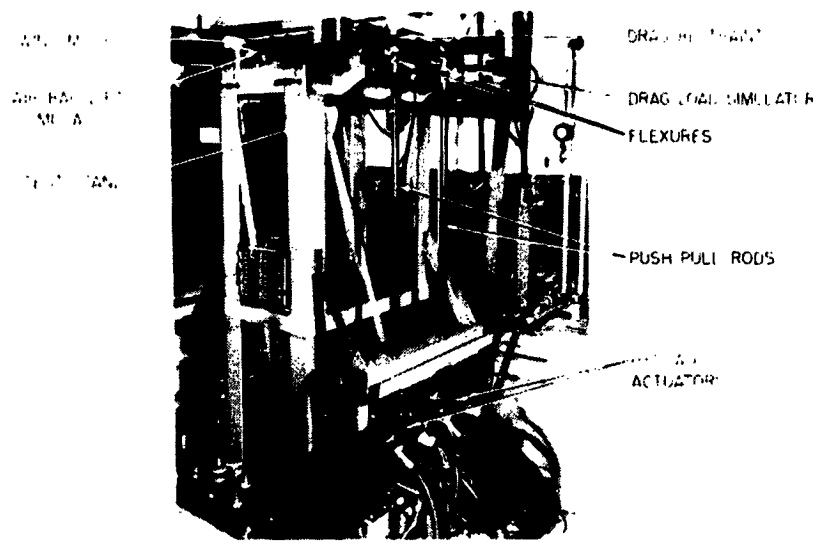


Figure 3.- Photograph of oscillating airfoil test stand.

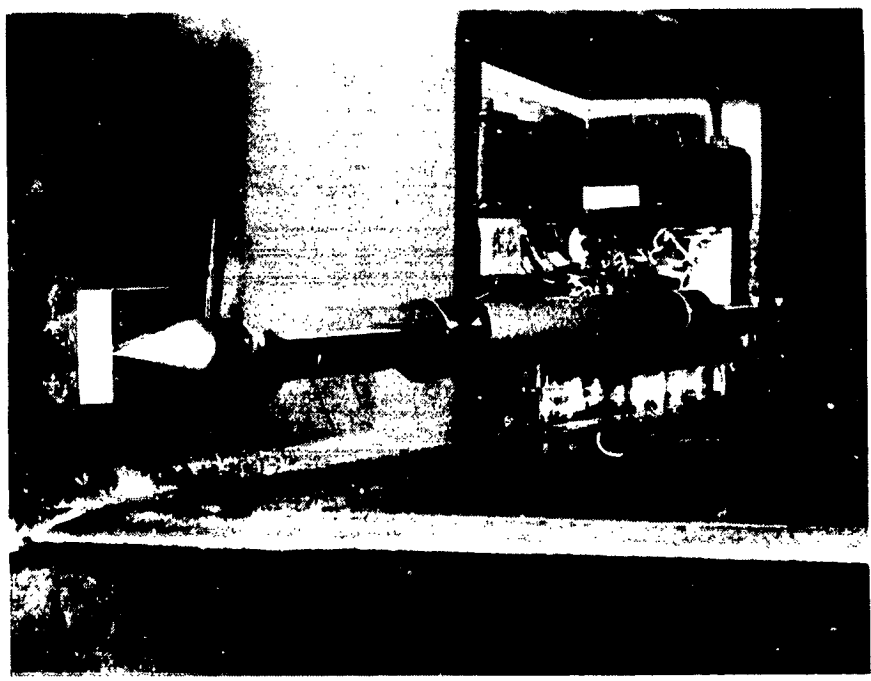


Figure 4.- Photograph of wing end section, drag restraint, side strut, and splitter plate.

ORIGINAL PAGE IS
OF POOR QUALITY

ORIGINAL PAGE IS
OF POOR QUALITY

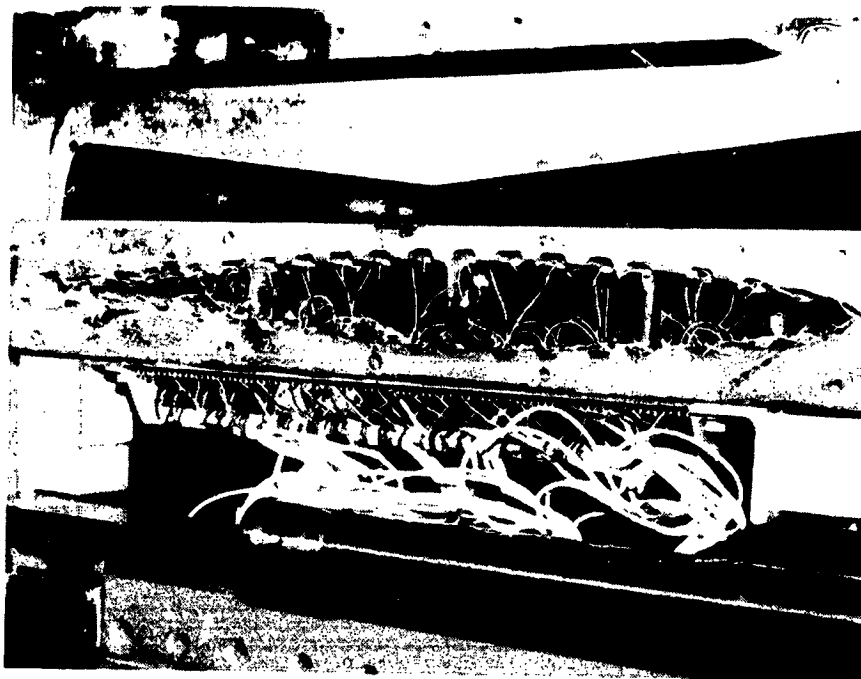


Figure 5.- Photograph of wing end section and access to instrumentation.

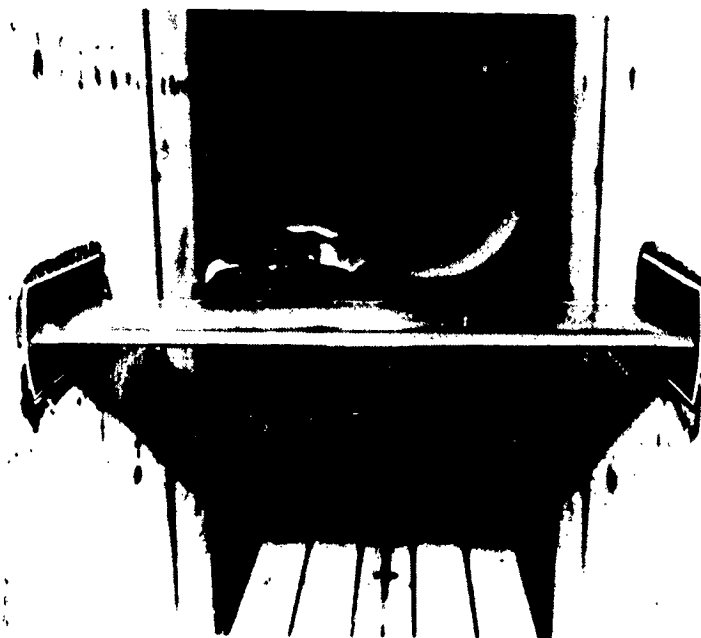


Figure 6.- Photograph of NACA 64A010 airfoil model mounted between splitter plates.

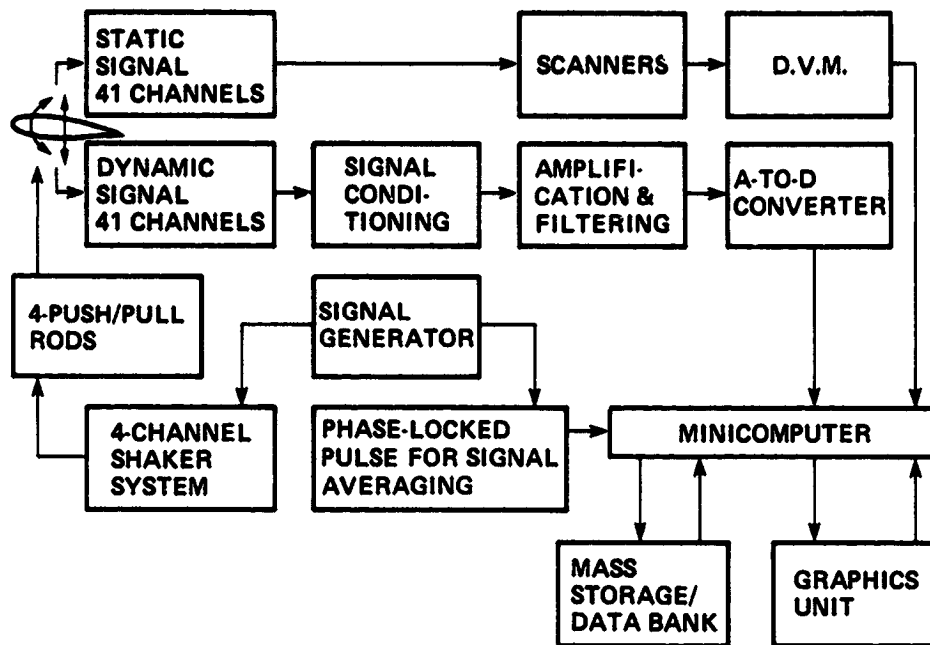


Figure 7.- Block diagram of the computational data-acquisition scheme for the two-dimensional oscillating airfoil apparatus.

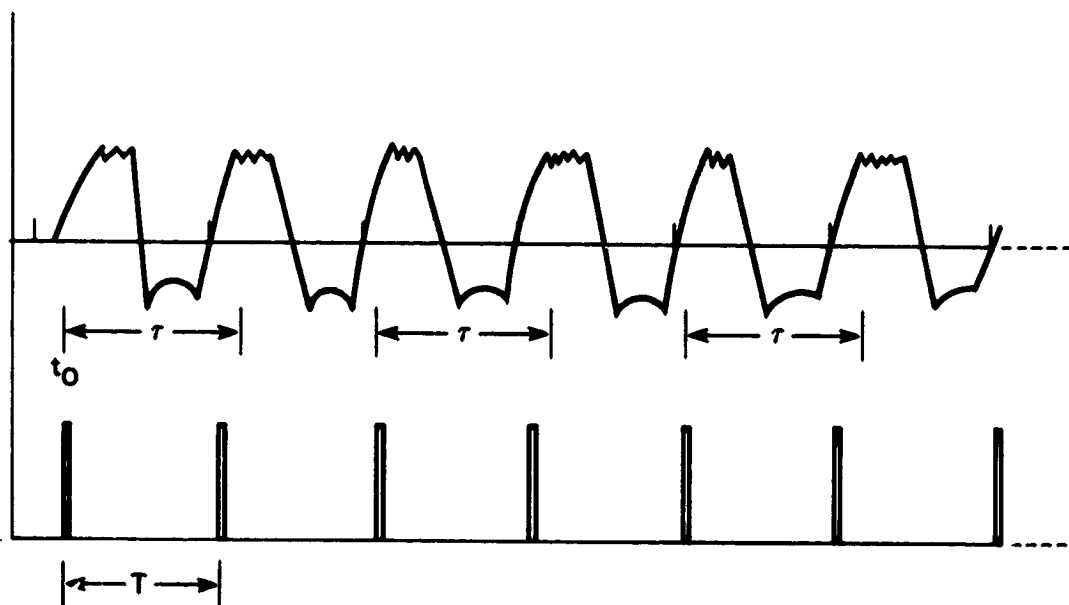


Figure 8.- Timing diagram for dynamic-data acquisition. Upper trace: dynamic-data signal, τ is slightly greater than 1 period. Lower trace: trigger for analog-to-digital conversion; T = Period; $n = 2$.

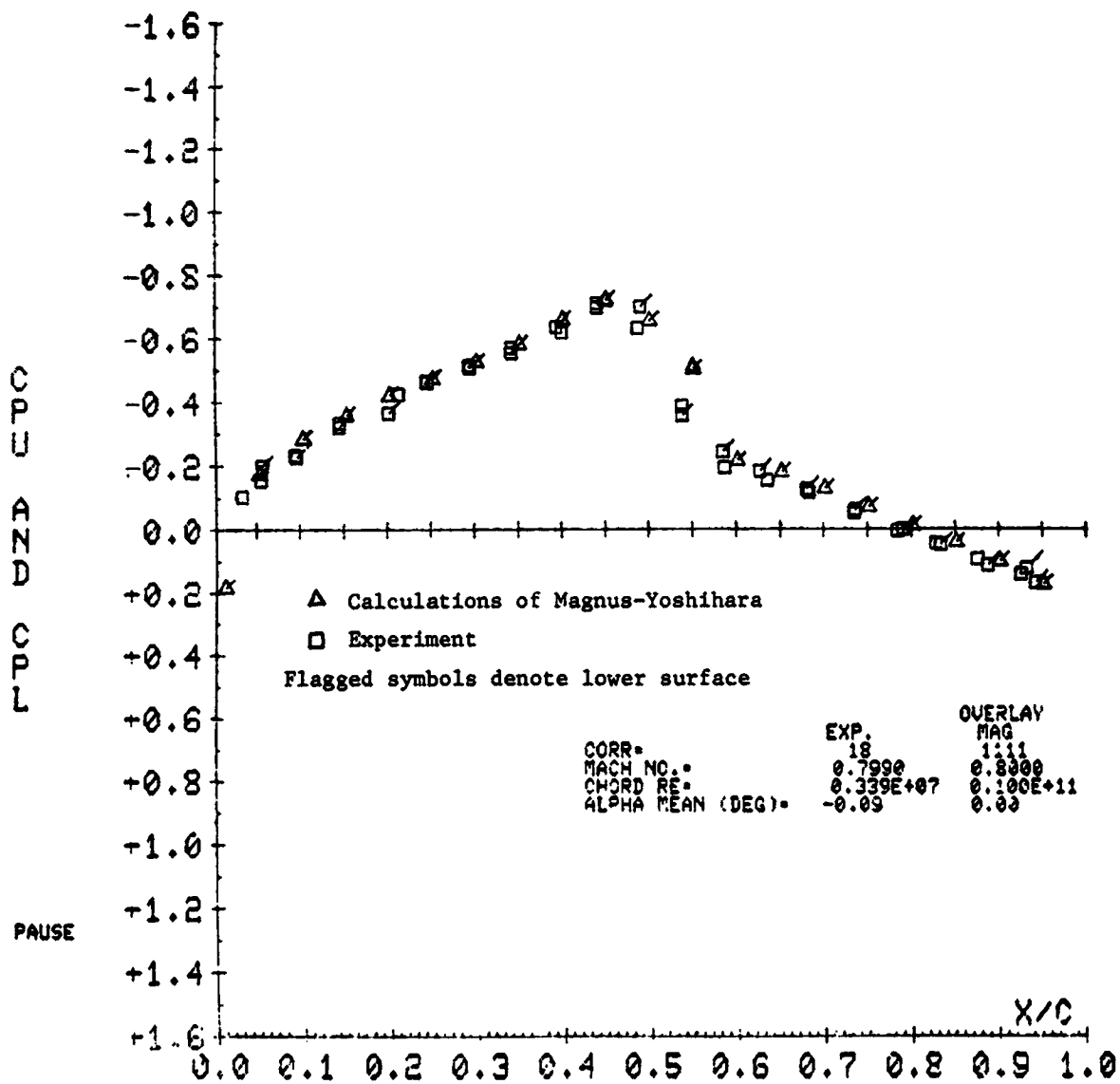


Figure 9.- Static pressure distribution on NACA 64A010 airfoil. $M_\infty = 0.8$;
 $\alpha = 0^\circ$. Record of 2/23/78: 21 h, 57 min.

PROJ PCOMP
 0 0 101677.4000JMT

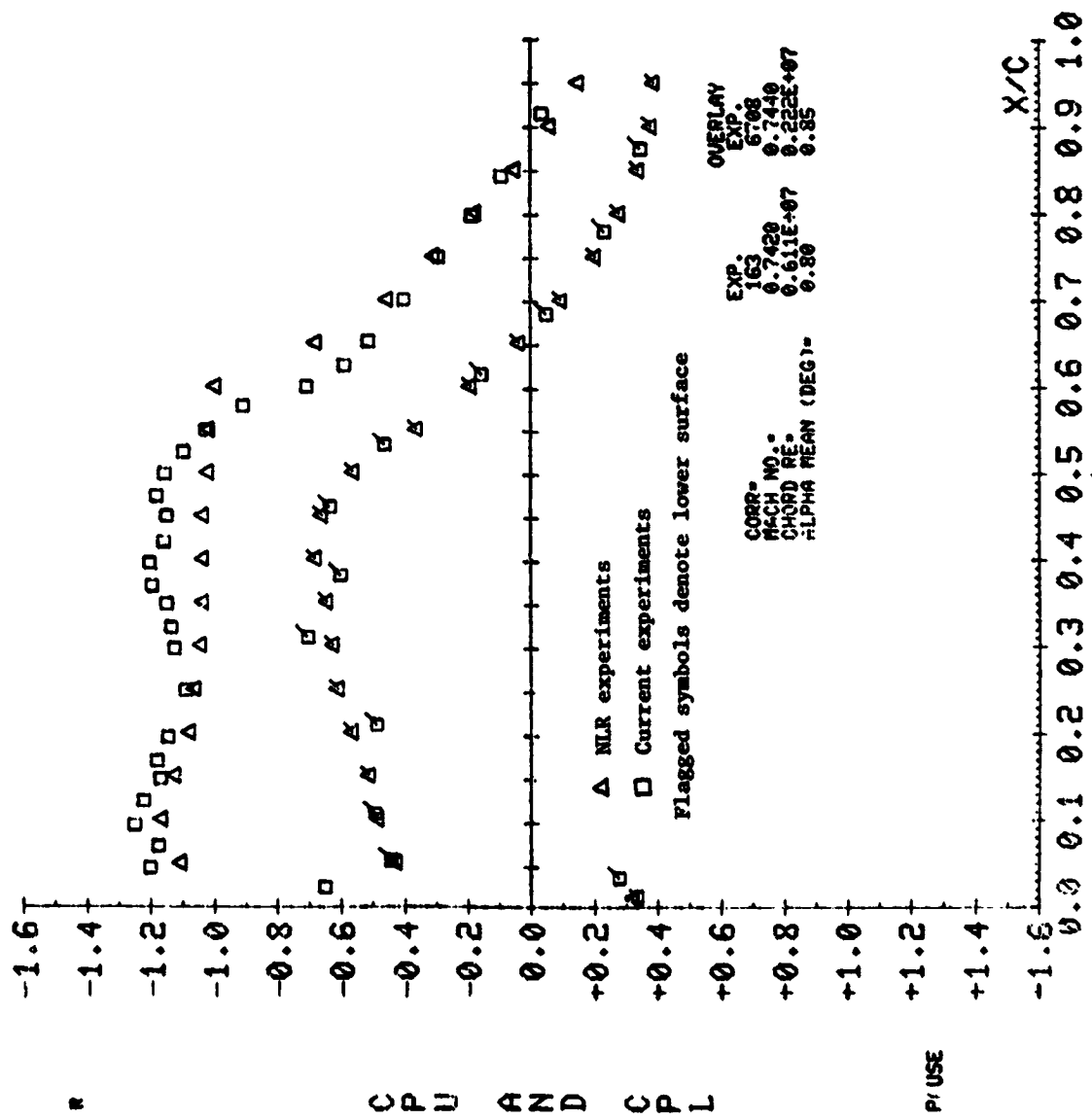


Figure 11.- Static pressure distribution on NLR 7301 supercritical airfoil.
 $M_\infty = 0.74$, $\alpha = 0.8^\circ$. Record of 3/18/78: 19 h, 55 min.

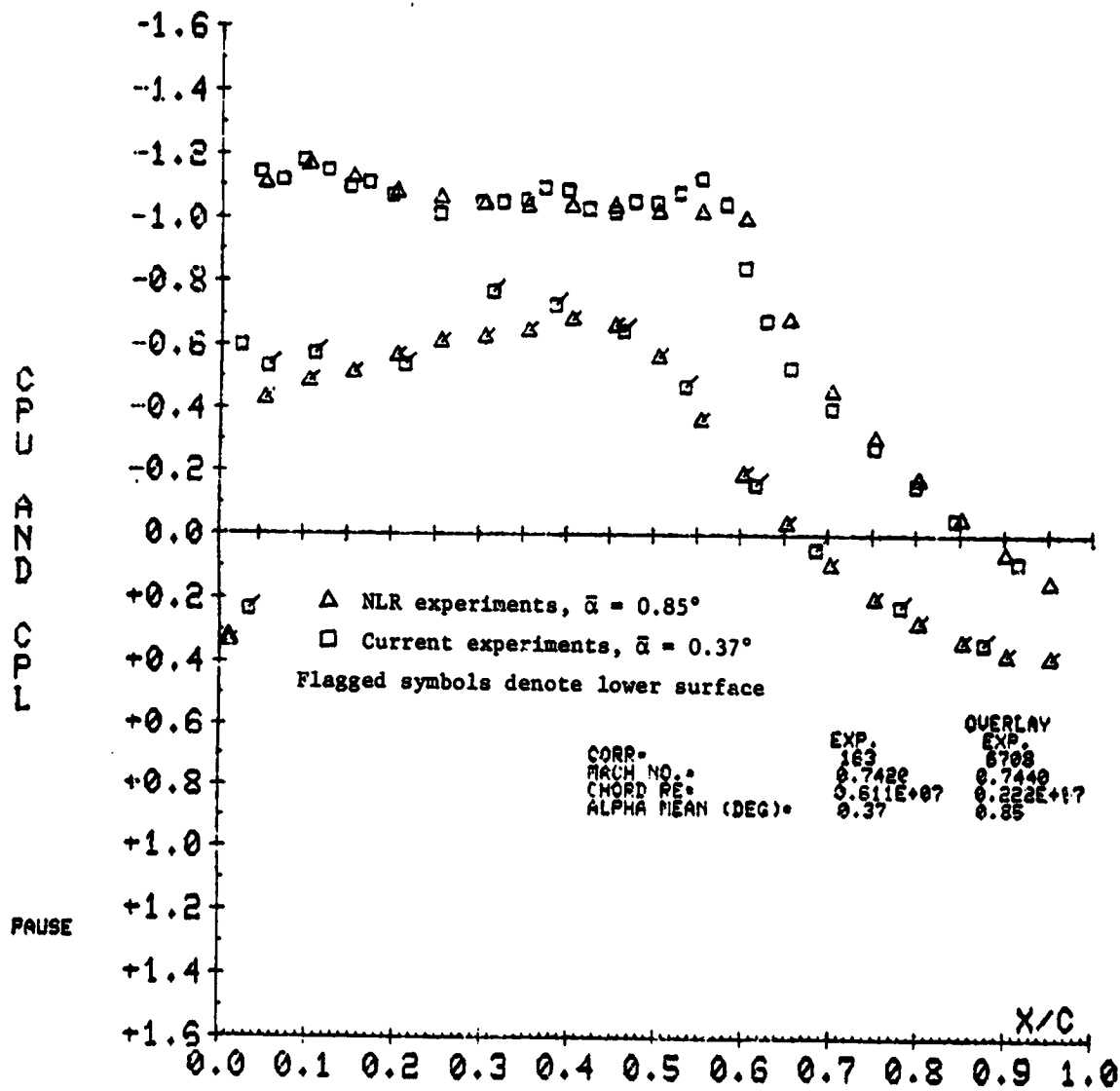


Figure 12.- Static pressure distribution on NLR 7301 supercritical airfoil showing best match between data. Record of 3/18/78: 19 h, 50 min.

SOME CALCULATIONS OF TRANSONIC POTENTIAL FLOW FOR
THE NACA 64A006 AIRFOIL WITH AN OSCILLATING FLAP

Robert M. Bennett and Samuel R. Bland
NASA Langley Research Center

SUMMARY

A method for calculating the transonic flow over steady and oscillating airfoils has recently been developed by Isogai. It solves the full potential equation with a semi-implicit, time-marching, finite difference technique. Steady flow solutions are obtained from time asymptotic solutions for a steady airfoil. Corresponding oscillatory solutions are obtained by initiating an oscillation and marching in time for several cycles until a converged periodic solution is achieved. In this paper the method is described in general terms, and results are compared with experimental data for both steady flow and for oscillations at several values of reduced frequency. Good agreement for static pressures is shown for subcritical speeds, with increasing deviation as Mach number is increased into the supercritical speed range. Fair agreement with experiment was obtained at high reduced frequencies with larger deviations at low reduced frequencies.

INTRODUCTION

The flutter critical portion of the aircraft flight envelope generally occurs at transonic speeds. This critical condition results from both the high dynamic pressures of operation and the dip in flutter speed or "bucket" that occurs at transonic Mach numbers. The dip in flutter speed is influenced by airfoil thickness and shape and cannot be satisfactorily treated by state-of-the-art aerodynamic analyses. Thus an important current topic in aerodynamic research is the development of methods for the calculation of unsteady aerodynamics for use in transonic flutter analysis. Many of the current efforts have built on the recent success of steady flow numerical finite difference solution procedures, and to date, have primarily been applied to two-dimensional airfoils as a means of evaluating and refining the analyses and algorithms involved. In this paper, a method developed at NASA Langley Research Center by Koji Isogai* (refs. 1 and 2) is described in general terms, and transonic results recently generated for the case of an oscillating flap are presented and discussed.

*NRC-NASA Resident Research Associate, on leave from National Aerospace Laboratory, Japan, 1975-1977.

SYMBOLS

a	nondimensional speed of sound
a_∞	nondimensional freestream speed of sound
c	airfoil chord
c_h	flap hinge moment coefficient, taken about hinge line, positive in direction of δ_f , (hinge moment)/ $q_\infty c^2$
c_l	lift coefficient, lift/ $q_\infty c$
c_m	pitching moment coefficient, taken about $c/4$, positive nose up, moment/ $q_\infty c^2$
C_p	pressure coefficient, $(p-p_\infty)/q_\infty$
C_p^*	pressure coefficient for sonic flow
ΔC_p	difference in pressure coefficient, $C_{p_{\text{lower}}} - C_{p_{\text{upper}}}$
Im	imaginary or out-of-phase part
k	reduced frequency, $\omega c/2V_\infty$
M	Mach number
p	pressure
q_∞	freestream dynamic pressure, $\frac{1}{2}\rho_\infty V_\infty^2$
Re	real or in-phase part
t	nondimensional time
U	nondimensional velocity component in x-direction
V	nondimensional velocity component in y-direction
V_∞	free-stream total velocity
x, y	coordinate distances

α	angle of attack
γ	ratio of specific heats
δ_f	flap deflection, positive trailing edge down
ρ_∞	free-stream density
ϕ	perturbation potential
ω	frequency of oscillation, rad/s

GENERAL DESCRIPTION OF THE METHOD

The full potential equation for two-dimensional time dependent flow is

$$(a^2 - U^2)\phi_{xx} - 2UV\phi_{xy} + (a^2 - V^2)\phi_{yy} \\ - 2U\phi_{xt} - 2V\phi_{yt} - \phi_{tt} = 0$$

where

ϕ = perturbation potential

$U = \cos \alpha + \phi_x$

$V = \sin \alpha + \phi_y$

$a^2 = a_\infty^2 - 0.5(\gamma - 1) (2\phi_t + U^2 + V^2 - 1)$

This equation is nonlinear because a , U , and V are functions of ϕ , and numerical finite difference techniques are generally used to obtain solutions. Use of the full potential equation yields a method that is intermediate in completeness and computational effort between methods that use the Euler equations (ref. 3) and those that use the small disturbance equation (refs. 4 and 5). One advantage of using the potential equation as compared with the Euler equations is that for the potential equation only the single variable ϕ has to be stored, whereas for the Euler equations ρ , p , U , and V must be stored.

A semi-implicit finite difference method has been developed by Isogai to obtain numerical solutions of the full potential equation in a time asymptotic manner for both steady and oscillatory cases. In reference 1, the basic method and several results are presented with emphasis on verifying the method. Additional computed examples are given in reference 2.

The semi-implicit finite difference technique alleviates some of the limits on time step, required for stability, that restrict explicit techniques. An unpublished addition to the algorithm described in reference 1 has also been made by Isogai which extends the permissible time step. It essentially is an additional implicit pass through the flow field. The time step is still restricted, however, which implies that the computer time increases as reduced frequency k decreases. The method also uses a rotated difference scheme to maintain numerical stability.

A stretched rectangular Cartesian grid system similar to that of reference 6 is used to map the infinite physical space to a finite computational region. The airfoil motion boundary condition is applied at the mean airfoil position. This assumption may restrict the valid range of amplitude of motion, but considerably simplifies the computer program as the airfoil and computation grid remain fixed in time. In addition, the finite difference method uses a quasi-conservative shock-capturing difference scheme to treat the moving shock waves. This treatment of shock waves ensures that the correct shock jump relations are maintained. It also simplifies the computer program as the moving shocks are treated automatically, but they are smeared over a few mesh spaces.

The current version of the computer program is dimensioned for a grid of up to 61 x 61 points. It requires 37 000 (114 Kg) locations of central computer memory. On a CYBER 175, operating under the NOS operating system with the FTN compiler, the program takes about 1/2 seconds of CPU time for each time step. About 3000 time steps are required to converge for a steady flow case and 1000 to 5000 steps for a typical oscillatory case.

RESULTS AND DISCUSSION

Several cases have been calculated for an NACA 64A006 airfoil with and without an oscillating quarter-chord flap. Experimental data for these cases have been obtained by Tijdeman and Schippers (refs. 7 and 8). For all calculations a 57 x 57 point grid system was used. The upper half of the grid is shown in figure 1 in physical space. One finite y -grid line and the lines at infinity are not shown. The mapping clusters points near the leading and trailing edges and near the airfoil surface, but no special consideration is given to shocks or hinge lines. For the grid system used (fig. 1), there are 29 points on each airfoil surface with the first and last points on the airfoil at 0.01c and 0.99c, respectively.

The steady pressure distribution for the NACA 64A006 airfoil with $\alpha = \delta = 0$ (considering airfoil thickness only) has been calculated for Mach numbers

ranging from 0.500 to 0.900. The results for Mach numbers 0.800 and 0.875 are shown in figures 2 and 3. Generally, good agreement exists for Mach number of 0.800 with some deviation from the experimental data at the trailing edge. The calculated results for a Mach number of 0.875 do not agree as well with experiment, primarily as a result of a calculated shock that is stronger and further aft than the experimental shock. These two cases illustrate portions of a trend found in comparing the calculated and experimental results. Good agreement was found at subsonic speeds, with some deviation over the aft end of the airfoil, but a gradual and increasing deviation between calculated and experimental results is apparent as Mach number increases into the supercritical speed range. The mismatch of experimental and computed shock locations has a strong effect on the unsteady results. The reasons for the mismatch of shock locations are not fully known but are possibly a result of boundary layer and wind tunnel wall effects. The calculations of reference 3 show that inclusion of porous wind tunnel wall boundary conditions can change the shock location by the same order of magnitude as the difference between the free-air calculations and experiment shown here (tunnel height/chord = 3.06 for these experimental data).

Results for the NACA 64A006 airfoil with an oscillating quarter-chord flap are shown in figures 4 and 5 for two values of reduced frequency k and for Mach number 0.875. The in-phase and out-of-phase parts of the first harmonic of the oscillatory pressure distributions are shown (fig. 4 and 5). For the higher reduced frequency, $k = 0.234$, the real part has two peaks, one at the shock location and one at the hinge line, and the imaginary part has a single peak at the shock location. Calculated trends correspond to experimental trends, but differences in shock location are apparent. Isogai (ref. 2) has shown improved agreement for this case if the calculations are made at a Mach number of 0.860 rather than 0.875 so that steady shock is near the experimental shock location. For the lower frequency case, there is significantly more deviation, particularly for the imaginary part. The lower frequency case involves a larger shock motion, and the unsteady results are apparently more sensitive to the steady shock location as well.

The calculated real and imaginary parts of the first harmonic of pitching moment, lift, and hinge moment coefficients (per unit flap deflection) are shown for several reduced frequencies in figures 6 to 8 and are compared with the experimental values of reference 8. All calculations shown are for a 1.08-degree flap amplitude which is the value for the experimental point at $k = 0.234$. The calculated results fluctuate with reduced frequency, whereas such fluctuations are not apparent in the experimental data. There is fair agreement of the theory with experiment at the two higher frequency experimental points. However, at the lower reduced frequencies there is a sizeable deviation from the experimental data. The relative agreement with experiment might be anticipated from figures 3 and 4, as the coefficients shown are integrals of the load distribution. The imaginary parts of the coefficients are zero at $k = 0$, and thus there must be a rapid variation near $k = 0$. Calculations for static deflection of the flap show that the coefficients are very nonlinear functions of the flap deflection. There may be similar nonlinearities in the low frequency unsteady results shown in figures 6 to 8.

Although a large number of calculated points are shown in figures 6 to 8, only a single grid size, time step, and amplitude of oscillation have been used. It is desirable to evaluate the influence of these parameters also, but such an investigation would require a significant expenditure of computer resources. For the cases of figures 6 to 8, it took about 5 minutes of CPU time on a CYBER 175 to calculate 6 cycles of oscillations at $k = 0.500$. This time increased to about 30 minutes to execute 3 cycles of oscillation at $k = 0.059$. Although the method gives results that offer considerable insight to transonic flows, it needs further development to reduce the computer time in order for it to be used as a production tool to study a wide variety of cases.

CONCLUDING REMARKS

The method of Isogai for calculating the transonic flow over steady and oscillating airfoils has been used to calculate several cases for the NACA 64A006 airfoil with an oscillating quarter-chord flap. The thickness pressure distributions were in good agreement with measured results at subcritical speeds but gradually deviated further from the data as Mach number was increased. Calculated unsteady results for a Mach number of 0.875 showed large frequency effects not apparent in the experimental results. Fair agreement was obtained at the higher reduced frequencies with larger deviations at low reduced frequencies. The method gives results that offer considerable insight to transonic unsteady flows, but needs further development to reduce the computer resources required.

REFERENCES

1. Isogai, Koji: Calculation of Unsteady Transonic Flow Over Oscillating Airfoils Using the Full Potential Equation. AIAA/ASME 18th Structures, Structural Dynamics & Materials Conference, Volume B (San Diego, California), Mar. 1977, pp. 245-256.
2. Isogai, Koji: Numerical Study of Transonic Flow Over Oscillating Airfoils Using the Full Potential Equation. NASA TP-1120, 1978.
3. Magnus, R. J.: Calculations of Some Unsteady Transonic Flows About the NACA 64A006 and 64A010 Airfoils, AAFDL-TR-77-46, U.S. Air Force, July 1977.
4. Weatherill, Warren H.; Sebastian, James D.; and Ehlers, F. Edward: The Practical Application of a Finite Difference Method for Analyzing Transonic Flow Over Oscillating Airfoils and Wings. NASA CR-2933, 1978.
5. Ballhaus, W. F.; and Goorjian, P. M.: Implicit Finite-Difference Computations of Unsteady Transonic Flows About Airfoils. AIAA J. vol. 15, no. 12, Jan. 1978, pp. 1728-1735.
6. Carlson, Leland, A.: Transonic Airfoil Flowfield Analysis Using Cartesian Coordinates, NASA CR-2577, 1975.
7. Tijdeman, H.; and Schippers, P.: Results of Pressure Measurements on an Airfoil With Oscillating Flap in Two-Dimensional High Subsonic and Transonic Flow (Zero Incidence and Zero Mean Flap Position). NLR TR 73078 U, Nat. Lucht - Ruimtevaartlab. (Amsterdam), July 13, 1973.
8. Tijdeman, H.; and Schippers, P.: Results of Pressure Measurements on a Lifting Airfoil With Oscillating Flap in Two-Dimensional High Subsonic and Transonic Flow. NLR TR 73018 L, Nat. Lucht - Ruimtevaartlab. (Amsterdam). Nov. 1974.

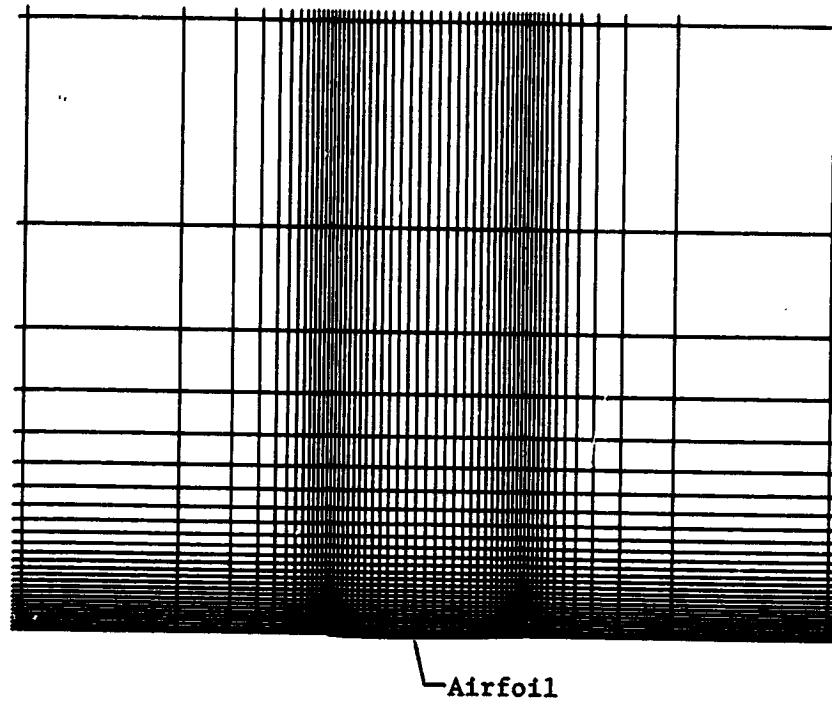


Figure 1.- Grid system used for calculations, 57 x 57.

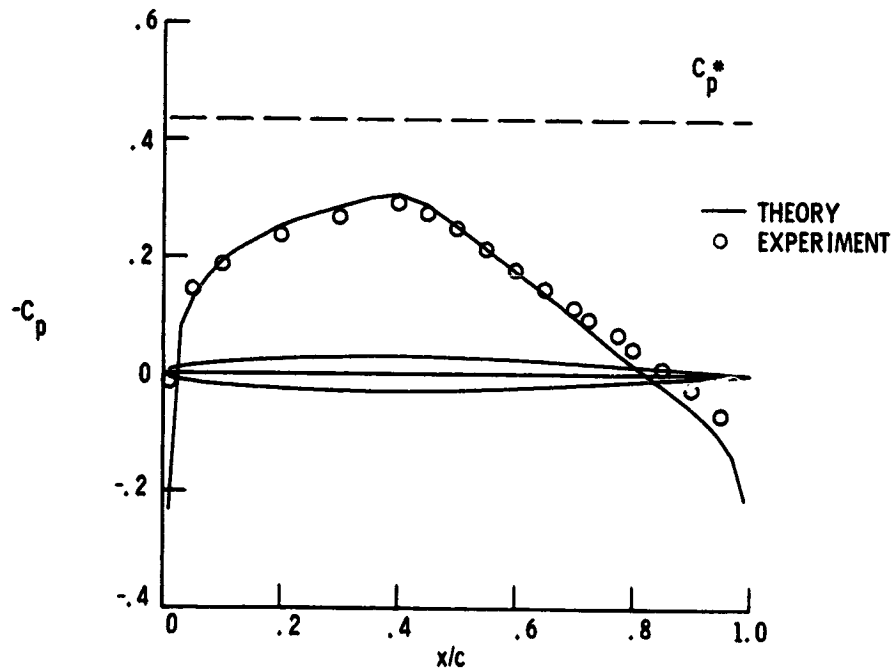


Figure 2.- Steady pressure distribution for the NACA 64A006 airfoil at $M = 0.800$ and $\alpha = 0^\circ$.

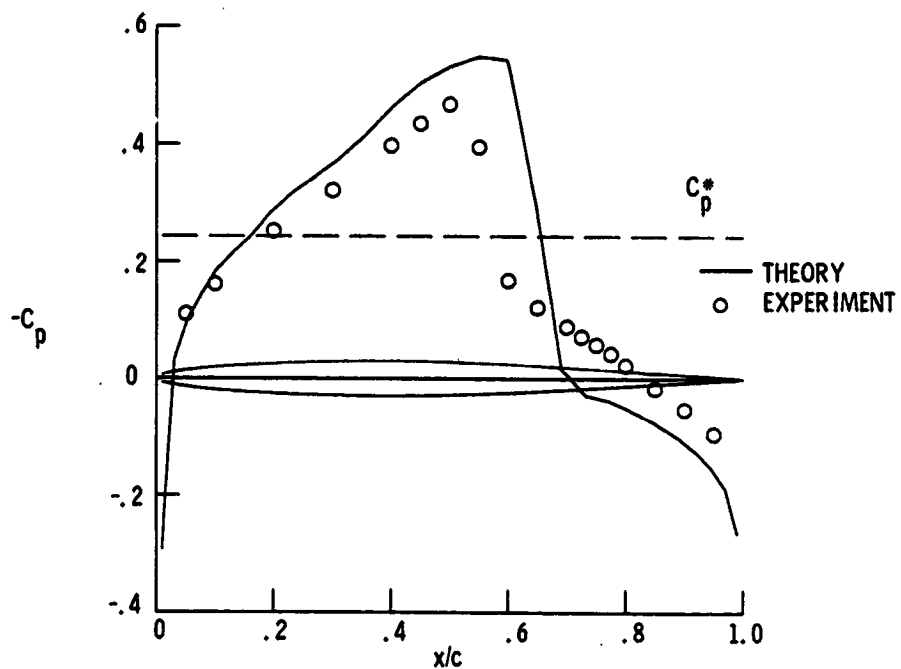
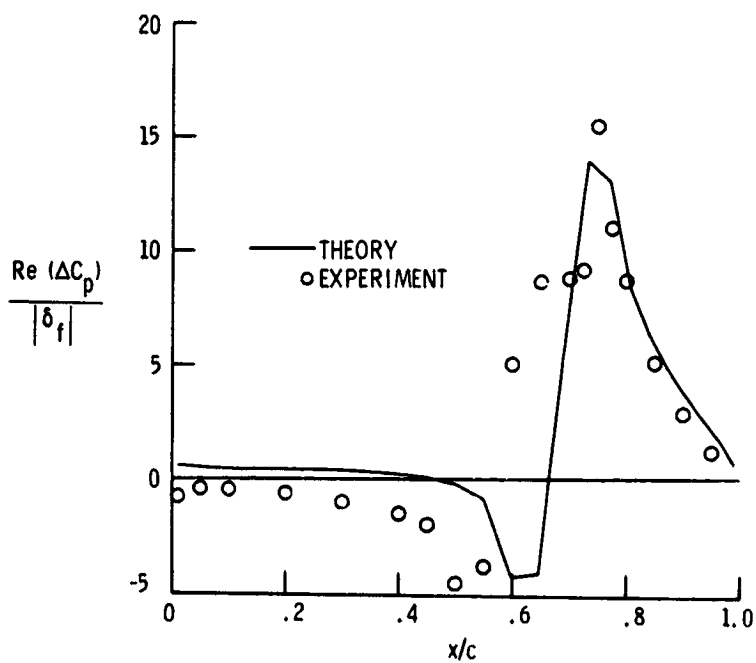
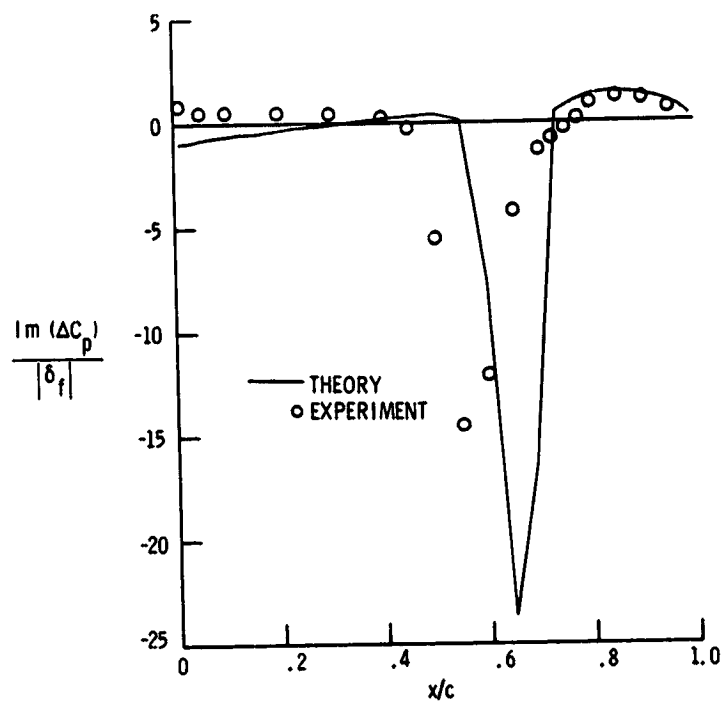


Figure 3.- Steady pressure distribution for the NACA 64A006 airfoil at $M = 0.875$ and $\alpha = 0^\circ$.



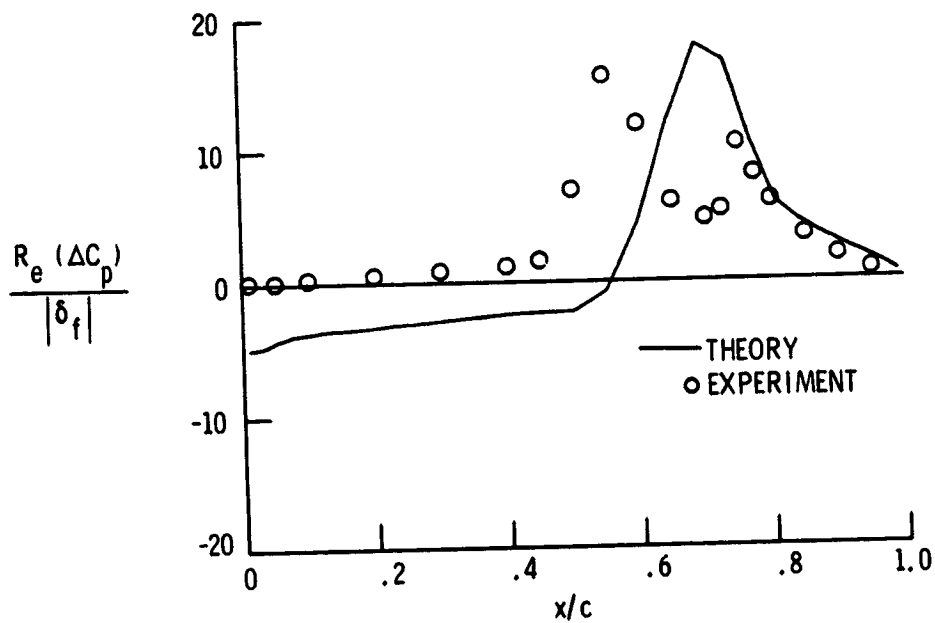
(a) Real part.

Figure 4.- Load distribution for an NACA 64A006 airfoil with an oscillating quarter-chord flap; $k = 0.234$, $M = 0.875$, $\alpha = 0.0^\circ$, and $|\delta_f| = 1.08^\circ$.



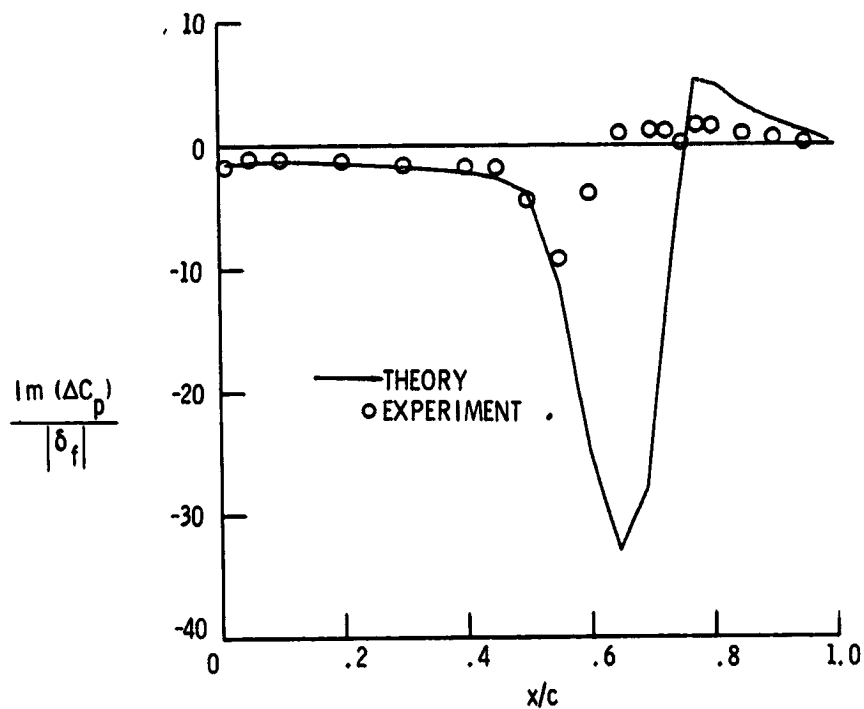
(b) Imaginary part.

Figure 4.- Concluded.



(a) Real part.

Figure 5.- Load distribution for an NACA 64A006 airfoil with an oscillating quarter-chord flap; $k = 0.059$, $M = 0.875$, $\alpha = 0.0^\circ$, and $|\delta_f| = 1.08^\circ$.



(b) Imaginary part.

Figure 5.- Concluded.

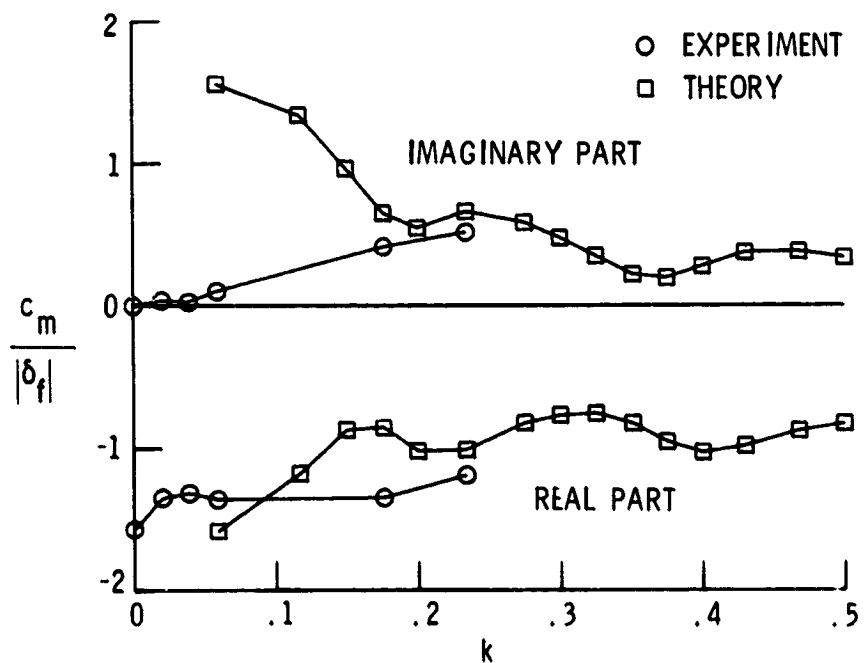


Figure 6.- Unsteady airfoil moment due to flap motion at $M = 0.875$ and $\alpha = 0^\circ$ with $|\delta_f| = 1.08^\circ$.

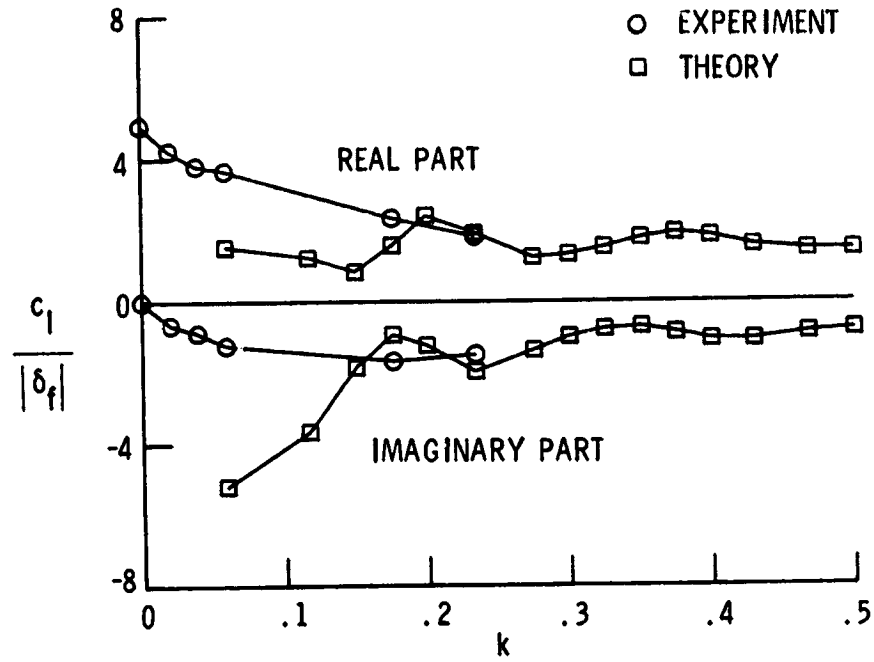


Figure 7.- Unsteady airfoil lift due to flap motion at $M = 0.875$ and $\alpha = 0^\circ$ with $|\delta_f| = 1.08^\circ$.

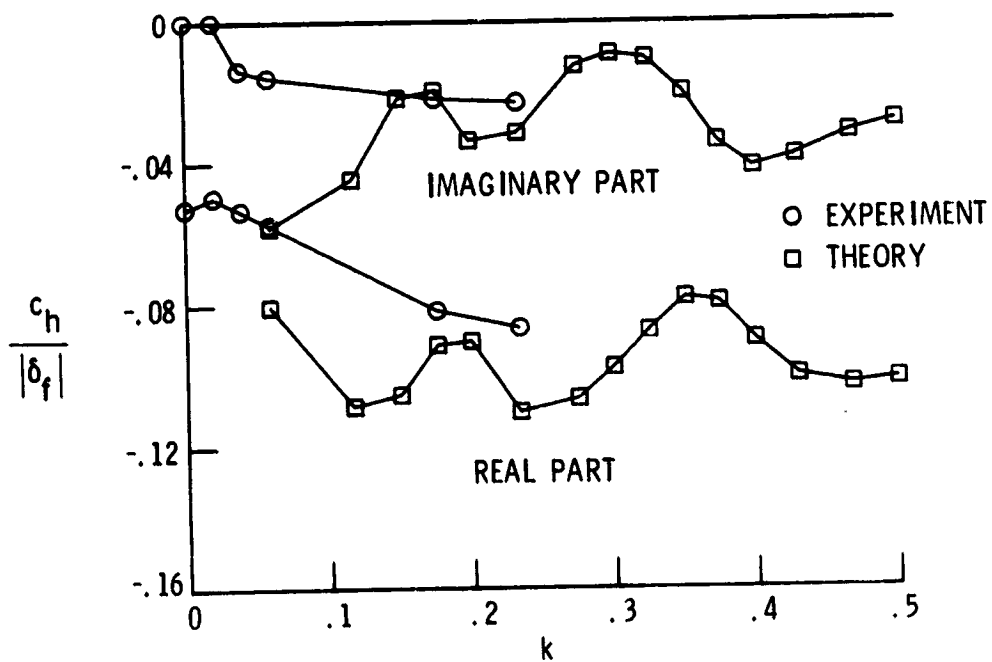


Figure 8.- Unsteady flap hinge moment due to flap motion at $M = 0.875$ and $\alpha = 0^\circ$ with $|\delta_f| = 1.08^\circ$.

OBSERVATIONS ON THE DYNAMIC STALL CHARACTERISTICS
OF ADVANCED HELICOPTER ROTOR AIRFOILS

L. Dadone
Boeing Vertol Company

SUMMARY

A significant amount of research has been devoted to understanding the mechanism of dynamic stall delay as applicable to the flow environment of a helicopter rotor in forward flight. One aspect of such research deals with the unsteady characteristics of two-dimensional airfoil sections over a Mach number range from 0.3 to 0.6, since such characteristics can be meaningfully related to rotor performance and loads.

This paper summarizes the results of several oscillatory tests carried out on conventional, transonic and BLC-equipped airfoils.

INTRODUCTION

There are two reasons to conduct oscillating airfoil tests. First, to identify the key elements in the unsteady flow environment and, second, to determine the unsteady characteristics of specific airfoils.

Until now an experimental approach has been necessary because dynamic stall cannot yet be quantified by theoretical means. Although empirical dynamic stall representation techniques have been developed, a fundamental understanding of the problem remains to be achieved.

Recently, considerable efforts have been directed to the definition of transonic airfoils applicable to helicopter rotors. This research was encouraged by the availability of new methods of analysis which greatly reduce the difficulty in designing airfoils with favorable transonic characteristics.

Now we have a large body of information from the oscillatory tests of several airfoils, and we can at least identify the most significant trends in the data. A review of these trends provides preliminary answers to questions concerning the comparison of transonic and conventional sections, further refinements in

airfoil design objectives, and generally, the purpose and usefulness of future unsteady airfoil testing.

SYMBOLS

Measurements and calculations were made in U.S. Customary Units and are presented in both the International System of Units (SI) and U.S. Customary Units.

b	airfoil semichord, m
c	airfoil chord, m
C_n	normal force coefficient
C_m	pitching moment coefficient
C_μ	blowing momentum coefficient, for sections employing active boundary layer control (BLC)
f	drive frequency of airfoil motion in pitch, Hz
k	reduced frequency, $\pi fc/V$
M	Mach number
P_T	tunnel test-section total pressure, N/m^2 (psia)
t	airfoil thickness, m
V	tunnel velocity, m/sec
α	angle of attack, deg
$\dot{\alpha}$	first differential of α with respect to time, deg/sec
γ	stall delay function
$\Delta\alpha$	amplitude of pitching motion, deg

SOURCE OF DATA

A thorough survey of current unsteady aerodynamics research is present in reference 1. However, until now the main source of oscillatory airfoil data applicable to helicopter rotors has been the two-dimensional subsonic insert of the Boeing Supersonic Wind Tunnel (BSWT).

A sketch of the oscillatory rig in the two-dimensional test section is shown in figure 1. The test section is 0.914m (36.0 in.) high and 0.304m (12.0 in.) wide. The wind tunnel is a blow-down facility with provisions for variable density operation, so that tests can be run at Reynolds numbers corresponding to full-scale blade chords with 6- to 7-inch chord models.

Solid floor and ceiling have been employed in all the oscillatory tests. Quasi-steady baseline data have been acquired in the presence of both solid and porous (4.9%) floor and ceiling. The oscillatory tests have been conducted within the following ranges of conditions.

Mach number, M	0.2 to 0.7
Mean angle of attack, α	-20° to $+20^\circ$
Amplitude of oscillation, $\Delta\alpha$	2.5° to 10°
Drive frequency, f	12 Hz to 100 Hz
Total Pressure, P_T	170,000 N/m ² to 520,000 N/m ² (25 psia to 75 psia)

The models of the airfoils were equipped with differential pressure transducers mounted as close to the pressure ports as possible. Each transducer/orifice cavity was sized to place the acoustic resonance frequency well beyond the tenth harmonic of the highest drive frequency of interest.

Table I lists the oscillating airfoil tests conducted in BSWT. Most of the tests have been documented and the data are available in references (2) through (5). The boundary layer control experiments on the V23010-1.58, and the VR-1 test have not been formally documented. Limited data from these tests are shown only to illustrate the relationship between static stall and aerodynamic damping.

Figure 2 shows typical pressures and integrated loads. The data were acquired during the tests of reference (5). The differential pressure coefficients are displayed as time-histories, while the normal force and pitching moment coefficients are shown as a function of angle of attack.

KEY PARAMETERS

Definition of Maximum Attainable Normal Force, $C_{n_{max}}$

The highest normal force achieved while an airfoil undergoes sinusoidal pitching motions over conditions ranging from fully attached flow to stall has been used as a measure of stall delay potential. The maximum attainable normal force is a function of reduced frequency and Mach number. Until now, it has not been successfully predicted by either theoretical or empirical means. Because of test limitations the maximum normal force cannot be always reached at model drive frequencies beyond 60 Hz.

Definition of Aerodynamic Damping

The area enclosed by the C_m, α trace, see figure 2, and the sense of motion around the loop have an important physical significance. The net work done by the airfoil on the surrounding air is proportional to the integral

$$W = \oint C_m d\alpha$$

This integral is proportional to the area enclosed by the C_m, α trace and it is positive for a counterclockwise circuit. If the circuit encloses a substantial area in a clockwise sense, the contribution of that area is negative, i.e., it represents energy extracted from the airstream by the airfoil.

For pitch oscillation about the quarter chord the theoretical damping is

$$\text{Damping} = \frac{-k}{4f}$$

The theoretical damping is used to non-dimensionalize the cycle damping value computed for each test condition. Details on the derivation of the theoretical damping are shown in reference 2.

Definition of Stall Delay Parameters

Reference (6) describes the formulation of an empirical method to represent dynamic stall. This method was specifically defined for rotor blade calculations.

The key to the method is the estimate of the delay in normal force and pitching moment stall angles as a function of instantaneous angular velocity $b\dot{\alpha}/V$ and Mach number. The rate of change of the stall angle with increasing $\sqrt{b\dot{\alpha}/V}$ at constant Mach number

has been called " γ -function." This quantity is different for the normal force and the pitching moment, and it decreases with Mach number. Figure 3 illustrates the derivation of γ -functions from oscillating airfoil data.

REVIEW OF CHARACTERISTICS

Maximum Normal Force

Figures 4 and 5 summarize the largest normal force attainable by several airfoils at $M = 0.4$ and 0.6 , respectively, over the range of reduced frequencies of interest for helicopter rotor operation.

The NACA 0006 and V13006-0.7 are thin airfoils ($t/c = 0.06$). The V0011 and V23010-1.58 are the airfoils employed on the CH-47A and CH-47B/C helicopters ($t/c = 0.11$ and 0.102) and, finally, the VR-1 ($t/c = 0.11$) and NLR 7223-62 ($t/c = 0.086$) are transonic sections.

The $M = 0.4$ condition is representative of the flow environment within which retreating blade stall takes place. The reduced frequency value of $k = 0.06$ is typical of 1/rev pitch changes. The maximum lift capability of all sections increases with reduced frequency above the static $C_{n_{max}}$ level. The rate of increase in stall margin with reduced frequency varies somewhat from airfoil to airfoil but, on the 1/rev basis, airfoils with low static $C_{n_{max}}$ do not gain enough additional lifting capability through unsteady effects to overcome a poor static stall performance. This fact was not obvious at the start of the stall delay research.

Compressibility effects reduce the boundaries at $M = 0.6$ for the same airfoils of figure 4. At $M = 0.6$ the stall delay effects are not as critical as they are at lower Mach numbers. Above $M = 0.5$ detrimental effects could result from operation at high lift in the presence of negative rates of change in angle of attack. Thin and transonic airfoils display larger $C_{n_{max}}$ changes at the higher subsonic Mach numbers than do the thick and conventional sections.

Aerodynamic Damping

The damping characteristics of six airfoils in 1/rev pitch oscillation at $M = 0.4$ are shown in figure 6. It is immediately evident that the thin and the transonic sections are positively damped through dynamic stall, while the conventional airfoils,

V0011 and V23010-1.58, are negatively damped. Although the aerodynamic damping from oscillating airfoil tests cannot be directly related to the rotor environment, it is useful as a measure of the stall recovery characteristics of the airfoils employed.

The aerodynamic damping is sensitive to Mach number and frequency changes, as illustrated in figure 7, but rotor test experience has shown the $M = 0.4$ condition and the lower frequencies to have dominant effects over the retreating blade.

A review of all the data for the airfoils of table I shows that positive damping at the 1/rev to 2/rev frequencies (k up to 0.12) is always associated with gradual quasi-steady stall, while negative damping during oscillation is typical of sections with abrupt static stall. The thin airfoils and the transonic sections considered here have a limited maximum lift range and gradual stall at $M = 0.4$, while at the same condition the V0011 and V23010-1.58 display leading edge stall (abrupt stall). This correlation between static stall and damping appears to hold generally true.

Figure 8 shows that as the stall character of the VR-1 airfoil changes with Mach number so do the 1/rev damping characteristics. As also illustrated in figure 8, one way to quantify stall is to determine experimentally the static stall hysteresis, since abrupt stall is associated with significant hysteresis effects.

All the data mentioned up to this point were for airfoils with high maximum lift potential and abrupt stall characteristics, or with a low maximum lift range and gradual stall. The only way of achieving high lift with gradual stall is through the attainment of trailing edge stall characteristics. Figure 9 is the only experimental evidence we have showing that trailing edge stall is beneficial in changing the aerodynamic 1/rev damping. Of course, since leading edge boundary layer control did not improve the maximum lift characteristics of the V23010-1.58 at $M = 0.4$, this method is not recommended unless positive damping is clearly essential.

Stall Delay Characteristics

The stall delay functions of three conventional airfoils are shown in figure 10. Figure 11 shows the stall characteristics of the VR-1 and NLR 7223-62, both transonic sections. A few general observations can be made:

- (a) Normal force always experiences a larger stall delay than the pitching moments.

- (b) Thin airfoils experience a larger lift-stall delay than thicker sections, but not enough to overcome the static maximum lift deficiency associated with thin airfoil stall.
- (d) Stall delay effects on the thin sections remain significant to higher Mach numbers.

The two transonic sections of figure 11 display strikingly similar trends. These trends are not substantially different from those of the conventional airfoils of figure 10, but the stall delay functions of the transonic sections do not decrease uniformly or vanish with increasing Mach number. The lift stall delay at Mach numbers above $M = 0.5$ is attributable to beneficial transonic effects not better quantified at this time, but it must be pointed out that stall delay at Mach numbers above $M = 0.5$ is not useful on present-day rotors.

CONCLUDING REMARKS

There are differences between the unsteady characteristics of conventional and transonic airfoils, but the transonic sections have no unusual stall delay characteristics at a Mach number M of 0.4, where such effect would be beneficial in compensating for a low static-lift capability. The transonic airfoils experience significant stall delay at Mach numbers above 0.5, a benefit which cannot be taken advantage of by present rotor technology.

The only favorable unsteady behavior we can deliberately design for is positive 1/rev and 2/rev aerodynamic damping at Mach numbers near $M = 0.4$. This can be accomplished by prescribing gradual static stall characteristics. Because of the high maximum lift requirements at $M = 0.4$, this means prescribing trailing edge stall.

Low maximum lift characteristics in the quasi-steady environment cannot be offset by a large dynamic stall delay.

The highest priority in unsteady aerodynamics research is the detailed understanding of the dynamic stall process. Until such understanding is reached, additional testing of airfoils is secondary to the detailed analysis of the data we already have, because approximate stall delay functions for most sections can be obtained by interpolating or extrapolating existing trends.

REFERENCES

1. McCroskey, W.J.: Some Current Research in Unsteady Fluid Dynamics. 1976 Freeman Scholar Lecture, March 1977, vol. 99, Journal of Fluids Engineering.
2. Liiva, J.; Davenport, F.J., Gray, L. and Walton, I.C: Two Dimensional Wind Tunnel Tests of Airfoils Oscillating Near Stall. U. S. Army AVLABS TR68-13, 1968.
3. Gray, L., Liiva, J., Davenport, F.J.: Wind Tunnel Tests of Thin Airfoils Oscillating Near Stall. U. S. Army AVLABS TR68-89A, 1969.
4. Gray, L., Dadone, L.U., Gross, D.W. and Child, R.F.: Wind Tunnel Investigation of Airfoils Oscillating in Reverse Flow. U. S. Army AVLABS TR70-4, 1970.
5. Dadone, L.U.: Two-Dimensional Wind Tunnel Test of an Oscillating Rotor Airfoil. NASA CR 2914 and 2915, December 1977.
6. Gross, D.W. and Harris, F.D: Prediction of Inflight Stalled Airloads from Oscillating Airfoil Data. 25th Annual National Forum of the American Helicopter Society, May 1969.

TABLE I
SUMMARY OF OSCILLATING AIRFOIL TESTS

AIRFOIL	APPLICATION	TYPE OF TEST
V0011	CH-47A	PITCH AND TRANSLATION
V23010-1.58	CH-47B/C	PITCH AND TRANSLATION
MACA 0006	RESEARCH	PITCH
V13006-0.7	AGB	PITCH
V23010-1.58 REVERSE FLOW	RESEARCH	PITCH
V23010-1.58 BLC	RESEARCH	PITCH (UNPUBL.)
VR-1	ADVANCED ROTOR	PITCH (UNPUBL.)
NLR 7223-62	ADVANCED ROTOR	PITCH

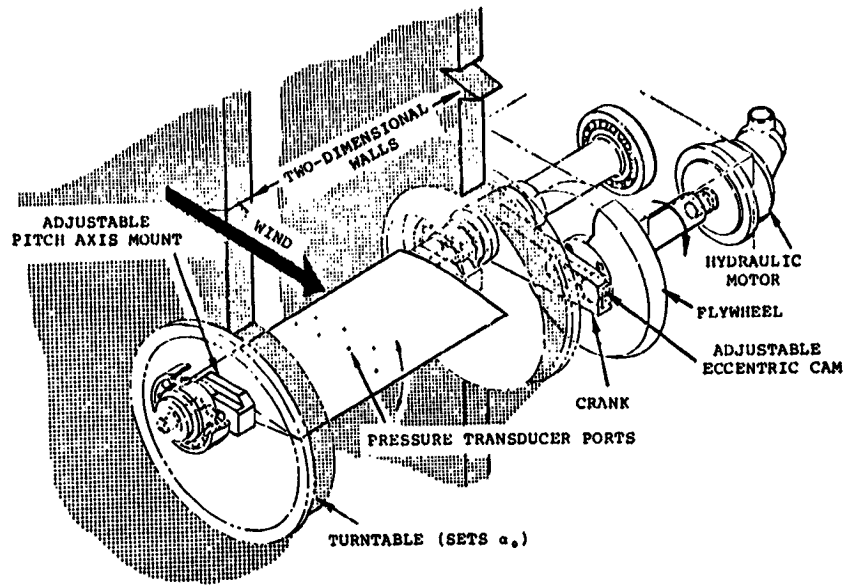


Figure 1.- Pitch oscillation mechanism.

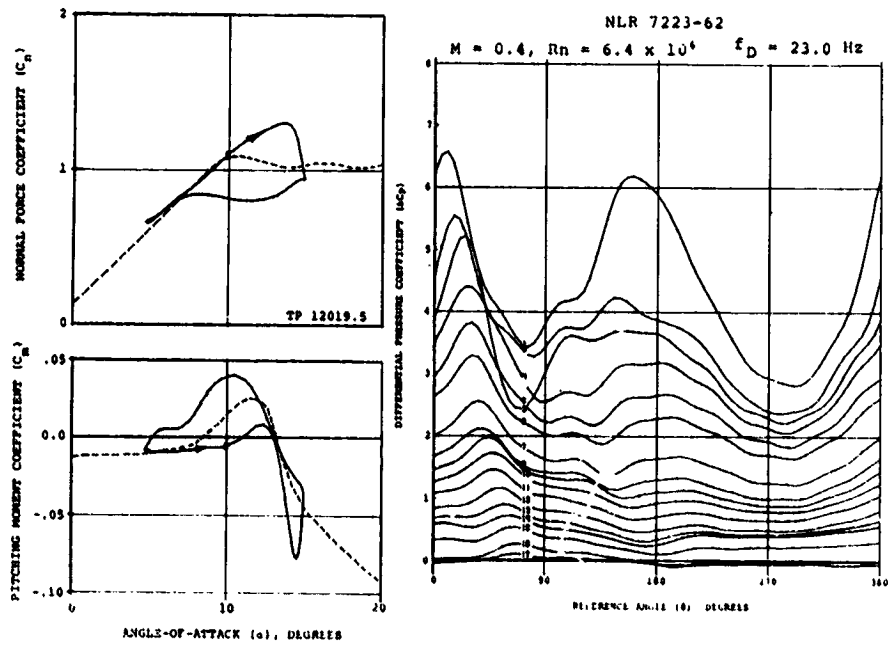


Figure 2.- Example of forced pitch oscillation data.

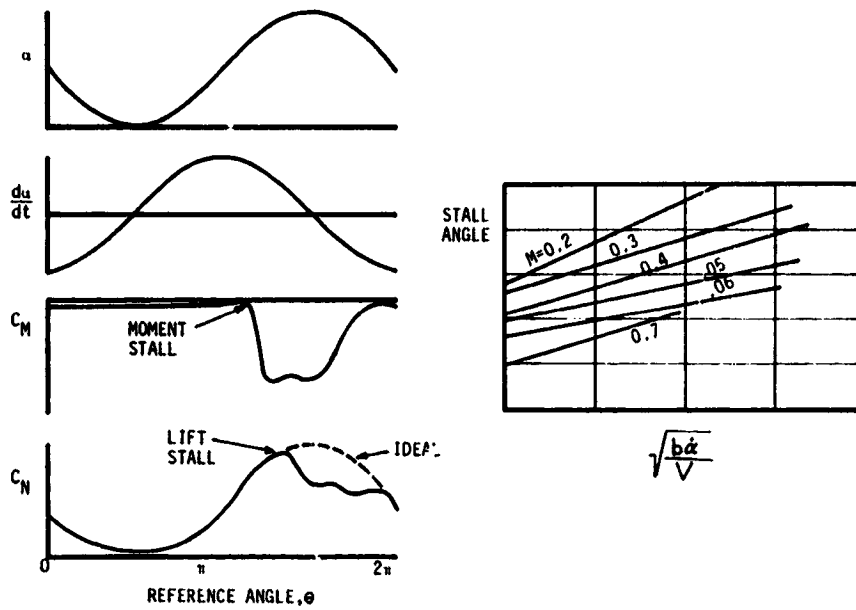


Figure 3.- Dynamic stall delay characteristics.

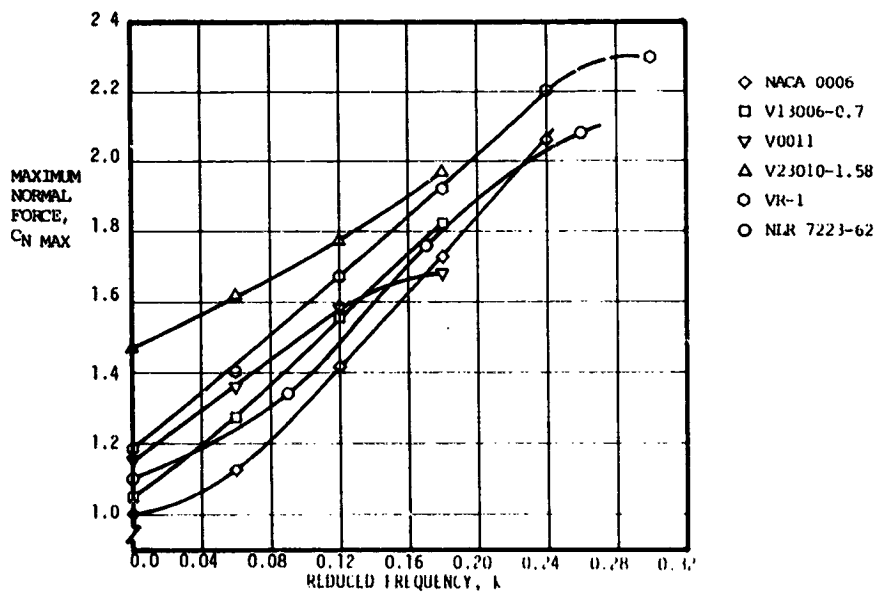


Figure 4.- Maximum attainable normal force at $M = 0.4$ and $\Delta\alpha = 5^\circ$.

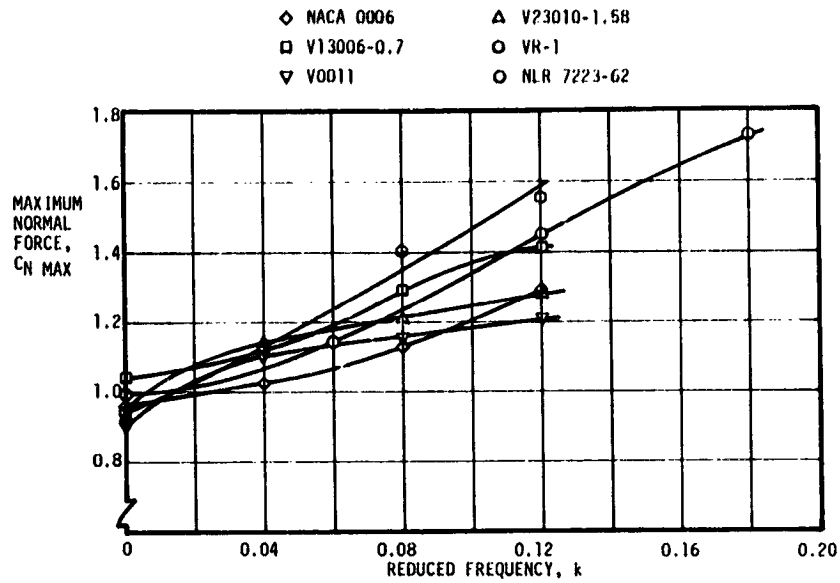


Figure 5.- Maximum attainable normal force at $M = 0.6$ and $\Delta\alpha = 5^\circ$.

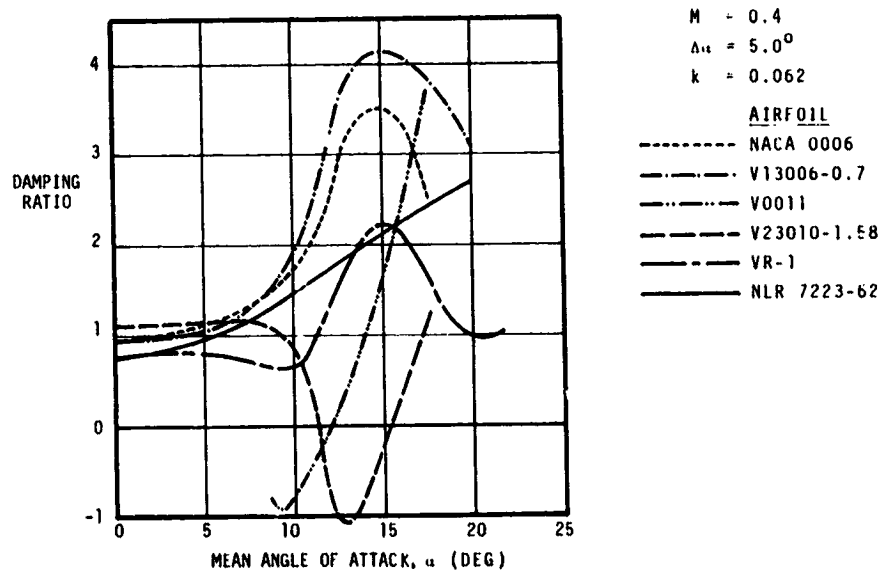


Figure 6.- Comparison of damping characteristics.

ORIGINAL PAGE
OF POOR QUALITY

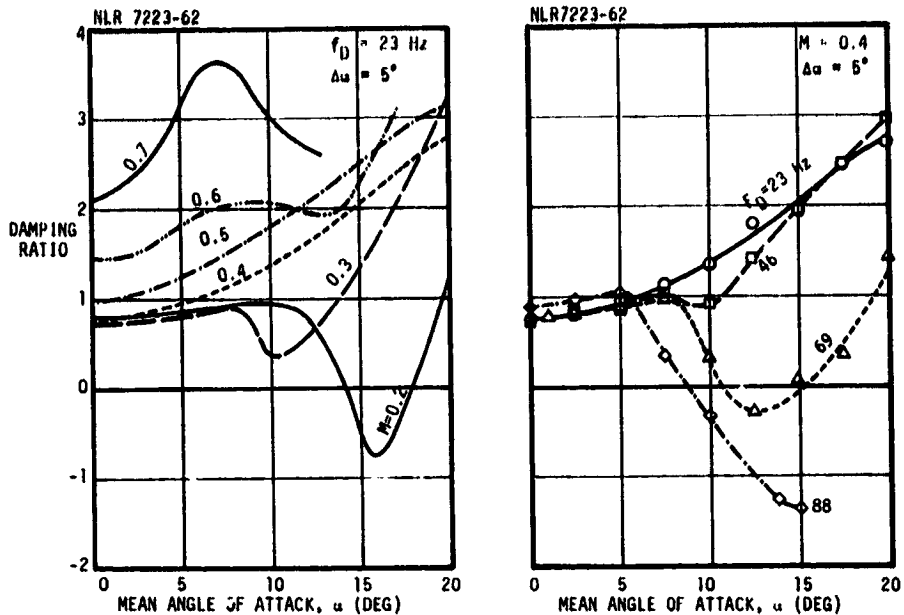


Figure 7.- Compressibility and frequency effects on damping.

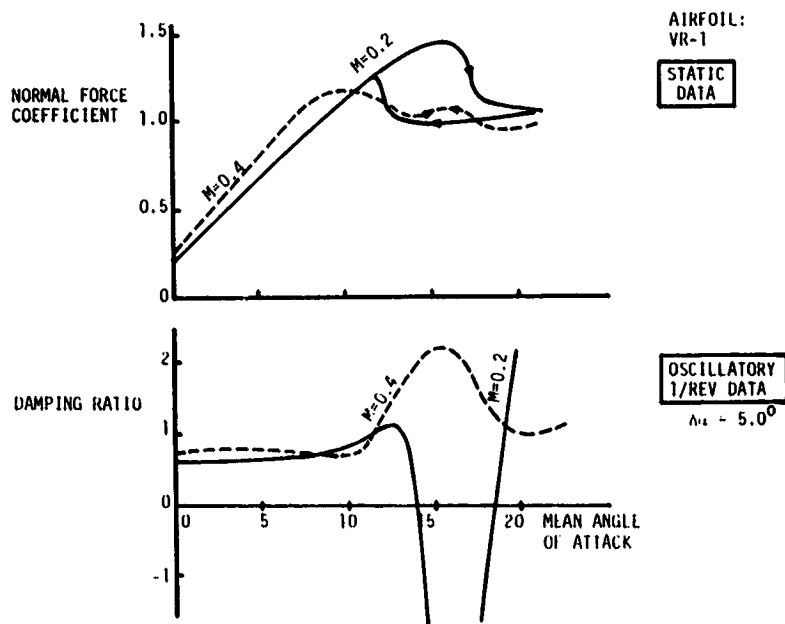


Figure 8.- Dependence of damping on static stall characteristics.

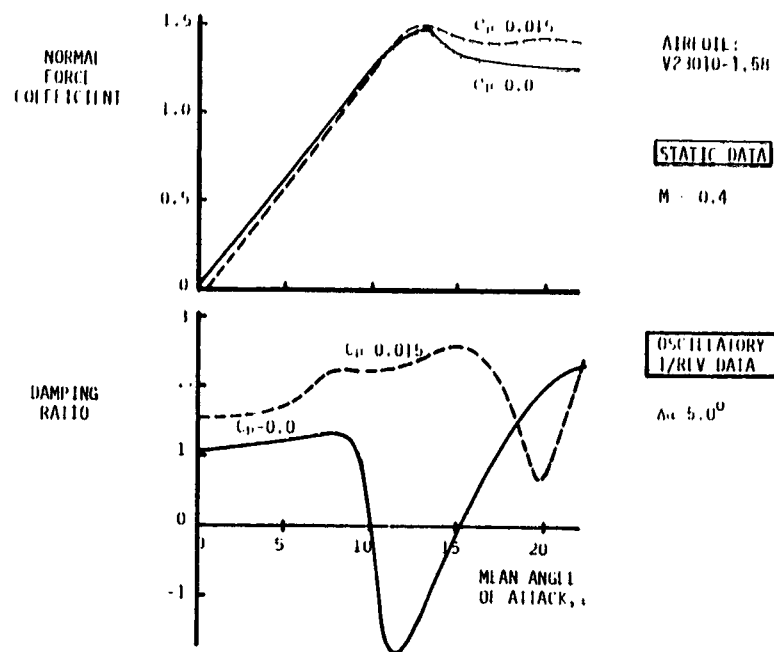


Figure 9.- Effect of leading-edge boundary-layer control on stall and damping.

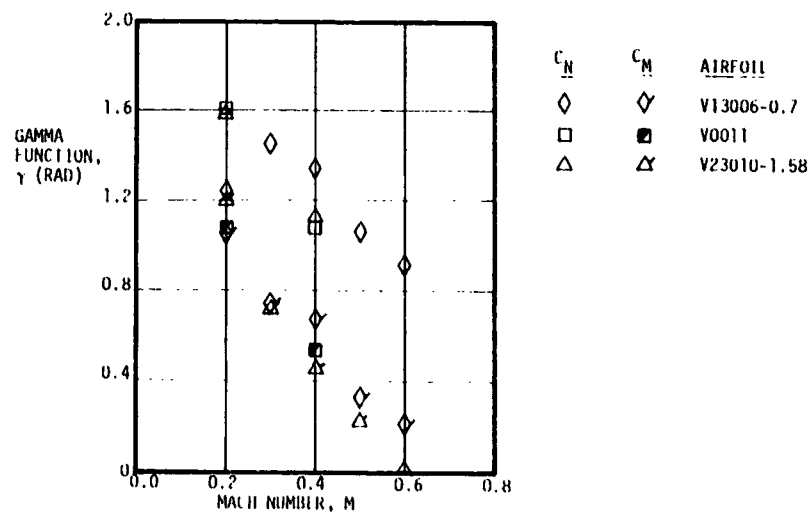


Figure 10.- Comparison of stall delay characteristics for three conventional airfoils.

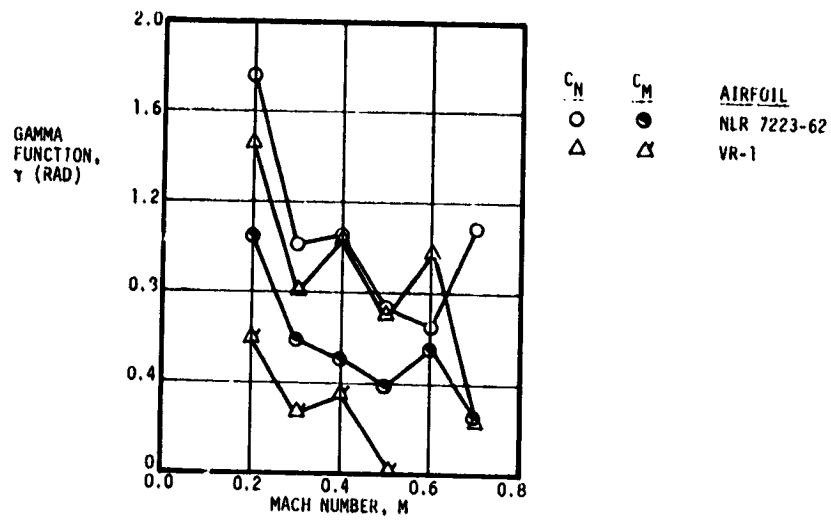


Figure 11.- Comparison of stall delay characteristics for two transonic airfoils.

TRANSONIC FLOW OVER THE NACA 64A006 WITH AN OSCILLATING FLAP -
CALCULATIONS BASED ON THE EULER EQUATIONS*

R. J. Magnus
General Dynamics Convair

SUMMARY

Exploratory calculations of transonic flows over the NACA 64A006 airfoil with a quarter-chord oscillating flap have been made using a program which obtains approximate solutions to the Euler equations with an explicit, shock-capturing, finite-difference scheme. The calculations, essentially inviscid and for the airfoil at zero angle-of-attack in a free-stream, are at Mach numbers and reduced frequencies which were tested in experiments by Tijdeman. The oscillatory lifts from analogous calculations by various investigators generally agree with one another better than they agree with Tijdeman's data. Inclusion in the calculations of an approximate modeling of boundary conditions expected at slotted wind tunnel walls tends to shift some of the results closer to the experimental values.

INTRODUCTION

Experimental work on transonic unsteady flows over the NACA 64A006 airfoil with a sinusoidally oscillating quarter-chord flap was described by Tijdeman and Bergh (reference 1) more than 10 years ago. Their results have inspired a number of attempts to calculate the flows over the configuration (references 2 through 9). The physical arrangement seems ideal for methods based upon perturbation equations (references 2, 3, 5, 6 and 8) -- a thin airfoil with small angle-of-attack and flap deflection.

By and large, the calculations made to date have assumed inviscid flow and that the airfoil is immersed in an unconstrained stream. In this paper, an abstraction of material in reference 9, it is demonstrated that including an approximate treatment of wind tunnel wall effects tends to bring some of the calculated features of the flow closer to the experimental data from reference 10.

*Work performed under contract with Air Force Flight Dynamics Laboratory,
Contract F33615-76-C-3018.

SYMBOLS

C	Airfoil chord
$C_{L\delta}$	Airfoil lift coefficient per radian of flap deflection amplitude
ΔC_p	The difference between lower and upper airfoil surface pressure coefficients per radian of flap deflection
$ \tilde{C}_{p\delta} $	Amplitude of first harmonic of oscillatory pressure coefficient per radian of flap deflection
k	Reduced frequency of flap oscillation based on airfoil semi-chord
p	Airfoil surface pressure
p_0	Free-stream total pressure
p^*	Free-Stream critical pressure
t	Time
u	Perturbation of chordwise velocity from free-stream value
U_∞	Free-stream velocity
v	Perturbation of normal (to airfoil chord) velocity from free-stream value
x	Distance aft of airfoil nose
y	Distance normal to airfoil chord, positive upward
ϕ	Lead angle of first harmonic of oscillatory response function
ω	Circular frequency of sinusoidal flap oscillation

DEFINITIONS

Reduced frequency:

$$k \equiv \omega C / 2U_\infty$$

Flap Motion:

$$\delta(t) = \delta_0 \sin \omega t$$

Trailing edge down considered as positive deflection

Typical first harmonic of a response function:

$$f(t) = f_0 \sin(\omega t + \phi)$$

ϕ positive, response leads flap motion

COMPUTATIONAL NOTES

The computer program used in the present work is closely related to the program used in work on the NACA 64A410, reference 11.

Equations, Scheme

The coupled system of four unsteady Euler equations in conservation form is solved numerically using a two-step, Lax-Wendroff, explicit, finite-difference scheme. Diffusion was added to suppress ragged overshoot in the calculated output near shocks and was also found to be needed to control short-wavelength oscillations in parts of the flow which were near-sonic.

Mesh Arrangements, Synchronization

On the order of 5000 mesh nodes arranged in several distinct grid systems were used to cover the field around the airfoil. Fine mesh was used around the airfoil nose; the basic mesh around the airfoil was 0.04 chord squares, and stretched and coarser meshes were used to extend the coverage to outer boundaries several chords from the airfoil.

Local, airfoil-oriented, coordinate systems were used to provide mesh nodes along the airfoil surface. Bands of fine mesh were inserted to provide detail on the loci of upper and lower surface shocks. In any single mesh system a uniform explicit time step would be applied at each node. Many time steps would be taken in the finest mesh for each time step in the coarsest. Exchanges of information between the developing solutions in contiguous grid systems were made by assignments and interpolations.

Boundary Conditions

To satisfy tangency boundary conditions along the airfoil surface, the flow at nodes on the time-averaged airfoil surface is calculated by the method cataloged as "Euler Predictor, Simple Wave Corrector" in the survey by Abbett, reference 12. By a similar process the upper and lower pressures and flow directions are matched along a line extending aft about 0.2 chord from the airfoil trailing edge. Further aft the wake discontinuity is allowed to become indistinct by numerical diffusion.

If the flow over the airfoil in an unrestricted stream was to be calculated the flow was held invariant at the field perimeter. On the examples calculated here, the upstream and downstream field boundaries were about 10 chords distant from the airfoil midchord and the lateral boundaries were placed further out by use of stretched mesh. A flow pattern due to a doublet and a vortex (strength commensurate with airfoil mean lift) plus free stream was maintained on the perimeter.

For the cases simulating flow over the airfoil in a slotted wall tunnel, an empirically determined boundary condition on perturbation velocities

$$u \pm 0.73v \pm 0.17v_x = 0$$

was specified on horizontal lines ± 1.53 chords from the airfoil. This empirical relation is based upon steady transonic calculations done in conjunction with tests which measured pressures on the slotted tunnel walls as well as on the airfoil model.

Computational Expense

The computer programs utilized are written in FORTRAN extended language and the calculations were run on a CDC 7600 computer. A relatively stable solution to a steady flow problem would be obtained in about 2400 passes through the field requiring 580 seconds of computation. Stationary solutions to the unsteady problems typically would be obtained after following the flow for about 3.5 cycles; this would require 2400 to 3100 seconds of computing; the expense depends inversely on the reduced frequency. Pressure fields at (typically) 36 steps in an oscillation cycle were recorded for further study.

RESULTS

Calculations were made at three Mach numbers; however, attention will be concentrated here on computations at Mach number 0.85. The steady free-air flow over the NACA 64A006 was calculated at zero angle-of-attack with the quarter-chord flap undeflected and deflected 1.0 degree; the unsteady flow for a reduced frequency of 0.179 with 1.0 degree flap amplitude was also calculated. These cases were also calculated with a slotted wind tunnel wall boundary condition included. The unsteady pressures were integrated to find the airfoil forces and moments and selected unsteady quantities were run through harmonic analysis to determine the magnitudes and phases of the fundamentals.

The magnitude and phase of the first harmonic of the lift due to sinusoidal flap deflection is shown in figure 1, together with similar results from calculations by Ballhaus and Goorjian, references 5 and 6, and Ehlers, reference 2. There is relatively good agreement between the four inviscid calculations; Tijdeman's experimental result (reference 10) (including viscous and wall interference effects) is considerably separated from the calculations.

The normalized lift due to flap deflection in steady flow (inviscid, free-air) is also shown in figure 1 along with results from a similar calculation by Traci, reference 3. The magnitudes of the calculated lifts are both more than double the steady lift measured by Tijdeman, reference 10.

The disagreement between the free-air inviscid calculations and Tijdeman's experimental results also shows in the zero-lift pressure distributions, figure 2. The calculated pressure distribution at Mach 0.85 is compared with Tijdeman's experimental data. At corresponding Mach numbers, the calculated pressures along the middle of the airfoil are considerably lower (and velocities higher) than the experimental values.

At first, it was surmised that a simple Mach number shift of about 0.02 might produce better agreement between calculation and experiment; viz., calculated Mach 0.85 resembles experimental Mach 0.875 in figure 2. An inspection of the distribution of lift in steady flow, however, indicates a notable difference between calculation and experiment; the experimental lift distributions at Mach 0.85 and 0.875 both show considerably less loading on the front part of the airfoil than the calculated, figure 3. The large spike in the calculated loading between 0.4 and 0.7 chord is due to movements of the upper and lower shocks upon deflecting the flap. The program calculates the pressure rises across shocks to be very nearly the "normal shock" values; the experimental recovery is considerably less because of interaction between shocks and boundary layers. Hence, the calculated loading spike due to shock migration is more extreme than the experimental.*

Adding a simulation of the slotted wind tunnel wall behavior to the calculations brings the calculated and experimental zero-lift pressure distributions closer to one another, figure 4. Similarly, the distribution of load due to deflecting the flap is brought into closer, but by no means precise, agreement with experiment by adding wall effect, figure 5.

The amplitudes and phase angles of the first harmonics of the oscillatory loadings in unsteady flow are shown in figures 6 and 7. Except in the region of the loading spike caused by shock movement, the inclusion of wind tunnel wall effects in the calculations results in reasonably satisfactory agreement with the experimental values. The noted agreement may, of course, be due to fortuitous combinations of errors; the agreements between calculation and experiment were not as impressive for steady flow, figures 4 and 5.

Inclusion of a simple practical means of weakening the pressure rise at shocks, i. e., a simple correction for the effects of shock interaction with the boundary layer, certainly would be desirable. This correction is needed for predictions of behavior of real configurations in free-air as well as for models in wind-tunnels.

*Additionally, the quasi-steady experimental results are derived from tests with 1.5 degrees flap whereas the calculations are for 1.0 degree flap. The loading due to shock movement is proportional to the area under the spike; spike height and breadth depend on flap amplitude in this particular style of presentation.

Upon integrating the pressures on the airfoil (as calculated including wall effect) to obtain the lift due to flap deflection, the results (square symbols in figure 1) are in considerably better agreement with the data than are the free-air results.

CONCLUDING REMARKS

When wind tunnel wall influence was added to the inviscid calculation of the steady, zero-lift flow over the airfoil, the airfoil pressure distribution changed in a manner as if the Mach number had been lowered by about 0.01. The wall influence lowers the amount of load developed on the front part of the airfoil upon deflecting the flap in steady flow and lessens the phase lag of pressure excursions on the front part of the airfoil in unsteady flow. The parts of the quasi-steady and unsteady loadings which are due to shock-migration are overestimated by the inviscid calculations studied here; a practical first-order means for describing the weakening of shocks by interaction with the boundary layer seems to be needed.

On the unsteady thin-airfoil problem studied, calculations done with programs based upon perturbation equations, references 2, 5 and 6, are in relatively good agreement with the results from the program based on the unsteady Euler equations; the perturbation programs obtain solutions at a very small fraction of the computing expense needed for an unsteady solution using the explicit unsteady Euler program.

REFERENCES

1. Tijdeman, H; and Bergh, H. : Analysis of Pressure Distributions Measured on a Wing With Oscillating Control Surface in Two-Dimensional High Subsonic and Transonic Flow. Rpt. NLR-TR F. 253, National Lucht-en Ruimtevaartlaboratorium, The Netherlands, March 1967.
2. Ehlers, F. Edward: A Finite Difference Method for the Solution of the Transonic Flow Around Harmonically Oscillating Wings. Rpt. NASA CR-2257, July 1974.
3. Traci, R. M.; Albano, E. D.; and Farr, J. L., Jr.: Small Disturbance Transonic Flows About Oscillating Airfoils and Planar Wings. Rpt. AFFDL-TR-75-100, Air Force Flight Dynamics Laboratory, August 1975.
4. Magnus, R.; and Yoshihara, H.: The Transonic Oscillating Flap. AIAA Paper No. 76-327, San Diego, July 1976.
5. Ballhaus, W. F.; and Goorjian, P. M.: Implicit Finite-Difference Computations of Unsteady Transonic Flows About Airfoils, Including the Treatment of Irregular Shock-Wave Motions. AIAA Paper 77-205, Los Angeles, California, January 1977.
6. Ballhaus, W. F.; and Goorjian, P. M.: Computation of Unsteady Transonic Flows by the Indicial Method. AIAA Paper 77-447, Dynamics Specialist Conference, San Diego, California, March 24-25, 1977.
7. Isogai, Koji: Calculation of Unsteady Transonic Flow Over Oscillating Airfoils Using the Full Potential Equation. AIAA Paper 77-448, AIAA Dynamics Specialist Conference, San Diego, California, March 24-25, 1977.
8. Yu, N. J.; Seebass, A. R.; and Ballhaus, W. F.: An Implicit Shock-Fitting Scheme for Unsteady Transonic Flow Computations. AIAA Paper 77-633, AIAA 3rd Computational Fluid Dynamics Conference, Albuquerque, New Mexico, June 27-28, 1977.
9. Magnus, R. J.: Calculations of Some Unsteady Transonic Flows About the NACA 64A006 and 64A010 Airfoils. AFFDL-TR-77-46, Air Force Flight Dynamics Laboratory, July 1977.
10. Tijdeman, H.; and Schippers, P.: Results of Pressure Measurements on an Airfoil With Oscillating Flap in Two-Dimensional High Subsonic and Transonic Flow (Zero Incidence and Zero Mean Flap Position). Rpt. NLR TR 73078U, National Lucht-en Ruimtevaartlaboratorium, The Netherlands, July 1973.
11. Magnus, R.; and Yoshihara, H.: Unsteady Transonic Flows Over an Airfoil. AIAA Journal, Vol. 13, No. 12, pp. 1622-1628, December 1975.

12. **Abbett, M. J.:** Boundary Condition Computational Procedures for Inviscid, Supersonic Steady Flow Field Calculations. NASA CR-114446, November 1971.

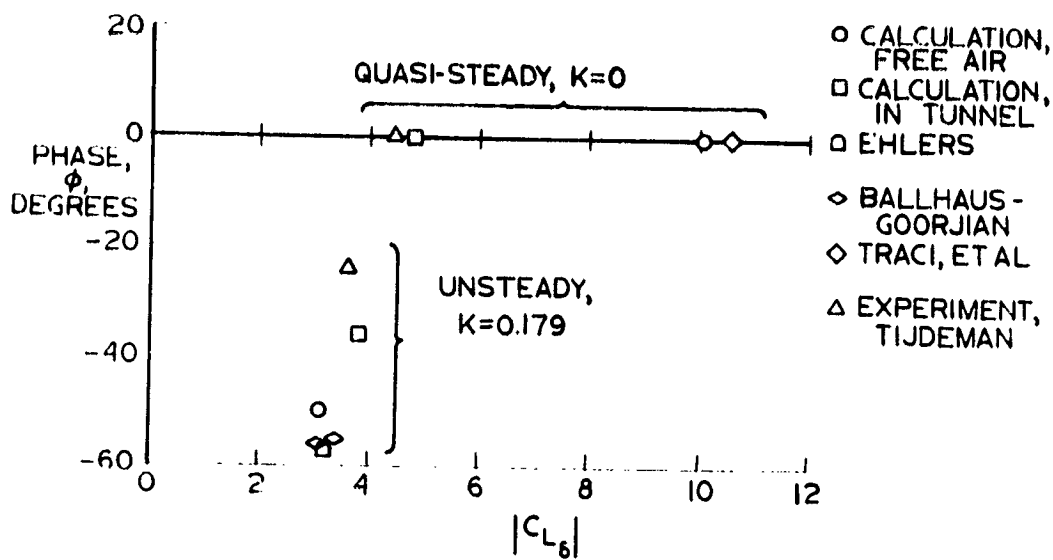


Figure 1.- Lift due to flap deflection for an NACA 64A006 airfoil with quarter-chord flap. $\alpha = 0^\circ$; $M = 0.85$.

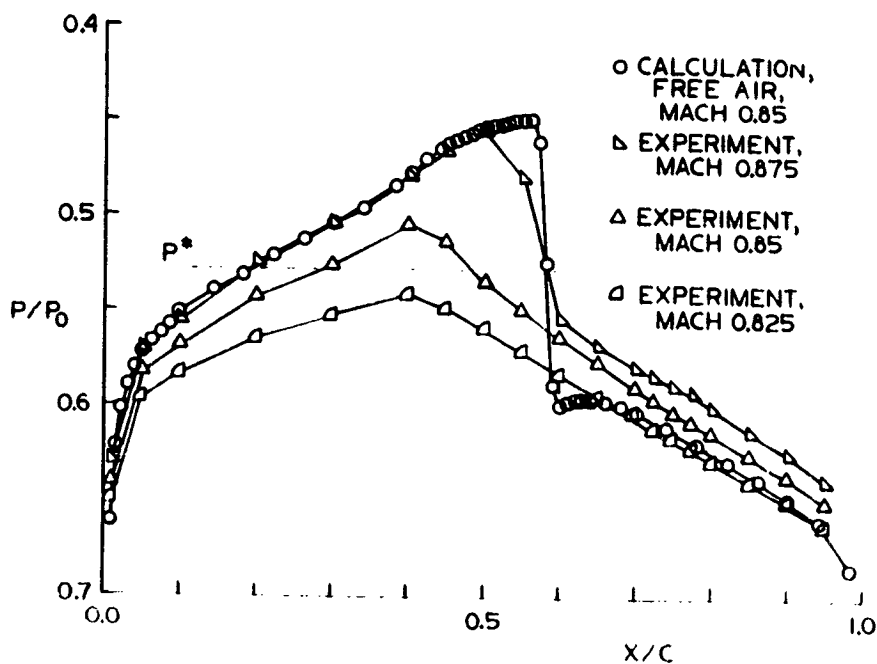


Figure 2.- Zero-lift pressure distributions for an NACA 64A006 airfoil. Free-air calculation at $M = 0.85$ compared with experimental values at three Mach numbers.

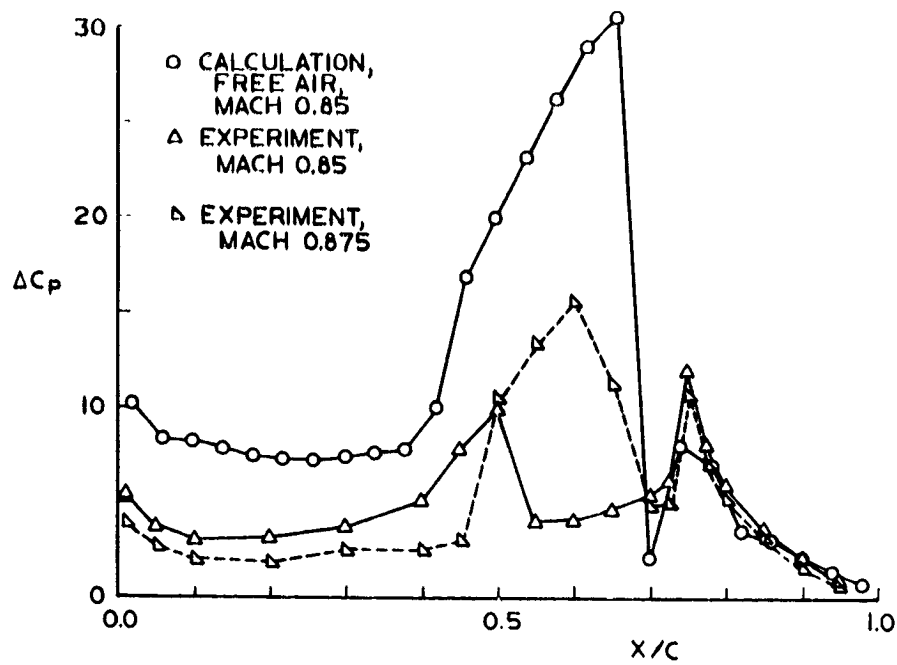


Figure 3.- Chordwise load distributions in steady flow. Free-air calculation at $M = 0.85$ compared with experimental values at two Mach numbers.

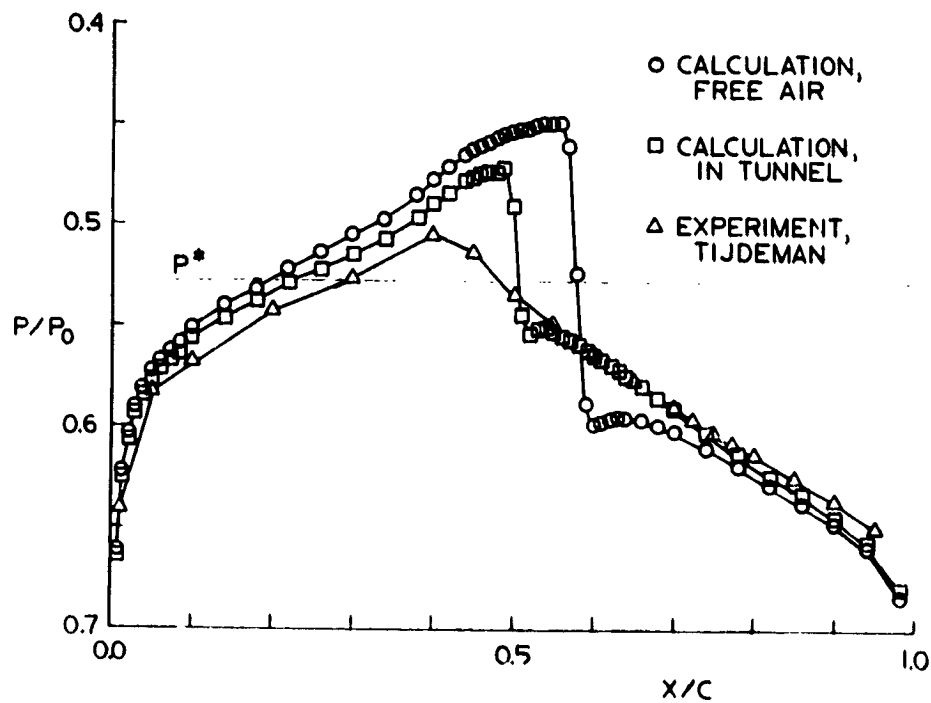


Figure 4.- Zero-lift pressure distributions at $M = 0.85$. Calculations in free air and including wind-tunnel wall influence compared with experimental values.

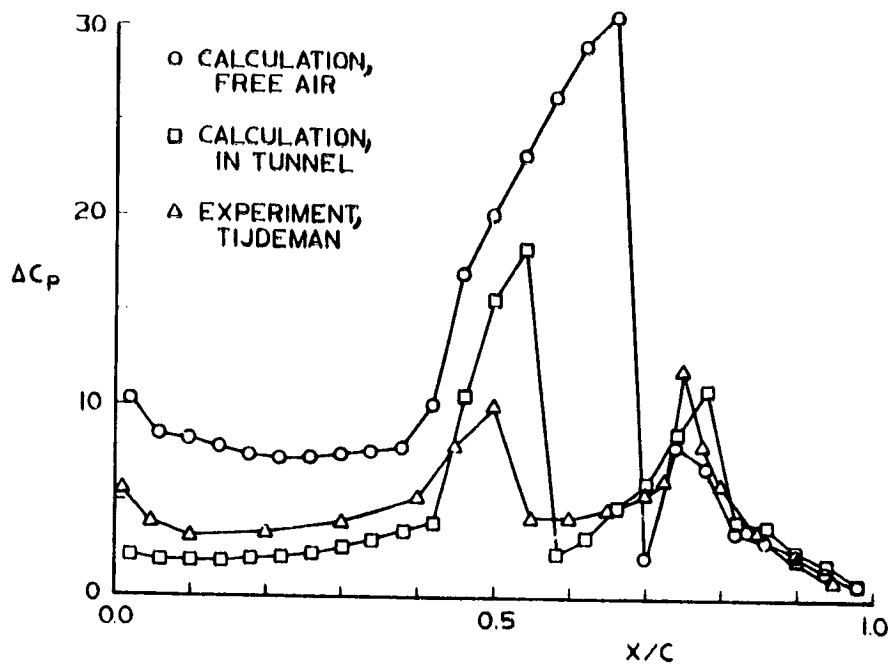


Figure 5.- Chordwise load distributions in steady flow at $M = 0.85$. Calculations in free air and including wind-tunnel wall influence compared with experimental values.

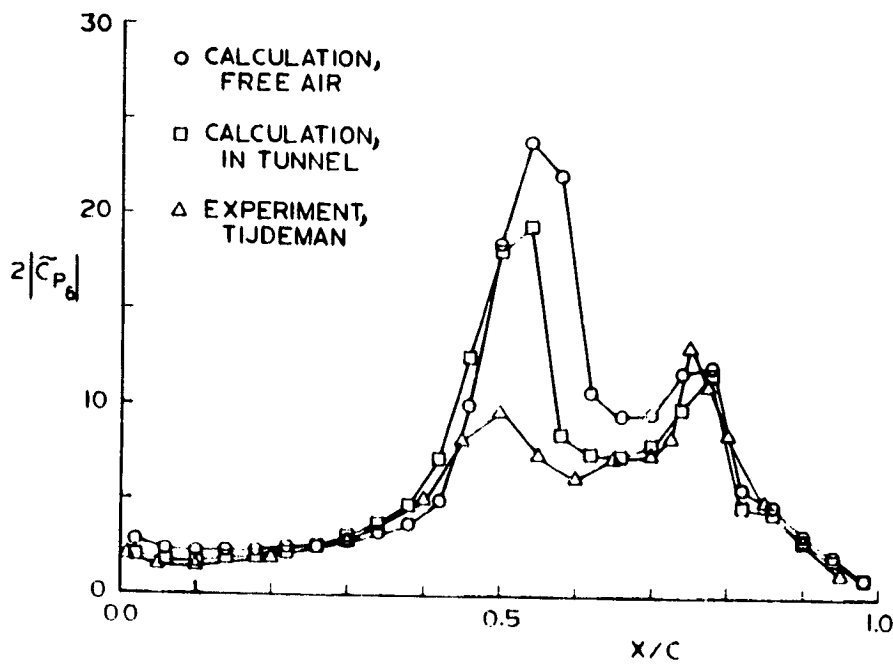


Figure 6.- Chordwise load distributions in unsteady flow at $M = 0.85$ for amplitudes of first harmonics. Calculations in free air and including wind-tunnel wall influence compared with experimental values.

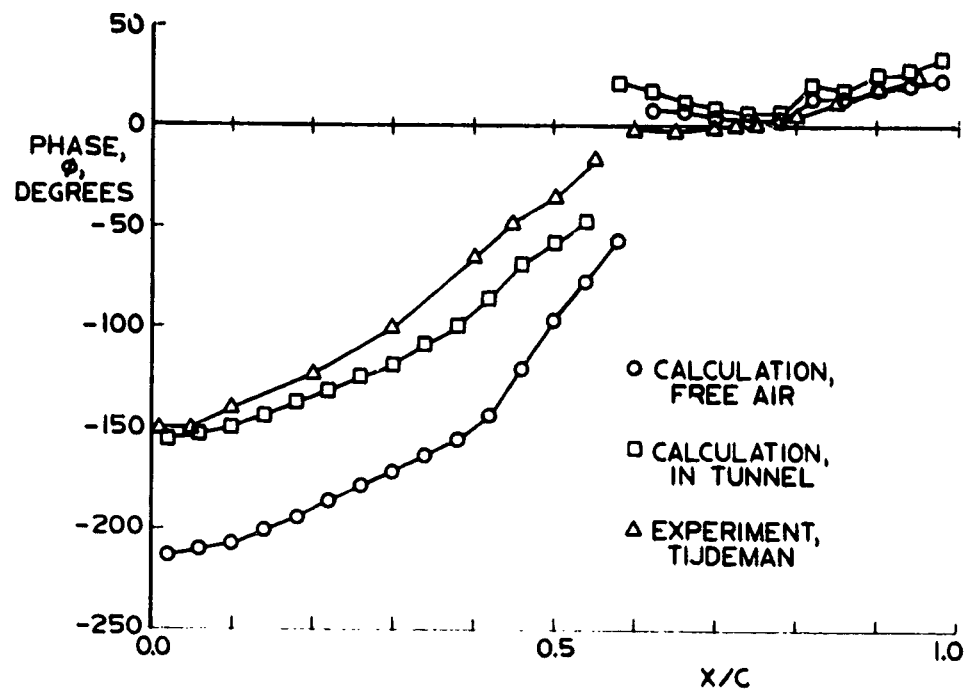


Figure 7.- Chordwise load distributions in unsteady flow at $M = 0.85$ for lead phase angles of first harmonics. Calculations in free air and including wind-tunnel wall influence compared with experimental values.

ROUNDTABLE SUMMARY AND CONFERENCE CONCLUSION

Cochairmen

Alfred Gessow, NASA Headquarters

Robert E. Bower, Langley Research Center

Participants:

Workshop Chairmen -

Percy J. Bobbitt, Langley Research Center
Gary T. Chapman, Ames Research Center
Alexander D. Hammond, Langley Research Center
Roger L. Winblade, NASA Headquarters
Theodore G. Ayers, Dryden Flight Research Center
William F. Ballhaus, USARDC, Ames Research Center
Joseph W. Stickle, Langley Research Center

Guests -

Ira H. Abbott, NASA Headquarters (Retired)
Helmut Sobieczky, Visiting Professor from DFILR (Germany) at
University of Arizona
Luis R. Miranda, Lockheed-California Company
Lars H. Ohman, National Aeronautical Establishment (Canada)
Andrew Z. Lemnios, Kaman Aircraft Corporation
Carl Rohrbach, Hamilton Standard Division, UTC
Harry A. James, Teledyne-Ryan Corporation
Bruce H. Carmichael, Consultant
Barnes W. McCormick, Jr., Pennsylvania State University

Floor Comments -

David C. Ives, Pratt and Whitney Aircraft Division
Dennis M. Bushnell, Langley Research Center
Theodore G. Ayers, Dryden Flight Research Center

ALFRED GESSOW:

The final wrap-up session of the conference is supposed to be one where we can all offer opinions as to how useful the program has been and where it should go. First, I should announce that the session is being recorded so that your words will become deathless prose when we print up the proceedings. I might just take a couple of minutes to review the objectives of the conference as they were laid out initially. There were three: One was to provide the aviation community with a review by NASA and its supporting contractors and grantees of all the latest information they've been doing on airfoil computational and experimental work. I might say that there were forty papers of that type, and about twenty-four independent papers from representatives of government, industry, and educational institutions. The second was to provide an opportunity for input and exchange between the various segments of the aircraft industry, the academic community, and other organizations. The third was to conduct a forum which engaged the community and all the aviation interests with an opportunity to provide an evaluation of NASA thrusts, goals, and progress. It is the third one, I think, that is the reason for us being here at this session. We would like to get your response to the program as it has gone, and we would like some constructive criticism as to where it should go in the future. In a way, this is a second ground of this nature, the first being at the 1975 industry-NASA workshop that I alluded to earlier in the conference.

I'd like to insert a few comments of my own before we begin. I think the turnout, the papers, and the scope of the information that have been presented here has been very gratifying to see. We have come a long way, although there is a lot more to go. It is also clear to me that the computational efforts that have come about in the normal course of events, that weren't spurred by the airfoil needs, really have enabled the state of the art in airfoils to be where it is today. At the same time, and I think Gary Chapman pointed it out to me this morning, the interest that this conference has elicited is an indication that the subject of airfoils is the one clear area where computations have come of age and have provided a direct application in a very visible way. We are beginning to see the influence of computational aerodynamics in many other areas of aircraft design but it is most clear in the airfoil business, and I think that is why we have made the progress and have the interest that we see today.

The way we are going to conduct this roundtable, and it will have to be conducted on a very tight schedule, is to have a number of invited guests express their views. There are two groups; one of these which Bob Bower will be chairing, will consist of the workshop chairmen from the conference. They will be representing the viewpoints of the applications people, the analysis people, those dealing with experimental techniques, and the like. They are seated along my right. Then, starting with Mr. Abbott on my left, we have a group of people who were invited because they represent areas of expertise, as well as the views of various segments of the industry, universities, and other government agencies. I am afraid that there is not going to be very much time for a lot of extra discussion. Instead, we plan that each of our speakers

here at the table take no more than five minutes in turn to present their views. After they are through, we will use the remaining time for comments and questions from the floor.

I've probably run past my time now, so let's start with Mr. Bower and his group.

ROBERT E. BOWER:

Thanks Al, I think we have quite a formidable task, particularly to start here with Bud and keep him to five minutes. We will get right on to it now. The first area that will be critiqued and summarized will be the analysis and design area. It will be shared by both Bud and Gary, but I think Bud will lead the show, and later Gary will make some additional comments, Bud.

PERCY J. BOBBITT:

The panel on "Analysis and Design: Needs and Issues" made a thorough although rapid assessment of the state of the art and identified a large number of problem areas. It was generally agreed that methods developed over the past half dozen years do provide good design and analysis tools for single and multielement systems with attached flow. There was, however, a great deal of concern expressed about the accuracy, or the lack of it, of our drag predictions. No matter how hard the theoreticians try they are still unable to consistently agree with experimental data; all sorts of reasons are offered why the experimental data isn't any good. Our drag prediction methods do need improvement but, in defense of the theoreticians, much of our experimental data is deficient as well. There isn't any, what boundary-layer people call, certified data. We need to have a series of experiments that are conducted in as interference-free a tunnel as we can identify, and it has to be coupled with some very detailed diagnostic work. It would be desirable to have at least one set of data that everybody (or most everybody) could put their faith in.

One panel member expressed concern that we may expend too much effort in trying to find improved drag-prediction methods. How accurate do we need our 2-D predictions to be?

Methods for calculating 2-D flows with large separated regions are now appearing. The panel thought that the data base for detailed flow-field measurements on airfoils with separation was not adequate for the theoreticians to validate their theories and improve flow-field models. There was also the suggestion that the separated flow theories be modified to include the effects of tunnel walls.

A whole array of suggestions were made regarding remarks on tunnel-wall interference. The major ones are as follows:

- Continued research on slotted walls still a necessity
- Streamline-wall tunnels show potential for subsonic and low supercritical conditions
- Sidewall treatments can be improved using theory
- Wall measured pressures for interference prediction should be pursued
- Wall interference calculations for unsteady flows needed

Streamline-wall tunnels show potential; we have a crude one working and a better one on the way. There are others around the world pursuing this approach for measurements up to the choke point. The use of pressures measured near the wall in combination with theory for interference assessments is another promising possibility for obtaining "interference-free" data.

The panel felt that we need to consider more of the 3-D environment in the design of airfoils, such as the effects of sweep and taper. Another factor of this type that should be taken into account is how much different the root environment is, say, from the middle of the wing or the tip. We also need to pay a lot more attention to off-design problems, particularly in optimizers. The difficulty here is what kind of logic to use. Clearly the computer program isn't going to provide the logic; people with practical experience must be involved along with those with an understanding of the flow physics and the mathematical processes before the proper criteria and constraints can be formulated. In carrying out off-design calculations using optimization routines boundary-layer and flow stability subroutines which determine separation and transition will become more important.

More high and low Reynolds number data at transonic speeds is needed particularly for the thicker supercritical sections. Hopefully the 20- by 60-cm cryo tunnel can contribute significantly to these needs.

Finally, a number of specific improvements to our analysis and design codes which are still required were identified. The four which seem to be most important and indeed are being worked on to varying degrees, are listed

- Boundary-layer and trailing-edge interaction "patches" for design and analysis codes
- Separation on spoilers and trailing-edge flaps - theory and experiment
- Improved turbulence models
- Faster codes (should be a general goal)

BOB BOWER:

Thank you very much Bud. Now Gary -

04

DR. GARY T. CHAPMAN:

Okay, I am just going to add a couple of comments to that. I would like to second Al Gessow's comment. This does represent an area where computational aerodynamics has really become of age. However there are still some outstanding issues. Bud Bobbitt has touched on some of them already. I am not going to use viewgraphs, I am just going to talk about several issues. First, we would all like to have one good set of transonic interference-free data. I can speak pretty much from the experimental side of the house and appreciate that as much as anybody else. Second, I think it is important to clean up some of the areas that we are still working on, particularly for attached flows where I think things are really in pretty good shape, and move on to more important areas of work. Third, Bud Bobbitt mentioned the need for high Reynolds number data, and I would like to make a plea for low Reynolds number data. It turns out there are a couple of special applications in the area of high altitude drone type aircraft where Reynolds numbers tend to run below 1 million, based on chord, and the people that do cascades and compressor type work indicate Reynolds numbers run from 100,000 to 1 million. The shock boundary-layer interaction problems encountered at these Reynolds numbers are going to be a lot different than in the high Reynolds number turbulence cases. Fourth, there are a lot of things that need to be done to improve the speed of optimization. The idea of making many many calculations as the method of getting to an optimum, is not necessarily the best way. I think there are some other things that can be done to improve this. We work with a 7600 and I never complain about time because we can do an optimization in one or two minutes. That's not much time, however many of you probably have a lot smaller machine. Hence I believe we have to do something to speed up the optimization process. Fifth, I think we are moving along very well in the area of multielement airfoils. However, we need some data to really check them out. Particularly for example in the work from Grumman by Volpe in transonic aerodynamics, there's really no good data for slotted transonic airfoil configurations. This is one area where the analysis tools are ahead of the experiments, with the exception of confluent boundaries where we still need a lot of work particularly on how we handle mixing. The sixth area of concern is massive separation. I was very impressed with some of the progress being made. However, here again we need experimental data, not only to validate the theories, but also to provide a better physical understanding of the nature of the flow and hence to develop simple modeling techniques. Finally we have the area of unsteady aerodynamics which is really just getting off the ground - It seems at this point that there are more computational tools than there are experimental data by an extensive margin. So here again there is a big need for experimental data and with that the need to understand unsteady wall interference. If we think the wind tunnel correction problems are bad for our static aerodynamic data, they are terrible when it comes to transonic unsteady aerodynamic data. I would like to conclude with a point on accuracy requirements. Bud Bobbitt quoted me as saying, why the importance on drag, and I'd just like to go back to Abbott's comment the other night: "We don't fly airfoils." So accuracy required is to be able to separate good airfoils from bad airfoils, so when you go to a 3-D design you have a reasonably good starting point. So I don't think we want to chase one drag count on drag calculations for airfoils.

BOB BOWFR:

Thank you Gary. The next area that we will be summarizing is in the area of facilities and techniques and Dudley Hammond will be summarizing that. Dudley.

ALEXANDER D. HAMMOND:

The first item listed below deals with an issue that was brought out in the analysis and design discussions by Bobbitt and Chapman as well as in yesterday's session on facilities. In light of the rapid development of airfoil design and analysis codes, there is a continuous need for us to get proven facilities and basic data for code verification and improvement.

- In light of the rapid development of airfoil design and analysis codes there is a continuing need to use proven facilities and provide basic data for code verification and improvement.
- Considerable discussion evolved around the issue of determining the validity of data.
 - Use of "standard airfoils"
 - Accurate determination of test conditions
 - Determination of the two-dimensionality of flow over airfoil at all test conditions
 - Elimination of wall interference and determination of residual effect on data
 - Tunnel flow quality and effect on data
 - Required accuracy of measurements and measurement requirements

Yesterday afternoon we had a considerable amount of discussion about the issue of determining the validity of the data that is obtained in facilities. Among the subjects of that discussion was the use of standard airfoils to provide a basic set of data and to help evaluate the data validity as was just mentioned. Determination of the test conditions and just how accurate do the test conditions need to be known was part of the discussion. The determination of the two-dimensionality of the flow over the airfoils at all test conditions was discussed, as well as elimination of wall interference and the effects of any residual wall interference on the data. Of course, the tunnel flow quality and its effect on the data is a valid concern that we need to continue to work. The required accuracy of measurements and the measurement requirements are dependent to some extent on how wide the data base is, and for what purposes the data will be used.

As has already been mentioned and is indicated in the added list below, we need a broad matrix of data, one as broad as you can reasonably accomplish for any one set of data as well as documentation of the test conditions under which that data was run, and some assessment of the effects of any known deficiencies in that data.

- As broad a matrix of data as can be reasonably accomplished for any one set of data is needed as well as documented test conditions and/or limitations.
- Development of adequate sidewall treatment for existing 2-D facilities needs to be expedited.
- Requirement for increase in research on adaptive walls to shorten the time before they become operationally usable.
- Assessment of tunnel flow quality by specifically designed programs for adequate documentation.
- Continue effort on nonintrusive flow-field measuring techniques - LDV and holography techniques and apply to 2-D facilities.

And of course, we need to develop an adequate sidewall treatment for existing 2-D facilities and this needs to be expedited. We are working the problem; however, it is a requirement that is going to develop further as we go along, and it certainly needs to be expedited. We need to have an increase of research on adaptive walls, to shorten the time before they become operational and useable. We have a research program going on at Langley, and others are doing research on various adaptive wall techniques. It all seems to move at a very slow rate, when one is anxiously waiting for the results of the tests before it can be put into operational use. The assessment of flow quality by specifically designed programs for adequate documentation refers back to the point that I mentioned a moment ago. We need to have a continued effort on nonintrusive flow-field measuring techniques; that is, LDV and holographic techniques that apply to 2-D facilities, and we need to work that problem more vigorously probably than we have in the past. It has been shown on other papers, for example, that intrusive measuring devices can give problems with regard to accurately determining flow-field characteristics. But that's not to say that some of that measuring does not need to be made even though it's intrusive. Even the intrusive measurements ought to be able to determine some aspects of the fluid mechanics flow in these highly separated regions to the degree of accuracy necessary for some applications.

This review of the facilities and techniques and the needs and issues involved has revealed challenging areas of research requirements. It has pointed out that although there are ongoing programs in all of these areas, the pace is slow and additional effort needs to be applied in nearly all of the areas covered.

BOB BOWER:

Thank you Dudley. Next area - Low and Medium Speed Applications - Roger Winblade.

ROGER WINBLADE:

We just very recently completed this session and in fact, most of the areas that we discussed have already been mentioned. The one area that received a great deal of discussion and in which I think we reached a general consensus is the extremely low Reynolds number field. This is an area in which we are not working but should be. Potential applications for this work include wind turbines, flight at very high altitudes, sailplanes and gliders. It was also suggested that more work is needed on 3-dimensional effects and the ability to predict transition. We then considered the whole range of real airplane effects. Airplanes have deicing boots on them, at least those airplanes that use the low and medium speed airfoils. The perturbations far exceed any of the perturbations generated in optimizing. A question of some concern was raised in viewing slides over the last couple of days. The start point and end point in optimizing the section were very close together, or appeared to be. Is that in fact within the manufacturing tolerance to produce in the light aviation arena, or in terms of variations during life time?

In discussing near term problem areas which we're not addressing, it was generally concluded that the activities underway are the ones that we have to live with. There's nothing that we could initiate now that would have any impact in the next two or three years. That is consistent with what we have seen in the past which is a 6-7 year time lapse. Long term activities that we are to keep in mind are the potential for new configurations such as canard concepts. It was also suggested that we be more adventuresome in our thinking as we were admonished and to not be constrained to follow the traditional line, but to keep the options open for different, but maybe not totally acceptable projects. A very interesting remark was made with respect to optimization techniques. The analogy was drawn with structural optimization and related to the very short time that Gary mentioned that it now takes to optimize a section. When you expand that to include more and more variables and eventually a full airplane, the time becomes excessive. When you start coupling that with the structural design systems, the total computer time becomes essentially prohibitive. There is then a high potential for either losing or backing away from the capability and going back to empirical testing just because of the complexity of the problems. The resulting suggestion was that we do as was previously recommended, concentrate on more efficient optimization techniques, rather than going through the extensive calculations.

BOB BOWER:

Thank you Roger. We had a classified session on supercritical applications. Within the constraints of this unclassified discussion, Ted Ayers from the Flight Research Center will discuss the issues in that area.

THEODORE G. AYERS:

Bob, although the Supercritical Applications session yesterday was classified because of the data being presented, so far as I know we did not discuss any classified material in the workshop session this morning. I think that what you've heard from the other people here indicates that almost everyone in the audience had a unified position because we had the same discussions in my workshop as the other did. In fact, when Bud first started to talk, I thought that he had come over and spied on us this morning. There were a couple of areas that have not been mentioned and I will bring those up. One of the things brought out was the need for the people working the codes to have better documentation for the user and to include some of the pitfalls that are in these programs, as well as the good things they do. Show some of the bad cases along with the good, so they can get a feel for what the capabilities and limitations of the programs are. Also, there was a plea to simplify the codes. Almost everyone cited a need for an experimental data base to validate the computational tools. This includes wind tunnel as well as flight data that NASA should be providing; data for high Reynolds number, thick boundary layers, shock boundary-layer interaction, wall effects, and turbulence modeling. I guess I would say there was a consensus of support for the National Aerodynamic Simulation Facility. One of the specific concerns for the experimental data base was the $c_{l,max}$ for supercritical airfoils. There is insufficient data in the $c_{l,max}$ range for two-dimensional airfoils to allow people to apply these airfoils in the three-dimensional sense. Another is the lack of data for spoilers which has already been mentioned. This was not only the analytical area but also an experimental area and pertains to the inability to predict spoiler effectiveness because of the unsteady nature of the flow for deflected spoilers. Our discussions got around quite a bit to the three-dimensional needs, since we are talking about supercritical applications. It is rather difficult to divorce supercritical applications from the 3-D case where people have to build an airplane with real wings. There were a number of areas brought up in the workshop which make it difficult to take 2-D data and transition it into a 3-D configuration. For example, an extension of the two-dimensional data out to higher design lift coefficients and lower thickness ratios is needed for those people who deal in the low aspect ratio, swept wing fighter area, or configurations indicative of supercruise type airplanes. I think that covers most of the areas. The others have already been discussed by other people.

BOB BOWER:

Thanks Ted. The next area is rotorcraft applications - Bill Ballhaus.

WILLIAM F. BALLHAUS:

The statement that we have heard over the past 2 1/2 days that "we don't fly airfoils" is certainly an understatement for helicopter rotors. A helicopter rotor operates in a highly three-dimensional, unsteady, viscous, and dynamic environment. Hence, new rotor designs based on two-dimensional, steady analyses will not necessarily result in better helicopter performance. The design problem is so complicated that no one seems to be able to define specifically how aerodynamic and/or aeroelastic phenomena influence rotor performance. These phenomena are usually described in general terms, such as "adverse transonic effects," or in terms of the integrated effect they produce, such as "excessive pitch link loads."

What is needed is a coordinated computational-experimental program to develop a clear understanding of the phenomena that limit rotor performance. Designers could then focus on these phenomena in efforts to extend present performance boundaries. In such investigations it is important to consider different operating environments corresponding to different helicopter missions. Body interference and the coupling between blade configuration and inflow condition, including wake interaction, should be addressed. Emphasis should be on advanced configurations designed to meet present and future requirements.

In the computational area, the technology is now available to begin detailed qualitative studies of the interacting effects of nonlinearity, three-dimensionality, viscosity, and dynamics. F. X. Caradonna of the U.S. Army AVRADCOM and researchers at ONEFA are investigating nonlinear, three-dimensional, unsteady rotor flows. Attempts are also being made to include viscous effects. These studies have provided information concerning the motion of shock waves on the surface of rotors near the tip and how these shock wave motions influence rotor load variations. Ultimately, quantitatively good unsteady force and especially pitching moment predictions will be required in the design of high performance rotors. Caradonna and his associates have already demonstrated the capability to predict advancing blade pressures that are in good agreement with experiment for simple nonlifting rotors.

In the experimental area, there is a concern over uncertainties in test data resulting from a failure to sort out facility effects. For example, there have been a large number of unsteady airfoil tests, but there appear to be few data points for parameters that overlap. A workshop participant suggests that the facilities be calibrated for the NACA 0012 airfoil in the following way: first, document the static stall point for $M_\infty = 0.3$ and 0.5 (this should be done before any unsteady testing). Then, for calibrating the unsteady tests, data should be correlated for reduced frequencies (based on the half chord) of 0.1 and 0.2 for the following cases: (1) $M_\infty = 0.3$, $\alpha = 10^\circ + 10^\circ \sin t$ and $\alpha = 15^\circ + 5^\circ \sin t$ (two different approaches to the same maximum angle), (2) $M_\infty = 0.5$, $\alpha = 10^\circ + 5^\circ \sin t$. The same standard conditions should also be used to calibrate facilities for other airfoils. Similar types of standards should also be established for low lift, high Mach number tests.

In the next few years there will be opportunities to construct and test advanced technology rotor configurations. For example, Hughes is building five rotors to be tested, under a contract with Ames Research Center, when the modification to the 40' x 80' wind tunnel is completed. Some of these configurations remain to be defined. It was suggested in the workshop session that: (1) the multi-point designs proposed by Blackwell, Bingham, and Hicks, all of which are based on two-dimensional, steady analyses, be considered as candidates for evaluation in this contracted effort, (2) in such design and design evaluation efforts, parameters be limited to focus on a few aspects of the rotor performance, and (3) a committee be established to coordinate NASA (Langley and Ames) and Army activity in this Area. In the future, more sophisticated designs, including planform and spanwise section variations, should be attempted. These designs would be based on three-dimensional, unsteady, viscous, and dynamic analyses, taking advantage of advanced computational methods as they become available.

Finally, I would like to include in this discussion a wish list ("what I would like to see accomplished in the next year") compiled by one of the workshop participants: (1) experiments with good flow visualization (especially of transition and vortex shedding phenomena), (2) static stall hysteresis loops reported in all airfoil stall experiments, (3) experimental data on Mach tuck, (4) investigations of the sensitivity of airfoil designs and its effect on blade tolerance requirements, (5) information on the extent to which laminar flow exists in flight, (6) results of wind tunnel tests on airfoil designs proposed by Blackwell, Dadone, and Hicks, (7) completion of a report on the AH-1G program, including power requirements and pitch link loads, and (8) better communication of technology among the NASA centers.

BOB BOWER:

Thanks Bill. The final area is perhaps a catchall - other applications. Joe Stickle will summarize the issues and needs there.

JOSEPH W. STICKLE:

Being in the "other" category this committee covered such things as sailing ships, hang gliders, RPV's, and things the other groups would like to but probably didn't talk about. The low Reynolds number requirement for data consistently came out throughout the conversation. One of the unique missions discussed for an RPV that I had not heard before was that of using an RPV as a Naval ship decoy; that is you send an RPV away from the ship at high speed and then loiter or cruise at a speed matching the ship cruise speed. The RPV acts as a radar reflector or decoy for the ship. It has to fly along about 40 knots. So there we have the requirement for low Reynolds number data that has to range from low speed all the way to high subsonic speed. It also means that it probably will be variable geometry. So there is a need for low Reynolds number data covering a wide range of parameters. In the way of wind

turbines, one of the requirements was looking at a wider range of useable angle of attack, and looking at such things as flat top lift curves. In the compressor, a need for cascade testing was brought out. Another area that was discussed is the radial flow effects on the boundary layer. The thickening of the boundary layer due to radial flow and its effect on the lift and drag for turbines and compressors need research. Multielement airfoil requirements have already been described. The fourth area we talked about was unsteady aerodynamics. The effects of the propeller wake on the performance of the wing airfoil sections needs to be understood. We go to a lot of trouble to design the airfoil in low turbulence pressure tunnels, fix the transition, and stick it behind the propeller and expect it to perform like the airfoil we designed it to be. I think we need some testing in the facilities to give us airfoils that will work better in the propeller wakes and they may or may not be the same airfoils that came up in steady wakes. Compressors have to be concerned with stall tolerance. Bill just mentioned about the rotorcraft airfoil being a very dynamic environment or critical environment to operate in, but people from Pratt and Whitney told us that the 4th compressor in a turbo engine has probably as harsh an environment to operate in as anything you can imagine. The committee ended up with another "other" category and that is a requirement not for the airfoil developers but rather for us in flight area or design mission area to do. If we are going to look at specific aircraft like an agricultural airplane or an RPV, we need to provide better mission criteria for the airplane from which then we can decide what this airfoil should be doing in terms that the designer can use.

BOB BOWER:

Thank you Joe. Al, I think we finished on schedule and I will turn the session over to you now.

AL GESSOW:

We sure did! I hope my team can do as well. I think we will start with "S" Abbott on my left. We are very happy to have him here and gain his insight and viewpoints on the work we have been doing.

IRA H. ABBOTT:

Well, let me say first I didn't realize until a few minutes ago that I was supposed to get up here to say something. I had presumed that other people knew as well as I did that I was no longer technically competent to deal out any words of wisdom about this research that you are doing.

I would like to say that I am favorably impressed by it. A lot of it I just didn't understand - not in detail anyway. I would like to emphasize that

I am favorably impressed by the whole thing, because I may end up making comments that may give you the impression that I am not, and that is not so, and I do not want to leave that impression with anybody. I am very much impressed by the work that has been done. I think it is good work. I think it should be continued, and I don't want any misunderstanding on that.

Now that I have said that, I want to say that I have an uneasy feeling about the whole thing too. It has been said many times that we never fly airfoil sections. We have probably beaten that to death, but it is something that can stand being beaten to death. Even in the old days 40 years ago this still needed to be beaten into people all the time, and I think that when I was actively working on airfoil sections I must have spent a third of my time telling people: Yes, we're doing a lot of work on the airfoil sections, but don't kid yourself, they are not wings. The miracle, of course, is that airfoil sections have had any significance whatsoever. The concept dates back to work of Prandtl in 1912, and that is a long while ago. The assumptions that were made in the theory which led to the concept of airfoil sections are so far from reality that it is a wonder that there is any reason why anybody should consider airfoil sections important. The wonder is not that the airfoil section concept does not lead to practical results on three-dimensional forms but that it has any validity that is worthwhile. Of course, it does. You all know that too. We also knew 30 years ago that even if you completely disregard the viscous and compressibility effects, which become overwhelming under many circumstances, that on planforms that we are commonly using today the curvature of the flow is such as to induce in an airfoil in many sections of the wing a negative camber which may greatly exceed the total amount of camber put in the wing section as designed for two-dimensional flow. So, all I am saying is, let's get on as fast as is feasible with three-dimensional cases. I know that everybody wants to. I know that the work here has to be done first. In all probability we have to learn to walk before we can run.

But don't become too enamoured by it. I have an uneasy feeling that at least some of the work is being done not because of perceived needs by the aircraft designers, but because a lot of people playing with computers have discovered problems that they can do and they are having one very good time. Now, I am not against research people having a good time. In fact I am in favor of it, but don't forget that while you're having a good time that there are more important problems to solve. So, instead of thinking up little modifications on this stuff, which might give you a little better result on this, that and the other thing, do a little thinking about how you are going to use these fine computers to solve some real problems. I don't know how you do that. You know more about it than I do. I just ask you to think about it once in awhile, when you are no longer enjoying yourself quite so much.

I have also noticed another thing - we're gradually changing our whole design philosophy, not only in aircraft but on other things - to optimization of this, that and the other thing instead of just selecting things and putting them together and coming up with a pretty good thing. This is good. It is necessary. But again don't forget that when you start optimizing things, what you get depends on what you optimize and how you do it. If you put too much faith in the optimization of things which are after all not going to work

the way you think they are going to, you may end up with something that overall is very very far from the optimum. Above all look at your optimum; if it is a nice smooth curve that is concave downward you can pick a maximum point without trouble. But if it has a sharp peak, forget it. Fair it off someplace otherwise you have nothing. Now, I have faith in designers, having talked to a great many of them over the years, so I think they are not going to be bothered too much by this, I am talking more to the research people now than I am to the designers.

One other thing I am impelled to say. I have heard a great deal about computer work, I have heard a great deal about wind tunnel work - you know I am an old wind tunnel man - I heard a little about flight work. But I want to make a plug for it. There is a great deal of this work that I think can only be properly done in flight. The question of transition is something that there is no other way to solve, or get basic information, except in flight. Now, I think I know something about low turbulence wind tunnels, and if you want a low Reynolds number low turbulence wind tunnel, I think you can get one that will be pretty good. But if you want to get into what we think of as real airplane Reynolds and Mach numbers at altitude - I will leave some of the little airplanes out of it for the moment - I think it is going to have to be done in flight. I am afraid there is some thought of flight research as flying an airplane and see what happens to that airplane, or getting some data on it. This is not the kind of flight research I mean. We are going to have to go out and modify airplanes to get the detailed data that would be obtained in wind tunnels if suitable tunnels were available. In the real world of flight you cannot only find out how or whether some definite aerodynamic promise can be achieved, but also how it has to be done so that when things go wrong you are not going to have penalties that are going to be too severe. So I would like to make a real plug for flight research.

I have said too much already. I thank you.

AL GESSOW:

Thank you very much "S". We certainly weren't disappointed in expecting and getting very meaningful comments. They were just the kind we are looking for. I think we will be hearing more about the extension from 2-D to 3-D as we move down the table. Our next speaker will be Helmut Sobieczky who is from Goettingen and is visiting at the University of Arizona.

DR. HELMUT SOBIECZKY:

The success of a conference like the one we have had the privilege of attending here depends critically on the amount of stimulation it provides through reports on major achievements and through work that we see remains to be done. This goal was achieved admirably here. The clear demonstration of

the advanced state of the art in two-dimensions, that is for airfoils, underlines this stimulating effect: we can now see more clearly, where advances are needed in applying airfoil results to the real world of wings and, indeed, the whole aircraft. To achieve this more advanced goal we need to interpret both the theoretical and the experimental results carefully.

The healthy interchange between experimentalists and analysts, aided by computers - certainly in evidence in this conference - is the best work to establishing realistic models of real flows as well as giving physically sound explanations for observed phenomena. Both theory and experiment have proven their value in airfoil research and also delineated its value and limitations in three-dimensional applications.

There is a difficulty, however, that it seems worth noting here. Numerical results, or as they were sometimes interpreted here, "analytical results" may suffer from the contamination of numerical errors. And the same is true of experimental results, particularly in the transonic regime. Only flight test data or "smart" wind tunnels avoid this latter difficulty. Results from such experiments are needed to supply or vindicate models for complex flow interaction problems. Parallel improvement of computer codes and test facilities based on systematic corroboration of results will surely lead to rapid progress with three-dimensional problems. I personally believe these will soon be comparable to the impressive results we have witnessed at this most stimulating and well organized conference.

AL GESSOW:

Thank you. Next is Luis Miranda of Lockheed and I must say that when we had him give his comments in '75, I kind of put him down when he kept pushing the 3-D area. I think the time has now come for more remarks on that subject.

LUIS R. MIRANDA:

Thank you. First of all, I would like to start, just as Ira Abbott did, by saying that I am very impressed with the systematic research that NASA has been conducting on 2-D flows. I think this work should be continued and encouraged. But after saying that, I would like to point out that, in the point of view of the airplane manufacturer (and I have to recognize that there are two types - those whose wing configurations are quasi two-dimensional and those that are highly three-dimensional), it appears that we are trying to perfect two-dimensional computational tools to the nth degree when we have much more difficult and significant problems in three-dimensional flows. I would like to see the same type of approach that emerged from the 1975 meeting in Washington regarding two-dimensional airfoils applied to the three-dimensional wing design problem. Perhaps it would be a good idea to organize a conference like this one but addressing the broader problem of 3-D wing design. The objective of this proposed conference would be to find out where

we are in terms of 3-D wing design technology and what kind of additional research is required to bring this technology to the same level of accuracy and completeness of 2-D airfoil design technology. Again, in order to avoid misinterpretation, I want to stress that the kind of work that we have seen presented on airfoil research in this conference should be continued. NASA is the proper place to become the focal and leading point in this type of research. But we should acknowledge that, from the airplane manufacturer's point of view, 2-D airfoil research may be reaching the point of diminishing returns in terms of actual design technology. I am fully aware that my opinions are biased because of our product lines, and that there are manufacturers to whom 2-D data is more useful than it is to us, but I believe that they represent the point of view of that large segment of the industry which works in highly three-dimensional environments. Thank you.

AL GESSOW:

Thank you very much, Lou. I think your point is well taken. "S" made a comment that we may not live long enough to reach that equivalent point, but I feel very optimistic that the computational procedures that have made such great advances in the last few years can be applied, and actually are now being applied very successfully, to 3-D design, particularly if we're talking about isolated wings. Next, Mr. Lars Ohman from NAE Ottawa who is quite experienced in experimental techniques as well as other areas.

LARS H. OHMAN:

I'm very glad to see that NASA is making a quantum jump into the high Reynolds number game, so at least now we can start comparing notes. As you know, we've been up to 50 million Reynolds number in some of our tests. There are a couple of points on 2-D testing that I feel need to be emphasized. First we have the sidewall boundary-layer problem, which has been mentioned but no real suggestion has been made on how to treat it. We think that our system of suction over an area around the airfoil is a good approach and our experimental data seems to support this. However, I believe something could be done here in the form of analysis. I'm sure that the boundary-layer methods available nowadays, that can treat the shock-wave boundary-layer interaction on airfoils, can also be used to treat the sidewall boundary layers. Perhaps in doing this one can arrive at some conclusion on what kind of suction to employ to get the best possible displacement surface of the sidewall boundary layer in order to eliminate, or at least minimize, its influence on the airfoil model. The emphasis that now goes into the adaptive wall concept is all fine, but the overwhelming problem is still going to be the sidewall boundary layer. Just a short comment on the wall interference effects. Wall pressure measurements should be mandatory on all 2-dimensional tests, of

course, so that sufficient data are at hand to employ some sort of wall interference correction. The trend seems to be for everybody to use the 0012 airfoil to evaluate new concepts. I think there is a very great danger in doing this, because that's an airfoil that's not particularly sensitive to wall effects. A supercritical airfoil is much more sensitive and you may find yourself entering into a completely new ballgame if you start evaluating the adaptive wall concepts with supercritical airfoils. One area of interest is 2-D high lift at low speed and I just want to make a short comment here. A wall configuration that has been successfully tried in Canada is that with a solid floor and a ventilated ceiling. This seems to give almost an ideal wall configuration for high lift testing, and this was successfully demonstrated at the University of British Columbia. Some further exploring of this concept would perhaps be well worthwhile. There is also the question of data accuracy. As I mentioned yesterday, I feel that in one way we are working in the dark because we have not established a target accuracy that we should strive for. We want to compare new calculation procedures and wind tunnel data and produce C_p plots, which may look beautiful, but very little attention is paid to what accuracy is actually required in such a comparison. I think that we should establish a target accuracy for what we want to accomplish instead of just carrying on ad infinitum improving things without even knowing if it is needed. The same applies, as was touched upon by one of the other gentlemen here, to model accuracy. This has not really been discussed at the conference, but we know, and it has been proven, that the supercritical airfoil is extremely sensitive to model inaccuracies. That's all I wanted to say. Thank you.

AL GESSOW:

Thank you. Our next speaker is Andy Lemnios from Kaman Aircraft.

ANDREW Z. LEMNIOS:

During this past two-and-one-half days, we have heard a great deal about new, powerful analytical techniques for the design of airfoils and comparisons of these advanced analyses with pressure distributions on newly developed airfoils. We have also heard, in the past two-and-one-half days, that you cannot fly an airfoil. I would like to expand that statement to say that you cannot fly a computer either.

With regard to rotorcraft applications, which was the subject of one specialist session this morning, Dr. Ballhaus very succinctly summarized some of the concerns and some of the "wish list" items for airfoils that are prevalent throughout the rotorcraft community. I support and strongly reinforce the comments by Dr. Ballhaus. Furthermore, I want to point out that in no other application do we have such strong interactions among the aerodynamics, dynamics, inertial, and control characteristics of an aerodynamic structure

as we do in the rotor blade. The aeroelastic effects in rotary wings can be much more significant and much more important than any airfoil improvements which we may be seeking.

In trying to develop advanced airfoils with improved performance, comparisons between two-dimensional airfoil tests and theory have been directed primarily at matching pressure coefficients and pressure distributions at constant or matched lift coefficients. As Dr. Ballhaus brought out earlier, rotor blade designers are equally interested in pitching moment coefficients and their variations with Mach number and angle of attack. In order to develop analytical tools that are useful to the rotorcraft aerodynamicist, added emphasis should be placed on matching pitching moment coefficients, in addition to lift coefficients.

Another point, which is important from a designer standpoint and from a fabrication standpoint, is that minor changes in surface contours on these new supercritical airfoils with trailing-edge cusps result in strong interactions and strong variations in the airfoil pressure distribution. Typically, rotor blades have chords that are on the order of one to two feet. Required contour tolerances on blades of this size are very difficult to achieve practically, thereby creating a problem for production. As a recommended approach to this production problem, we should determine the influence on pressure distribution of minor variations and tolerance differences over the leading-edge portion and the trailing-edge cusp of the blade. What would these contour differences do to supercritical flow? Would they, in fact, create more problems than they solve?

A final point is that many of these new airfoil shapes for fixed wing applications are based on a single point design condition, such as cruise. In rotorcraft applications, we have a multi-point design problem. We have to design for a cruise condition which has a wide variation in flow over one cycle and we have to design for maneuvers. What happens when you go into a 1.5 g pull-up or a 0.5 g pushover? What does this do to the air loads? Perhaps we can design an efficient airfoil section and blade for a particular cruise condition, but it may have a hard stall. The point there is that we need to look at a forgiving airfoil - one with a gentle stall. This point was brought out yesterday in one of the papers. Thank you.

AL GESSOW:

Thank you very much, Andy. Our next speaker represents another type of rotating airfoil application, Mr. Carl Rohrbach from Hamilton Standard who represents propellers, wind generators, and other types of rotating machines.

CARL ROHRBACH:

Thank you for inviting me to participate in the roundtable discussion of the material presented at this outstanding conference. I would like to comment on an application of advanced airfoils other than for wings and rotors and that is for high speed propellers. The rather unique requirement in this case is that the airfoil sections range from two to ten percent thick over the important working portions of the blade. Unfortunately, very little design and experimental data are available on advanced airfoils for this thickness range.

For years, Hamilton Standard have been satisfied with the NACA Series 16 Airfoils on our propeller blades because tests show this airfoil family to have high critical Mach numbers and good lift-to-drag ratios over fairly wide ranges of angle of attack and Mach number. But now, with the supercritical airfoil emerging, it looks like we may be able to achieve some improvement in the high speed performance characteristics of the propeller along with improvement in off-design operation. However, our concern is that all the work done to date has been on the relatively thick airfoils, i.e., 10-percent thick and above. We know that NASA Langley have plans to include the design and test of thin airfoils and urge that they expedite this work.

I was particularly impressed when Dick Whitcomb indicated that we could use the codes now, in lieu of wind tunnel testing, to confidently design new airfoil sections. However, for propeller design and performance prediction, we need airfoil data over a broad range of Mach numbers and angle of attack. Moreover, we require such data above the section critical Mach number as well as below. Thus, we would need to use the codes to develop these data where perhaps they may not yet be applicable. Finally, I am concerned about the large performance sensitivity the supercritical airfoils have to small configuration variation which for propeller blades are probably within manufacturing tolerance. Accordingly, we would like to see some test data on thin supercritical airfoils covering the broad operating ranges I mentioned previously.

In summary, I would urge that NASA expedite and expand their plan to design and test several very thin supercritical airfoils and establish whether they offer a performance advantage over conventional airfoils as has been demonstrated for the thicker versions.

AL GESSOW:

Thank you. The next speaker is Mr. Harry James of Teledyne-Ryan who represents the RPV community.

HARRY A. JAMES:

The trend I see for the high altitude RPV vehicles is the need for new data in the extremely low Reynolds number regime. The regime between 1 and 3 million, I think is now pretty well documented and we are very grateful to Dr. Whitcomb for his help in the application of the supercritical airfoils for the high subsonic regime. When we got into Mini-RPV's, particularly the low speed propeller driven RPV's for high endurance, I am starting to see Reynolds numbers as low as 20,000 on propeller blade sections. We have very little substantiation of the efficiency of the propellers that would operate in that regime. On the wing sections of the Mini-RPV that Mr. Reed of Dryden is planning to launch from a high balloon at about 100,000 feet, the Reynolds numbers can be as low as 100,000. This area was not addressed at this conference. Okay, one little comment about the other end of the Reynolds number regime. TRA is now involved in a Mach 2 RPV for low altitude which will operate in an extremely high Reynolds number area. During the preliminary design test process development, I noted that we had very little confidence in the available analytical procedures for the selection of the airfoils so we used the old cut and try reliable wind tunnel tests involving many configurations to solve your problems. I think it's a cumbersome way. I didn't see anything on supersonic airfoils at this conference. Perhaps it was irrelevant.

AL GESSOW:

Thank you very much. Our next speaker is Mr. Bruce Carmichael.

BRUCE H. CARMICHAEL:

First, I think we all owe Mr. Ken Pierpont and his wonderful staff a vote of thanks for an extremely well organized, informative, and exciting symposium.

My own interests cover viscous fluid phenomena over the entire Reynolds number range. As the late Dr. Sighard Hoerner so beautifully put it-- "From butterflies at 1000 to bombers at 100,000,000." Perhaps we should expand that to, "From the fractional Reynolds numbers of falling dust motes to that of nuclear submarines at 1,000,000,000." I would like to address three regimes in this expanse for about one minute each.

First the regime from 10,000 to 100,000. You may think this will mainly help your children as they strive to win model airplane contests and perhaps this is not a bad reason for research, but I assure you that in addition it applies to a project of major national and international importance. You will be hearing about this mind boggling project next year. Scientifically, the problem is that of the long laminar separation bubble on wing upper surfaces. To define the separation bubble, its separation point, its transition, its turbulent reattachment point, the pressure distribution under and

downstream of the bubble, and its effects on lift and drag and moment is a fine challenge. There has been excellent work done at higher Reynolds numbers but the question arises as to whether these generalized laws hold down to this particular Reynolds number range. Fortunately, this is the case where the wind tunnel is inexpensive and provides excellent guidance in a situation where theory is still somewhat limited. Low turbulence wind tunnel design is well established. Force and pressure distribution data can be supplemented by smoke flow visualization giving unusually good insight into the physics of the problem in this most exciting realm of research.

The second regime of ultra-light flight at Reynolds numbers from 300,000 to 1,000,000 I will share with you for your enjoyment and entertainment. It started with the Parawing of NASA's beloved Francis Rogallo. He never intended it for manned flight but the lads started using them as crude gliders. They have evolved in one decade into the super kite which is stable, controllable, maneuverable, portable, and with sufficiently high performance to allow soaring flight in light thermal and ridge lift conditions. Recently, I saw a young man stride into a clearing with a bundle over his shoulder 9 inches in diameter, 18 feet long, weighing about 50 pounds. Over the other shoulder he had a 25 pound assembly consisting of a 7 foot tube with a little 2 cycle engine on one end and a 52 inch diameter propeller on the other. He assembled his craft in about 10 minutes, attached himself to it with a harness, started the engine, took a few steps into the wind, and took off and climbed like a Sopwith Camel. He flew into a thermal, shut off his engine, soared for an hour, descended, and 15 feet above the ground went into deep stall and landed lightly as a bird at zero forward speed. Now this is flying as man always envisioned it. It is a genuine folk movement developed outside the mainstream of aeronautical effort. If you have been priced out of power flying and even sailplane flying I suggest you look at ultra-light flight. If you're getting to my age and your personal landing gear is no longer stressed for this, there are also ultra-lights with wheels and/or skids.

The third regime and subject is one I have devoted a lifetime to: Airplanes with highest possible efficiency having extensive laminar flow at Reynolds numbers from 1,000,000 to 50,000,000. First, natural laminar flow. The research was largely done two, three, and even four decades ago. We now need to address the practical problems. Remember what Mr. Abbott told us today. He recommended doing the work three dimensionally, doing it in flight, and tackling the practical problems rather than further refining the theory or conducting more wind tunnel experiments. We have more theory than we need now. We also have high Reynolds number proof of all the elements we need and we have had it for a couple of decades. So let's tackle these practical problems and get some useful high efficiency airplanes in the air!

Natural laminar flow will always have its upper Reynolds number limit where amplification of small disturbances causes transition. Distributed suction through the surfaces greatly extends laminar flow even in the case of adverse pressure gradient and in the presence of wing sweepback. Flight verification and high Reynolds number low turbulence wind tunnel verification of complete laminar flow on wings and fuselages had been obtained in the 50's

and 60's by our group working under Dr. Werner Pfenninger at Northrop Aircraft. Following those exciting days, I experimented with laminar flow under water for over 15 years. The Navy, who backed some of this work, was interested in laminar torpedoes, but it applies equally well to laminar aircraft fuselages. We have worked both with and without distributed suction and also surface temperature differential. The research and development is largely done. It is now time to reap the benefits with useful vehicles.

AL GESSOW:

Thank you Mr. Carmichael. Last, but certainly not least, is my good friend Barney McCormick, Chairman of the Aerospace Department at Penn State. He represents the university viewpoint in rotorcraft and a number of other good areas.

DR. BARNES W. McCORMICK, JR.:

I am pleased to represent the academic community. As we have seen at this meeting, the academic community has certainly contributed to the area of computational fluid mechanics. Particularly noteworthy is the work of Lee Carlson at Texas A&M, Joe Thompson at Mississippi State, the group at Wichita State University, and the airfoil center which has now been established at Ohio State. I would also like to mention some research at Penn State in an area which has not been touched on here. This concerns the field of hydrodynamics. We have a large water tunnel at Penn State and have had an extensive research project ongoing for many years concerned with underwater propulsion, particularly torpedo propellers and pump jets. Through the application of aerospace technology we have been able to significantly improve the cavitation performance of torpedo propellers. Classified at the time, we succeeded with the application of series 16 airfoils in doubling the silent speed of torpedos. I certainly think that the supercritical technology has some place in hydrofoil development for fully wetted sections. One is concerned there with the same limitations which are encountered in compressibility effects; that is, how high can you get the value of the minimum pressure coefficient.

I might add something other than an aerodynamic consideration concerning the design of propellers, some things one would normally not foresee. Just last week I visited a propeller manufacturer in connection with a research project we have with NASA Langley on propellers. I asked them if they were considering going to supercritical sections of some kind for their propellers. The response was not too enthusiastic because they were concerned about the fact that, in operation, a propeller becomes nicked on the edges. The edges look to them to be far from the neutral axis of the section for a supercritical airfoil and they are concerned about fatigue problems.

AL GESSOW:

I certainly thank the speakers here at the table. Now Bob Bower will take over and utilize the remainder of the time to get some comments from the floor.

BOB BOWER:

Thank you Al. I see that we've been so obedient in staying within our time that we now have about 15 minutes left before we're scheduled to complete this conference. So, I think we would like to open up the discussion now to the floor and invite any comments that you may have. Well, a real bashful bunch. One down here please, David C. Ives.

DAVID C. IVES:

I'm from an engine company, Pratt-Whitney. If you count the number of planes flying, most of them have engines, and a lot of these engines are jet engines, and if you count the number of blades in the engines it's 500 to a 1000. So I think the number of blades have the number of wings outnumbered by at least 2 orders of magnitude. We need some basic research on Reynolds numbers from 100,000 to a million, with levels of turbulence from nothing to 5 percent. That's what we really need. The rest of the tools you people have developed can be applied quite quickly. But, that's the one thing we're lacking.

BOB BOWER:

Thank you. Behind you over there. Dennis Bushnell.

DENNIS M. BUSHNELL:

I'd like to comment on a question of the calculation of turbulence separated regions. I think first of all we'll have calculation methods for turbulent separated regions way before we have accurate calculations. The comment by Bradshaw in a 1978 AGARDograph is we know virtually nothing about the turbulence structure and turbulent separated flows. The fundamental problem is probably at least threefold: There is breathing of the separated regions which superimposes on the turbulence, there is generation of 3-dimensional vortex structures, and there is interaction between these 3-dimensional vortex structures. As a final comment, the actual work going on now in the structure of turbulence and separated flows is not very much; in

fact, it's extremely small. At the present rate of progress, we may never get there within Al's lifetime, as he commented before.

BOB BOWER:

Thank you. Now Ted Ayers.

THEODORE G. AYERS:

I'd like to make a couple of comments, Bob. One of the things that I didn't mention earlier was that people are saying that NASA ought to have faster dissemination of data. The manpower situation is what dictates when we can get the data out, generally. The other thing I'd like to say is "thank you" to Ira Abbott for saying what I would like to have said about flight.

BOB BOWER:

I thought you'd like those words Ted. Are there any other comments? Before I officially close the conference I think I would like to say a few words. We've all been looking forward to this conference for a long time - in fact some people for ten years - we've been looking forward to the time when we would be able to have the data as well as our theoretical tools to talk about and to exchange. So it has been a very gratifying experience to see it come off with such attendance. A conference is not an end in itself. As had already been mentioned, one of the primary purposes of a conference is to stimulate thinking, stimulate exchange of ideas, and I think with an attendance here of 450 people we have done that. I want to thank all of the participants, not only in this session this morning, but also for the past three days. And again, I'd like to ask the individual who is really the one most responsible for the conference, Ken Pierpont, to stand up. He has finally come in here and joined us. As Ken indicated to me at coffee break, he organized this conference to be one that he would like to go to. I think that he has been extremely successful in putting on one tremendous conference. With that, I would like to officially close our conference on airfoil research and thank you again for coming.